8-2010

Prediction of Liquid Crystalline Content and Molecular Structures Present in Carbonaceous Pitches

Ward Burgess
Clemson University, wab800@hotmail.com

PREDICTION OF LIQUID CRYSTALLINE CONTENT AND MOLECULAR STRUCTURES PRESENT IN CARBONACEOUS PITCHES

A Dissertation
Presented to
the Graduate School of
Clemson University

In Partial Fulfillment
of the Requirements for the Degree
Doctor of Philosophy
Chemical Engineering

---

by
Ward A. Burgess
August 2010

Accepted by:
Prof. Mark C. Thies, Committee Chair
Prof. David A. Bruce
Prof. Dan D. Edie
Prof. Christopher L. Kitchens
Prof. Steven J. Stuart

ABSTRACT

Previous research at Clemson has shown that multistage, packed column, supercritical extraction (also called dense-gas extraction, or DGE) of petroleum pitches is a promising technique for the production of carbonaceous precursors that can be processed into a variety of carbon products, including activated carbons and high thermal conductivity carbon fibers. As the existence (or lack thereof) of a liquid crystalline phase, or mesophase, plays a key role in establishing the suitability of a potential precursor material for a given application, we developed the SAFT-LC (liquid crystal) equation of state by combining Maier-Saupe theory for multicomponent mixtures with the SAFT equation. SAFT-LC was used with some success to predict the effect of temperature and pressure, as well as pitch and solvent composition, on the formation of mesophase at both supercritical and ambient conditions. Unfortunately, the lack of information about the actual molecular structures present in petroleum pitch hindered the development of an appropriate set of pure-component parameters for use with SAFT-LC. Thus, the second half of this dissertation focused on structural characterization.

Previous efforts to characterize the molecular structures of the major species present in pitches have been limited by an inability to fractionate the pitch into cuts of narrow molecular weight (mol wt). However, by using DGE followed by preparatory-scale gel permeation chromatography (prep-scale GPC), we are now able to fractionate petroleum pitch into its constituent oligomers. Subsequent analytical characterization of these oligomers using high-performance liquid chromatography with photodiode array

detection (HPLC/PDA), matrix-assisted, laser desorption and ionization, time-of-flight mass spectrometry (MALDI), MALDI-post source decay (PSD), and UV-Visible spectrophotometry (UV-Vis) has determined that M-50 monomer is primarily comprised of benzenoid, polycyclic aromatic hydrocarbon (PAH) "backbones" (the most prevalent of which are pyrene, chrysene, benz[a]anthracene, triphenylene, benzo[a]pyrene, benzo[e]pyrene, and benzo[ghi]perylene), substituted with from 0 to 4 alkyl (primarily methyl) groups. The most prevalent dimers are formed from the condensation reaction of two of the most prevalent monomer units, such that four hydrogens are lost and a five-membered, connecting ring is formed to create a fluoranthenoid PAH. For trimers and tetramers, MALDI, UV-Vis, and transmission FT-IR results are all consistent with the linkage of the most prevalent lower-order oligomeric units via a single, five-membered ring. Thus, the body of evidence indicates that the highly PAH-condensed structure previously proposed for such pitches does not exist.

DEDICATION

I dedicate this work to my parents, Dick and Jenny Burgess, for the constant support and encouragement they gave me during my years in graduate school.

ACKNOWLEDGMENTS

I would like to thank the following individuals for their various contributions to this dissertation:

My research advisor Prof. Mark C. Thies, who encouraged me to pursue graduate school and who gave me the opportunity to learn how to be a researcher.

My Ph. D. advising committee members, Profs. David Bruce, Dan Edie, Christopher Kitchens, and Steven Stuart for reviewing this work.

Jennifer Pittman and Prof. Ken Marcus, for their indispensable help with HPLC analyses.

Kim Ivey, for her prompt and able help with IR analyses.

Dan Sweeney, with whom I spent nearly a month in South Korea as a guest researcher, and from whom I learned a lot about how to get things done in the lab.

Prof. Dan Edie, who provided the funding and contacts to make the Korea research experience possible.

Jay McAliley, for teaching me how to use Visual FORTRAN.

Eduardo Cervo, Sourabh Kulkarni, Sarah Mena, David Esguerra, and Julian Velez for their friendship and for being so patient and easy to work with.

My brother, Richard Burgess, Jr., for his constant pep talks.

TABLE OF CONTENTS

Page

Page

Page

Page

Page

LIST OF TABLES

LIST OF FIGURES

CHAPTER 1

INTRODUCTION

Carbonaceous pitch is the name given for a class of materials consisting primarily of relatively large polycyclic aromatic hydrocarbons (PAHs), with both alkyl (particularly methyl) and/or naphthenic substitution occurring.[1,2,3,4,5,6] There are three major classes of pitches: (i) coal-tar pitches,[7] the residue remaining after the high-temperature distillation of coal-tar, (ii) petroleum pitches,[8] produced by the heat-soaking of fluid catalytic cracking (FCC) decant oil (a byproduct of the catalytic cracking of the heavy gas oil fraction of crude oil), and (iii) synthetic pitches produced from the thermal or catalytic polymerization of a pure compound, such as anthracene[9] or naphthalene.[5] In 1965, Brooks and Taylor[10] demonstrated that all of these pitches form an ordered, discotic, liquid-crystalline phase, or mesophase, upon heating to elevated temperatures. In addition, a commercially available, isotropic (0% mesophase) petroleum pitch such as M-50 can be processed into mesophase by removal of the lower molecular weight (mol wt) components, thereby concentrating the high mol wt species.[11] Thus, these materials have characteristics in common with both thermotropic and lyotropic liquid crystals.[12,13,14] Because of these unique characteristics, pitches can serve as precursors for a variety of carbon products.[15] For example, to produce high modulus, high thermal-conductivity carbon fibers, the starting pitch should be liquid-crystalline at processing conditions.[16] Thus, this precursor material should consist primarily of moderate to high mol wt (500-1000 Da) molecules,[11] which will spontaneously align upon melting to form the desired liquid-crystalline mesophase. On the other hand, production of the matrix phase of a

carbon-carbon composite requires a lower mol wt pitch fraction that remains isotropic, yet has a high carbon yield.[17]

The work contained in this dissertation focused on two problems encountered in producing such precursor materials. As mentioned in the preceding paragraph, precursor pitches of different mol wts are required, depending on the properties desired in the final carbon product. Thus, a major focus of the Carbon Research Group at Clemson has been the preparation of carbonaceous pitches of controlled mol wt distribution (MWD) that would serve as precursors for carbon products. For the following reasons, we have found that petroleum pitches are quite suitable for this work: (i) they are inexpensive (M-50 petroleum pitch costs only \$0.23/lb[18]), (ii) the oxidative stabilization rates for fibers made from petroleum pitch are much faster than for those made from coal-tar pitch,[6] and (iii) by applying Clemson's dense-gas/supercritical extraction (DGE/SCE, or DGE for short) process[11] for the extraction and precipitation of selected species, pitch precursors can be produced with a wide range of mol wts and, as a result, a wide range of softening points and mesophase contents.[11]

The empirical solution of the appropriate DGE operating conditions for producing a pitch of a given mol wt, MWD, and mesophase content is time-consuming; furthermore, optimum regions of operation could be entirely missed. Thus, thermodynamic models of our DGE processes have always been of interest. This chapter therefore begins with a discussion of past studies by Clemson researchers with respect to modeling the relevant phase behavior for such extraction processes. Next, a discussion of previous work by other researchers in modeling the formation of mesophase is presented.

In the course of carrying out the modeling work described herein, it became apparent that improvement in the thermodynamic modeling of both the extraction and mesophase formation processes was being limited by our inability to accurately describe the molecular composition of petroleum pitches. Thus, the focus of the final half of this dissertation is concerned with the analytical characterization of petroleum pitches, with the goal of determining the specific, major molecular structures that exist therein.

Modeling Supercritical Extraction of Petroleum Pitches – Previous Work

The work of Hutchenson

Hutchenson et al.[19] modeled vapor-liquid equilibrium (VLE) between A-240 petroleum pitch and toluene at elevated temperatures and pressures using the Peng-Robinson (PR) equation. Such phase behavior was relevant to his investigation of one-stage SCE processing of pitch with supercritical (SC) toluene. The PR model was chosen both for its simplicity and for its ability to model the SC region with at least fair accuracy, even though work by Alexander[20] and Schwartz and Prausnitz[21] indicated that a perturbed hard chain-type equation of state may be more accurate for predicting the overall phase behavior of a complex mixture such as petroleum pitch. Hutchenson modeled the molecular composition of A-240 pitch by using the 3 pseudocomponents (PCs) defined by Dickinson[1] for A-240 pitch (this work will be discussed in greater detail later in this chapter). The pure-component PR characteristic constants a_C, b, and κ for each of the three PCs were then determined by the following procedure:

Hutchenson et al. first compiled a list of T_c, P_c, and ω (calculated from the available vapor pressure data) for 43 model PAHs. These pure-component properties were then used to calculate the corresponding pure-component a_C, b, and κ for each of the 43 model PAHs. They then showed that each of these characteristic constants could be expressed a linear function of the most statistically relevant molecular structure parameters: M_N, the number average mol wt of the PC; C_{aro}, the number of aromatic carbons for the PC; C_1, the number of aromatic nonbridge carbons for the PC; R_S, the number of alkyl substituent groups for the PC; and $\%c_{A,}$ the weight percent of the PC that consists of aromatic carbon.

Modeling results indicated that the PR equation does an adequate job in calculating both the solvent and overall pitch content in both the extract and residue phases at conditions of VLE. However, experimental results indicated that high operating temperatures (674 K) were necessary in order to achieve even modest extraction yields (~ 20 wt % of pitch feed) into the top phase. With the weak extractive power of the SC solvent at these operating conditions, it was not possible to produce a residue that was high enough in mol wt so as to permit the formation of bulk mesophase.

The work of Hochgeschurtz, Bolaños, Dauché, and Zhuang

Following the work of Hutchenson et al.,[19] Hochgeschurtz[22] and Bolaños[23] investigated a region of liquid-liquid equilibrium located at elevated temperatures and pressures. These workers discovered that the heavier, pitch-rich liquid phase frequently contained the proper mol wt/MWD required to form mesophase pitch. Dauché et al.[24]

then conducted a more thorough study of this region of liquid-liquid equilibrium (LLE). In particular, they fractionated an isotropic Conoco petroleum pitch via one-stage extraction with SC toluene at various pressures (45 to 155 bar), temperatures (583 to 633 K), and solvent-to-pitch (S/P) ratios (2.5 to 4.0); see Fig. 1.1. There was marked improvement in the experimental extraction yields obtained, compared to Hutchenson's earlier work. Measurements of the extraction yield indicated that the majority of the pitch was extracted into the top phase; upon drying of the residue phase, the mesophase content was observed to range from 38 to 100%.

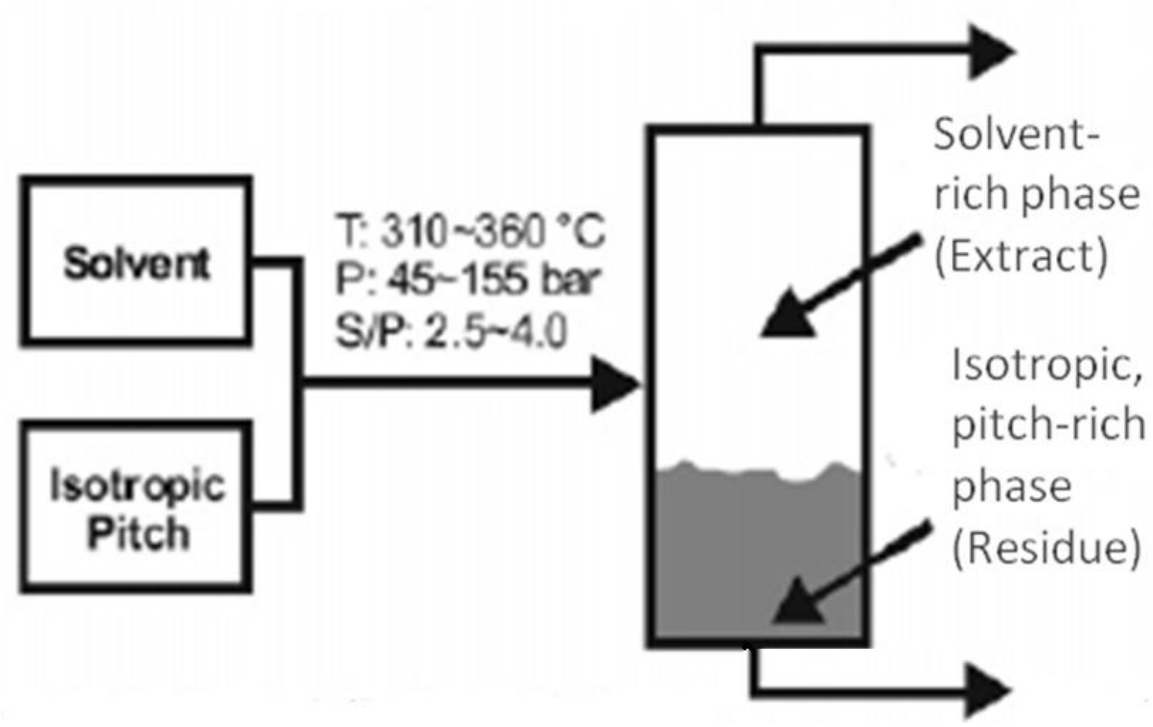

Figure 1.1. A single-stage liquid-liquid extraction process using near-critical (NC) or SC toluene to create pitch precursors that possessed various mesophase contents upon solvent removal. Reprinted with permission;[25] copyright American Chemical Society.

In order to model the liquid-liquid extraction process for pitch-toluene mixtures, Dauché initially considered the PR equation for its relative simplicity. However, it was

soon discarded after preliminary calculations by both Zhuang[26] and Pigott[27] indicated that cubic equations of state (including the PR equation) gave inaccurate predictions for the liquid-liquid phase equilibrium of interest. Because of the relative success of the SAFT (Statistically Associating Fluid Theory) equation of state for modeling LLE for polymer-solvent mixtures[28] and phase equilibria for the extraction of bitumen with SC CO_2, [29] this model was selected for further investigation.

In SAFT theory, a molecule is assumed to be a chain, composed of a number of equally sized segments. For each component, required inputs to the SAFT equation include 3 pure-component fitting parameters: u_i^0, an energy parameter representing the temperature-independent depth of the square well potential between two molecules of species i; v^{00}, the temperature-independent volume of a chain segment; and m, the number of segments in a chain.

In order to determine the SAFT parameters for a given pitch, it is first necessary to replace the essentially continuous nature of the MWD of pitch with a defined number of PCs. To this end, Bolaños[30] generated PCs from experimental gel permeation chromatography (GPC) data for A-240 pitch using a quadrature method. In particular, he expressed the GPC curve as the sum of three normal distribution functions. Then, using the Gauss-Chebyshev quadrature technique,[31] he generated 7 quadrature points for each normal distribution function (NDF), with each quadrature point representing a PC, for a total of 21 PCs. PC mol wts were directly obtained from the prepared GPC calibration curve of mol wt vs. retention time, by noting the retention time associated with each quadrature point comprising the NDFs, and calculating the associated mol wt. Finally,

the mass fractions of each PC were determined according to the Gauss-Chebyshev method.

Folowing the approach of Bolaños, Zhuang[26] resolved the MWD of a Conoco feed pitch (vs. A-240) into 21 PCs. Using these PCs as input into the SAFT equation, he correlated the predicted toluene solvent weight fractions to the experimentally determined values by adjusting the binary interaction parameters k_{ij}. For lack of a better alternative, the SAFT parameters for each pitch PC were calculated from the mathematical relationships developed by Huang and Radosz[29] for bitumen PCs. Required inputs to these equations were the PC mol wt and carbon-to-hydrogen (C/H) ratio (additional structural information, including the molecular structure itself, was not necessary). However, realistic values for the C/H ratios did not yield good results, so this parameter was treated as an adjustable parameter; with the best fit to the experimental data occurring at a C/H ratio of 1.0 (this C/H ratio was erroneously reported as being equal to 1.10[26]). The SAFT model was shown to correctly predict the experimentally observed solvent weight fractions present over a range of experimental, SC conditions with a reasonable degree of accuracy (see Fig. 1.2a). In addition, it correctly predicted the marked increase in extraction yield observed at elevated pressures (see Fig. 1.2b). However, at the time these studies were made, it was not possible to confirm the accuracy of the MWDs predicted for the top and bottom phases.

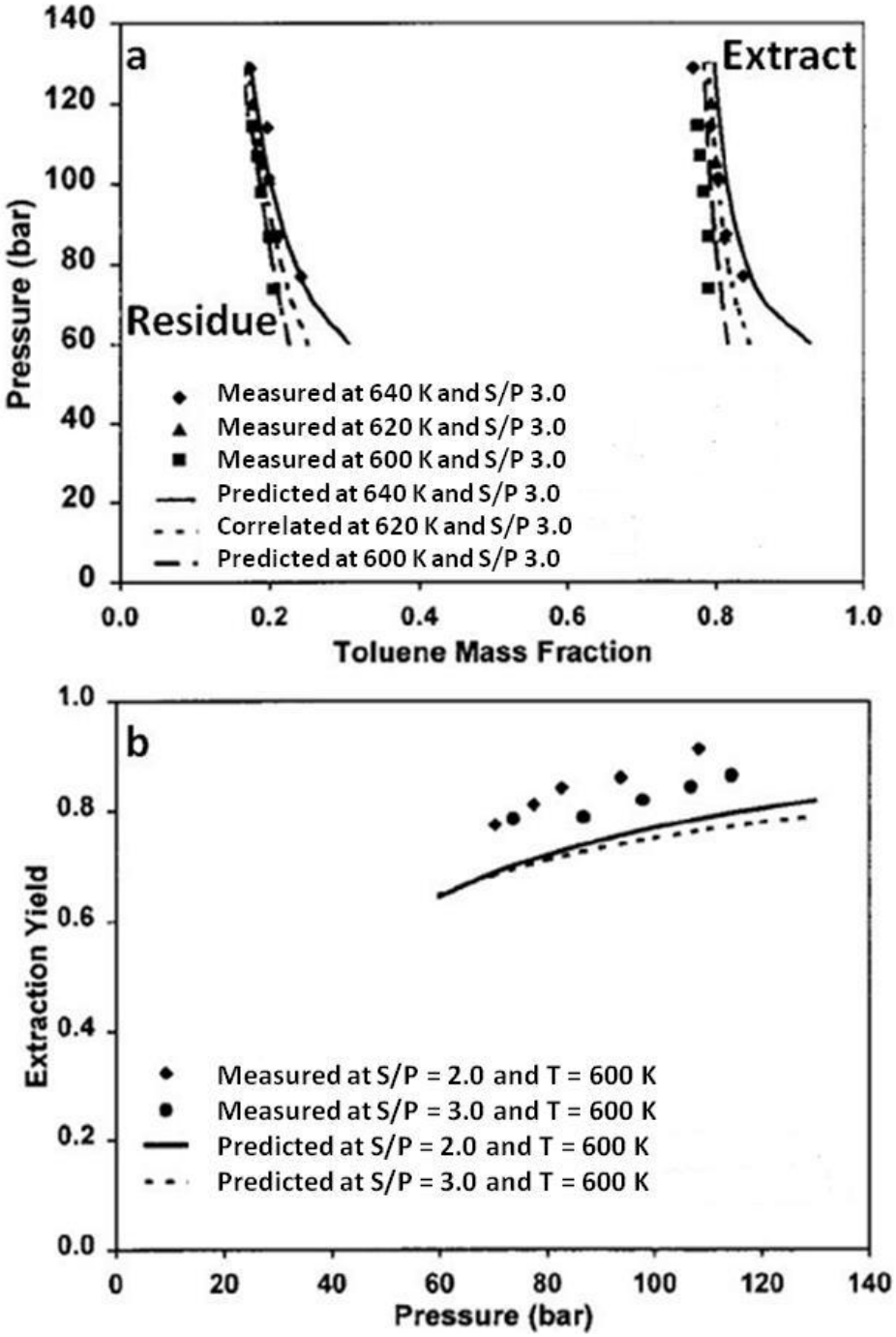

Figure 1.2. In panel a, SAFT predictions of the toluene compositions in both the pitch-rich phase (residue) and solvent-rich phase (extract) are in close agreement with experimental data.[26] The data in panel b indicate the ability of the SAFT equation to predict the elevated extraction yields achieved when using denser NC or SC solvents. Reprinted with permission;[26] copyright American Chemical Society.

While useful, the above work was limited in that the SAFT model cannot be used to predict the extent of liquid crystal (LC)/mesophase formation in either phase. Therefore, the next topic of discussion will concern the work of previous researchers in modeling the formation of mesophase.

Modeling to Predict Mesophase Formation – Previous Work

LC Theory of Maier and Saupe

In the late 1950s, Maier and Saupe[32,33,34] developed a theory in which the liquid-crystalline mesophase formation is assumed to arise as the result of an anisotropic potential that exists for a mesogen (that is, a mesophase-forming molecule) interacting in the mean field generated by its neighbors. In this chapter, we denote this potential as the anisotropic energy parameter ε. Based on the work of Maier and Saupe, for a pure mesogen, the following relationship holds for ε:

$$\varepsilon = 4.541 kT_{cl} \tag{1.1}$$

In Equation 1.1, k is Boltzmann's constant and T_{cl}, the clearing temperature, is the temperature at which a phase transition from ordered mesophase to a disordered, isotropic phase occurs. Only an isotropic phase is observed at temperatures above T_{cl}. In this manner, the anisotropic potential energy parameter is related to the macroscopic variable, T_{cl}. In developing this theory, Maier and Saupe assumed that mesogens can be represented by long, cylindrical rods, as indicated in Fig. 1.3. Each individual molecule is oriented at an angle θ_1 relative to a preferred state, or director. In Fig. 1.3, the director

is denoted by **n**. The Helmholtz free energy of molecular orientation A^{ori} (see Equation 1.2 below), is a function of ε and $T_{cl,}$. The order parameter $\overline{P}$ in Equation 2 is a function of the ensemble average angle of orientation for all molecules.

$$A^{ori} = \frac{N}{m}\left[\frac{\varepsilon \overline{P}^2}{2} - kT \ln\left(\int_0^{\pi/2} \exp^{\frac{\varepsilon \overline{P}}{kT}\left(\frac{3}{2}\cos^2\theta_i - \frac{1}{2}\right)} \sin\theta_i d\theta_i\right)\right] \quad (1.2)$$

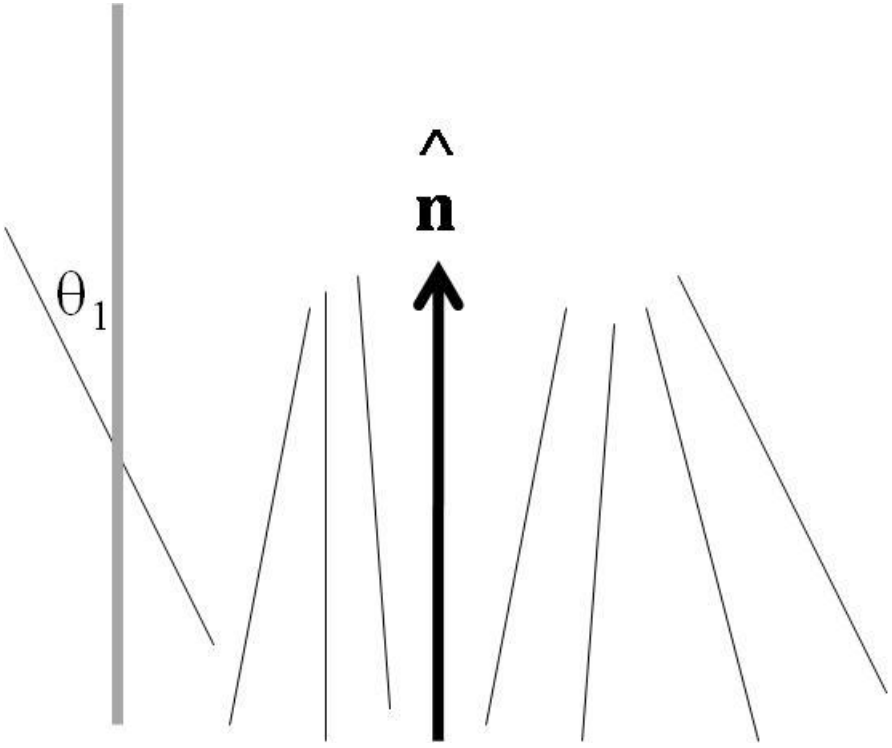

Figure 1.3. Each mesogen is oriented at a unique angle θ_1 relative to the director **n** (or preferred orientation). Maier and Saupe proposed that the mesophase molecules can be represented as long rods.

Extension of Maier-Saupe Theory to Multicomponent Mixtures

In the early 1970s, Humphries et al.[35,36,37] extended Maier-Saupe theory to mixtures of liquid-crystalline molecules. The desired, corresponding equation is shown below as Equation 1.3. The authors then used the theory to successfully predict a nematic-isotropic phase diagram for a mixture of 2 nearly identical, rodlike nematogens (see Fig. 1.4). nematogen I is p-phenylene dianisate and nematogen II is 4-(4-methoxybenzoxy)phenyl-4-methoxybicyclo[2.2.2]octane-1-carboxylate.

$$A^{ori} = \frac{N}{2}\sum_i \sum_j x_i x_j \varepsilon_{ij} \overline{P_i}\,\overline{P_j} - NkT\sum_i x_i \ln\left(\int_0^{\pi/2} \exp \frac{\sum_j x_j \varepsilon_{ij} \overline{P_j}}{kT}\left(\frac{3}{2}\cos^2\theta_i - \frac{1}{2}\right)\sin\theta_i d\theta_i\right) \quad (1.3)$$

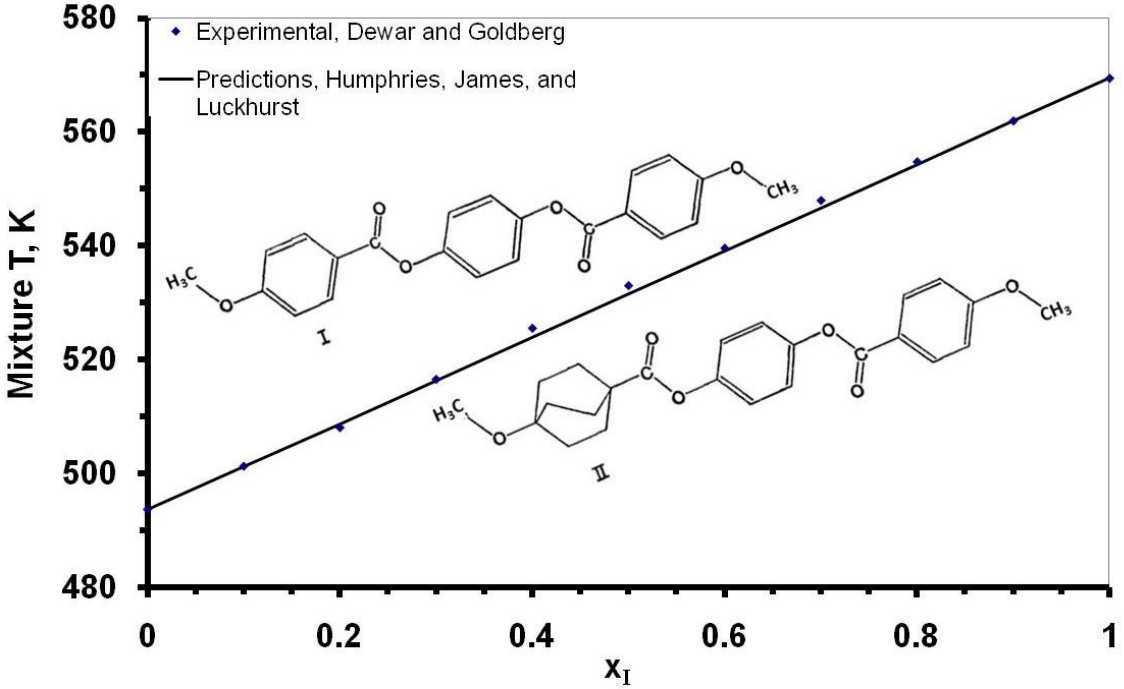

Figure 1.4. Maier-Saupe theory (as modified by Humphries, James, and Luckhurst) predictions for the nematic-isotropic transition are close to the experimentally observed data points obtained by Dewar and Goldberg[38] for a binary mixture of two nematogens. These nematogens are p-phenylene dianisate (I) and 4-(4-methoxybenzoxy)phenyl-4-methoxybicyclo[2.2.2]octane-1-carboxylate (II). Adapted from Humphries et al.[35]

Maier-Saupe Theory for Modeling of Phase Equilibrium of Pitch-Containing Mixtures

In 1997, Shishido et al.[39] used Maier-Saupe theory (as expanded to multicomponent mixtures by Humphries et al.[35,36,37]) to predict the nematic-isotropic phase transition behavior for mesophase pitches at atmospheric pressure and elevated temperatures. Mochida and Korai[40] had previously determined phase boundaries for a pitch system experimentally as follows. First, benzene-soluble (isotropic) and benzene-insoluble (typically mesophase-forming) fractions of a coal-tar pitch were mixed together in various proportions. Next, Mochida and Korai[40] observed the phase transition behavior of these mesophase pitches on a hot stage via optical microscopy (see Fig. 1.5). They observed that the pitch could be in one of three states: (i) a nematic, liquid-crystalline phase, (ii) a fully isotropic liquid phase, or (iii) a nematic liquid-crystalline phase in equilibrium with a fully isotropic liquid phase.

To model these phase equilibria, Shishido et al.[39] had to by necessity assume a binary mixture of two (i. e., benzene-soluble and benzene-insoluble) components. Isotropic interactions between these two species were governed by the ideal solution model, and anisotropic interactions by Humphries et al.'s extension[35,36,37] of Maier-Saupe theory. Even though mesophase pitch is comprised of disclike, rather than rodlike, mesogens, model predictions were in qualitative agreement (see Fig. 1.5) with the experimental data of Mochida and Korai.

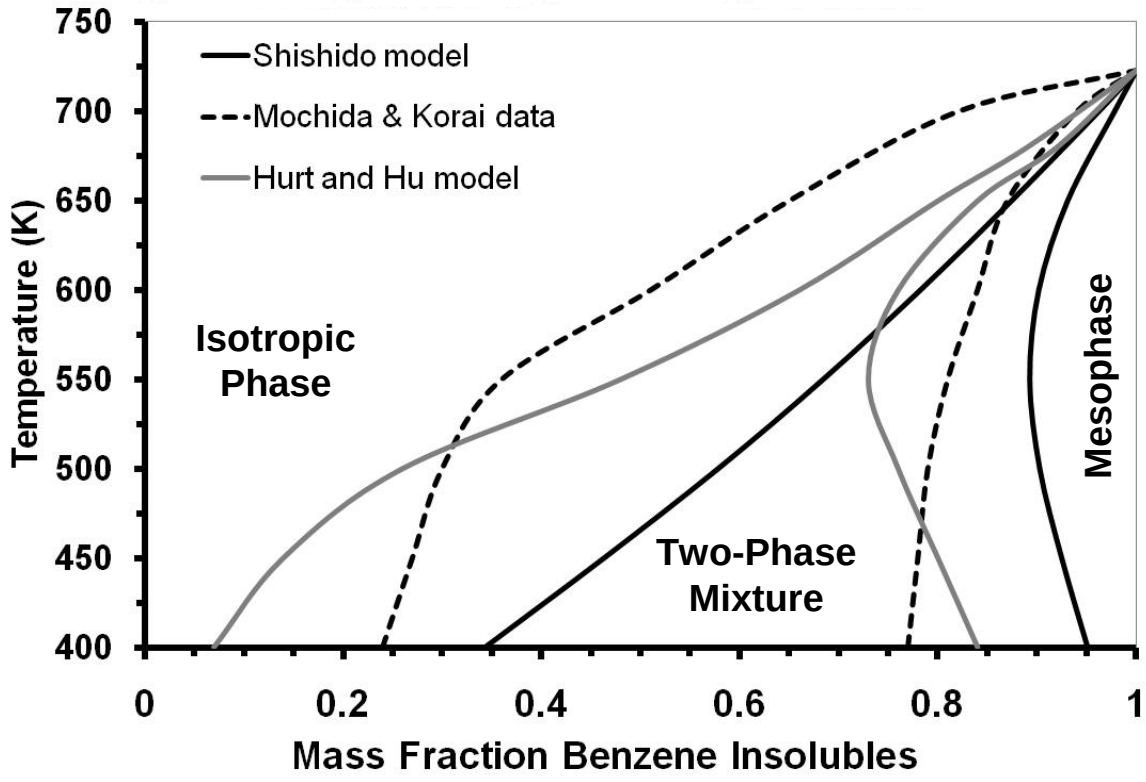

Figure 1.5. Thermodynamic models used to predict the nematic-isotropic phase behavior for a mixture of benzene solubles and benzene insolubles (determined experimentally by Mochida and Korai[40] for a coal-tar pitch).

Coupling of Maier-Saupe Theory to Regular Solution Theory – The work of Hurt and Hu

Hurt and Hu[41] then extended the modeling work of Shishido et al.[39] with a thermodynamic model that included not only anisotropic (that is, liquid-crystalline) but also other nonideal (that is, differences in mol wt and chemical composition of the various components present) effects. Because of the nonpolar nature of carbonaceous pitches, a model based upon both regular solution theory and Flory-Huggins theory was chosen to thermodynamically model these additional nonideal mixing effects. An assumption in regular solution theory is that there is no excess entropy of mixing – that

is, all mixing occurs because of enthalpic effects. However, in order to account for the combinatorial entropy of mixing molecules with large differences in molecular size (such as the light and heavy pitch molecules), the combinatorial portion of the Flory-Huggins theory (this theory is used to model phase equilibrium for molecules which vary greatly in size, such as polymer chains and solvent) was used. In Equation 1.4 below, the model of Hurt and Hu[41] is expressed in terms of the Gibbs free energy of mixing, ΔG_{mix}

$$\Delta G_{mix} = \Delta G^{ideal} + \Delta G^{enthalpic} + \Delta G^{combinatorial} + G^{ori} \qquad (1.4)$$

where ΔG^{ideal} accounts for ideal solution mixing effects, $\Delta G^{enthalpic}$ is the enthalpic contribution to the Gibbs free energy of mixing (from regular solution theory), $\Delta G^{combinatorial}$ is the contribution to the Gibbs free energy of mixing by the combinatorial entropy (from Flory-Huggins), and G^{ori} is the contribution to the Gibbs free energy of mixing by the anisotropic potential, which causes molecular orientation and, therefore, mesophase formation. The G^{ori} term was adapted from the statistical theory of Humphries and coworkers[35,37] discussed earlier and denoted in Equation 1.3 in terms of A^{ori}. Because Hurt and Hu modeled phase equilibria for systems at ambient pressures, they assumed that $P\Delta V^{ori}$ (the difference between G^{ori} and A^{ori}) was inconsequential under these circumstances and that it could therefore be neglected (thus, $G^{ori} = A^{ori}$).

The model of Hurt and Hu was tested against the experimental data of Mochida and Korai[40] (see Fig. 1.5) and yielded somewhat better agreement with the data than the method of Shishido et al.[39] It was also successfully tested against the hot-stage observations of Lewis[12] and the petroleum pitch MWD data of Greinke and Singer.[42]

However, neither the model of Shishido et al.[39] nor that of Hurt and Hu[41] could be used to predict phase equilibrium at the SC conditions typical of DGE, as the ideal solution reference state does not exist at these conditions.

Of equal importance was the fact that input to the above models had thus far been qualitative at best. For example, benzene-solubles and benzene-insolubles are hardly definitive molecules, nor are average mol wts of pitches of broad MWD. Thus, with such limited characterization data, it was to a large extent uncertain as to how much of the observed deviations between experiment and theory were due to the model itself, or the inadequacy of the characterization of the system of interest.

Characterization of Pitches – Previous Work

One of the first quality characterizations of petroleum pitch was made in 1984 by Dickinson.[1] First, he successively fractionated A-240 pitch using 3 solvents: a 90:10 mixture of cyclohexane and acetone, a 50:50 mixture of cyclohexane and acetone, and toluene. He then characterized these three fractions using vapor pressure osmometry (VPO), proton NMR, ^{13}C NMR, and elemental analysis. By applying Knight's method, average molecular structures (see Fig. 1.6) were obtained for each fraction. Note that these structures consist of PAHs with limited methyl and ethyl substitution. As 11% of the pitch was insoluble, no information on this higher mol wt portion of the pitch was obtained.

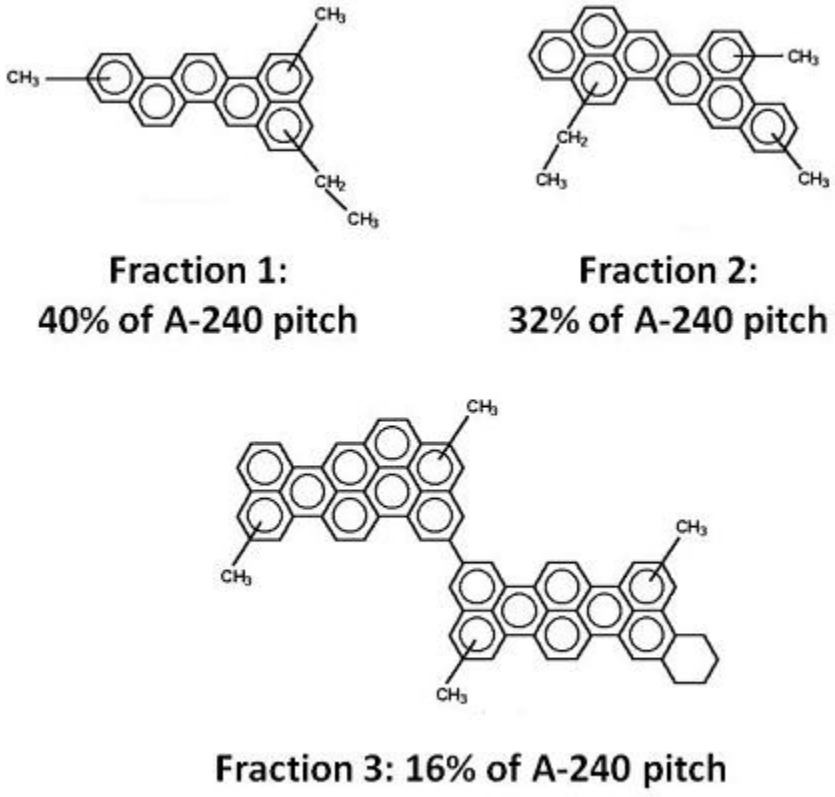

Figure 1.6. Average molecular structures for three solvent fractions of A-240 pitch, as proposed by Dickinson.[1] All percentages denote weight fractions.

While useful, this work was limited in that it yielded only average molecular structures, which reflected the overall composition of the pitch fraction in question, as opposed to structures for the actual species present in the pitch. Furthermore, the whole pitch was expressed as a mixture of only 3 PCs, which is not a high degree of precision.

A number of techniques have been used to obtain information concerning the mol wt, structure, and composition of petroleum pitches (see Table 1.1). VPO yields the average mol wt of a sample, but gives no information concerning the MWD. Some methods, such as elemental analysis and Fourier Transform-Infrared (FT-IR) spectroscopy, do not require the use of a solvent. However, elemental analysis, while

Table 1.1. Advantages and disadvantages of methods used to characterize carbonaceous pitches.

Method of Characterization	Measured Properties	Advantages and Disadvantages	Reference
Elemental Analysis	C/H ratio	Solubility not an issue; can be used to approximate aromaticity but is of limited use otherwise	1, 4
FT-IR	Functional groups present	Solubility not an issue: is primarily used to obtain qualitative information concerning functional groups present in a mixture (such as the presence and position of methyl groups on various pitch species). Cannot provide structural information for individual species present in mixtures, but only for the mixture as a whole.	3, 16
GPC	MWD	Is a well-established technique for determining MWDs for polydisperse samples, but not all pitches are fully soluble in GPC mobile phases.	43, 44, 45
MALDI-TOF-MS	Absolute mol wt, MWD	Measures actual mol wts of species in distribution; appropriate matrix material needed. Can be performed on either solvent-based or solvent-free basis. Carbon Group research on using MALDI to quantify the MWD of pitches, while very promising, is still in its early stages.	11, 46, 48, 49, 50
Proton NMR and ^{13}C NMR	Relative presence of different types of hydrogen and carbon atoms	These two well-established techniques yield useful quantitative information concerning the different types of hydrogen and carbon atoms present in a mixture. However, they cannot be applied to heavier pitch fractions which have low solubility in common NMR solvents.	1,3,4
VPO	Average mol wt	Yields number average mol wt of a sample, but is time-consuming and does not yield the mol wts of individual species present.	1,43,54
UV-Visible Spectro-photometry	UV, visible light absorbance	Is capable of unequivocal identification of PAHs. However, samples must be highly pure.	3,56,58, 60

providing useful information concerning aromaticity in the form of the molecular C/H ratio, is of limited value otherwise. Meanwhile, FT-IR provides useful information concerning the different functional groups present on a molecule. For example, FT-IR spectra of carbon fibers subjected to various degrees of oxidation yield information concerning the atomic makeup of the intermolecular linkages that form at various stages during the fiber stabilization process.[16] However, the technique is primarily used for qualitative (vs. quantitative) characterization.

Proton NMR yields structural information concerning the relative presence of aromatic and alkyl protons, while ^{13}C NMR yields structural information concerning the relative presence of different types of carbon atoms (aromatic, naphthenic, etc.). However, the technique cannot be applied to heavier pitch fractions, which have low solubility in common NMR solvents such as deuterated chloroform.

GPC is the traditional technique for determining the MWD of pitches[42,43,44] and continues to have its uses. However, it does have its drawbacks. Even when high-temperature GPC, with aggressive solvents such as 1,2,4-trichlorobenzene is used,[45] portions of the pitch are insoluble. Rapid degradation of the column[24] occurs when attempts are made to analyze the entire pitch by GPC, probably because the insoluble, highest mol wt species plug the column pores. Another drawback of GPC is the difficulty of finding suitable calibration standards that mimic the behavior of pitch, especially at mol wts above 500 g/mol.

Seeking an alternative to GPC, Edwards et al.,[46] showed that a relatively new mass spectrometry technology, matrix-assisted laser desorption and ionization, time of

flight mass spectrometry (MALDI-TOF-MS, or MALDI for short) could be used to obtain reproducible mass spectra for partially insoluble carbonaceous pitches. The MALDI technique has two distinct advantages: (1) analyses can be conducted using either solvent-free or solvent-based sample preparation methods, thus eliminating pitch solubility as an area of concern, and (2) unlike other mass spectrometry techniques, which require that the species of interest be at least somewhat volatile, MALDI can be applied to the whole mol wt range of the pitch. Edwards[46,47,48] and then Cervo[11,49] successfully used MALDI (with solvent-free sample preparation) to characterize pitch cuts isolated by DGE. The quantitative determination of the MWD of pitches is the subject of ongoing research in our laboratory.[50]

For many of the methods described above, proper characterization of a carbonaceous pitch requires that the pitch be separated into narrow mol wt fractions, such that molecular information on the various types of species that comprise pitches can be obtained. Furthermore, once the separation of pitches into a well-defined fraction is accomplished, other analytical techniques that heretofore have not been applied to pitches, but have been applied to other complex mixtures of chemically homologous materials, may become quite useful. Methods used for the fractionation of pitches, as well as analytical characterization techniques that may prove to be useful as narrow mol wt pitch fractions become available, are discussed next.

Methods Previously Used for the Fractionation of Pitches

DGE

DGE is a multistage, countercurrent extraction technique that has been in use by the Carbon research group for the fractionation of petroleum pitches for about five years, and is a significant improvement over the previously discussed single-stage extraction processes employed by earlier Carbon group researchers. DGE was invented by Zosel,[51] who used this technique to fractionate a wide range of chemical mixtures. For example, he fractionated a mixture of α-olefins (carbon numbers 16, 18, 20, 22, 24, and 26) into narrow, single-oligomer cuts of 95-99% purity using ethane at elevated pressure as the dense-gas solvent. However, none of the mixtures separated were chemically similar to pitches, so significant changes for column design, operating conditions, and solvent type have been investigated and developed by the Carbon group at Clemson over the past several years.[47,48,52,53]

For DGE fractionation of a representative petroleum pitch, M-50, a dense-gas (typically at SC temperatures upon entering the extraction column) solvent is used to produce cuts of desired composition. As shown in Fig. 1.7, M-50 pitch can be classified as oligomeric, as there are four distinct groups of species. Of course, the oligomers themselves are not pure, as the starting material, FCC decant oil, is itself a mixture. However, for simplicity, we call the species comprising the first broad peak monomer (marked with a 1 in Fig. 1.7). Those comprising the second, third, and fourth broad peaks are called dimer (2), trimer (3), and tetramer (4), respectively. The DGE process

depicted in Fig. 1.7 yields a narrow, oligomeric fraction comprised of high-purity M-50 monomer. DGE has also been used by the Thies group to yield high-purity dimer[52,53] and trimer-rich[47] cuts.

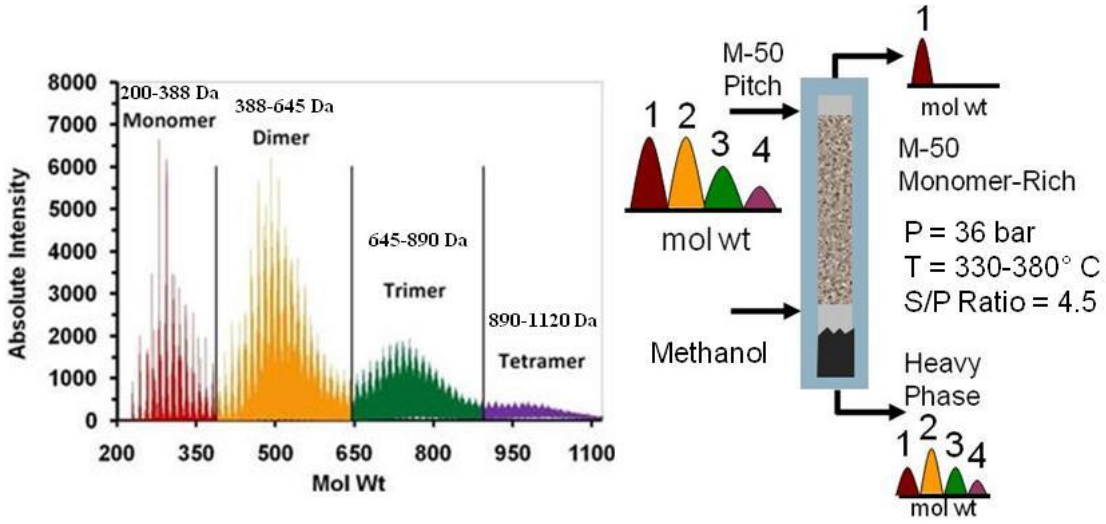

Figure 1.7. MALDI spectrum of M-50 pitch (left panel; adapted from Cervo and Thies[52]), and a schematic of the DGE process by which a narrow fraction rich in M-50 monomer is produced (right panel). A temperature gradient is imposed throughout the column such that the bottom section is at 330° C, the middle section at 350° C, and the top section at 380° C.

Preparatory-Scale (Prep-Scale) GPC

Another method that has been used to prepare pitch fractions for further analysis is prep-scale GPC. In 1980, Greinke and O'Connor[43] used prep-scale GPC to obtain calibration standards for the characterization of petroleum pitches by analytical-scale GPC (with the stationary phase being Styragel). The material fractionated was a polymerized isotropic petroleum pitch; the toluene-insoluble fraction was subjected to

reductive ethylation and then mixed with the toluene-soluble portion. This mixture was then fractionated using hot quinoline at 87°C as the GPC mobile phase. The average mol wt of each fraction was determined using VPO. Results indicated that there was a linear relationship between log mol wt and the retention volume of the collected fractions.

In 1990, Boenigk, Haenel, and Zander[54] fractionated a coal-tar pitch using prep-scale GPC, using pyridine at 60° C as the mobile phase. The stationary phase was Sephadex LH-20. Like Greinke, they used VPO to determine the mol wts for each of the fractions collected. They confirmed that the relationship between the log of the mol wt of the collected coal-tar pitch fractions and the retention volume is indeed linear at these operating conditions. Again, however, no information concerning the mol wt range of the collected fractions was given.

In 1998, Kandiyoti, Herod, and co-workers[55] fractionated a coal-tar pitch using prep-scale GPC. The stationary phase was 10 micron poly(divinylbenzene), and the mobile phase was unstabilized tetrahydrofuran (THF). Eluent fractions were collected at 1 minute intervals. MALDI analysis revealed that most of the species in the fractions containing the lightest species (i. e., below ~ 500 Da) fell within a range of 100-200 Da. Clearly, further analyses of chromatographic fractions of the pitch would have been necessary if one wished to obtain more definitive information on the types of species that exist within pitches.

Methods Previously Used for the Structural Characterization of PAHs and Carbonaceous Pitches

High-Performance Liquid Chromatography

In 1995, Fetzer and Kershaw[56] analyzed chromatographic fractions of a coal-tar pitch that were previously prepared using open-column liquid chromatography. For these analyses, high-performance liquid chromatography with UV-Vis/photodiode array detection (HPLC/PDA) was used. For the chromatographic separation, a Bakerbond C-18 reversed-phase PAH column was used. From this work, it was possible to unequivocally identify almost two dozen PAHs present in the pitch. Later, Somers and Wornat[57] used HPLC/PDA to identify the species present in the SC pyrolysis product of 1-methylnaphthalene (see Fig. 1.8). Even though many species were present in this complex mixture, it was possible to unequivocally identify dozens of PAHs present. In both of these studies, species were identified by matching the UV-Vis spectra of the eluent stream at a specific instant in time to those of known reference standards. For example, the close match of the UV-Vis spectrum for species A in Fig. 1.8, eluting at 40 min, with that of a reference standard, establishes the identity of species A as dibenzo[a,i]fluorene (see Fig. 1.9a). Species E is similarly identified as naphtho[2,1-a]pyrene (see Fig. 1.9b). This work and other efforts[58,59,60] have clearly established the usefulness of HPLC/PDA for both separating and unequivocally identifying mixtures of PAHs with mol wts < ~ 450.

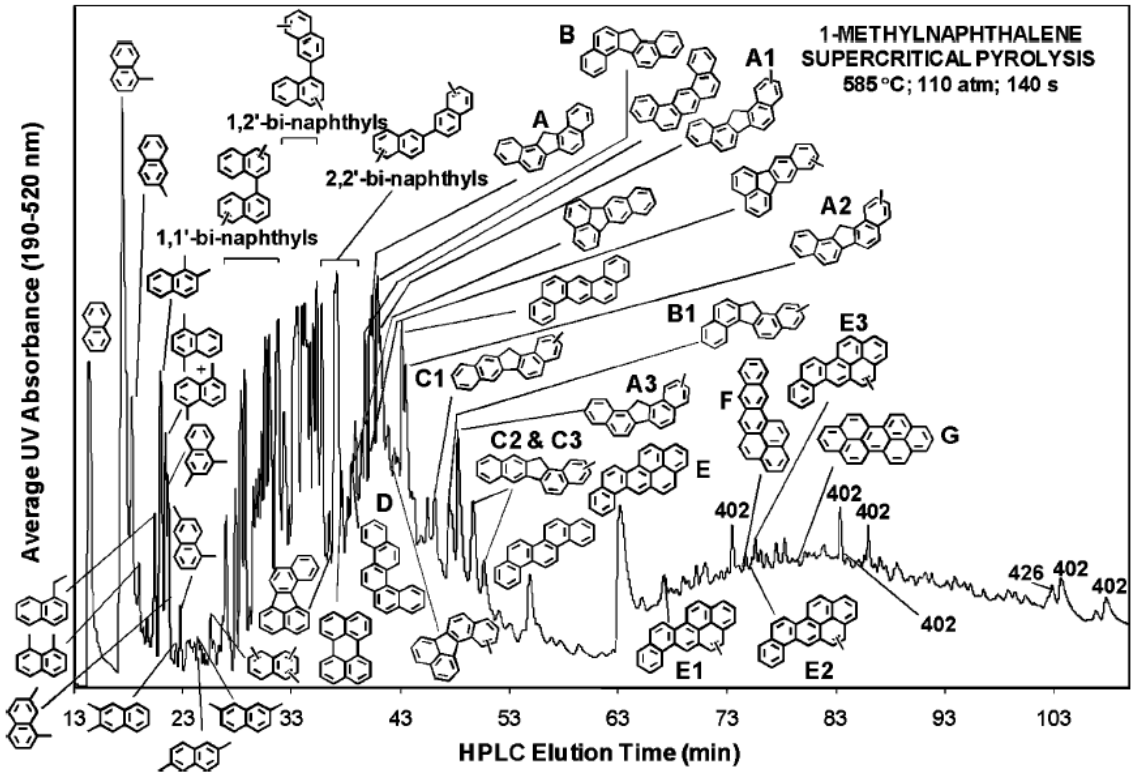

Figure 1.8. HPLC chromatogram, obtained by Somers and Wornat,[57] for the SC pyrolysis product of 1-methylnaphthalene. Reprinted with permission; copyright Taylor & Francis.

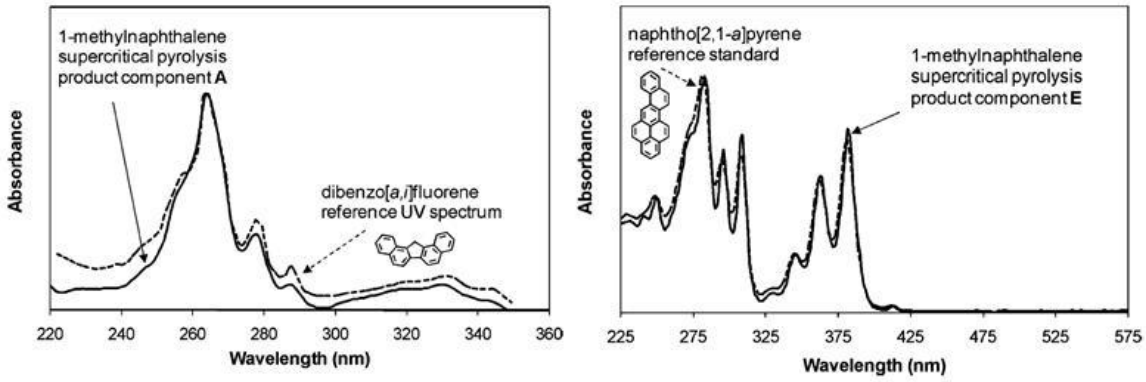

Figure 1.9. Comparison, by Somers and Wornat,[57] of the UV-Vis spectra obtained at HPLC elution times of 40 and 63 min unequivocally confirm that species A and E are dibenzo[a,i]fluorene and naphtho[2,1-a]pyrene, respectively. Reprinted with permission; copyright Taylor & Francis.

In 2007, Wang and Eser[61] analyzed FCC decant oils using a Shimadzu GC-17A gas chromatograph coupled to a QP-5000 mass spectrometer. FCC decant oils are particularly of interest to us because these materials are the precursors that are thermally polymerized at elevated temperatures to form petroleum pitch. Wang and Eser determined that naphthalene, phenanthrene, pyrene, chrysene, and alkylated derivatives of these compounds (possessing, at most, four methyl groups) were prominent species in the decant oils (see Fig. 1.10). However, because of poor peak resolution, it was not possible to identify heavier compounds present. Therefore, HPLC with mass spectrometer detectors in tandem (HPLC/MS/MS) was used for identification of these species (which included benzo[a]pyrene, benzo[e]pyrene, benzo[ghi]perylene, and alkylated derivatives thereof; see Fig. 1.10). A Finnigan mass spectrometry MAT TSQ 7000 triple-stage quadrupole instrument equipped with an atmospheric pressure chemical ionization source was used to obtain the mass spectra.

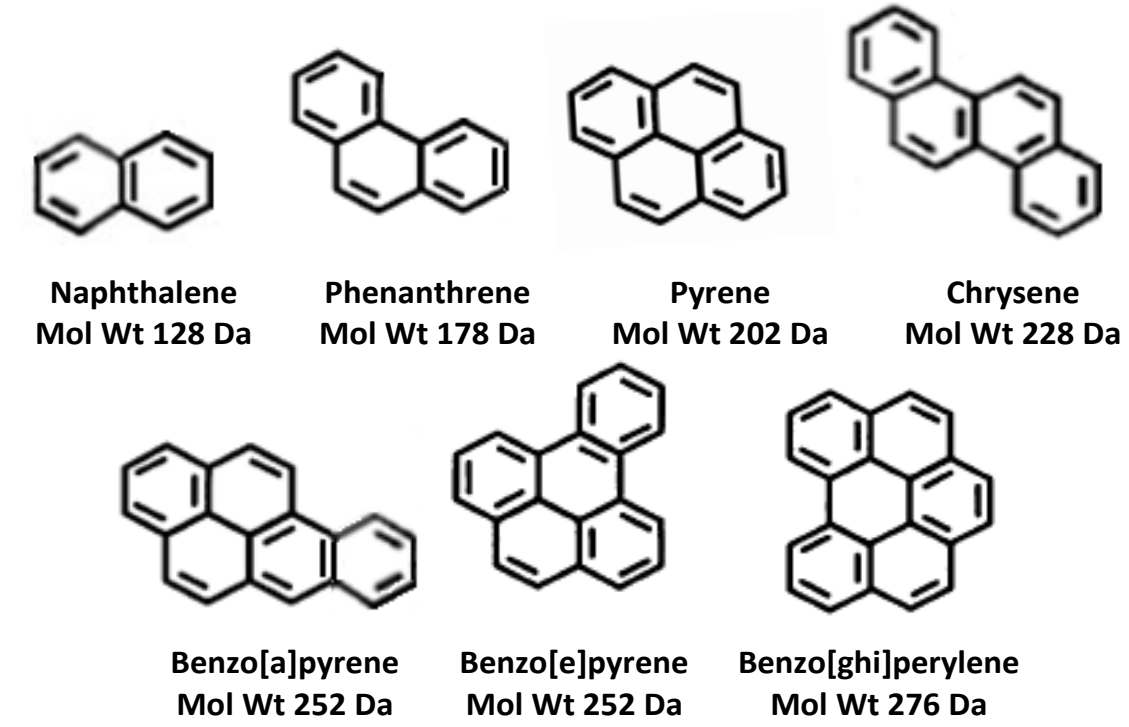

Figure 1.10. Molecular structures for the aromatic PAH backbones present in FCC decant oils analyzed by Wang and Eser.[61] The majority of the decant oil is comprised of alkylated derivatives of these species possessing up to 4 methyl groups.

Post-Source Decay (PSD)

Another technique that is useful for obtaining MS/MS information is post-source decay (PSD). This technique is available on many MALDI machines; it can be used to perform molecular fragmentation analyses on a specific ion (or ions) within a mixture. When ionization occurs, provided a sufficient laser power is applied, the energy absorbed by the molecule will be enough to bring about metastable fragmentation. Because the length of

the MALDI time-of-flight (TOF) tube is much greater than the length of the ion acceleration region immediately before the TOF tube, it can be assumed that the vast majority of molecular fragmentation occurs in the TOF tube. If fragmentation occurs in the TOF tube, the parent ion of a particular mol wt and all fragments derived from it travel at the same velocity, as no energy is lost in the fragmentation process.[62]

An ion gate consisting of alternating negative and positive voltages arranged in a Venetian blind sequence is used to allow only the ions of interest to reach the ion detector. When activated, ions approaching the gate are deflected toward the walls of the time-of-flight tube of the MALDI instrument, where they lose their charge. Only when the ion gate is deactivated are ions able to pass through it and reach the reflector, which is a voltage grid with the same polarity as the ions traveling through the TOF tube. The reflector deflects incident ions toward the detector. Therefore, the parent ion and all associated fragment ions, which were all bunched together in a tight packet upon reaching the reflector, are now separated according to mol wt. This separation occurs because the ions of different mol wt are accelerated by the reflector such that they possess equal kinetic energies. Thus, smaller ions are accelerated at higher velocities than the larger ones, which penetrate the reflector to a greater depth. At reflector voltages sufficient to reflect the heaviest fragments and the parent ion, it is not feasible to reflect the smaller and medium mol wt ions with enough accuracy so that they reach the detector. Therefore, in order to provide an accurate representation of the mol wt of each fragment, it is necessary to sum several spectra, each taken at a different reflector voltage, gradually stepping it down. At greatly reduced reflector voltage, smaller ions

can be focused on the detector with accuracy, while large ions have enough momentum to fully penetrate the reflector voltage grid[62] (and are therefore not reflected at all).

To illustrate the potential usefulness of PSD to our work, we consider as an example the 2007 work of Frache et al.[63] This group analyzed a mixture of diesel engine exhaust particles by performing MS analyses on product ions produced via the post-source decay of precursor ions produced by LDI-TOF-MS (that is, MALDI with no matrix). They used a Bruker Reflex IV MALDI-TOF mass spectrometer (Bruker Daltonics, Bremen, Germany). This instrument was equipped with a nitrogen laser (wavelength 337 nm).

Frache et al.[63] showed that PSD could be used to detect the presence of alkylation on PAHs. These PAHs included aromatics substituted with long alkyl chains (an example of such a compound is 6-n-butylchrysene; see Fig. 1.11a). PSD could also detect the presence of methylation if a compound (such as 1,4,6,7-tetramethylnaphthalene; see Fig. 1.11b) was substituted with multiple methyl groups. They also showed that the performance of PSD on non-alkylated PAHs yielded no fragment peaks.

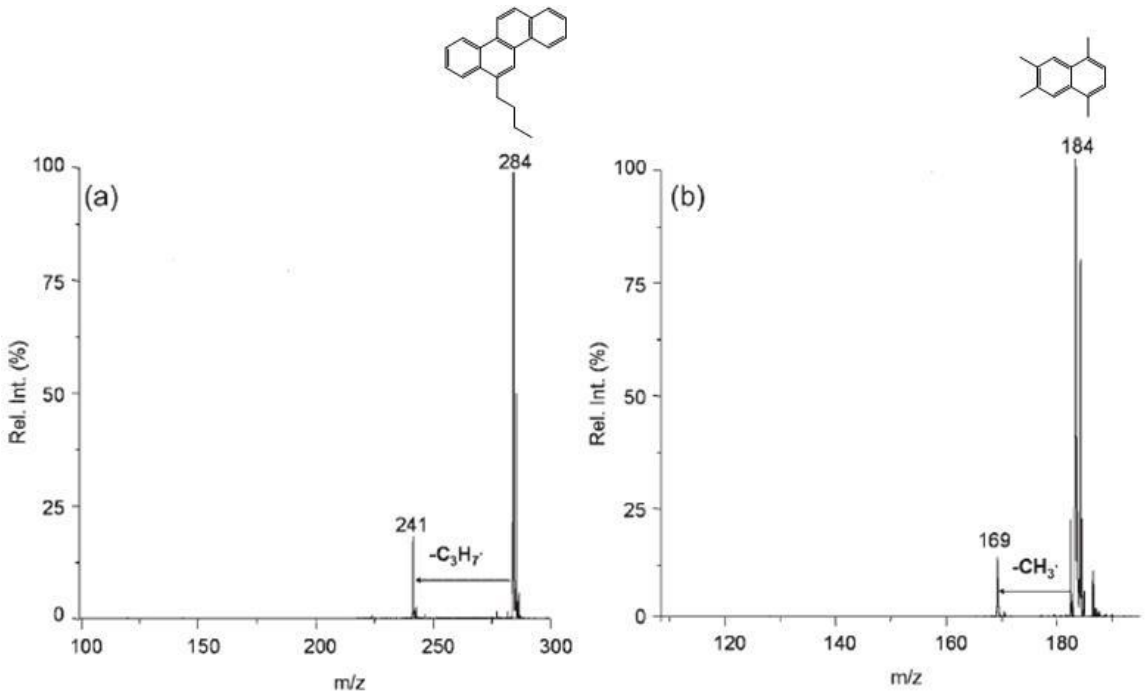

Figure 1.11. PSD spectra obtained by Frache et al.[63] for 6-n-butylmethylchrysene (panel a), and (1,4,6,7-tetramethylnaphthalene (panel b). Reprinted with permission; copyright John Wiley and Sons. The superimposed molecular structures have been generated by the author of this dissertation.

Goals of Dissertation

One of the long-term goals of the Carbon research group at Clemson University has been the development of a thermodynamic model that is reliable for the prediction of SC phase equilibria for pitch-solvent mixtures. It is also desired that this model have the capability to predict mesophase formation. Chapter 2 represents both a correction and an extension of the work of Zhuang, who (1) used SAFT to predict phase equilibria for pitch-solvent mixtures and (2) combined the orientational Helmholtz energy term of Humphries et al.[35,36,37] with SAFT theory to create a new equation of state, SAFT-liquid crystal (SAFT-LC). In this chapter, which has been previously published in slightly

modified form,[25] a detailed discussion of SAFT, Maier-Saupe theory, and Humphries et al.'s extension is given. The manner in which GPC and Gauss-Chebyshev quadrature were used to generate pitch PCs in discussed next. Then, by fitting the new equation of state (EoS) to both phase equilibrium and mesophase content data for a pitch-toluene system, we tested the ability of SAFT-LC to predict the formation of mesophase during extraction processes conducted at SC conditions.

The focus of Chapter 3 was on improving the method of predicting necessary inputs to the SAFT-LC model derived in the previous chapter. Specifically, the focus was on improving the method of determining feed pitch MWD, and the method of predicting the SAFT parameters for the PCs comprising said MWD. First, MALDI was used to estimate the MWD of the feed pitch. MALDI was chosen in favor of the methods used to determine the MWD in Chapter 2 because of the conclusion in Chapter 2 that the mol wts of the heaviest species were likely significantly overestimated. The MALDI spectrum for the feed pitch was resolved into 10 PCs; SAFT parameters for each PC were calculated using the correlations of Huang and Radosz, which were developed for bitumen. The EoS was fitted to the same phase equilibrium and mesophase content data as in Chapter 2, and comparisons were made. This chapter has been previously published[64] in slightly modified form.

It was shown that SAFT-LC does at least a fair job at predicting the formation of mesophase resulting from supercritical extraction processes. However, there still exist cases in which model predictions differ significantly from the trends observed experimentally. We concluded that the method of predicting SAFT parameters for the

PCs comprising the MWD of the feed pitch must be improved, which would require the knowledge of the molecular structure for each species comprising the MWD of the pitch.

The second phase of this work was to determine the actual molecular structures of the major components of the pitch, so as to obtain a definitive set of compounds that could be used as a starting point for future parameter determinations with the SAFT EoS. In Chapter 4, the major monomeric compounds present in M-50 pitch were determined. DGE was used to produce g-sized quantities of monomer-rich cuts of M-50 pitch. Prep-scale GPC was then used to separate pitches into narrower fractions of purities that are not obtainable using DGE. These cuts were then subjected to MALDI and PSD analyses, thus determining the mol wts and molecular structural information for the most prevalent monomer species. Selected cuts and fractions were also analyzed using HPLC/PDA to identify the major aromatic backbone species present in M-50 monomer. Using these analytical techniques, actual, rather than average, molecular structures are presented for the major components of M-50 petroleum pitch monomer.

In Chapter 5, additional clarifying discussions concerning the work conducted in Chapter 4 are given.

In Chapter 6, molecular structures for the higher oligomers comprising M-50 pitch were determined. As before, the sequence of DGE followed by prep-scale GPC was used to produce narrow oligomeric fractions of M-50 pitch. Prep-scale GPC was also used to fractionate a less polydisperse anthracene pitch produced by Conoco, Inc. These fractions were characterized using UV-Vis spectrophotometry to determine the

nature of the bonding between the monomer species comprising the major oligomers present. MALDI and PSD analyses were used to determine the mol wts and nature of the substituent groups present on these molecules, respectively. This information, along with the knowledge of reaction mechanism, and the most prevalent M-50 pitch monomer structures obtained in Chapter 4, was used to predict the dominant molecular structures present in the M-50 dimer, trimer, and tetramer.

In Chapter 7, additional clarifying discussions concerning the work conducted in Chapter 6 are given.

In Chapter 8, the conclusions from the work presented in this dissertation are presented. Recommendations are made concerning future work for the characterization of, and thermodynamic modeling of, petroleum pitches.

References

[1]Dickinson, E. M. Average Structures of Petroleum Pitch Fractions by $^{1}H/^{13}C$ N.M.R. Spectroscopy. *Fuel* **1985**, *64*, 704-706.

[2]Hutchenson, K. W.; Roebers, J. R.; Thies, M. C. Fractionation of Petroleum Pitch with Supercritical Toluene. *J. Supercrit. Fluids* **1991**, *4*, 7-14.

[3]Cristadoro, A.; Kulkarni, S. U.; Burgess, W. A.; Cervo, E. G.; Räder, H. J.; Müllen, K.; Bruce, D. A.; Thies, M. C. Structural Characterization of the Oligomeric Constituents of Petroleum Pitches. *Carbon* **2009**, *47*, 2358-2370.

[4]Kershaw J. R.; Black K. J. T. Structural Characterization of Coal-Tar and Petroleum Pitches. *Energy Fuels*, **1993**, *7(3)*, 420-25.

[5]Korai, Y.; Yoon, S.-H.; Oka, H.; Mochida, I.; Nakamura, T.; Kato, I.; Sakai, Y. The Properties of Co-Oligomerized Mesophase Pitch from Methylnaphthalene and Naphthalene Catalyzed by HF/BF_3. *Carbon* **1998**, *36(4)*, 369-375.

[6]Mochida, I.; Yoon, S.-H.; Korai, Y.; Kanno, K.; Sakai, Y.; Komatsu, M. Carbon Fibers from Aromatic Hydrocarbons. *CHEMTECH* **1995**, *25*, 29-37.

[7]Whelan, T. *Polymer Technology Dictionary*, 1st ed.; Chapman & Hall: London, 1994, p.78.

[8]MSDS for M-50 Pitch. http://www.mapllc.com/MSDS/0275MAR019.pdf

[9]Scaroni, A. W.; Jenkins, R. G.; Walker, P. L. Carbonization of Anthracene in a Batch Reactor. *Carbon* **1991**, *29(7)*, 969-980.

[10]Brooks, J. D.; Taylor, G. H. Formation of Graphitizing Carbons from the Liquid Phase. *Nature* **1965**, *206*, 697-699.

[11]Cervo, E. G.; Thies, M. C. Controlling the Oligomeric Composition of Carbon-Fiber Precursors by Dense-Gas Extraction. *J. Am. Ceram. Soc.* **2008**, *91*, 1416-1422.

[12]Lewis, I. C. Thermotropic Mesophase Pitch. *Carbon* **1978**, *16*, 503.

[13]Diefendorf, R. J.; Riggs, D. M. Forming Optically Anisotropic Pitches. U. S. Patent 4,208,267, June 17, 1980.

[14]Hurt, R. H.; Chen, Z. Y. Liquid Crystals and Carbon Materials. *Phys. Today* **2000**, *53(3)*, 39-44.

[15]*Introduction to Carbon Technologies*. Marsh, H., Heintz, E. A., Rodriguez-Reinoso, F., Eds.; University of Alicante Secretariado de Publicaciones: Alicante:Universidad, 1997.

[16]Beauharnois, M. E.; Edie, D. D.; Thies, M. C. Carbon Fibers from Mixtures of AR and Supercritically Extracted Mesophases. *Carbon*, **2001**, *39*, 2101-2111.

[17]Buckley, J. D.; Edie, D. D. Carbon-Carbon Matrix Materials. *Carbon-Carbon Materials and Composites;* Noyes Publications: Park Ridge, New Jersey, 1993; Chapter 5.

[18]Wobser, J. Marathon Petroleum Company LLC. Personal communication, 2010.

[19]Hutchenson, K. W.; Roebers, J. R.; Thies, M. C. Fractionation of Petroleum Pitch by Supercritical Fluid Extraction. *Carbon* **1991**, *29(2)*, 215-223.

[20]Alexander, G. L.; Schwarz, B. J.; Prausnitz, J. M. Phase Equilibria for High-Boiling Fossil-Fuel Distillates. 2. Correlation of Equation-of-State Constants with Characterization Data for Phase Equilibrium Calculations. *Ind. Eng. Chem. Fundam.* **1985**, *24*, 311-315.

[21]Schwarz, B. J.; Prausnitz, J. M. A Correlation for Thermodynamic Properties of Heavy Fossil-Fuel Fractions. *Ind. Eng. Chem. Res.* **1988**, *27*, 882-892.

[22]Hochgeschurtz, T.; Hutchenson, K. W.; Roebers, J. R.; Liu, G. Z.; Thies, M. C. Production of Mesophase Pitch by Supercritical Fluid Extraction. *ACS Symposium Series* **1993**, *514*, 347-362.

[23]Bolaños, G.; Liu, G. Z.; Hochgeschurtz, T.; Thies, M. C. Producing a Carbon Fiber Precursor by Supercritical Fluid Extraction. *Fluid Phase Equilib.* **1993**, *82*, 303-310.

[24]Dauché, F. M.; Bolaños, G.; Blasig, A.; Thies, M. C. Control of Mesophase Pitch Properties by Supercritical Fluid Extraction. *Carbon*, **1998**, *36*, 953-961.

[25]Burgess, W. A.; Zhuang, M. S.; Hu, Y.; Hurt, R. H.; Thies, M. C. SAFT-LC: An Equation of State for Predicting Liquid Crystalline Phase Behavior in Carbonaceous Pitches. *Ind. Eng. Chem. Res.* **2007**, *46*, 7018-7026.

[26]Zhuang, M. S.; Thies, M. C. Extraction of Petroleum Pitch with Supercritical Toluene: Experiment and Prediction. *Energy and Fuels* **2000**, *14*, 70-75.

[27]Pigott, R. T. Economic Analysis of a Supercritical Extraction Process for Producing Mesophase Pitch. M. S. Thesis. Clemson University, 2003.

[28]Huang, S. H.; Radosz, M. Equation of State for Small, Large, Polydisperse, and Associating Molecules. *Ind. Eng. Chem. Res.* **1990**, *29*, 2284-2294.

[29]Huang, S. H.; Radosz, M. Phase Behavior of Reservoir Fluids V: SAFT Model of CO_2 and Bitumen Systems. *Fluid Phase Equilibria* **1991**, *70*, 33-54.

[30]Bolaños, G. Production of Mesophase Pitch by Supercritical Fluid Extraction: A Study of the Region of Liquid-Liquid Equilibrium. Ph. D. dissertation, Clemson University, 1995.

[31]Carnahan, B.; Luther, H. A.; Wilkes, J. O. *Applied Numerical Methods*. John Wiley and Sons, Inc.: New York, 1969; pp 115-116.

[32]Maier, V. W.; Saupe, A. Eine Einfache Molekulare Theorie des Nematischen Kristallinflüssigen Zustandes. *Z. Naturforschg.* **1958**, *13a*, 564-566.

[33]Maier, V. W.; Saupe, A. Eine Einfache Molekular-Statistische Theorie der Nematischen Kristallinflüssigen Phase. Teil I. *Z. Naturforschg.* **1959**, *14a*, 882-889.

[34]Maier, V. W.; Saupe, A. Eine Einfache Molecular-Statistische Theorie der Nematischen Kristallinflüssigen Phase. Teil II. *Z. Naturforschg*. **1960**, *15a*, 287-292.

[35]Humphries, R. L.; James, P. G.; Luckhurst, G. R. A Molecular Field Treatment of Liquid Crystalline Mixtures. *Symp. Faraday Soc.* **1971**, *5*, 107-118.

[36]Humphries, R. L.; James, P. G.; Luckhurst, G. R. Molecular Field Treatment of Nematic Liquid Crystals. *J. Chem. Soc. Faraday Trans. II* **1972**, *68*, 1031-1044.

[37]Humphries, R. L.; Luckhurst, G. R. A Statistical Theory of Liquid Crystalline Mixtures: Phase Separation. *Proc. R. Soc. Lond., Ser. A* **1976**, *352*, 41-56.

[38]Dewar, M. J. S.; Goldberg, R. S. The Role of p-Phenylene Groups in Nematic Liquid Crystals. *J. Amer. Chem. Soc.* **1970**, *92*, 1582-1586.

[39]Shishido, M.; Inomata, H.; Arai, K.; Saito, S. Application of Liquid Crystal Theory to the Estimation of Mesophase Pitch Phase Transition Behavior. *Carbon* **1997**, *35*, 797-799.

[40]Mochida, I.; Korai, Y. *J. Fuel Soc. Japan*. **1985**, *64*, 796.

[41]Hurt, R. H.; Hu, Y. Thermodynamics of Carbonaceous Mesophase II. General Theory for Nonideal Solutions. *Carbon* **2001**, *39*, 887-896.

[42]Greinke, R. A.; Singer, L. S. Constitution of Co-Existing Phases in Mesophase Pitch During Heat Treatment: Mechanism of Mesophase Formation. *Carbon* **1988**, *26(5)*, 665-670.

[43]Greinke, R. A; O'Connor, L. H. Determination of Molecular Weight Distributions of Polymerized Petroleum Pitch by Gel Permeation Chromatography with Quinoline Eluent. *Anal. Chem.* **1980**, *52*, 1877-1881.

[44]Lewis, I. C.; Petro, B. A. Molecular Weight Analysis of Pitches and Polymeric Pitches by Gel Permeation Chromatography. *J. Polym. Sci., Polym. Chem. Ed.* **1976**, *14*, 1975-1985.

[45]Geiculescu, C. Preparation of Petroleum Pitch Pseudocomponents by Gel Permeation Chromatography. M. S. Thesis. Clemson University, 1994.

[46]Edwards, W. F.; Jin, L.; Thies, M. C. MALDI-TOF Mass Spectrometry; Obtaining Reliable Mass Spectra from Insoluble Carbonaceous Pitches. *Carbon* **2003**, *41*, 2761-2768.

[47]Edwards, W. F.; Thies, M. C. Fractionation of Pitches by Molecular Weight Using Continuous and Semibatch Dense-gas Extraction. *Carbon* **2006**, *44*, 243-252.

[48]Edwards, W. F.; Thies, M. C. Dense Gas Fractionation and MALDI Characterization of Carbonaceous Pitches. *Energy & Fuels* **2005**, *19*, 984-991.

[49]Cervo, E. G.; Thies, M. C. Control of the Molecular Weight Distribution of Petroleum Pitches via Dense-Gas Extraction. *Chem. Eng. Technol*. **2007**, *30*, 742-748.

[50]Kulkarni, S. U.; Thies, M. C. Solvent-based vs. Solvent-free MALDI-TOF-MS Sample Preparation Methods for the Quantitative Analysis of Petroleum Macromolecules. Preprints - American Chemical Society, Division of Petroleum Chemistry (2010), 55(1), 108-111.

[51]Zosel, K. Process for the Separation of Mixtures of Substances. US patent 3969196, 1976.

[52]Cervo, E. G.; Thies, M. C. Control of Molecular Weight Distribution of Petroleum Pitches via Multistage Supercritical Extraction. *J. Supercrit. Fluids*, **2010**, *51*, 345-52.

[53]Cervo, E. G.; Thies, M. C. Isolating Petroleum Pitch Oligomers by Continuous, Countercurrent Dense Gas Extraction. Submitted for publication to *J. Supercrit. Fluids*, 2010.

[54]Boenigk, W.; Haenel, M.; Zander, M. Structural Features and Mesophase Fraction of Coal-Tar Pitch Fractions Obtained by Preparative Size Exclusion Chromatography. *Fuel* **1990**, *69*, 1226-1232.

[55]Johnson, B. R.; Bartle, K.; Domin, M.; Herod, A. A.; Kandiyoti, R. Absolute Calibration of Size Exclusion Chromatography for Coal Derivatives Through MALDI-m.s. *Fuel* **1998**, *77*, 933-945.

[56]Fetzer, J. C.; Kershaw, J. R. Identification of Large Polycyclic Aromatic Hydrocarbons in a Coal Tar Pitch. *Fuel* **1995**, *74(10)*, 1533-36.

[57]Somers, M. L.; Wornat, M. J. UV Spectral Identification of Polycyclic Aromatic Hydrocarbon Products of Supercritical 1-Methylnaphthalene Pyrolysis. *Polycyclic Arom. Compd.* **2007**, *27*, 261-80.

[58]McClaine, J. W.; Oña, J. M.; Wornat, M. J. Identification of a New $C_{28}H_{14}$ Polycyclic Aromatic Hydrocarbon as a Product of Supercritical Fuel Pyrolysis: Tribenzo[cd,ghi,lm]perylene. *J. Chromatogr. A* **2007**, *1138*, 175-183.

[59]Fetzer, J. C. The Chemistry and Analysis of Large PAHs. *Polycyclic Arom. Compd.* **2007**, *27(2)*, 143-162.

[60]Oña, J. O.; Wornat, M. J. Identification of the $C_{30}H_{16}$ Polycyclic Aromatic Hydrocarbon Benzo[cd]naphtho[1,2,3-lm]perylene as a Product of the Supercritical Pyrolysis of a Synthetic Jet Fuel. *Polycyclic Arom. Compd*. **2007**, *27(3)*, 165-183.

[61]Wang, G.; Eser, S. Molecular Composition of the High-Boiling Components of Needle Coke Feedstocks and Mesophase Development. *Energy Fuels* **2007**, *21*, 3563-3572.

[62]Paul Kowalski, Bruker Daltonics. Personal communication.

[63]Frache, G.; Krier, G.; Müller, J.-F.; Manuelli, P. Post-Source Decay of Alkylated and Functionalized Polycyclic Aromatic Compounds. *Rapid Commun. Mass Spectrom.* **2007**, *21*, 2601-2607.

[64]Burgess, W. A.; Thies, M. C. SAFT-LC: Predicting Mesophase Formation from a Statistical Mechanics-Based Equation of State. *Fluid Phase Equilib.* **2007**, *261*, 320-326.

CHAPTER 2

SAFT–LC: AN EQUATION OF STATE FOR PREDICTING LIQUID CRYSTALLINE PHASE BEHAVIOR IN CARBONACEOUS PITCHES

Introduction

Carbonaceous pitches are obtained from the thermal polymerization of decant oil, a by-product of the fluid catalytic cracking (FCC) of a vacuum bottoms fraction of crude oil. They are oligomeric in nature and have a broad molecular weight (mol wt) distribution (MWD), ranging from about 250 to at least 2000 g/mol.[1,2] Pitches consist primarily of polycyclic aromatic hydrocarbons (PAHs), with both methyl and naphthenic substitution being abundant,[3,4] and can also be made from coal tar, or the thermal or catalytic polymerization of pure PAHs.[5]

Surprisingly, this complex mixture of molecules can exhibit liquid crystalline behavior, as first reported by Brooks and Taylor[6] in 1965. Furthermore, the formation of the discotic nematic mesophase is initiated by changes in either temperature or composition. Thus, these unusual materials have characteristics in common with both thermotropic and lyotropic liquid crystalline phases.[7-9]

Pitches are versatile materials that serve as precursors for a wide range of carbon products.[10] Depending on the final application, pitches with different phase behaviors, average molecular weights, and compositions are desired. For example, to produce high thermal conductivity carbon fibers, the starting pitch should be liquid crystalline and so should consist primarily of higher mol wt (>800-1000) molecules, which will spontaneously align upon melting to form the desired mesophase.[11] On the other hand, a

carbon-carbon composite may consist of an isotropic matrix phase into which a stronger, reinforcing material is dispersed.[12]

A more fundamental understanding of the relationship between pitch composition and phase behavior is of significant interest to researchers; thus, the development of thermodynamic models to describe the isotropic/mesophase transition is an important focus of our research program on carbonaceous pitches.

The first attempt to thermodynamically model the phase behavior of pitches was by Shishido et al.[13] In their work, the statistical theory of liquid crystalline mixtures, developed by Humphries et al.[14-16] as an extension to the pure-component liquid crystal theory of Maier and Saupe,[17-19] was used to predict the phase behavior obtained by mixing benzene-soluble and benzene-insoluble fractions of coal-tar pitch. The benzene-soluble fraction was modeled as a nonmesogenic (i.e., having no liquid-crystal-forming tendency) pseudocomponent, and the benzene-insoluble fraction as a mesogenic pseudocomponent. Because ideal solution behavior is assumed in the theory, the predicted phase split was caused entirely by orientational effects.

Hu and Hurt[20] were the first to propose a more general theory of phase behavior for carbonaceous pitches, taking into account both the orientational free energy (following Humphries et al.[14-16]) and nonideal solution behavior (using Flory-Huggins and regular solution theory[21]) that such systems exhibit. For pitch of a given MWD, their model contained two adjustable parameters, one based on the solubility parameters and another on the clearing temperatures of the pitch pseudocomponents.

Zhuang and Thies[22] used the SAFT equation version of Huang and Radosz[23-24] to describe the liquid–liquid phase split that occurs for solvent–pitch mixtures at supercritical solvent conditions. The mol wt of each pseudocomponent was used to determine pure-component parameters, and the binary interaction parameters were assumed to be well-behaved with respect to mol wt, as has been shown to be the case when SAFT is applied to other systems.[25]

With our interest in using supercritical extraction processes to produce both isotropic and mesophase pitch fractions of defined MWD[2,26-27], a versatile equation of state for modeling such systems is of significant interest. In this paper, we develop such an equation by adding the free energy of orientation term described above to the SAFT equation. We call this equation SAFT–liquid crystal (SAFT–LC). The efficacy of SAFT–LC was tested by using it to model both the extraction of pitch with supercritical toluene and the percent mesophase present in the dried, high mol wt extraction product. In addition, the ability of SAFT–LC to predict the experimentally observed property of high mol wt pitch fractions to dissolve large amounts of solvent, while still maintaining their liquid crystalline nature, was evaluated.

Development of SAFT–LC Equation

The SAFT Equation

The Statistical Associating Fluid Theory (SAFT) equation of state is discussed in detail elsewhere,[23-24,28] so only a brief synopsis is given here. The residual molar

Helmholtz free energy (A^{res}) in dimensionless form for a nonassociating fluid is described by SAFT as follows:

$$\frac{A^{res}}{RT} = \frac{A^{seg}}{RT} + \frac{A^{chain}}{RT} = m\left(\frac{A_0^{hs}}{RT} + \frac{A_0^{disp}}{RT} \right) + \frac{A^{chain}}{RT} \tag{2.1}$$

Here A^{seg}, A^{chain}, $A_0{}^{hs}$, and $A_0{}^{disp}$ are the segment, chain, segment hard sphere, and segment dispersion contributions to the residual free energy of the mixture. m is the average segment number of the mixture, weighted by the pure-component mole fractions:

$$m = \sum_i x_i m_i \tag{2.2}$$

The segment hard sphere term is given by[28]

$$\frac{A_0^{hs}}{RT} = \frac{6}{\pi\rho}\left[\frac{(\xi_2)^3 + 3\xi_1\xi_2\xi_3 - 3\xi_1\xi_2(\xi_3)^2}{\xi_3(1-\xi_3)^2} - \left[\xi_0 - \frac{(\xi_2)^3}{(\xi_3)^2} \right] \ln(1-\xi_3) \right] \tag{2.3}$$

where

$$\xi_0 = \left(\frac{\pi\rho}{6} \right) \sum_i x_i m_i \tag{2.4a}$$

$$\xi_1 = \left(\frac{\pi\rho}{6} \right) \sum_i x_i m_i d_{ii} \tag{2.4b}$$

$$\xi_2 = \left(\frac{\pi\rho}{6} \right) \sum_i x_i m_i (d_{ii})^2 \tag{2.4c}$$

$$\xi_3 = \left(\frac{\pi\rho}{6} \right) \sum_i x_i m_i (d_{ii})^3 \tag{2.4d}$$

and

$$d_{ii} = \sigma_i \left[1 - 0.12 \exp\left[\frac{-3u_i^o}{kT} \right] \right] \tag{2.5}$$

Here, ρ = number of molecules/Å^3, x_i = mole fraction, d_{ii} = temperature-dependent hard sphere diameter of component i, and u_i^o/k = temperature-independent energy parameter (in K) for component i. The temperature-independent hard sphere diameter σ_i is related to the temperature-independent segment volume parameter v_i^{oo} by[28]

$$\sigma_i = \left(\frac{10^{24} v_i^{oo} \sqrt{2}}{N_{Av}} \right)^{1/3} \tag{2.6}$$

where the units of v_i^{oo} are in cc/mol and those of σ_i are in Angstroms.

The contribution to A^{res} due to the formation of chains is given by[24,28]

$$\frac{A^{chain}}{RT} = \sum_i x_i (1 - m_i) \ln\left(g_{ii}(d_{ii})^{hs} \right) \tag{2.7}$$

where the pair correlation function $g_{ii}(d_{ii})$ for hard spheres is

$$g_{ii}(d_{ii})^{hs} = \frac{1}{1-\xi_3} + \frac{3d_{ii}}{2} \frac{\xi_2}{(1-\xi_3)^2} + 2\left[\frac{d_{ii}}{2} \right]^2 \frac{\xi_2^2}{(1-\xi_3)^3} \tag{2.8}$$

Finally, we define the dispersion contribution to A^{res} as[28]

$$\frac{A_0^{disp}}{RT} = \sum_{i=1}^{4} \sum_{j=1}^{9} D_{ij} \left[\frac{u}{kT} \right]^i \left[\frac{\xi_3}{\pi\sqrt{2}/6} \right]^j \tag{2.9}$$

The D_{ij} values are universal constants[28] and are defined by Chen and Kreglewski. Van der Waals one-fluid theory mixing rules are used to extend this equation to mixtures:

$$\frac{u}{kT} = \frac{\sum_{i=1}^{n}\sum_{j=1}^{n} x_i x_j m_i m_j \left[\frac{u_{ij}}{kT}\right] v_{ij}^{o}}{\sum_{i=1}^{n}\sum_{j=1}^{n} x_i x_j m_i m_j v_{ij}^{o}} \tag{2.10}$$

where

$$u_{ij} = (1 - k_{ij})(u_{ii} u_{jj})^{1/2} \tag{2.11}$$

and

$$u_{ii} = u_i^{o}\left(1 + \frac{10}{T}\right) \tag{2.12}$$

Also,

$$v_{ij}^{o} = \left[\frac{1}{2}\left[(v_i^{o})^{1/3} + (v_j^{o})^{1/3}\right]\right]^3 \tag{2.13}$$

and

$$v_i^{o} = v_i^{oo}\left[1 - 0.12\exp\left[\frac{-3u_i^{o}}{kT}\right]\right]^3 \tag{2.14}$$

A^{orient} term for SAFT–LC

A statistical treatment of nematic mesophase based on molecular field theory was first developed by Maier and Saupe (M-S).[17-19] Their theory is able to predict both the temperature dependence of molecular orientation and the nematic-isotropic phase transition. Humphries et al.[14-15] extended M-S theory to multicomponent mixtures, and their model forms the basis of our approach. As the theoretical development of A^{orient} is

reported elsewhere,[14-15,29] our discussion here is brief and focused on those aspects most relevant to application to our work with carbonaceous pitches.

For a multicomponent mixture, the orientational internal energy for a molecule of component i is given by

$$U_i = \sum_{j=1}^{n} x_j \varepsilon_{ij} \bar{P}_j P_i \tag{2.15}$$

Here, x_j is the mole fraction of component j (which includes i), and ε_{ij} is the energy interaction parameter for the anisotropic potential between two molecules i and j. P_i is the order parameter describing orientational order of the molecule i and is defined using the second Legendre polynomial:

$$P_i = \frac{3}{2}\cos^2\theta_i - \frac{1}{2}, \tag{2.16}$$

where θ_i is the angle between the axis of molecular symmetry (this is the short axis that runs through the center of a disc-like molecule) and the director $\hat{\mathbf{n}}$. In a discotic mesophase, the short axes of the molecules preferentially align themselves along a single direction, which is called the director (see Fig. 2.1). $\bar{P}_j$ is the ensemble average order parameter for the species j. Note that for the isotropic phase, $\bar{P}_j$ is zero, as the molecular axes point in all directions with equal probability. For typical liquid crystalline material, $\bar{P}_j$ decreases as the temperature is increased and ranges in value from 0.3 to 0.8.[29]

For mixtures containing components that differ significantly in size (and thus, molar volumes), Humphries and Luckhurst[30] extended M-S theory to obtain the following expression for the energy parameter ε_{ij}:

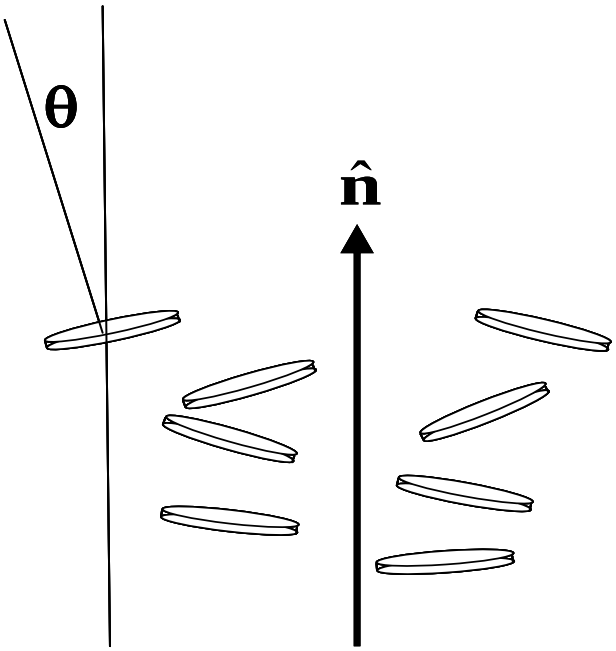

Figure 2.1. In a nematic discotic mesophase, the molecules tend to align themselves along a director, denoted by the vector $\hat{\mathbf{n}}$. Θ is the angle between the axis of molecular symmetry and $\hat{\mathbf{n}}$.

$$\varepsilon_{ij} = \frac{\tilde{\varepsilon}_{ij}\sqrt{V_i V_j}}{\sum_{k=1}^{n} x_k V_k} \tag{2.17}$$

where V_k is the liquid molar volume of component k and $\tilde{\varepsilon}_{ij}$ is the composition-independent energy parameter:

$$\tilde{\varepsilon}_{ij} = -4.542k\sqrt{T_{cl_i} T_{cl_j}} \tag{2.18}$$

We wish to point out that the volume dependence of ε_{ij} is not well-established,[29] so the above form was chosen because it was successful in fitting experimental clearing

temperatures for binary mixtures of nematogens[30] (i.e., mesogens). The clearing temperature T_{cl_i} is the temperature of the phase transition between the liquid crystalline and the isotropic (i.e., the "clear") state. Note that Equation 2.18 from M-S theory provides the key link between the molecular and macroscopic states.

The probability Pr_i of a molecule i in the mixture being oriented at an angle θ_i from the director $\hat{\mathbf{n}}$ is assumed to be represented by the Boltzmann distribution

$$Pr_i = \frac{\exp\left[-\frac{U_i}{kT}\right]}{Z_i} = \frac{\exp\left[-\frac{U_i}{kT}\right]}{\sum_{i=1}^{n}\exp\left[-\frac{U_i}{kT}\right]}, \tag{2.19}$$

where the orientational partition function Z_i is given by (using integration over spherical space instead of summation)

$$Z_i = \int_0^{\pi}\exp\left[-\frac{U_i}{kT}\right]\sin\theta_i d\theta_i \int_0^{2\pi} d\varphi = 2\pi\int_0^{\pi}\exp\left[-\frac{1}{kT}\sum_{j=1}^{n} x_j \varepsilon_{ij}\bar{P}_j P_i\right]\sin\theta_i d\theta_i, \tag{2.20}$$

and $\bar{P}_j$, the ensemble average order parameter, is calculated from

$$\bar{P}_j = \int_0^{\pi} P_j Pr_j \sin\theta_j d\theta_j \int_0^{2\pi} d\varphi = \frac{2\pi\int_0^{\pi} P_j \exp\left[-\frac{1}{kT}\sum_{i=1}^{n} x_i \varepsilon_{ij}\bar{P}_i P_j\right]\sin\theta_j d\theta_j}{Z_j} \tag{2.21}$$

Now the ensemble average internal energy of a single molecule of species i $\langle U_i \rangle$ is calculated from the expression

$$\langle U_i \rangle = \int_0^{\pi} U_i Pr_i \sin\theta_i d\theta_i \int_0^{2\pi} d\phi \tag{2.22}$$

to obtain

$$\langle U_i \rangle = \sum_{j=1}^{n} x_j \varepsilon_{ij} \bar{P}_j \bar{P}_i \tag{2.23}$$

Finally, the total orientational molar internal energy U is obtained by summing over i molecules, multiplying by N, Avogadro's number of molecules, and then dividing by 2 so that we count only pairs of molecules:[14]

$$U=U^{orient} = \frac{N}{2} \sum_{i=1}^{n} \sum_{j=1}^{n} x_i x_j \varepsilon_{ij} \bar{P}_j \bar{P}_i \tag{2.24}$$

To determine the entropy of the system, we begin with the entropy of a single molecule of component i in the mixture:[31]

$$S_i = \frac{\langle U_i \rangle}{T} + k \ln Z_i = \frac{1}{T} \sum_{j=1}^{n} x_j \varepsilon_{ij} \bar{P}_j \bar{P}_i + k \ln Z_i \tag{2.25}$$

Summing over all i components and multiplying by N, we obtain the total orientational molar entropy:

$$S=S^{orient} = \frac{N}{T} \sum_{i=1}^{n} \sum_{j=1}^{n} x_i x_j \varepsilon_{ij} \bar{P}_j \bar{P}_i + Nk \sum_{i=1}^{n} x_i \ln Z_i \tag{2.26}$$

Finally, the overall Helmholtz orientational molar free energy is given by

$$A = A^{orient} = U^{orient} - TS^{orient} = -\frac{N}{2} \sum_{i=1}^{n} \sum_{j=1}^{n} x_i x_j \varepsilon_{ij} \bar{P}_j \bar{P}_i - NkT \sum_{i=1}^{n} x_i \ln Z_i \tag{2.27}$$

Details of calculating the order parameters, partition functions, and A^{orient} are given elsewhere.[32]

Finally, this A^{orient} term is added to the SAFT terms from Equation 2.1 to obtain the desired SAFT–LC equation:

$$\frac{A^{res}}{RT} = m\left(\frac{A_0^{hs}}{RT} + \frac{A_0^{disp}}{RT}\right) + \frac{A^{chain}}{RT} + \frac{A^{orient}}{RT} \qquad (2.28)$$

Application of SAFT–LC to Carbonaceous Oligomeric Pitches

For a complex mixture such as pitch, pseudocomponents must be defined for use in an equation of state. The approach taken here was to generate pseudocomponents mathematically from a measured MWD for the pitch of interest. Specifically, gel permeation chromatography (GPC) was used to determine the MWD of a heat-soaked, isotropic petroleum pitch obtained from Conoco Inc. and fluxed with hot toluene to remove the insolubles.[22] (This pitch is very similar to the A-240 brand of pitch commercially sold by Ashland Oil for many years.) The GPC data were then normalized (so that the area under the curve summed to one) and fit to the sum of three normal distribution functions (NDFs). Numerical integration by 9-point Gauss-Chebyshev (G-C) quadrature[33] was then applied to each of the NDFs (fewer quadrature points are inadequate for fitting a NDF). Each of the 9 quadrature points defined a pitch pseudocomponent, whose mass fraction was determined by multiplying the value of the normal distribution function at the quadrature point by the appropriate G-C weighting factor. Quadrature points 1 and 9 were discarded because their mass fractions were negligible (i.e., on the order of 10^{-5} each), giving us 7 pseudocomponents per NDF, for a total of 21 pseudocomponents. Finally, the mol wts of the pseudocomponents were obtained from a GPC calibration curve of mol wt as a function of retention time. Details of the procedure are given elsewhere.[34] The normalized GPC data, the three NDFs, and the overall curve created by summing the distributions are given in Fig. 2.2. Note that a

good fit to the original GPC data is obtained with the summed curve. Parameters for each of the normal distributions, along with the mass fractions and mol wts of each of the 21 quadrature-generated pseudocomponents, are given in Table 2.1.

For each pitch pseudocomponent, several pure-component parameters had to be determined in SAFT–LC. The SAFT-based parameters v^{oo}, m, and u_i^o/k were estimated from correlations developed by Huang and Radosz[35] for bitumen components of varying aromaticity. Necessary inputs to the correlations were the C/H atomic ratio and the molecular weight. Because no other information was available, we initially assumed that all pseudocomponents had the same C/H ratio as was experimentally measured for the parent Conoco pitch. For any defined components used in combination with the pitch (e.g., solvents), literature values for the pure-component SAFT parameters were used.[23]

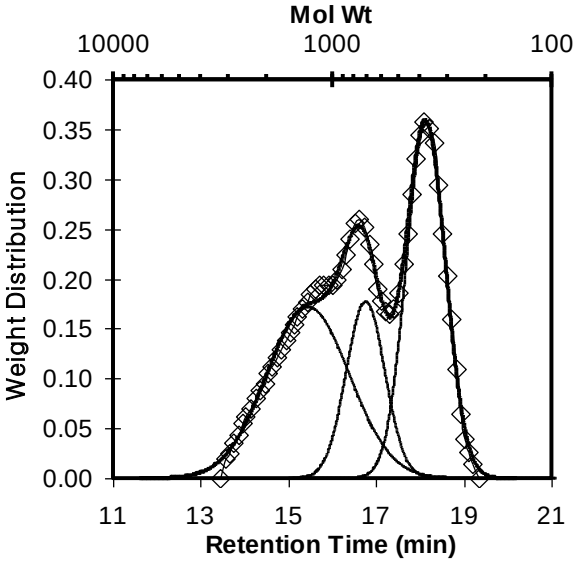

Figure 2.2. GPC chromatogram of Conoco petroleum pitch and the 3 fitting NDFs used to generate the quadrature points (i.e., pseudocomponents): GPC data (◊); NDFs (—); Overall curve (—). Mol wts are given by the calibration equation $\log_{10}$ MW = 6.13394 – 0.19659*(ret. time).

Table 2.1. Quadrature-Generated Pseudocomponents for Modeling MWD of Conoco Petroleum Pitch

Pseudocomponent No.	GPC Retention Time (min)	Molecular Weight	Mass Fraction
	NDF 1 (μ = 15.45, σ = 0.942, ω = 0.4049)[a]		
1	12.19	5476	0.0003
2	13.03	3741	0.0063
3	14.16	2239	0.0831
4	15.45	1249	0.2256
5	16.74	697	0.0831
6	17.87	417	0.0063
7	18.71	285	0.0003
	NDF 2 (μ = 16.72, σ = 0.448, ω = 0.1986)		
8	15.17	1418	0.0001
9	15.57	1183	0.0031
10	16.11	927	0.0408
11	16.72	703	0.1105
12	17.33	533	0.0408
13	17.87	418	0.0031
14	18.27	349	0.0001
	NDF 3 (μ = 18.14, σ = 0.4455, ω = 0.3965)		
15	16.60	743	0.0003
16	17.00	620	0.0062
17	17.53	487	0.0815
18	18.14	370	0.2205
19	18.75	281	0.0815
20	19.28	220	0.0062
21	19.68	184	0.0003

[a] μ = NDF mean; σ = NDF standard deviation; ω = NDF mass fraction.

The "LC-based" pure-component parameters consisted of the parameters *a* and *b* and the liquid molar volumes V_k. Based on physically realistic assumptions,[20,36] we assumed the following linear relationship between mol wt and clearing temperature (°C) for the pitch pseudocomponents:

$$T_{cl,i} = a + b * MW_i \tag{2.29}$$

Here, $T_{cl,i}$ is the clearing temperature and MW_i is the mol wt of pseudocomponent i. Thus, the adjustable pure-component parameters *a* and *b* characterize the mesophase-forming tendency of a given pitch pseudocomponent. The liquid molar volumes V_k in the A^{orient} term were assumed to be constant and were calculated by dividing the mol wt of each pseudocomponent by the liquid mass density (1.20 g/cc) of A-240 pitch.[37] Solvent molar volumes were fixed to their literature values at the normal boiling point. With these assumptions, we note that A^{orient} is independent of fluid density, but knowledge of the density dependence of the molecular interaction term ε_{ij} is not understood well enough to make alternative assumptions.[29]

In addition to *a* and *b*, SAFT–LC contains three adjustable parameters, A, B, and C, which are needed to calculate the binary interaction parameters (these fitting parameters are used as a correction to the geometric mean combining rule for the cross dispersion energy parameter u_{ij} as indicated in Equation 2.11) between pitch pseudocomponents, and between pitch pseudocomponents and solvent. Following the previous approach of Thies and co-workers,[22] we assumed that the interaction parameters between the solvent and pitch pseudocomponents were linear with respect to mol wt:

$$k_{1,j} = A*MW_j + B \tag{2.30}$$

where

$k_{1,j}$ = interaction parameter between the solvent (1) and the jth pseudocomponent,
MW_j = mol wt of the jth pseudocomponent,
A, B = adjustable parameters.

The interaction between pitch components was computed using the following expression:

$$k_{i,j} = C|MW_i - MW_j| \tag{2.31}$$

where

$k_{i,j}$ = interaction parameter between pseudocomponents i and j,
MW_i = molecular weight of the ith pseudocomponent,
C = adjustable parameter.

SAFT–LC for the Solvent Extraction of Carbonaceous Pitches

We test the efficacy of SAFT–LC by using it to model the solvent extraction of carbonaceous pitches. Such processes have been used both commercially[8,38-39] and on a laboratory scale[11,26] to produce mesophase pitch. A simplified schematic of a near critical/supercritical extraction process used at Clemson that is representative of such processes is shown in Fig. 2.3. The process is initiated by combining an isotropic feed pitch (e.g., Conoco or A-240 petroleum pitch) with the solvent of interest and allowing the mixture to come to equilibrium. At temperatures, pressures, and solvent-to-pitch (S/P) ratios corresponding to those shown in the figure, two phases form in the phase separator: a top, solvent-rich fluid phase and a bottom, pitch-rich liquid phase. The pitch components distribute between the two phases, with lower mol wt species being concentrated in the top and higher mol wt pitch components in the bottom phase. The

bottom phase is then dried to remove the solvent, and the remaining pitch fraction is the desired product, which can consist of anywhere from 0 to 100% mesophase.

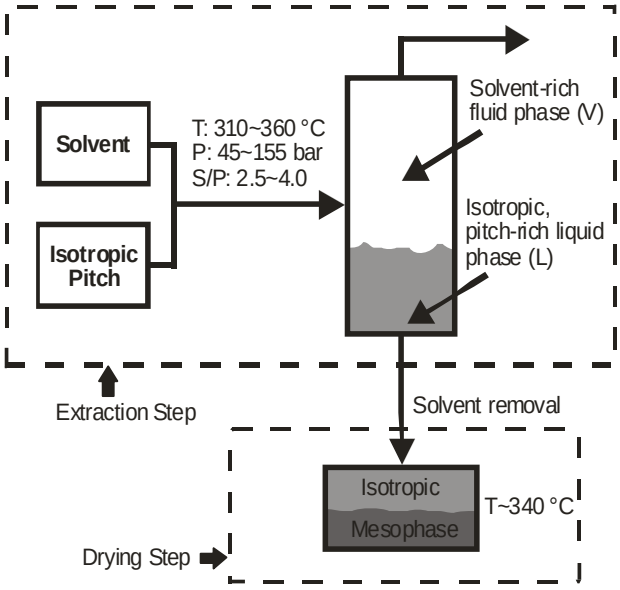

Figure 2.3. The process for producing mesophase pitch by supercritical extraction consists of an extraction step and a drying step.

We were interested in the use of SAFT–LC to model both steps of the process, that is, the extraction step and the drying step. For the extraction step in Fig. 2.3, a two-phase flash calculation incorporating the so-called "negative flash algorithm" [32,40] was used. By allowing phase fractions (e.g, V/F) to be less than 0, convergence of phase equilibrium calculations is enhanced with this algorithm. Input consisted of the pseudocomponent compositions of the feed pitch (i.e., the Conoco pitch given in Table 2.1), the S/P ratio, and the temperature and pressure of the phase separator. All K-values were calculated via SAFT–LC. Integration to determine the order parameter $\overline{P}_j$ in the A^{orient} term (see Equation 2.21) was accomplished numerically using 10,000 segment slices. A converged

solution for $\bar{P}_j$ was readily obtained by successive substitution using an initial guess of 0.6. Output from the flash calculation consisted of the amounts, compositions, and densities of the V and L phases.

For the drying-step calculation (see Fig. 2.3), the solvent toluene is removed from the pitch-rich liquid phase isolated in the extraction step (i.e., L), and a two-phase "negative flash" is performed on the overall composition of the "dried" pitch mixture to determine mesophase content. This flash calculation was performed at 340 °C and 50 bar, as these conditions are representative of those at which mesophase pitch is processed (e.g., melt-spun into nonstabilized carbon fibers[11]).

All calculations involving SAFT-LC were performed using a computer program written in the Visual FORTRAN programming language. In this program, a parameterized version of the SAFT equation is used in order to keep the size of the program at a minimum; Huang and Radosz discuss it in depth in the Appendix of their 1991 paper.[24]

Results and Discussion

SAFT–LC for Prediction of Solvent Extraction and Drying Steps

Dauche et al.[26] investigated supercritical extraction with toluene (T_c = 591.8 K, P_c = 41.1 bar) for the single-stage fractionation of carbonaceous pitches, using the process illustrated in Fig. 2.3. In particular, top-phase (V) and bottom-phase (L) solvent compositions were measured for 17 different combinations of temperature, pressure, and S/P ratio, see Table 2.2. Following the solvent extraction process, Dauche et al.[26] dried

the bottom L phase under vacuum at 340 °C to remove the solvent, and then determined the softening point (a simple melting-point test) and the percent mesophase by polarized light microscopy (see Table 2.2).

We used SAFT–LC for both the correlation and prediction of Dauche et al.'s results. For correlation, Extraction Runs 1-8 in Table 2.2 were used, as they all contained less than 100% mesophase in the dried bottom-phase samples, and thus were the most useful ones for fitting. These runs were used to fit the adjustable SAFT–LC parameters

Table 2.2. Experimental, correlated, and predicted solvent compositions and mesophase contents for extraction of Conoco petroleum pitch with supercritical toluene (also see Fig. 2.3).

	Operating Variables	Toluene Mass Fraction--Extraction Step				Dried Bottom Phase		
Extract Run No.	Press/Temp S/P Ratio	Top Phase (V)		Bottom Phase (L)		Softening Point (°C)	Percent Mesophase	
		Expt.	Correl.	Expt.	Correl.	Expt.	Expt.	Correl.
1	46/320/2.5	0.784	0.750	0.258	0.301	203	38	29.0
2	45/310/3.0	0.792	0.780	0.222	0.268	210	50	51.2
3	81/360/2.5	0.785	0.733	0.254	0.305	212	38	56.6
4	46/320/3.5	0.844	0.805	0.239	0.272	214	44	53.7
5	81/360/3.5	0.847	0.796	0.227	0.284	228	59	76.4
6	45/310/4.0	0.836	0.823	0.216	0.244	231	85	73.4
7	84/340/3.0	0.801	0.767	0.230	0.256	234	98	91.2
8	77/330/3.0	0.785	0.769	0.218	0.250	236	95	88.8
		Expt.	Predicted	Expt.	Predicted	Expt.	Expt.	Predicted
9	94/320/2.5	0.738	0.734	0.245	0.240	238	100	91.8
10	77/330/4.0	0.831	0.816	0.201	0.235	262	100	100
11	94/320/3.5	0.820	0.795	0.221	0.228	269	100	100
12	94/310/3.0	0.771	0.771	0.214	0.229	272	100	94.5
13	154/360/2.5	0.741	0.722	0.232	0.246	274	100	100
14	94/310/4.0	0.821	0.817	0.184	0.217	284	100	100
15	155/330/3.0	0.764	0.766	0.173	0.232	298	100	100
16	155/330/4.0	0.814	0.814	0.171	0.223	306	100	100
17	154/360/3.5	0.804	0.787	0.184	0.247	319	100	100

(i.e., A, B, C; *a* and *b*) by minimizing an objective function consisting of the sum of the squares of (1) the experimental minus calculated toluene mass fractions in the top and

bottom phases and (2) the experimental minus calculated mesophase fractions in the dried bottom phases. In addition, a weighting factor of 0.5 was assigned to the deviation in mesophase fractions so that its contribution to the objective function would be approximately the same as the deviation in mole fraction. A downhill simplex method was used for the minimization.[41] Some constraints were set to these adjustable parameters. In particular, we assumed that the resulting $k_{1,j}$'s and $k_{i,j}$'s would be in-line with our previous work[22] and with what has been observed by previous workers.[35] Furthermore, the values of *a* and *b* were constrained to physically realistic ranges.[36] The optimized fitting parameters obtained were A = 2.42E-05, B = 7.00E-02, C = 1.21E-05, *a* = 99.2K, and *b* = 0.350. These values, when input into eqs. 30 and 31, yield binary interaction parameters ranging from <0.01 to 0.20. From Equation 2.29, the clearing temperature for a pseudocomponent of mol wt 500 is predicted to be approximately 0 °C. This is on the low side of estimates obtained from theory, but still consistent with previous work.[36]

The correlations developed by Huang and Radosz[35] for estimating the pure-component SAFT parameters v^{oo}, m, and u_i^o/k yielded significantly better results when we allowed the C/H ratio to deviate from the experimentally measured value for Conoco pitch. In particular, a C/H ratio of 0.71 for all pseudocomponents was found to provide the best fit to the experimental data – a significant deviation from the experimentally measured value of 1.5 for A-240 (or Conoco) pitch.[3,4] We note that Huang and Radosz's correlations were developed from cuts of bitumen, with their C/H ratios ranging from 0.55 to 0.72, whereas fractions of A-240 (or Conoco) pitch can have C/H ratios that vary

from 1.2 to 1.8.[2] In retrospect, one could not have expected "bitumen" correlations to have performed well, when used so far out of their experimentally determined range.

The above parameters were then used to predict (not fit) the solvent compositions and mesophase percentages in the dried bottom phase L for Extraction Runs 9-17 (see Table 2.2). Comparing the correlated to the predicted toluene mass fractions, we see that the SAFT–LC parameters behave "globally", as the predicted results (Runs 9-17) are of comparable accuracy to those obtained by correlation (Runs 1-8). For the percent mesophase calculations, the correlated values (Runs 1-8) are generally within 15 wt % of the experimentally measured values, which is in-line with the typical experimental accuracy for this measurement.[26] For Runs 9-17, SAFT–LC correctly predicts the experimentally measured values of 100% mesophase for all but Runs 9 and 12.

Phase amounts, phase densities, and pseudocomponent compositions are shown for two representative cases of solvent extraction, Runs 4 and 11, in Tables 2.3 and 2.4. In addition, the impact of the extraction process on the distribution of pseudocomponents (PCs) in each phase is shown in Figs. 2.4 and 2.5. These results indicate several interesting trends. First, SAFT–LC predictions for the density of the toluene-dominated vapor phase are in agreement with experimentally observed values for pure toluene[42] at the conditions given in Table 2.2. Because the SAFT parameters for toluene, and the heavier PAHs phenanthrene and anthracene (the latter two compounds have mol wt 178) fit experimental liquid density data (from conditions ranging from ambient to near-critical) to better than 3% difference,[23] liquid phase density predictions for the pitch-dominated bottom phase are also expected to be reasonable. Second, the predicted yields

of pitch (i.e., the percentage of the feed pitch) in the bottom phase L of 17% for Run 4 and 11% for Run 11 are in good agreement with the 10-20% typically obtained when mesophases are produced in the laboratory.[26]

Table 2.3. Phase amounts, densities, and pseudocomponent compositions as predicted by SAFT–LC for Extraction Run No. 4 (see Table 2.2).[a]

Run 4 (P = 46 bar, T = 320° C, S/P = 3.5)

		V = 0.948	L = 0.0523
		ρ_{pred} = 0.503 g/cc	ρ_{pred} = 0.685 g/cc
PC Number	Mol Wt	Mass Fraction	Mass Fraction
Solvent	92.1	0.805	0.272
1	5476	3.16E-10	1.18E-03
2	3741	2.17E-06	2.68E-02
3	2239	0.002	0.313
4	1249	0.041	0.218
5	697	1.81E-02	2.55E-02
6	417	1.41E-03	1.25E-03
7	285	6.25E-05	4.63E-05
8	1418	2.23E-05	1.86E-04
9	1183	5.90E-04	2.60E-03
10	927	8.70E-03	1.98E-02
11	703	2.40E-02	3.43E-02
12	533	9.26E-03	9.81E-03
13	418	6.99E-04	6.21E-04
14	349	3.11E-05	2.51E-05
15	743	5.98E-05	9.22E-05
16	620	1.37E-03	1.68E-03
17	487	1.81E-02	1.79E-02
18	370	4.94E-02	4.10E-02
19	281	1.84E-02	1.35E-02
20	220	1.41E-03	9.67E-04
21	184	6.26E-05	4.14E-05

[a] Phase amounts V and L are reported on a mass basis.

As discussed in the introduction, a goal of pitch extraction processes is the concentration of higher mol wt pitch molecules (i.e., mesogens) that can form mesophase. In Fig. 2.4, the PC distribution of the feed pitch F is compared with those of the products V and L. Here, we see that the shift to higher mol wts in the distribution for L is

significant – significant enough to result in the experimentally observed (and predicted) formation of ~50% mesophase when the phase is dried to remove the solvent. In Fig. 2.5, we see that the more aggressive extraction conditions of Run 11 produce an L phase that is significantly enriched in the higher mol wt pseudocomponents relative to Run 4, resulting in a dried L phase that contains 100% mesophase.

Finally, we note that when a three-phase flash was carried out on the extraction step shown in Fig. 2.3, the presence of a mesomorphic third phase was predicted for some of the runs (e.g., Run 11). This mesophase typically was found to consist of about 7 wt % toluene, with the PC composition consisting of more than 90 mass % PC 2 (mol wt = 3741). The predicted amount of this third phase was always less than 0.01 mass fraction. As can be seen in Fig. 2.2, the GPC curve stops at a retention time of ~13.4 min, which corresponds to a mol wt of 3160. Thus, the existence of PC 2 was caused by application of the NDF/quadrature method to the experimental GPC data. Because (1) we had no experimental evidence supporting the existence of this *in situ* mesophase, (2) its predicted amount was so small, and (3) the phase disappeared if PCs 1 and 2 were eliminated from the pitch, we used the two-phase flash described earlier for all extraction-step calculations (see Fig. 2.3) and thus did not take into account the presence of this third phase.

Table 2.4. Phase amounts, densities, and pseudocomponent compositions as predicted by SAFT–LC for Extraction Run No. 11 (see Table 2.2).[a]

Run 11 (P = 94 bar, T = 320° C, S/P = 3.5)

		V = 0.968	L = 0.0316
		ρ_{pred} = 0.552 g/cc	ρ_{pred} = 0.721 g/cc
PC Number	Mol Wt	Mass Fraction	Mass Fraction
Solvent	92.1	0.795	0.228
1	5476	3.96E-11	1.95E-03
2	3741	1.42E-06	4.44E-02
3	2239	3.43E-03	0.479
4	1249	4.75E-02	0.131
5	697	1.85E-02	1.60E-02
6	417	1.42E-03	9.22E-04
7	285	6.25E-05	3.78E-05
8	1418	2.78E-05	1.25E-04
9	1183	6.67E-04	1.53E-03
10	927	9.21E-03	1.16E-02
11	703	2.46E-02	2.14E-02
12	533	9.37E-03	6.69E-03
13	418	7.02E-04	4.57E-04
14	349	3.12E-05	1.94E-05
15	743	6.17E-05	5.66E-05
16	620	1.40E-03	1.09E-03
17	487	1.83E-02	1.25E-02
18	370	4.96E-02	3.13E-02
19	281	1.83E-02	1.11E-02
20	220	1.40E-03	8.34E-04
21	184	6.23E-05	3.69E-05

[a] Phase amounts V and L are reported on a mass basis.

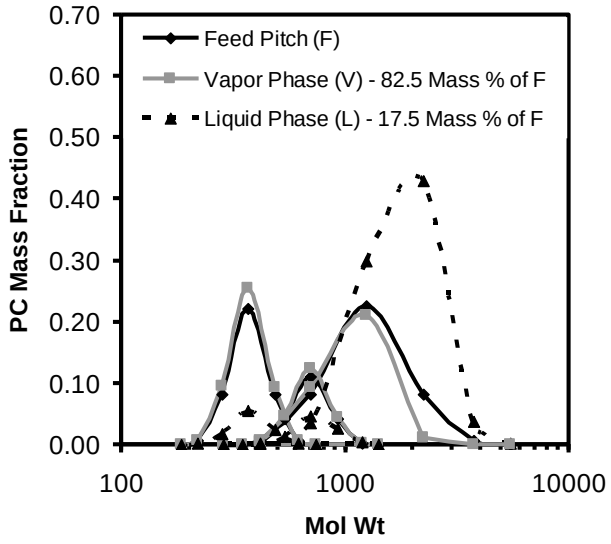

Figure 2.4. PC mass fractions (converted to a solvent-free basis for this and following figures) for the feed pitch (F), and for the vapor (V), and liquid (L) phases upon solvent removal, for Extraction Run 4 (see Table 2.2). The curves connecting the PCs are to show readers their NDF origin. The extraction process causes a shift to a higher MWD.

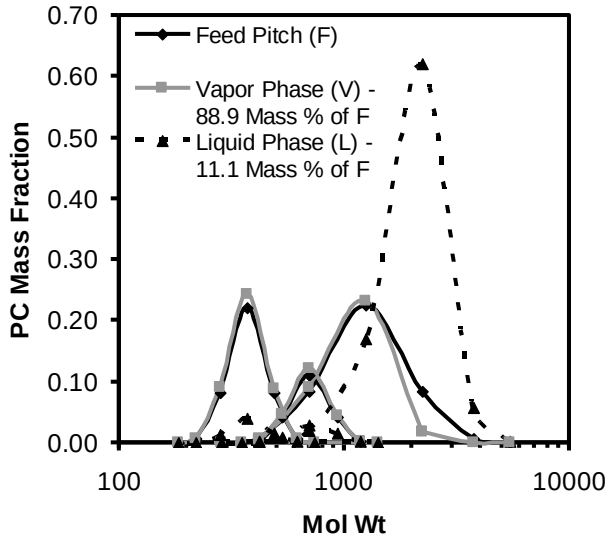

Figure 2.5. PC mass fractions for the feed pitch (F), and for the vapor (V) and liquid (L) phases upon solvent removal, for Extraction Run 11 (see Table 2.2). Note the higher MWD of the L phase compared to Run 4.

SAFT–LC for Predicting the Effect of Solvent Addition on Mesophase Formation

In the early 90s, researchers at Conoco[39] discovered that high-melting, mesogen-containing pitch fractions can dissolve up to 20 wt % toluene and still consist of 100% mesophase. We therefore evaluated the capability of SAFT–LC, used in a purely predictive mode, to model this effect. In particular, the addition of toluene to three, dried (i.e., solvent-free) bottom (L) phases from Extraction Runs 11, 13, and 17 (with softening points of 269, 274, and 319 °C, respectively) was simulated using SAFT–LC. Both experimental work and prediction indicate that in the dried, solvent-free state, these fractions consist of 100% mesophase (see Table 2.2). Calculations were performed with the SAFT–LC pure-component and binary interaction parameters previously determined above. The temperature and pressure used in the simulation were representative of spinning conditions for carbon fiber, that is, 340 °C and 50 bar.[11] Moderate deviations in temperature and pressure from these conditions had little effect on the results obtained, as long as all phases present remained in the condensed state.

As shown in Fig. 2.6, SAFT–LC does predict the "solvating"[39] effect of mesophase, as the L phases from all three runs still consist of 100% mesophase when significant amounts (i.e., 5-10 wt % toluene) are added. Representative PC compositions for both the isotropic and the mesophases formed by the addition of toluene to the L phase from Run 11 are shown in Figs. 2.7 and 2.8. At the point of incipient isotropic phase formation, when ~5 wt % toluene has been added (Fig. 2.6), we see that the isotropic phase has a significantly lower mol wt than the feed and mesophase pitch (Fig.

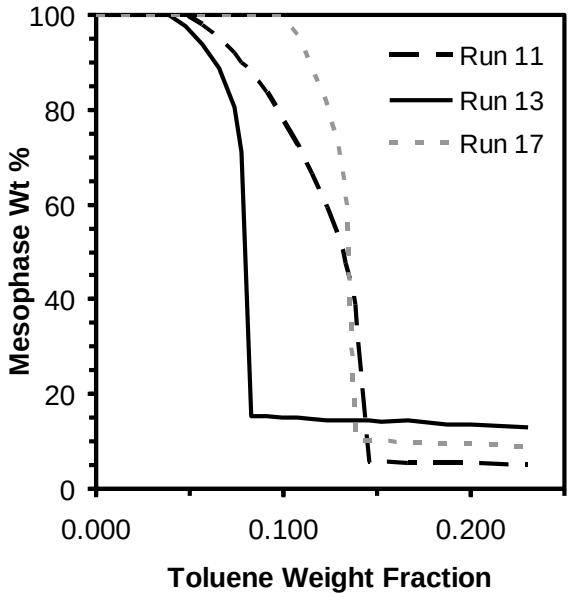

Figure 2.6. Effect of added toluene solvent on the mesophase content of the dried pitch fraction "L" resulting from three different extraction runs as predicted by SAFT–LC. These pitch fractions, denoted as Run 11, Run 13, and Run 17, comprise 11.1, 4.6, and 6.3 wt % of the pitch feed F, respectively.

2.7). Note that the feed and mesophase MWDs are essentially superimposed on each other. With the overall addition of ~13 wt % toluene, the isotropic phase has grown to essentially half of the total phases present (Fig. 2.6). Now the differences in the PC distribution between the isotropic and mesophases (Fig. 2.8) are less significant. Finally, as shown in Fig. 2.6, when the overall toluene addition reaches 15 wt %, the percent mesophase for Run 11 plateaus out at about 5 wt % and essentially remains flat for further additions of toluene. However, we note that this residual mesophase consists of more than 90 wt % PC 2 (mol wt = 3741), whose existence, as discussed above, is uncertain. In the absence of PC 2, SAFT–LC predicts only one (isotropic) phase at these higher solvent contents for Runs 11, 13, and 17 (because the clearing temperature of PC 2

in the solvent-free state is predicted, via Equation 2.29, to be 1036° C, it is expected that significantly higher temperatures and/or solvent contents would be necessary to achieve a mesophase content of 0% in the L phases resulting from Runs 11, 13, and 17). In Fig. 2.6, it is hypothesized that the abrupt manner in which the mesophase content falls is caused by the fact that these mesophase fractions are dominated by one PC, PC 3 (a more gradual, continuous change would be expected were a variety of species over a range of mol wts present in relatively equal amounts).

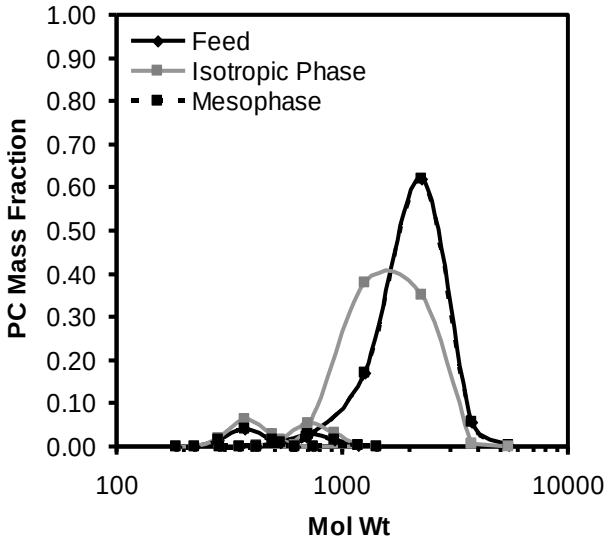

Figure 2.7. SAFT–LC predictions of the PC composition of the feed (the dried L phase resulting from Run 11), isotropic phase, and mesophase at the point of incipient isotropic phase formation after solvent addition. The overall toluene content is 4.8 wt % (see Fig. 2.6).

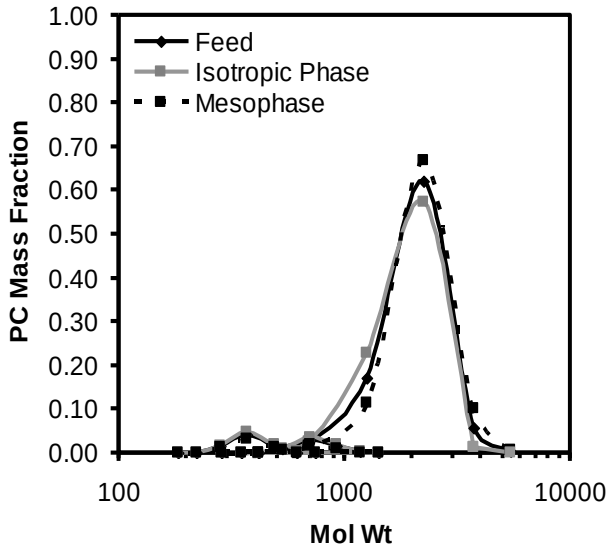

Figure 2.8. SAFT–LC predictions of the PC composition of the feed (the dried L phase resulting from Run 11), isotropic phase, and mesophase at 50 wt % mesophase after solvent addition. The overall toluene content is 13 wt % (see Fig. 2.6).

Conclusions

As originally developed, SAFT cannot predict liquid crystalline behavior. However, by adding an orientational free energy term based on Maier–Saupe theory, we have developed an equation of state that can be used to predict the phase behavior of carbonaceous, oligomeric pitches over a wide range of conditions, where either excess free energy or orientational free energy effects dominate, both with and without solvents. For example, SAFT–LC can be used to identify supercritical solvent extraction conditions for producing pitch fractions that, upon solvent removal, consist of 100% liquid crystalline mesophase. In addition, SAFT–LC can predict the experimentally observed ability of mesophases to dissolve significant amounts of solvent while still maintaining their 100% mesophase character. These "solvated" mesophases have dramatically lower melting points, facilitating their processing into carbon artifacts.[39]

References

[1]Edwards, W. F.; Jin, L.; Thies, M. C. MALDI-TOF Mass Spectrometry: Obtaining Reliable Mass Spectra from Insoluble Carbonaceous Pitches. *Carbon* **2003**, *41*, 2761-2768.

[2]Edwards, W. F.; Thies, M. C. Fractionation of Pitches by Molecular Weight Using Continuous and Semibatch Dense-gas Extraction. *Carbon* **2006**, *44*, 243-252.

[3]Dickinson, E. M. Average Structures of Petroleum Pitch Fractions by $^{1}H/^{13}C$ N.M.R. Spectroscopy. *Fuel* **1985**, *64*, 704-706.

[4]Hutchenson, K. W.; Roebers, J. R.; Thies, M. C. Fractionation of Petroleum Pitch with Supercritical Toluene. *J. Supercrit. Fluids* **1991**, *4*, 7-14.

[5]Mochida, I.; Yoon, S. H.; Korai, Y.; Kanno, K.; Sakai, Y.; Komatsu, M. Carbon Fibers from Aromatic Hydrocarbons. *CHEMTECH* **1995**, *25*, 29-37.

[6]Brooks, J. D.; Taylor, G. H. Formation of Graphitizing Carbons from the Liquid Phase. *Nature* **1965**, *206*, 697-699.

[7]Lewis, I. C.; Thermotropic Mesophase Pitch. *Carbon* **1978**, *16*, 503.

[8]Diefendorf, R. J.; Riggs, D. M. Forming Optically Anisotropic Pitches. U. S. Patent 4,208,267, June 17, 1980.

[9]Hurt, R. H.; Chen, Z. Y. Liquid Crystals and Carbon Materials. *Phys. Today* **2000**, *53*, 39-44.

[10]*Introduction to Carbon Technologies*; Marsh, H., Heintz, E. A., Rodriguez-Reinoso, F., Eds.; University of Alicante Secretariado de Publicaciones: Alicante, Spain, 1997.

[11]Beauharnois, M. E.; Edie, D. D.; Thies, M. C. Carbon Fibers from Mixtures of AR and Supercritically Extracted Mesophases. *Carbon* **2001**, *39*, 2101-2111.

[12]Murdie, N.; Ju, C. P.; Don, J.; Wright, M. A. Carbon-Carbon Matrix Materials. In *Carbon–Carbon Materials and Composites;* Buckley, J. D.; Edie, D. D. , Eds.; Noyes Publications: Park Ridge, New Jersey, 1993; Chapter 5.

[13]Shishido, M.; Inomata, H.; Arai, K.; Saito, S. Application of Liquid Crystal Theory to the Estimation of Mesophase Pitch Phase-Transition Behavior. *Carbon* **1997**, *35*, 797-799.

[14]Humphries, R. L.; James, P. G.; Luckhurst, G. R. A Molecular Field Treatment of Liquid Crystalline Mixtures. *Symp. Faraday Soc.* **1971**, *5*, 107-118.

[15]Humphries, R. L.; James, P. G.; Luckhurst, G. R. Molecular Field Treatment of Nematic Liquid Crystals. *J. Chem. Soc., Faraday Trans. 2* **1972**, *68*, 1031-1044.

[16]Humphries, R. L.; Luckhurst, G. R. A Statistical Theory of Liquid Crystalline Mixtures: Phase Separation. *Proc. R. Soc. Lond., Ser. A* **1976**, *352*, 41-56.

[17]Maier, V. W.; Saupe, A. Eine Einfache Molekulare Theorie des Nematischen Kristallinflüssigen Zustandes. *Z. Naturforsch.*, **1958**, *13a*, 564-566.

[18]Maier, V. W.; Saupe, A. Eine Einfache Molekular-Statistische Theorie der Nematischen Kristallinflüssigen Phase. Teil I. *Z. Naturforsch.*, **1959**, *14a*, 882-889.

[19]Maier, V. W.; Saupe, A. Eine Einfache Molecular-Statistische Theorie der Nematischen Kristallinflüssigen Phase. Teil II. *Z. Naturforsch*. **1960**, *15a*, 287-292.

[20]Hurt, R. H.; Hu, Y. H. Thermodynamics of Carbonaceous Mesophase II. General Theory for Nonideal Solutions. *Carbon* **2001**, *39*, 887-896.

[21]Prausnitz, J. M.; Lichtenthaler, R. N.; Gomes de Azevedo, E. *Molecular Thermodynamics of Fluid Phase Equilibria*, 3rd ed.; Prentice Hall PTR: Upper Saddle River, New Jersey, 1999; pp. 390-402.

[22]Zhuang, M. S.; Thies, M. C. Extraction of Petroleum Pitch with Supercritical Toluene: Experiment and Prediction. *Energy Fuels* **2000**, *14*, 70-75.

[23]Huang, S. H.; Radosz, M. Equation of State for Small, Large, Polydisperse, and Associating Molecules. *Ind. Eng. Chem. Res.* **1990**, *29*, 2284-2294.

[24]Huang, S. H.; Radosz, M. Equation of State for Small, Large, Polydisperse, and Associating Molecules: Extension to Fluid Mixtures. *Ind. Eng. Chem. Res.* **1991**, *30*, 1994-2005.

[25]Yu, M. L.; Chen, Y. P. Correlation of Liquid-liquid Phase Equilibria Using the SAFT Equation of State. *Fluid Phase Equilib.* **1994**, *94*, 149-165.

[26]Dauché, F. M.; Bolaños, G.; Blasig, A.; Thies, M. C. Control of Mesophase Pitch Properties by Supercritical Fluid Extraction. *Carbon* **1998**, *36*, 953-961.

[27]Edwards, W. F.; Thies, M. C. Dense-Gas Fractionation and MALDI Characterization of Carbonaceous Pitches. *Energy Fuels* **2005**, *19*, 984-991.

[28]Ting, P. D.; Joyce, P. C.; Jog, P. K.; Chapman, W. G.; Thies, M. C. Phase Equilibrium Modeling of Mixtures of Long-chain and Short-chain Alkanes Using Peng-Robinson and SAFT. *Fluid Phase Equilib.* **2003**, *206*, 267-286.

[29]Wojtowicz, P. J. Generalized Mean Field Theory of Nematic Liquid Crystals. In *Introduction to Liquid Crystals*; Priestley, E. B.; Wojtowicz, P. J.; Sheng, P., Eds.; Plenum Press: New York, 1974; Chapter 4.

[30]Humphries, R. L.; Luckhurst, G. R. A Statistical Theory of Liquid Crystalline Mixtures. Components of Different Size. *Chem. Phys. Lett.* **1973**, *23*, 567-570.

[31]McQuarrie, D. A.; Simon, J. D. *Molecular Thermodynamics*. University Science Books: Sausalito, California, 1999, Chapter 6.

[32]Zhuang, S.-Z. Supercritical Fractionation of Petroleum Pitches: Experiment and Prediction. Ph. D. Dissertation, Clemson University, Clemson, SC, 2001.

[33]Carnahan, B.; Luther, H. A.; Wilkes, J. O. *Applied Numerical Methods*. John Wiley and Sons, Inc.: New York, 1969; pp 115-116.

[34]Bolaños, G. Production of Mesophase Pitch by Supercritical Fluid Extraction: A Study of the Region of Liquid–Liquid Equilibrium. Ph. D. Dissertation, Clemson University, Clemson, SC, 1995.

[35]Huang, S. H.; Radosz, M. Phase Behavior of Reservoir Fluids V: SAFT Model of CO_2 and Bitumen Systems. *Fluid Phase Equilib.* **1991**, *70*, 33-54.

[36]Hurt, R. H.; Hu, Y. Thermodynamics of Carbonaceous Mesophase. *Carbon* **1999**, *37*, 281-292.

[37]Boyer, C. Marathon Petroleum Company LLC. Personal communication, 1989.

[38]Greenwood, S. H. Treatment of Pitches in Carbon Artifact Manufacture. U. S. Patent 4,277,324, July 7, 1981.

[39]Kalback, W. M.; Romine, H. E.; Bourrat, X. M. Solvated Mesophase Pitches. U. S. Patent 5,538,621, July 23, 1996.

[40]Whitson, C. H.; Michelsen, M. L. The Negative Flash. *Fluid Phase Equilib.* **1989**, *53*, 51-71.

[41]Press, W. H.; Flannery, B. P.; Teukolsky, S. A.; Vetterling, W. T. *Numerical Recipes*. Cambridge University Press: Cambridge, Great Britain, 1986; Chapter 10.

[42]Goodwin, R. D. Toluene Thermophysical Properties from 178 to 800 K at Pressures to 1000 bar. *J. Phys. Chem. Ref. Data* **1989**, *18(4)*, 1565.

CHAPTER 3

SAFT-LC: PREDICTING MESOPHASE FORMATION FROM A STATISTICAL MECHANICS-BASED EQUATION OF STATE

Introduction

Carbonaceous pitches are polycyclic aromatic, oligomeric materials that have a molecular weight (mol wt) range from about 200 up to over 1000 g/mol (see Fig. 3.1).[1] They are produced via the thermal polymerization of decant oil, a by-product of the fluid catalytic cracking (FCC) of crude oil fractions. In 1965, Brooks and Taylor discovered that carbonaceous pitches, when heated to elevated temperatures such that a fluid phase forms, form a nematic, discotic, liquid crystalline phase, or mesophase.[2] Other researchers subsequently discovered that mesophase formation is also influenced by pitch composition; thus, these unique materials have characteristics in common with both thermotropic and lyotropic liquid crystals.[3]

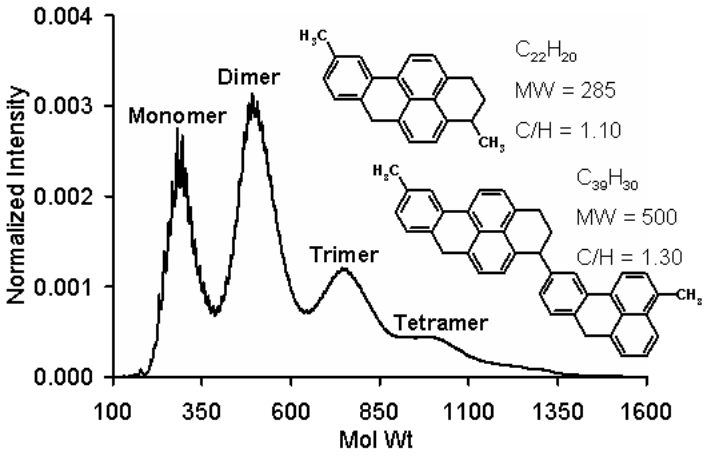

Figure 3.1. MALDI mass spectrum of M-50 petroleum pitch and suggested structures for typical monomer and dimer species.[1]

It is often necessary to process carbonaceous pitches in the liquid crystalline state. Such is the case when they serve as precursors for high modulus, high thermal conductivity carbon fibers.[4] On the other hand, a carbon-carbon composite may consist of an isotropic matrix into which a stronger, reinforcing material is dispersed. Thus, the degree to which a potential precursor pitch forms mesophase at processing conditions strongly influences its suitability for a given use.

With both temperature and molecular composition affecting the isotropic/nematic phase equilibria of pitches, a predictive model is of significant interest to researchers. In Chapter 2, we presented the development of such an equation, the Statistical Associating Fluid Theory – Liquid Crystal equation of state, or SAFT–LC.[5] In brief, our approach has been to combine the SAFT equation of Huang and Radosz[6] with the liquid crystal theory of Maier and Saupe.[7] Thus, this model accounts not only for the nonideal free energy of mixing (via SAFT), but it also accounts for the orientational free energy exhibited by liquid crystalline systems (via Maier-Saupe).

Near critical and supercritical extraction (SCE) processes are of interest for the fractionation of carbonaceous pitches into cuts with a range of mesophase-forming tendencies. In this paper, we use SAFT–LC to explore the effect of SCE operating conditions on the oligomeric composition of pitch fractions and on isotropic–nematic phase equilibria.

Previously, we used gel permeation chromatography (GPC) in tandem with a Gauss-Chebyshev quadrature technique to resolve the complex mol wt distribution (MWD) of the Conoco feed pitch into discrete pseudocomponents (PCs).[5] There was

some uncertainty as to the accuracy of the GPC calibration curve predictions for the mol wts of the largest PCs. Therefore, for this work, the mass spectrum of the pitch, obtained via matrix-assisted laser desorption/ionization, time-of-flight mass spectrometry (MALDI-TOF-MS, or MALDI for short), was used as the starting point for resolution of the MWD of the feed pitch into PCs. Unlike GPC, MALDI provides absolute mol wt values for the species comprising the MWD of the pitch.

Supercritical Extraction for the Production of Mesophase Pitch

A schematic illustrating the production of mesophase pitch via the supercritical extraction of carbonaceous pitches is shown in Fig. 3.2. Note that the process is divided into two steps. The first step is an extraction in which an isotropic feed pitch and solvent are fed into an extractor, which is simply a single-stage flash vessel. Over the range of temperatures, pressures, and solvent-to-pitch (S/P) ratios shown in Fig. 3.2, two phases form in the extractor: a lighter, solvent-rich phase (denoted by V) and a heavier, pitch-rich liquid phase (denoted by L). Lower mol wt pitch components concentrate in the top V phase, while heavier pitch components tend to concentrate in the bottom L phase. In the second step of the process, the L phase is dried to remove all solvent, yielding the final product. Depending on the experimental conditions and the feed pitch used, this final product can range from being completely isotropic to being 100% mesophase.

The SAFT-LC Equation

Background

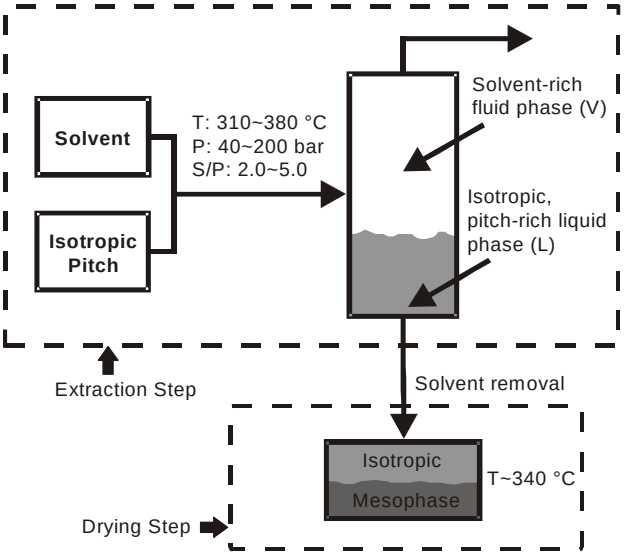

Figure 3.2. Schematic of a supercritical extraction process for fractionating carbonaceous pitches in order to produce mesophase pitch. Adapted from Burgess et al.[5]

The development and details of SAFT–LC are presented elsewhere,[5] so only a brief description is given here. The expression for the orientational Helmholtz free energy, as defined by Maier and Saupe[7] and extended to multicomponent mixtures by Humphries et al.[8] is

$$A = A^{orient} = U^{orient} - TS^{orient} = -\frac{N}{2}\sum_{i=1}^{n}\sum_{j=1}^{n} x_i x_j \varepsilon_{ij} \overline{P}_j \overline{P}_i - NkT\sum_{i=1}^{n} x_i \ln Z_i \qquad (3.1)$$

Here, N is Avogadro's number, x_i and x_j are species mole fractions, k is Boltzmann's constant, T is temperature, ε_{ij} is the anisotropic potential energy parameter between

molecules i and j, Z_i is the orientational partition function for the species (this term encompasses a summation of all of the energy states that arise because of the anisotropic interactions of a molecule in the mean field generated by the neighboring molecules), and $\overline{P}_j$ is the average order parameter for all the molecules of species j. Both Z_i and $\overline{P}_j$ are dependent upon the angle θ at which a particular molecule tends to align relative to a director, or preferred state; this concept is discussed in greater detail in Chapter 2.

The orientational partition function Z_i represents a summation of the different energy states which arise because of the anisotropic interactions between a molecule and the mean nematic field generated by its neighbors. Thus, this is an intermolecular (vs. the classic intramolecular) partition function. Assuming that the distribution of these possible orientational energy states is continuous, Z_i can be expressed as an integral as shown in Equation 3.3 (by integrating over all possible orientation states, which are dependent upon θ and the azimuthal angle ϕ). The observed energy state of a nematogen is dependent upon the angle θ_1 at which it is oriented relative to the fully oriented, preferred state denoted by the director. This is a representation of a laboratory-based coordinate system (see Chapter 2, pp. 44-45).

Note that this orientational partition function is not the same as the rotational partition function, which is based upon a summation of rotational energy states within a particular molecule; these rotational energy states do not depend upon interactions with another molecule. Also, the rotational energy states are calculated using a molecular-based coordinate system instead of our laboratory-based coordinate system.

The energy parameter ε_{ij} is obtained from[9]

$$\varepsilon_{ij} = \frac{\tilde{\varepsilon}_{ij}\sqrt{V_i V_j}}{\sum_{k=1}^{n} x_k V_k} \tag{3.2a}$$

where V_i and V_j are species molar volumes at ambient conditions, x_i is the composition of a species, and the parameter $\tilde{\varepsilon}_{ij}$ is the composition-independent energy parameter, which itself is given by

$$\tilde{\varepsilon}_{ij} = -4.542\,k\sqrt{T_{cl_i} T_{cl_j}} \tag{3.2b}$$

Here the parameter T_{cl} is the clearing temperature of a species, that is, the temperature at which the phase transition from the anisotropic to isotropic state takes place. Thus, the equation links the molecular to the macroscopic state.

From statistical mechanical arguments, it can be shown that the orientational partition function is given by

$$Z_i = \int_0^{\pi} \exp\left[-\frac{U_i}{kT}\right] \sin\theta_i d\theta_i \int_0^{2\pi} d\varphi = 2\pi \int_0^{\pi} \exp\left[-\frac{1}{kT}\sum_{j=1}^{n} x_j \varepsilon_{ij} \bar{P}_j P_i\right] \sin\theta_i d\theta_i \tag{3.3}$$

and the average order parameter by

$$\bar{P}_j = \int_0^{\pi} P_j Pr_j \sin\theta_j d\theta_j \int_0^{2\pi} d\varphi = \frac{2\pi \int_0^{\pi} P_j \exp\left[-\frac{1}{kT}\sum_{i=1}^{n} x_i \varepsilon_{ij} \bar{P}_i P_j\right] \sin\theta_j d\theta_j}{Z_j} \tag{3.4}$$

In Equation 3.4, the probability that a molecule has a particular degree of orientation is given by the term Pr_j. The P_j term represents to the order parameter for a particular molecule of species j. It is related to the angle of orientation θ_j as shown in Equation 3.4a below:

$$P_j = \frac{3}{2}\cos^2\theta_j - \frac{1}{2} \tag{3.4a}$$

In order to obtain SAFT–LC, we add the Helmholtz orientational free energy term described above to the segment and chain contributions from the SAFT equation, A^{seg} and A^{chain} :[6]

$$\frac{A^{res}}{RT} = \frac{A^{seg}}{RT} + \frac{A^{chain}}{RT} + \frac{A^{orient}}{RT} \tag{3.5}$$

The use of SAFT-LC to model the supercritical extraction of pitch using toluene as the solvent, and to predict the mesophase content of the unextracted dried bottoms phase, is described below.

Application of SAFT–LC to Carbonaceous Pitches; Definition of Pitch PCs and SAFT–LC Parameters

In order to apply the SAFT-LC equation to a poorly defined system such as carbonaceous pitch, the pitch must be represented as a mixture of discrete PCs. To this end, the MWD of a pitch obtained from Conoco (denoted by the company as PB35A/B; CAS 68187-58-6) was obtained by matrix-assisted laser desorption/ionization, time-of-flight mass spectrometry (MALDI-TOF-MS). Details of the development of this analytical method for carbonaceous pitches are presented elsewhere.[10] We note that MALDI, because it gives the absolute mol wt of individual pitch species, is a significant improvement over the traditional method for determining the mol wt of pitches, GPC.

In Fig. 3.3, the MALDI spectrum obtained is presented in terms of the normalized intensity of the MALDI detector response, so that the total area under the MALDI spectrum is equal to unity. In order to define PCs for the pitch, the plot was then divided into 10 regions, with each oligomeric peak being divided into 2 sections. Next, the number average molecular weight ($\overline{M}_n$) and the area under the curve for each region was calculated. Each region was assumed to represent one PC, and the area fraction of the curve in that region was assumed to equal the PC mole fraction. Work in progress in our laboratory indicates that this latter assumption is a good first approximation. Each region was divided into thin vertical slices (approximately 1000 per region), the mol wt in the middle of each slice was determined, as was the area of each slice as a fraction of the total area encompassed by the respective region; from these data, the number average molecular weight for each region could be calculated. The results of these calculations are summarized in Table 3.1.

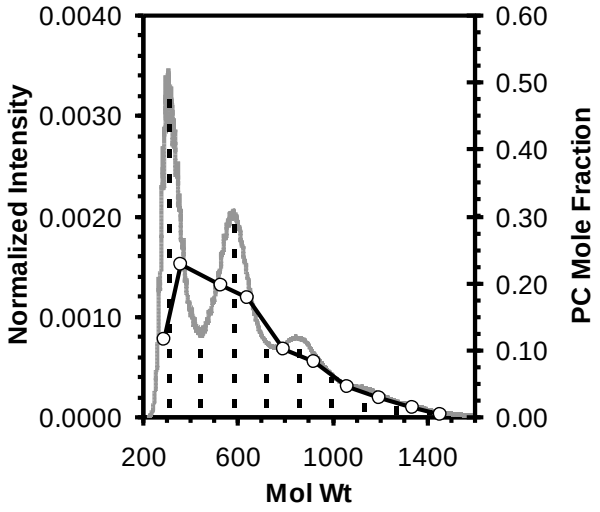

Figure 3.3. MALDI-TOF-MS mass spectrum (grey line, left axis) of PB35A/B petroleum pitch. PC mass fractions (right axis) are denoted by the open circles. The vertical, dashed lines bound the mol wt ranges assigned to each of the 10 PCs.

It was then necessary to determine the pure-component SAFT parameters for each PC. These parameters (v^{00}, m, and u^o/k) were obtained using correlations developed by Huang and Radosz for bitumen.[11] Required inputs to the correlations are the PC mol wts and the atomic carbon-to-hydrogen (C/H) ratio. For each PC, the values for the C/H ratios (Table 3.1) were predicted using a correlation developed in our labs that relates the MALDI-determined number average mol wt of a particular pitch fraction produced by dense-gas extraction to the C/H ratio of that fraction.[12]

The final pure-component parameters to be determined were the clearing temperatures for each PC. Following the work of Hurt and Hu,[13] we assumed that clearing temperature was a linear function with respect to molecular weight:

$$T_{cl,i} = a + b * MW_i \tag{3.6}$$

where $T_{cl,i}$ represents the clearing temperature of PC i (in K), MW_i represents the mol wt of said component, and the parameters *a* and *b* are adjustable.

Table 3.1. Physical and chemical properties of the 10 pitch PCs.

Pitch PC data			
PC #	Mol Wt	Mole Fraction (MALDI Area)	C/H Ratio
1	287	0.1161	1.14
2	360	0.2290	1.21
3	527	0.1970	1.36
4	641	0.1777	1.46
5	793	0.1018	1.60
6	922	0.0839	1.71
7	1064	0.0456	1.84
8	1198	0.0300	1.96
9	1335	0.0146	2.09
10	1452	0.0044	2.19

In order to calculate the binary interaction parameters between the various species, we followed our previous approach with SAFT.[14] That is, binary interaction parameters between the solvent and the various pitch PCs were assumed to be a linear function of mol wt:

$$k_{1,j} = A * MW_j + B \tag{3.7}$$

Here, $k_{1,j}$ represents the interaction parameter between the solvent "1" and pitch PC j, A and B are adjustable fitting parameters, and MW_j is the mol wt of PC j. Binary interaction parameters between the pitch PCs were defined as follows:

$$k_{i,j} = C * \left| MW_i - MW_j \right| \tag{3.8}$$

where $k_{i,j}$ represents the interaction parameter between the pitch PCs i and j, and C is a fitting parameter.

Results and Discussion

Dauché et al.[15] investigated the phase behavior of mixtures of petroleum pitch and toluene at supercritical conditions, determining the mass fractions of solvent in the top (V) and bottom (L) phases at 17 different sets of experimental conditions (see Fig. 3.2 and Table 3.2). In addition, the mesophase content in the solvent-dried, bottom product (L) was determined by polarized light microscopy.

All SAFT-LC calculations were performed using a computer program written in the Visual FORTRAN programming language. In this program, a parameterized version of the SAFT equation described by Huang and Radosz[6] was used in order to minimize the amount of programming necessary.

The adjustable parameters A, B, C, *a*, and *b* in SAFT-LC were fit to the solvent phase compositions and mesophase percentages for Runs 1-8 using a downhill simplex method. We chose these runs as fitting points because the experimentally determined mesophase content in the dried bottoms phase was less than 100%, maximizing the sensitivity of SAFT-LC to changes in mesophase composition and therefore providing a more rigorous test for SAFT–LC (as indicated in Table 3.2, many pitches can form 100% mesophase; however, the values obtained for these five adjustable parameters are not greatly affected if they are fit to all 17 sets of experimental data). For the percent mesophase calculation, it was assumed that P = 50 bar, and T = 340° C, as these conditions are representative of those at which mesophase pitch is processed into carbon products, such as fibers.

The above optimization process yielded SAFT–LC parameter values of A = 2.65E-4, B = -0.123, C = 1.03E-4, *a* = 146.6 K, and *b* = 0.541. We note here that these values of A, B, and C yield binary interaction parameters for pitch–solvent interactions ranging from -0.047 to 0.26 for the lightest and heaviest PCs, respectively. Slight changes in the values of these $k_{i,j}$'s (e.g., setting the negative values for the 2 lightest PCs to zero) have a negligible impact on the predicted phase behavior. We also note that from Equation 3.6, PC 6 (MW = 922) has a clearing temperature of 645 K, in good agreement with the theoretical work of previous workers.[13]

Table 3.2
Experimental, correlated, and predicted solvent compositions and mesophase contents for extraction of PB35A/B petroleum pitch with supercritical toluene.

Extract Run No.	Press/Temp S/P Ratio	Top Phase (V)		Bottom Phase (L)		Percent Mesophase	
		Expt.	Correl.	Expt.	Correl.	Expt.	Correl.
1	46/320/2.5	0.784	0.776	0.258	0.188	38	70.4
2	45/310/3.0	0.792	0.807	0.222	0.187	50	73.9
3	81/360/2.5	0.785	0.789	0.254	0.221	38	43.0
4	46/320/3.5	0.844	0.840	0.239	0.210	44	46.4
5	81/360/3.5	0.847	0.868	0.227	0.284	59	27.0
6	45/310/4.0	0.836	0.853	0.216	0.200	85	56.5
7	84/340/3.0	0.801	0.807	0.230	0.199	98	65.6
8	77/330/3.0	0.785	0.805	0.218	0.192	95	75.4
		Expt.	Predicted	Expt.	Predicted	Expt.	Predicted
9	94/320/2.5	0.738	0.757	0.245	0.140	100	100
10	77/330/4.0	0.831	0.851	0.201	0.203	100	60.0
11	94/320/3.5	0.820	0.818	0.221	0.151	100	100
12	94/310/3.0	0.771	0.790	0.214	0.140	100	100
13	154/360/2.5	0.741	0.758	0.232	0.177	100	100
14	94/310/4.0	0.821	0.836	0.184	0.146	100	100
15	155/330/3.0	0.764	0.786	0.173	0.142	100	100
16	155/330/4.0	0.814	0.832	0.171	0.145	100	100
17	154/360/3.5	0.804	0.819	0.184	0.187	100	100

After the adjustable parameters in SAFT–LC were determined, the equation was used to predict the experimental conditions given in Table 3.2 for Runs 9-17. It is encouraging to note that the predictions are of approximately the same accuracy as those obtained in the fitting step (Runs 1-8), indicating that the parameters are to a significant extent global.

Finally, we were somewhat surprised to find that the correlations developed by Huang and Radosz[11] for determining the SAFT parameters m, v^{oo}, and u^o/k have in fact yielded reasonable results, because these correlations were developed from the analytical characterization of cuts of bitumen, which, with C/H ratios ranging from 0.55 to 0.72, are

much more aliphatic than our pitches, which have C/H ratios that range from 1.2 to 1.86.[12]

Because a long-term objective of our work on the solvent extraction of pitches is control of the oligomeric composition of carbonaceous pitches, SAFT-LC was then used to predict the impact of the extraction pressure on the PC mass distribution in the dried L phase (see Fig. 3.2). For a temperature of 330 °C and a S/P ratio of 3.0 (toluene solvent), pressures of 40, 77 (Run 8), and 155 (Run 15) bar were examined. The change of the PC mass distribution with pressure is given in Fig. 3.4.

These results reveal some interesting trends. First, for the dried residues formed at lower extraction pressures (40 and 77 bar), two phases, one isotropic and one nematic, exist at the mesophase determination conditions of 340° C and 50 bar. As the extraction pressure is increased, the PC distribution in the bottom phase shifts to the right. The effect of the denser solvent is a more aggressive extraction, with a key contribution to the increase in mesophase content being the marked decrease in the presence of PCs 1-5 as the pressure is increased from 40 bar to 77 bar. Even higher extraction pressures are required for the bottom L phase to consist entirely of 100% mesophase. At 155 bar, SAFT–LC predicts that there are only trace amounts of PCs 1-4, with PC 5 being present at only about 1 wt %. Thus, the primary mesophase-forming species are the five heaviest PCs.

The PC distributions predicted by SAFT–LC for the isotropic phase and the mesophase separately, for the extraction conditions and overall bottom phase L shown in Fig. 3.4, are given in Fig. 3.5. Of interest is the fact that the average mol wt of the

isotropic phase increases with extraction pressure as its overall fraction of the bottom L phase decreases. The mesophase PC distribution, on the other hand, goes through a minimum in mol wt as the L phase changes from a two-phase mixture to 100% mesophase.

The effect of SCE pressure on the mesophase content of the dried L phase, as predicted by SAFT–LC, is shown in Fig. 3.6. For a S/P ratio (toluene solvent) of 3.0 and extraction temperatures of 330, 350, and 380 °C, pressures of 90, 130, and 180 bar, respectively, are required to obtain 100% mesophase. Consistent with our recent experimental results,[1] we also see that for a given extraction pressure an L phase with a higher percentage of mesophase is obtained at lower extraction temperatures, where the solvent is more liquid-like.

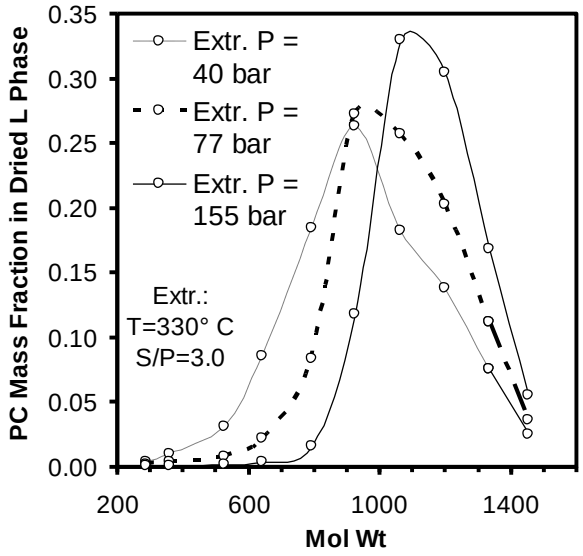

Figure 3.4. Change in PC mass distribution in the bottom L phase (upon solvent removal) with extraction pressure as predicted by SAFT-LC at T = 330° C, S/P = 3.0, and various extraction pressures (P). Mesophase content is predicted to be 32.3% at P = 40 bar (thin dashed black line), 75.4% at P = 77 bar (thick dashed black line), and 100% at P = 155 bar (thin black line). PC mass fractions are denoted by open circles, and the lines are only to guide the eye.

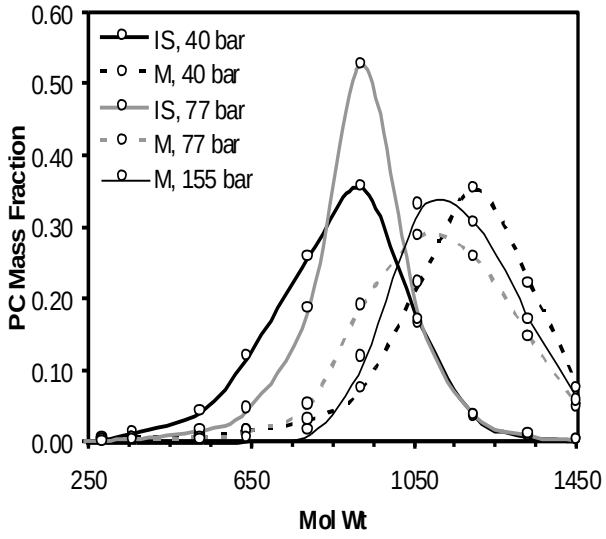

Figure 3.5. SAFT-LC predictions for PC mass distributions for the isotropic (IS) phase and mesophase (M) fractions contained in the L phases shown in Fig. 3.4.

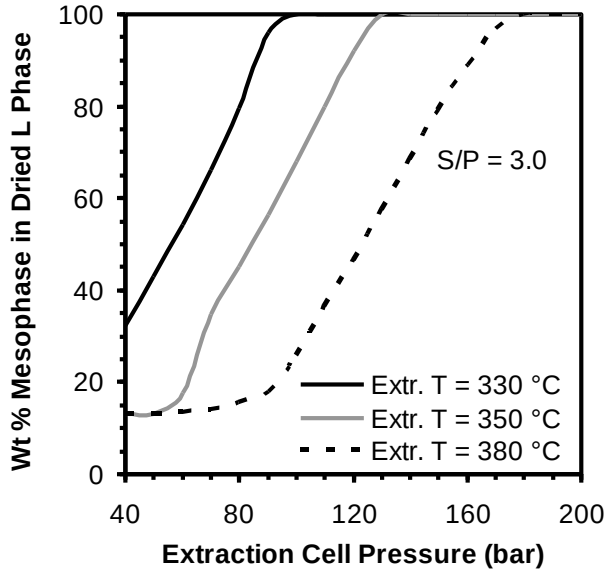

Figure 3.6. Effect of SCE pressure on the predicted mesophase content of the dried L phase (see Fig. 3.2). SAFT–LC predictions were made at an S/P ratio of 3.0 and three operating temperatures.

The effect of S/P ratio on mesophase content in the L phase was also investigated. Results for a constant extraction temperature of 330 °C and several extraction pressures are given in Fig. 3.7. SAFT–LC predictions of a decrease in mesophase content in L with an increase in S/P ratio are counterintuitive and, in fact, contradict the experimental results given in Table 3.2 (e.g., compare Runs 1 and 4, 2 and 6, 8 and 10; for these pairs, only the S/P ratio was changed). SAFT–LC also predicts (not shown) that the fraction of the feed pitch which remains unextracted and ends up as the L phase increases from 20 to 30 wt % as the S/P ratio is increased from 2.0 to 5.0 at 330 °C and 90 bar. Prediction of an increase in bottom-phase yield of this magnitude would, indeed, lead to a lower average mol wt and less mesophase content. Our investigation of what aspects of SAFT–LC are leading to this anomalous behavior are in progress, and tentatively point to the pure-component parameters that were derived from bitumen data.

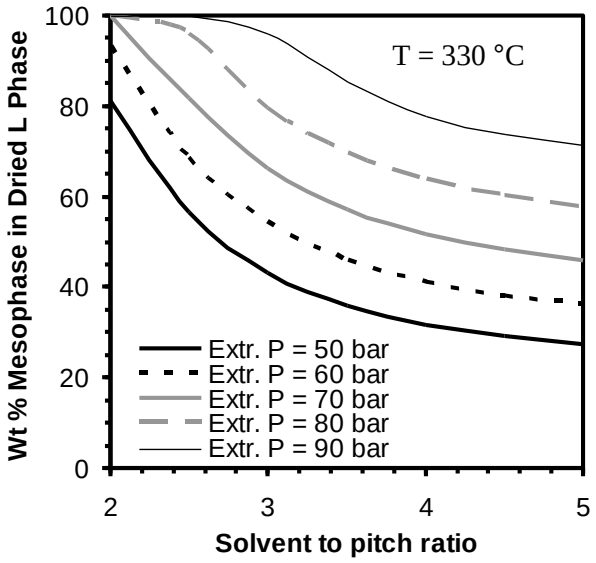

Figure 3.7. Effect of solvent-to-pitch ratio (toluene solvent) on the mesophase content in the dried L phase for a SCE temperature of 330° C, as predicted by SAFT–LC.

Finally, we evaluated the ability of SAFT–LC to predict the surprising behavior of carbonaceous mesophase pitches to absorb up to 20 wt % solvent and still consist of 100% mesophase.[16] To this end, phase diagrams were generated that illustrate system phase behavior as a function of temperature for the addition of toluene solvent to L phases consisting of 100% mesophase, generated by the SCE process shown in Fig. 3.2. As an example, Fig. 3.8 shows a phase diagram at 50 bar for 100% mesophase pitch fractions produced at three different SCE conditions: (1) an L phase obtained at extraction conditions of 330 °C, 100 bar, and a S/P ratio of 3.0 (Fraction 1); an L phase obtained at the same T and S/P ratio, but 155 bar (Fraction 2); and an L phase obtained at the same T and S/P ratio, but 200 bar (Fraction 3).

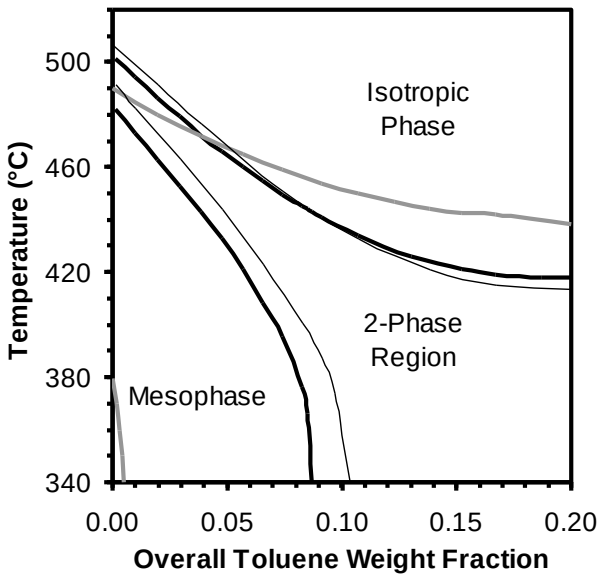

Figure 3.8. Calculated binary phase diagram for the addition of toluene to 100% mesophase pitch fractions at 50 bar. Pitch fractions were obtained at extraction conditions of T = 330° C, S/P ratio = 3.0, and pressures of (i) 100 bar (gray phase boundaries), (ii) 155 bar (thick black phase boundaries), and (iii) 200 bar (thin black phase boundaries)

Several trends are apparent from an examination of Fig. 3.8. First, we note that for the fractions produced at higher extraction pressures, and with higher average mol wts, increasing amounts of toluene are required before we cross the phase boundary to create an isotropic phase (analogous to a bubble point). For example, at a temperature of 340 °C an isotropic phase forms from Fraction 1 with the addition of only 0.5 wt % toluene; however, no phase split occurs for the higher mol wt fractions until the toluene wt % reaches 8.5 and 10.5 wt %, respectively.

A different behavior is observed at the boundary between the 2-phase region and the isotropic phase (the clearing temperature; analogous to the dew point). At low concentrations of solvent (< ~ 0.04 weight fraction), the behavior is as expected, with the clearing temperatures increasing with the average mol wt of the fraction. However, at solvent concentrations > ~ 0.04, this trend reverses itself, as Fraction 1 becomes the toluene/pitch mixture with the highest overall clearing temperature. Although we have no immediate explanation for this phenomenon, we note that Fraction 1, having the lowest average mol wt, in fact contains the lowest mole fraction of solvent. Therefore, the presence of solvent may have less of an impact on this fraction than those of higher average mol wt. Finally, we also note that as the extraction pressure increases, the size of the two-phase region decreases markedly. At 0 percent toluene, Fraction 1 has a "bubble point" of 380 °C and a clearing temperature of 490 °C. However, for Fraction 3, the two phase transitions differ by less than 20 °C. For all fractions, the addition of toluene greatly expands the size of the two-phase region, while significantly lowering the fraction clearing temperature.

Conclusions

SAFT–LC has shown itself to be a versatile equation of state for application to carbonaceous pitches, a unique class of materials that can form discotic nematic mesophases at appropriate oligomeric compositions. In general, both the supercritical extraction conditions required to produce 100% mesophase fractions and the effect of solvent addition on system phase behavior were successfully predicted. However, the extent to which SAFT–LC can accurately predict the oligomeric distribution of the fractions isolated will require the measurement of new phase equilibrium data, including the molecular composition of the recovered fractions. Fortunately, with the recent development of MALDI mass spectrometry as an effective analytical tool for carbonaceous pitches, this is now an achievable objective.

Another important task is the modification of the set of pure-component SAFT parameters so that they are appropriate for carbonaceous pitches, which possess a significantly higher aromatic content than the cuts of bitumen for which the correlations of Huang and Radosz (which were used to define SAFT parameters for this study) were defined. These correlations were defined based primarily on SAFT parameter data for aliphatic compounds; in addition, in deriving these correlations, Huang and Radosz only considered aromatic compounds up to a mol wt of 228 Da (triphenylene). Thus, the accuracy of SAFT parameters predicted for PCs of highly aromatic pitches is highly questionable.

Finally, in order to use group contribution theories to obtain a new set of pure-component SAFT parameters, it will be necessary to determine a new MWD for the feed pitch, along with molecular structures for each of its constituents.

Comparison of the Performance of SAFT-LC Models Presented in Chapters 2 and 3: Which one is Better?

In this section, the effect of the methods presented in Chapters 2 and 3 for predicting the mol wt distribution and SAFT parameters on the SAFT-LC model predictions presented in each chapter is investigated. In Fig. 3.9, the solvent compositions for the V and L phases given in Tables 2.2 and 3.2 are presented in graphical form. In Fig. 3.9, Model 1 refers to the SAFT-LC model predictions presented in Chapter 2, in which GPC and Gauss-Chebyshev quadrature were used to resolve the feed pitch into 21 PCs and each PC was assumed (for the sake of modeling) to have the same C/H ratio, with this value being set as a fitting parameter. Model 2 refers to the SAFT-LC model predictions presented in Chapter 3, in which an MWD obtained via MALDI mass spectrometry was resolved into 10 PCs, with the molecular C/H ratio for each PC obtained from a correlation developed in our labs that relates the MALDI-determined number average mol wt of a particular pitch fraction produced by dense-gas extraction to the average C/H ratio of that fraction. Finally, Model 3 refers to SAFT-LC calculations obtained using the same 10 PCs as Model 2, but with the C/H ratio set as a fitting parameter)just as in Chapter 2, the optimum value for C/H ratio = 0.71.

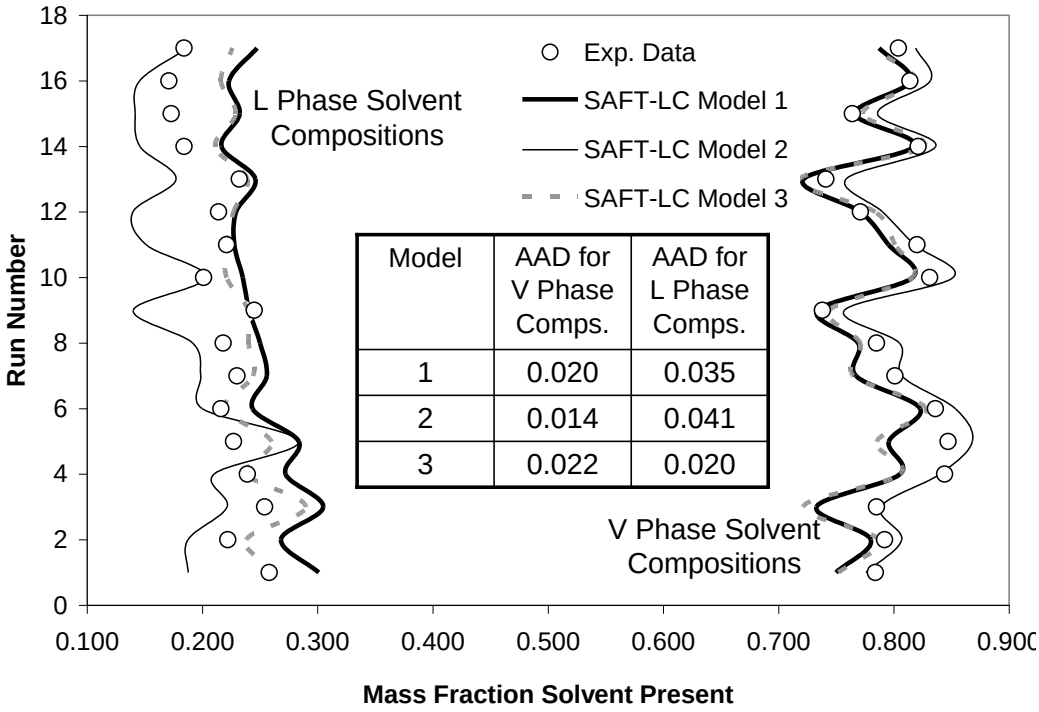

Model	AAD for V Phase Comps.	AAD for L Phase Comps.
1	0.020	0.035
2	0.014	0.041
3	0.022	0.020

Figure 3.9. Toluene solvent compositions in the V and L phases obtained at the extraction conditions denoted in Tables 2.2 and 3.2. Average absolute differences (AADs) between experimental and correlated/predicted solvent compositions for V and L phases indicate that use of Models 1 and 3 is typically more effective at reproducing experimental results.

From Fig. 3.9, it is apparent that there is a high degree of similarity between the solvent compositions predicted using Models 1 and 3. That is, under the constraints of Models 1 and 3, SAFT-LC tends to overpredict solvent compositions in the L phase, and it underpredicts them in the V phase. The correlated/predicted values yielded by Models 1 and 3 for the mesophase content in the dried L phase are also similar (although the correlations and predictions obtained using Model 1 are superior to those obtained using Model 3, as indicated by the AAD values given in Fig. 3.10).

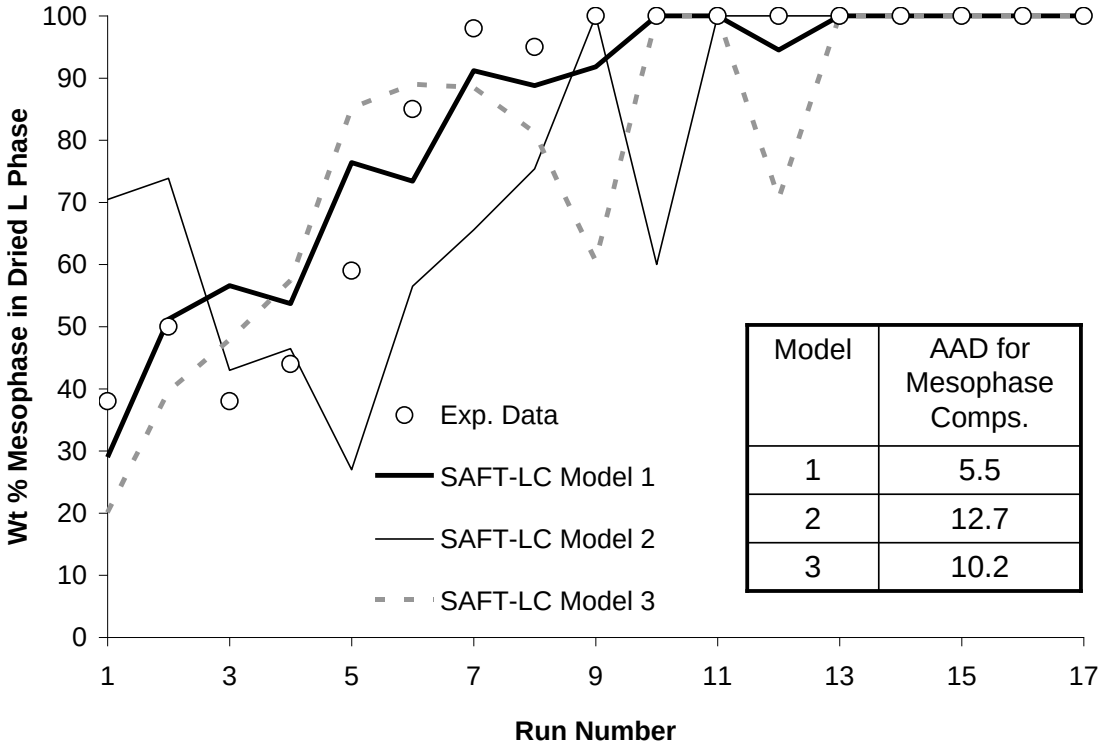

Figure 3.10. Mesophase compositions in the dried L phases resulting from extractions at the conditions denoted in Tables 2.2 and 3.2. Models 1 and 3 are clearly more closely correlated to the experimental results for runs 1-8 than Model 2, as indicated by the AADs between experimental and correlated/predicted mesophase compositions.

While otherwise identical (both treat the C/H ratio as an adjustable parameter), Models 1 and 3 incorporate different methods of resolving the MWD of the feed pitch into PCs (GPC and Gauss-Chebyshev quadrature in the first case, and MALDI in the second). It is very notable that the difference in the number of PCs (21 vs. 10) utilized in each case does not greatly impact the model predictions for solvent phase compositions and mesophase contents. Nor does the great difference in the width of the MWD (for Model 1, PC mol wts range from 184 to 5476, while for Model 3, PC mol wts range from 287 to 1452) have a great impact on the model predictions. Therefore, it appears unlikely

that changing the spacing of the intervals for the MALDI spectrum in Fig. 3.3 so that the PC distribution more closely models the MWD of the feed pitch, or altering the number of such intervals to change the number of PCs would greatly impact the model predictions either.

Based on the data analysis presented within this section, Model 1 yields the best correlations/predictions for mesophase content in the dried L phase. Because the accurate prediction of mesophase content is essential to controlling the mesophase content of pitches produced from such extraction processes, Model 1 is the best of the three models. This is true even though the GPC-derived MWD is skewed to the high side and SAFT parameters are predicted using a C/H ratio that is not indicative of that present in carbonaceous pitches. Because the fit results were best when C/H ratio was set as an adjustable parameter, the correlations of Huang and Radosz used to predict the SAFT parameters for the pitch PCs must be replaced.

Parameter sensitivity analyses were conducted by perturbing one adjustable fitting parameter (A, B, C, a, or b), typically ±10%, while holding all others constant. For SAFT-LC Model 1, analysis results indicate that such moderate deviations in the value of one parameter have a small but noticeable effect on the predictions for toluene-pitch phase behavior and mesophase formation in the dried bottom L phase (see Figs. 3.11-3.15). Model 1 and Model 3 were considerably more tolerant than Model 2 of equally sized perturbations in the adjustable fitting parameters, with the phase equilibrium and mesophase content data generated using Model 1 being the least affected by perturbations in the fitting parameters.

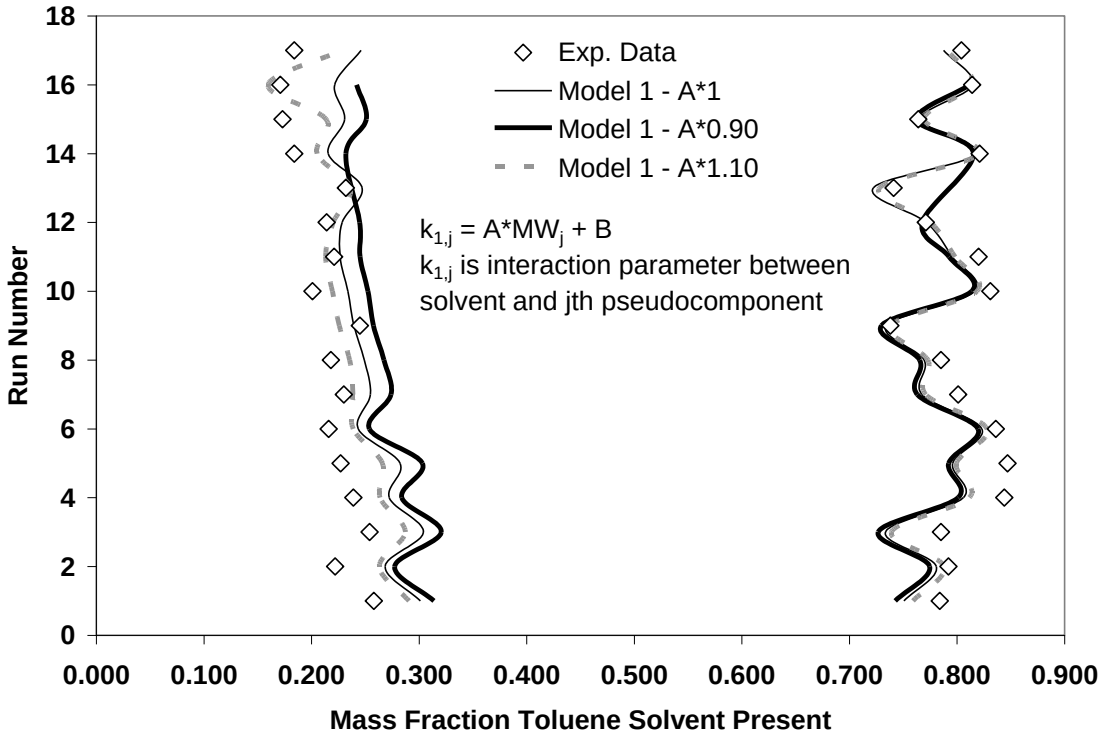

Figure 3.11. Sensitivity analysis results for perturbation of the A parameter in SAFT-LC Model 1.

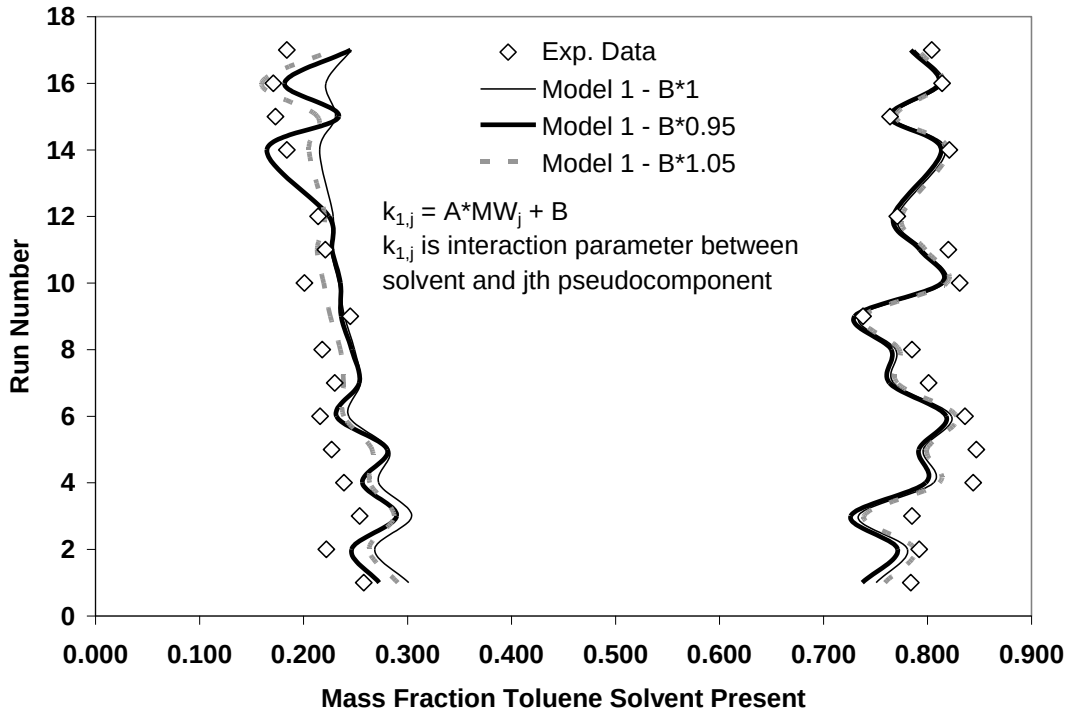

Figure 3.12. Sensitivity analysis results for perturbation of the B parameter in SAFT-LC Model 1.

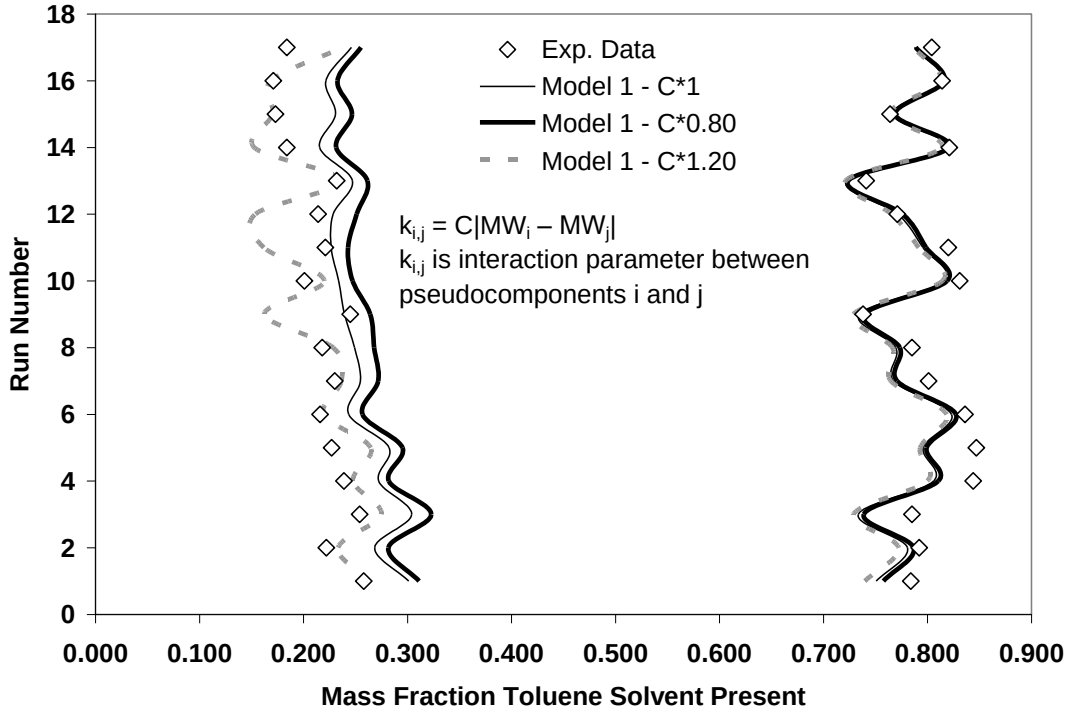

Figure 3.13. Sensitivity analysis results for perturbation of the C parameter in SAFT-LC Model 1.

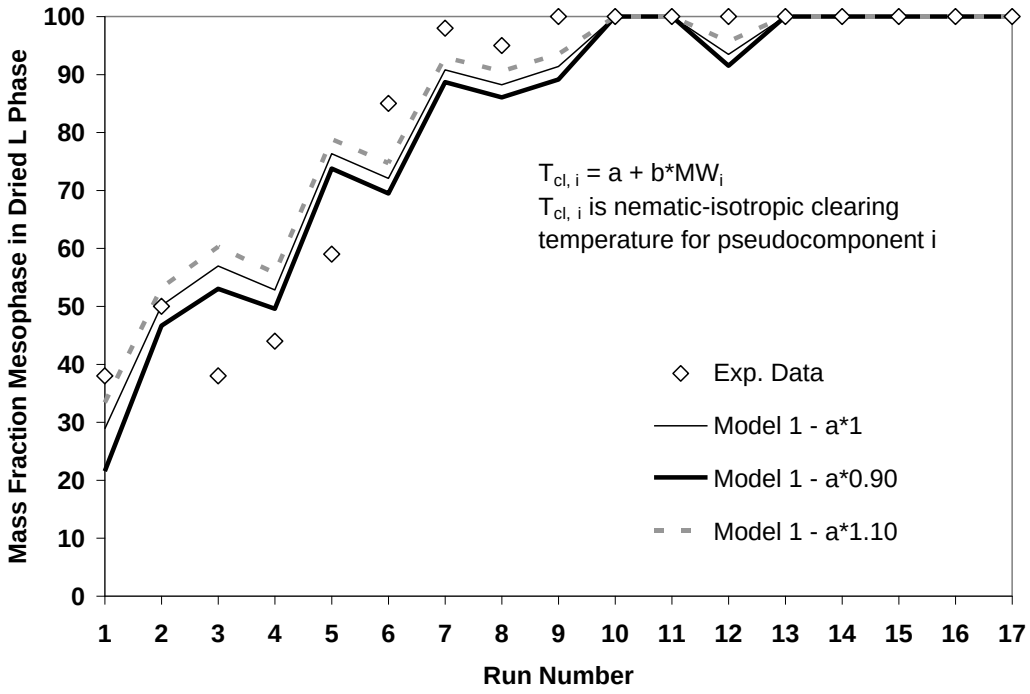

Figure 3.14. Sensitivity analysis results for perturbation of the a parameter in SAFT-LC Model 1.

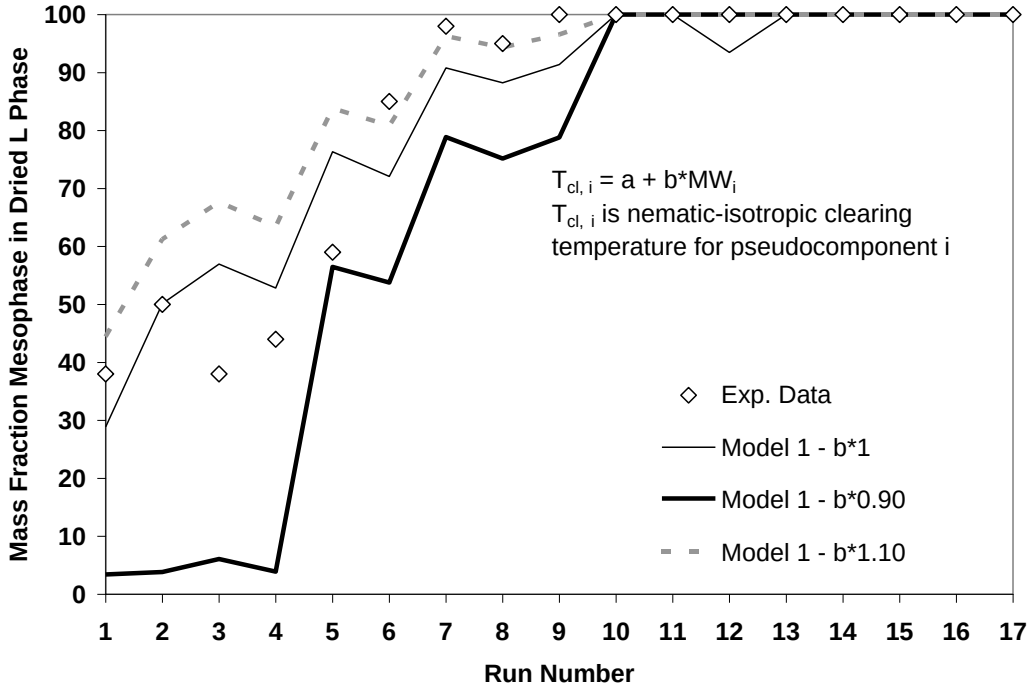

Figure 3.15. Sensitivity analysis results for perturbation of the b parameter in SAFT-LC Model 1.

References

[1]Cervo, E. G.; Thies, M. C. Control of the Molecular Weight Distribution of Petroleum Pitches via Dense-Gas Extraction. *Chem. Eng. Technol*. **2007**, *30*, 742-748.

[2] Brooks, J. D.; Taylor, G. H. Formation of Graphitizing Carbons from the Liquid Phase. *Nature* **1965**, *206*, 697-699.

[3]Hurt, R. H.; Chen, Z. Y. Liquid Crystals and Carbon Materials. *Phys. Today* **2000**, *53*, 39-44.

[4]F. M. Dauché, A. B. Barnes, N. C. Gallego, D. D. Edie, M. C. Thies. Ribbon-Shaped Carbon Fibers from Supercritically Extracted Mesophase Pitches. Carbon 36 (1998) 1238-1240.

[5]W. A. Burgess, M. S. Zhuang, Y. Hu, R. H. Hurt, M. C. Thies. SAFT-LC: An Equation of State for Predicting Liquid Crystalline Phase Behavior in Carbonaceous Pitches. *Ind. Eng. Chem. Res.* **2007**, *46*, 7018-7026.

[6]Huang, S. H.; Radosz, M. Equation of State for Small, Large, Polydisperse, and Associating Molecules: Extension to Fluid Mixtures. *Ind. Eng. Chem. Res.* **1991**, *30*, 1994-2005.

[7]Maier, V. W.; Saupe, A. Eine Einfache Molecular-Statistische Theorie der Nematischen Kristallinflüssigen Phase. Teil II. *Z. Naturforsch.* **1960**, *15a*, 287-292.

[8]Humphries, R. L.; James, P. G.; Luckhurst, G. R. A Molecular Field Treatment of Liquid Crystalline Mixtures. *Symp. Faraday Soc.* **1971**, *5*, 107-118.

[9]Humphries, R. L.; Luckhurst, G. R. A Statistical Theory of Liquid Crystalline Mixtures. Components of Different Size. *Chem. Phys. Lett.* **1973**, *23*, 567-570.

[10]Edwards, W. F.; Jin, L.; Thies, M. C. MALDI-TOF Mass Spectrometry: Obtaining Reliable Mass Spectra for Insoluble Carbonaceous Pitches. *Carbon* **2003**, *41*, 2761-2768.

[11]Huang, S. H.; Radosz, M. Phase Behavior of Reservoir Fluids V: SAFT Model of CO_2 and Bitumen Systems. *Fluid Phase Equilib.* **1991**, *70*, 33-54.

[12]Edwards, W. F.; Thies, M. C. Fractionation of Pitches by Molecular Weight Using Continuous and Semibatch Dense-gas Extraction. *Carbon* **2006**, *44*, 243-252.

[13]Hurt, R. H.; Hu, Y.. Thermodynamics of Carbonaceous Mesophase II. General Theory for Nonideal Solutions. *Carbon* **2001**, *39*, 887-896.

[14] Zhuang, M. S.; Thies, M. C. Extraction of Petroleum Pitch with Supercritical Toluene: Experiment and Prediction. *Energy Fuels* **2000**, *14*, 70-75.

[15] Dauché, F. M.; Bolaños, G.; Blasig, A.; Thies, M. C. Control of Mesophase Pitch Properties by Supercritical Fluid Extraction. *Carbon* **1998**, *36*, 953-961.

[16]Kalback, W. M.; Romine, H. E.; Bourrat, X. M. Solvated Mesophase Pitches. U. S. Patent 5,538,621, July 23, 1996.

CHAPTER 4

STRUCTURAL IDENTIFICATION OF THE MONOMERIC CONSTITUENTS OF PETROLEUM PITCH

Introduction

Petroleum pitches are generally obtained from the thermal polymerization of fluid catalytic cracking (FCC) decant oil,[1-2] a byproduct of the catalytic cracking of the heavy gas oil fraction of crude oil. These polycyclic aromatic hydrocarbons (PAHs) possess a higher degree of alkyl substitution[3] than do coal-tar pitches and are more likely to contain methylene bridges[4] between carbon atoms. As shown in Fig. 4.1a and validated independently by several researchers,[3,5-8] these materials are oligomeric in nature, with a molecular weight (mol wt) range that extends from about 200 to more than 1000.[5-6]

Petroleum pitches can serve as raw materials for a wide variety of carbon products, including high thermal conductivity carbon fibers[9], carbon electrodes[10], activated carbon fibers[11-12], and as an impregnating agent for the densification of carbon-carbon composites.[13] For several of the above applications, conversion of the initially isotropic pitch to a liquid-crystalline mesophase must also be carried out. Although the mol wt and structure of pitches are known to play a role in their suitability for a given application,[5,9,14] this understanding has been limited because of an inability to properly characterize the constituents of pitch.

The focus of this paper was the identification of the key monomeric species that exist in a representative petroleum pitch. For this study, Marathon M-50[15] was chosen,

primarily because of its similarity to its well-known predecessor, Ashland A-240, which had a significant commercial market for many years. Monomer information about such pitches is needed to assist in the prediction of the molecular structures of the dimer and higher-order oligomers present in petroleum pitch, as these oligomers serve as key precursors for the advanced carbon materials described above.

Previous work in this area has been limited. The material safety data sheet (MSDS)[15] for M-50 pitch reports the concentration of several persistent bioaccumulative toxins (PBTs) present in M-50 pitch. However, this list is hardly inclusive, as the vast majority of species present in M-50 pitch are not on the list (only 6 of the many species present in M-50 pitch, covering four mol wt values, are listed). Fetzer and Kershaw[16] used reversed-phase high performance liquid chromatography with photodiode array/UV-Vis detection (HPLC/PDA) to identify individual species present in chromatographic fractions of pitch, but it was a coal-tar pitch that was studied. Basova et al.[17] used gas chromatography-mass spectrometry (GC-MS) to identify monomeric components present in both a Korean and a Conoco petroleum pitch. However, because no pre-fractionation of the pitches was carried out, good resolution between the pitch components was not achieved. In addition, as shown by Wang and Eser,[18-19] GC-MS is less suitable for species above a mol wt of 250, as they become increasingly difficult to resolve and elute. Furthermore, it is not always possible to distinguish between the mass spectra of PAH isomers.

Also of interest to us is the characterization of FCC decant oils. Because they are the starting materials for petroleum pitch, we would expect similarities between these species

and the monomer fraction of pitch, although the processes of polymerization and volatilization would also be expected to create differences. Eser and co-workers[18-19] used GC-MS, HPLC/PDA, HPLC/MS/MS, and laser desorption/mass spectrometry (LD/MS) to characterize a number of different decant oils. Their work showed that the decant oils were composed primarily of methylated derivatives of 3-6 ring PAHs, including phenanthrene, pyrene, chrysene, perylene, the benzopyrene isomers, and benzo[ghi]perylene.

Recently, Cristadoro et al.[3] investigated the monomer and dimer fractions of M-50 petroleum pitch, using both fractionation and characterization techniques. Monomer- and dimer-rich fractions of the pitch were isolated using the method of dense-gas extraction (DGE).[20-21] These fractions were then characterized by a wide variety of techniques, including matrix-assisted, laser desorption and ionization, time-of-flight mass spectrometry (MALDI-TOF-MS, or MALDI for short), MALDI-post-source decay (MALDI-PSD, or PSD for short), UV-Vis spectrophotometry, IR spectroscopy, and ^{1}H NMR. A key finding of this work was that the major PAH species comprising M-50 monomer are grouped into well-defined, Gaussian-like distributions, with each distribution consisting of an aromatic backbone substituted (primarily β–) with from 0 to 6 methyl (and occasionally ethyl) groups. However, the molecular structures of the aromatic backbones could not be unambiguously established.

Thus, the motivation of this paper was twofold: (1) identify all important PAH series present in the monomer fraction of M-50 pitch (which comprises almost half of the entire pitch[22]), and (2) unambiguously determine the PAH backbones for these monomer series.

To meet these objectives, narrow mol wt fractions of M-50 monomer separated by DGE were fractionated into even narrower cuts by preparatory-scale gel permeation chromatography (prep-scale GPC). The degree of separation achieved by this 2-step process was such that many of the individual species present were then isolated, and thus could be analyzed. MALDI-TOF-MS and PSD were subsequently applied to selected fractions, and the species therein, to obtain mol wt distribution (MWD), molecular structure, and series distribution information. Finally, these fractions were analyzed by reversed-phase HPLC/PDA in order to conclusively identify the major PAH backbone species present in M-50 monomer.

Experimental

Materials

M-50 petroleum pitch (CAS number 68187-58-6), was obtained from Marathon Petroleum Company LLC. The mass spectrum of M-50, as obtained by MALDI, is given in Fig. 4.1a. The broad peaks are classified in terms of oligomers as follows: monomer (210 to 388 Da), dimer (388 to 645 Da), trimer (645 to 890 Da), and tetramer (890 to 1120 Da). As described below in Section 2.2, three narrow mol wt, monomeric fractions of the M-50 pitch were isolated by DGE and also served as materials in this study.

Both toluene (HPLC grade, CAS number 108-88-3) and methanol (HPLC grade, CAS number 67-56-1) were obtained from Fisher Scientific and used as DGE solvents. GPC-grade 1,2,4-trichlorobenzene (TCB; CAS number 120-82-1) was used as the mobile phase for the prep- scale GPC work and was supplied by J. T. Baker. For reversed-phase

HPLC work, the solvents acetonitrile (ACN; HPLC grade, CAS number 75-05-8) and water (HPLC grade, CAS number 7732-18-5) were supplied by Burdick and Jackson and Thermo Scientific, respectively. For UV-Vis spectrophotometry, the solvent cyclohexane (CAS number 110-82-7) was obtained from Sigma-Aldrich. For MALDI and PSD analyses, the matrix 7,7,8,8-tetracyanoquinodimethane (TCNQ; CAS number 1518-16-7) was supplied by TCI America.

DGE Pitch Cuts

It was necessary to generate 3 fractions of M-50 monomer in order to subsequently isolate and characterize species in the low (270 Da and below), medium (270-335 Da), and high (335-388 Da) mol wt ranges. These fractions are shown as DGE Pitch Cuts 1-3 in Figs. 4.1b-4.1d, respectively. DGE Pitch Cut 1 was produced from M-50 pitch by continuous DGE using methanol as the extractive solvent. The column operating pressure was 36 bar; a positive temperature gradient was employed throughout the DGE column such that the bottom section was held at 330° C, the middle at 350° C, and the top at 380° C. Additional details are given elsewhere.[3] DGE Pitch Cut 2, identified as Fraction 4 in Table 3 of Reference 3, was generated from M-50 pitch via semibatch DGE, using toluene as the extractive solvent. Column temperatures and pressures were the same as those described above.

DGE Pitch Cut 3 was also prepared by semibatch DGE, but here the feed charge was not M-50 but rather a dimer-rich cut containing only the heaviest monomer species. Conditions were the same as described for DGE Pitch Cut 2 above, except that the

column operating pressure was 29 bar. The dimer-rich charge itself was produced from M-50 pitch using a 2-column DGE process, as developed by Cervo and Thies,[21] and is referred to in that paper as "Dimer-Rich B". Details of its preparation are given there.

Prep-scale GPC

Prep-scale GPC was used to produce narrow mol wt fractions from DGE Pitch Cuts 1-3, using hot TCB as the mobile phase at 140° C. Hutchenson et al.[23] found that nearly ideal elution behavior (i.e., a linear relationship between log mol wt and retention time) was obtained when hot TCB was used as the mobile phase. In addition, past solubility tests[24] indicate that petroleum pitch is > 99% soluble in hot TCB over a concentration range of 1.5 to 100 mg/mL.

An analytical-scale Waters Alliance GPCV 2000 was used for our work; several modifications were made so that it could be used on the preparative scale. In particular, both the viscometer and the solvent preheater loop were bypassed so that the mobile-phase flow rate could be increased to 2.50 mL/min at an operating temperature of 140° C. Two prep-scale GPC columns (25 mm i. d. x 300 mm long) were supplied by Polymer Laboratories. The packing material was PLgel, with a particle size of 10 microns. The packing material in the first column (part number PL1210-6125) had a pore size of 500 Å, and in the second column (part number PL1210-6120) a pore size of 100 Å.

DGE Pitch Cuts 1 and 2 were prepared for GPC fractionation at a concentration of 10 mg/mL. Because of its scarcity, DGE Pitch Cut 3 was prepared at a lower concentration of 3 mg/mL. It should be noted that higher pitch concentrations were

generally avoided, so as to extend column life and maintain column efficiency[25]. Samples were filtered with a 0.5 micron filter prior to injection and were then injected at a volume of 1.08 mL. Sample collection was achieved by diverting the column eluent stream to a Waters Fraction Collector (model 1). A refractive index (RI) detector was used to obtain the GPC chromatogram.

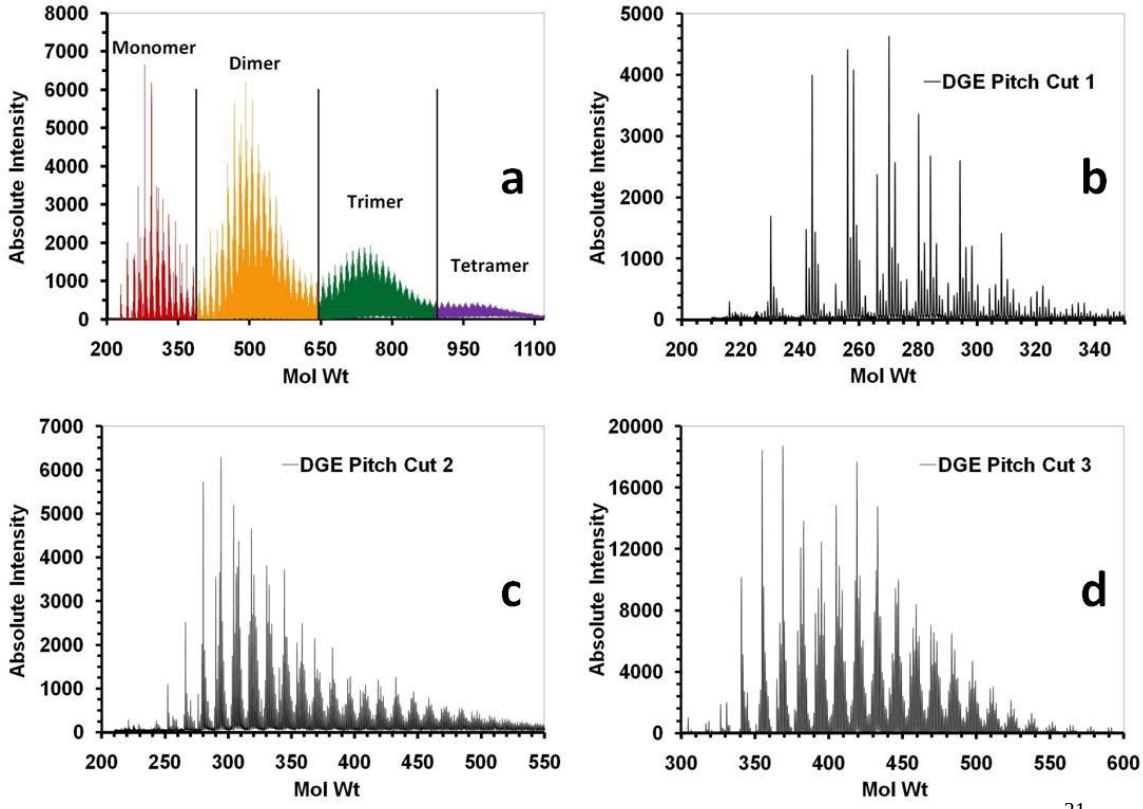

Figure 4.1. MALDI spectra for (a) M-50 pitch (adapted from Cervo and Thies[21]), (b) DGE Pitch Cut 1, (c) DGE Pitch Cut 2, and (d) DGE Pitch Cut 3.

Pitch species identification by HPLC/PDA

HPLC/PDA was used to unequivocally identify species present in three pitch fractions: DGE Pitch Cut 1 and GPC Fractions 6 and 7, which were isolated from DGE Pitch Cut 2 via prep-scale GPC. Analysis of DGE Pitch Cut 1 was conducted by

dissolving the sample in pure ACN at a concentration of 7 mg/mL. Such a high concentration had to be used because of the relatively broad MWD of this sample. With the two GPC fractions being of much narrower MWD, a lower concentration could be used. GPC Fractions 6 and 7 were first dried at 110° C and 15 torr to remove the GPC mobile phase TCB. These samples were then dissolved in 1 mL of ACN at a concentration of about 0.1 mg/mL, and water was subsequently added to the solution until the UV-Vis absorbance measured from 0.5 to 0.6 absorption units at 254 nm and an optical path length of 1.0 cm. Typically, the ACN:water ratio was 1:1 by volume. The sample volume injected onto the HPLC column was 10 μL in all cases.

Reversed-phase HPLC was chosen in favor of normal-phase HPLC because of the success of previous workers[16,26-29] in utilizing this technique to separate mixtures of PAHs with mol wts up to 450 Da. In this study, a C18 reversed-phase column (length 250 mm, inner diameter 4.6 mm, particle size 5μm) manufactured by Restek (Pinnacle II, product no. 9214575) was used. Gradient elution was performed with a quaternary Waters model 626 solvent pump at a mobile phase flow rate of 1.0 mL/min. The initial makeup of the mobile phase was 30/70 v/v ACN/water on a volume basis, with the mobile-phase ACN concentration being increased by 1 volume percent per minute until pure ACN was the eluent. The run then proceeded for 20 more min under these conditions. A Waters model 996 PDA detector was used to obtain the UV-Vis spectra of the eluent stream exiting the column every 1.0 second. In order to identify the species eluting from the HPLC column, these UV-Vis spectra were compared to those of reference standards. Standards were prepared using water/ACN solutions at

concentrations identical to those of the HPLC mobile phase at elution time. For the analysis of DGE Pitch Cut 1, fractions of the column eluent were collected for subsequent MALDI analysis; typically, the collection time was 20 seconds.

MALDI and PSD

Both MALDI and PSD analyses were performed on GPC fractions 1-12, using a Bruker Daltonics Autoflex MALDI mass spectrometer with a 337 nm nitrogen laser. MALDI was used to obtain the absolute mol wt of the most prominent species in a given fraction; this was followed up with PSD on said prominent species, in order to obtain specific molecular structure information on those species. We have previously described the operating parameters for both MALDI and PSD in detail elsewhere.[3] Because of the low amounts of pitch present in each collected GPC or HPLC eluent fraction (the amounts are on the order of micrograms), the following sample preparation procedure was followed in order to minimize the amount of sample necessary for MALDI analysis. First, the TCNQ matrix was ground into a fine powder with the aid of a ball mill (Thermo Electron Corp., Wig-L-Bug model). The TCNQ was then deposited onto the MALDI target using water spotting, a method developed by our group at Clemson.[6] Next, a drop of the fraction of interest was spotted onto the dried TCNQ. Once dry, the sample was subjected to analysis.

UV-Vis Spectrophotometry

UV-Vis analyses were performed on selected GPC fractions with a Spectral Instruments 400 Series spectrophotometer. The GPC fractions were first dried for 2 hours at a temperature of 120° C and a pressure of 25 torr to remove the TCB mobile phase. They were then re-dissolved in cyclohexane, the UV cutoff wavelength of which is ~ 110 nm less than that of TCB. This action allowed measurement of the UV-Vis spectrum over a wider wavelength range. The concentrations of the GPC fractions analyzed were controlled by adding cyclohexane solvent until the maximum light absorbance value recorded fell below 2.0.

Results and Discussion

MALDI-PSD to detect alkyl substitution on PAH backbones

The MALDI spectrum of M-50 pitch, focused in on the monomer region, is given in Fig. 4.2. Previous work[3] had established that species within the monomer fraction could be resolved into Gaussian signal distributions, created by the distribution of methyl (and, to a limited extent, ethyl) substituents on base PAH backbone(s) of a given mol wt. The "blue rectangle" series originating at a mol wt of 216 Da, the "yellow ring" series beginning at 228 Da, and the "orange dot" series starting at 252 Da had been previously identified, but their PAH backbones had not been identified. In addition, for the "yellow ring" series the extent of alkyl substitution could not be determined because we were not able to properly isolate the species in this series for PSD analysis.

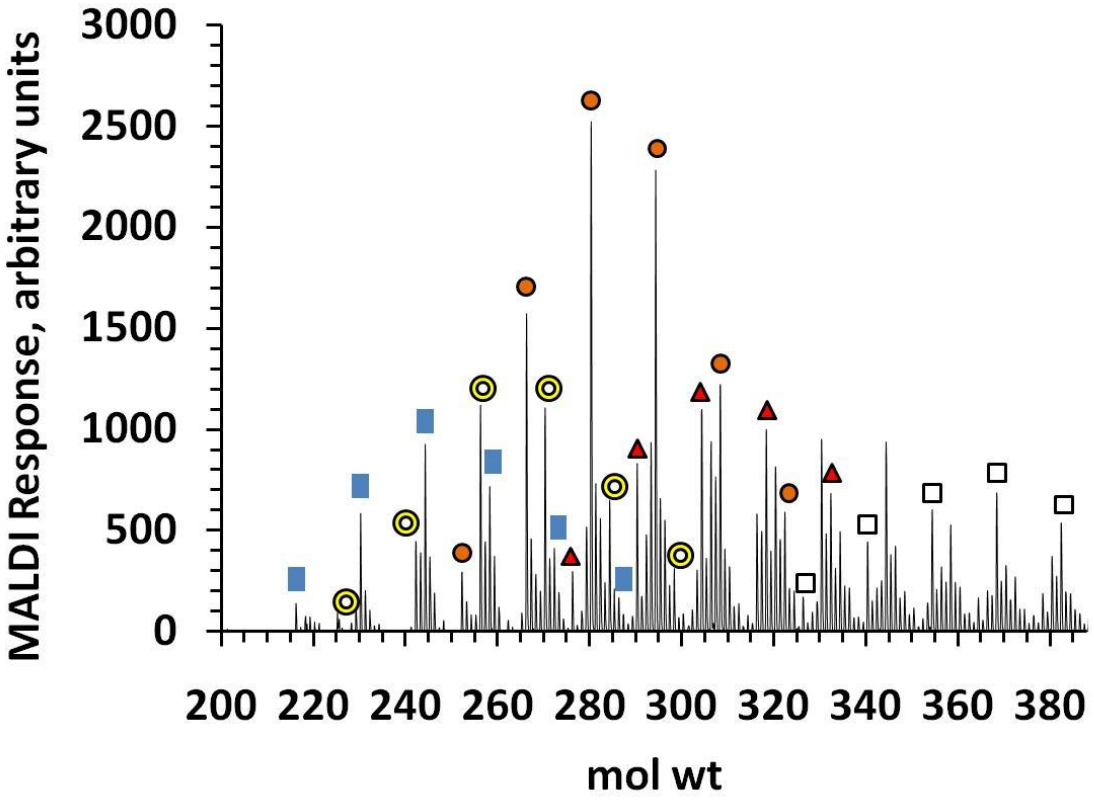

Figure 4.2. MALDI of M-50 pitch, showing only the mol wt range of the monomer (210-388 Da). Major species signal distributions are highlighted. The "red triangle" and "white square" signal distributions are new and have not been previously reported.

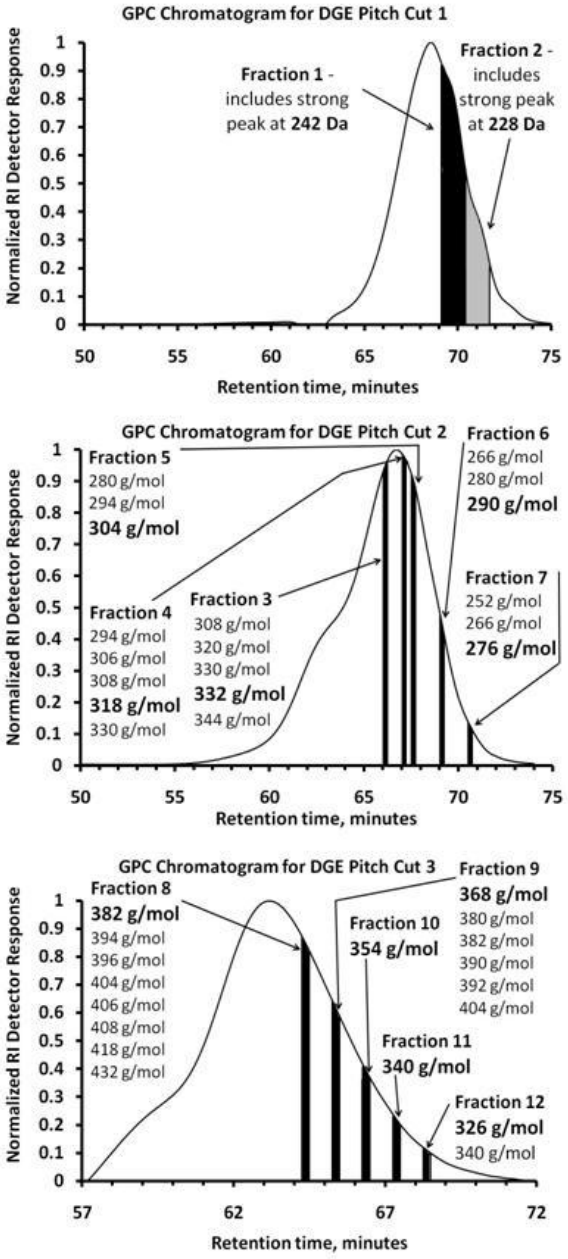

Figure 4.3. GPC chromatograms for DGE Pitch Cuts 1-3, showing the 12 fractions that were selected for MALDI-PSD analyses. The actual, isolated species selected for analysis are denoted in boldface.

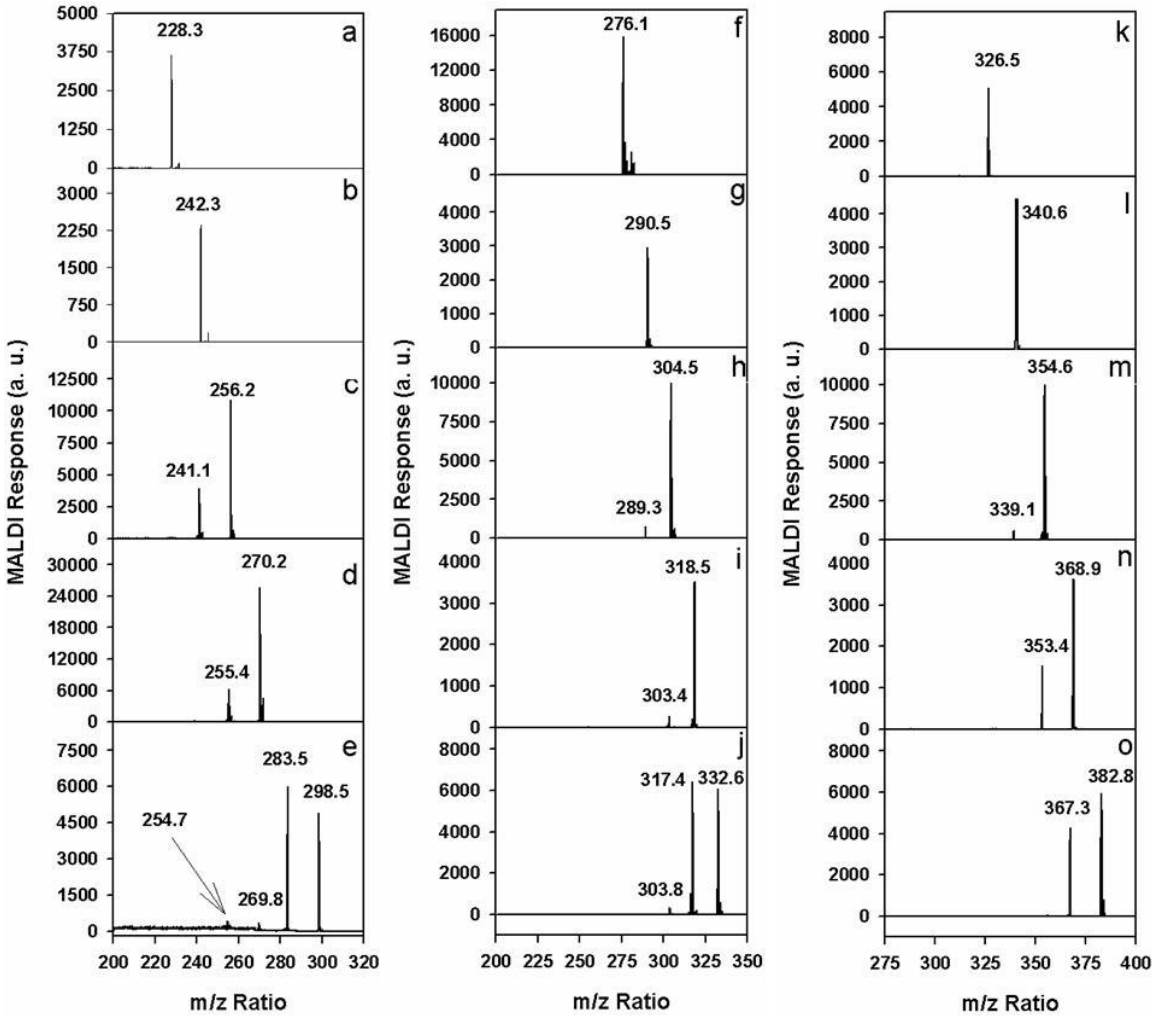

Figure 4.4. MALDI-PSD fragmentation analyses for individual species comprising the "yellow ring" (left panel), "red triangle" (center panel) and the "white square" (right panel) distributions given in Fig. 4.2. PSD spectra given in a-b and f-o were obtained from GPC Fractions 1-12 (see Fig. 4.3), while the spectra given in c-e were previously obtained[3] directly from DGE Pitch Cut 1.

In this work, such isolation was successfully carried out by applying prep-scale GPC to DGE Pitch Cuts 1-3. Up to 31 GPC fractions per DGE Pitch Cut, with each cut typically being collected over a 15-second time span, were obtained. MALDI analysis was performed on these fractions, and 12 of these had prominent peaks well-isolated such that they could be readily analyzed for molecular structure by PSD (see Fig. 4.3). PSD

analyses for the "yellow ring" signal distribution in Fig. 4.2 are given in Figs. 4.4a-e. Analysis of the m/z = 228 peak in Fraction 1 and of the 242 peak in Fraction 2 produced no fragmentation (Figs. 4.4a and 4.4b), a result that occurs for both unsubstituted aromatics and those substituted with only a single methyl group. However, for parent peaks of m/z = 256.2, 270.2, and 298.5 (see Figs. 4.4c-e), signals with m/z of 15 less than those of the parent species appear, with the magnitude (and thus, the abundance of these peaks) generally increasing with respect to the mol wt of the parent species. As PSD mass spectra for PAHs containing two or more methyl groups exhibit strong peaks at m/z of 15 less than the parent species,[30-31] we conclude that the yellow-ring series originates with an unsubstituted PAH backbone with a mol wt of 228.3 Da, with the other species containing the same PAH backbone with varying degrees of methylation (in Fig. 4.4e, the peak at m/z = 269.8 indicates the limited presence of ethyl groups).

Investigation of the "red triangle" series in Fig. 4.2, beginning with the signal at m/z = 276.1 Da, was carried out by PSD analysis of GPC Fractions 3-7, obtained by fractionating DGE Pitch Cut 2 (see Fig. 4.3). Neither the fragmentation analyses for the parent species of 276.1 Da (see Fig. 4.4f) nor 290.5 Da (see Fig. 4.4g) display peaks indicating the loss of a methyl group, a result consistent with what has already been observed for the "blue rectangle", "yellow ring", and "orange dot" signal distributions. PSD analyses for the parent species of mol wts 304.5 (Fig. 4.4h) and 318.5 Da (Fig. 4.4i) exhibit peaks indicating the presence of a de-methylated species, while the fragmentation pattern for the parent species of mol wt 332.6 Da (Fig. 4.4j) indicates the presence of both methyl and ethyl groups. These trends, as well as the increase in size of the de-

methylation peak with increasing degree of alkylation, indicate that the "red triangle" series of Fig. 4.2 is comprised of one or more PAH backbones of mol wt 276 that possess varying degrees of alkylation.

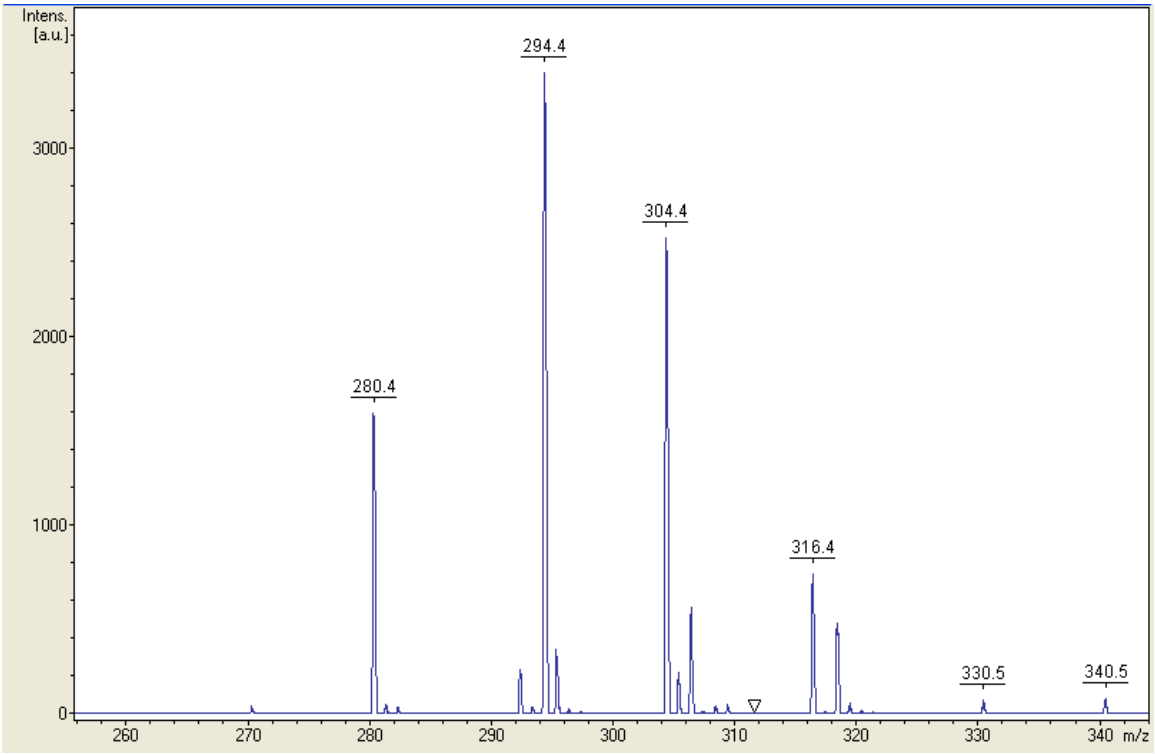

Figure 4.5. MALDI spectrum for GPC Fraction 5, produced by prep-scale fractionation of DGE Pitch Cut 1.

The benefits of our 2-step fractionation process (i.e., DGE followed by GPC) are illustrated by examining the MALDI (not PSD) spectrum for GPC Fraction 5, given in Fig. 4.5. Because the signal at m/z = 304.4 is strong with respect to the nearest neighboring species (i.e., those within m/z = 5-10), the Bradbury-Nielsen ion gate is able to fully screen out all ions except those arising from the parent species.

PSD of the "white square" signal distribution was carried out by analysis of GPC Fractions 8-12, obtained by the fractionation of DGE Pitch Cut 3 (see Fig. 4.3). The trends observed in the fragmentation analyses for this series (see Fig. 4.4k-o) are similar to those observed for the two signal distributions previously described herein. However, it is notable that no peak indicating the presence of de-ethylated ions is observed in Fig. 4.4o, in which case the peak denoting the parent ion appears at m/z = 382.8 Da.

HPLC/PDA Analysis of Monomer Pitch Fractions

HPLC/PDA Analysis of DGE Pitch Cut 1

In Fig. 4.6, the HPLC chromatogram for DGE Pitch Cut 1 is given. Here, the average absorbance from 200 to 450 nm (the range of wavelengths over which light absorption is measured) was plotted against time in order to allow for the fact that different compounds absorb strongly at different wavelengths. For unsubstituted PAHs, only matching of each unknown UV-Vis spectrum against the molecular "fingerprint" of a reference standard is necessary for unequivocal compound identification. The UV-Vis spectrum for species A, which elutes at a time of 48.82 min (see Fig. 4.6), is compared to that of pyrene in Fig. 4.7a. The results indicate close agreement between the two spectra. For the eluting species, the rise in baseline between 250-260 nm is due to the presence of a co-eluting species (likely an alkylated phenanthrene). In addition, the UV-Vis spectrum for species B, which elutes at a time of 51.52 min, compares favorably to that of triphenylene in Fig. 4.7b. These two spectral matches confirm, for the first time, that triphenylene and pyrene are present in M-50 pitch. Chrysene (species C) and

benz[a]anthracene (species D), both of mol wt 228, were detected in comparable amounts (see Fig. 4.6). Other unsubstituted aromatics detected in DGE Pitch Cut 1, albeit at lower levels than the aforementioned species, include phenanthrene (mol wt 178), anthracene (178), benzo[b]fluorene (216), benzo[e]pyrene (252), and benzo[a]pyrene (252).

The discovery that pyrene (mol wt 202) is present in considerable amounts in DGE Pitch Cut 1 suggests that the "blue rectangle" signal distribution in Fig. 4.2, originating at 216 Da, actually begins at 202 Da. Therefore, we sought to determine if methylpyrenes and other alkylpyrenes were present in DGE Pitch Cut 1.

Two of the strongest peaks in Fig. 4.6, labeled A1 and A2, occur at 54.77 and 55.86 min. The UV-Vis spectra obtained at both of these elution times are similar to that of pyrene (see Figs. 4.8a and 4.8b). A slight bathochromic (that is, in the direction of higher wavelengths) shift in the UV-Vis spectra of these eluting compounds relative to that of pyrene is observed, as would be expected for an alkylpyrene;[26] furthermore, the mol wts of species A1 and A2 (see Figs. 4.8d and 4.8e) as observed by MALDI correspond in both cases to that of a methylpyrene (216 Da). Finally, comparison of the UV-Vis spectra to the reference spectra of Freidel[32] confirms that peak A1 represents 4-methylpyrene and peak A2 2-methylpyrene.

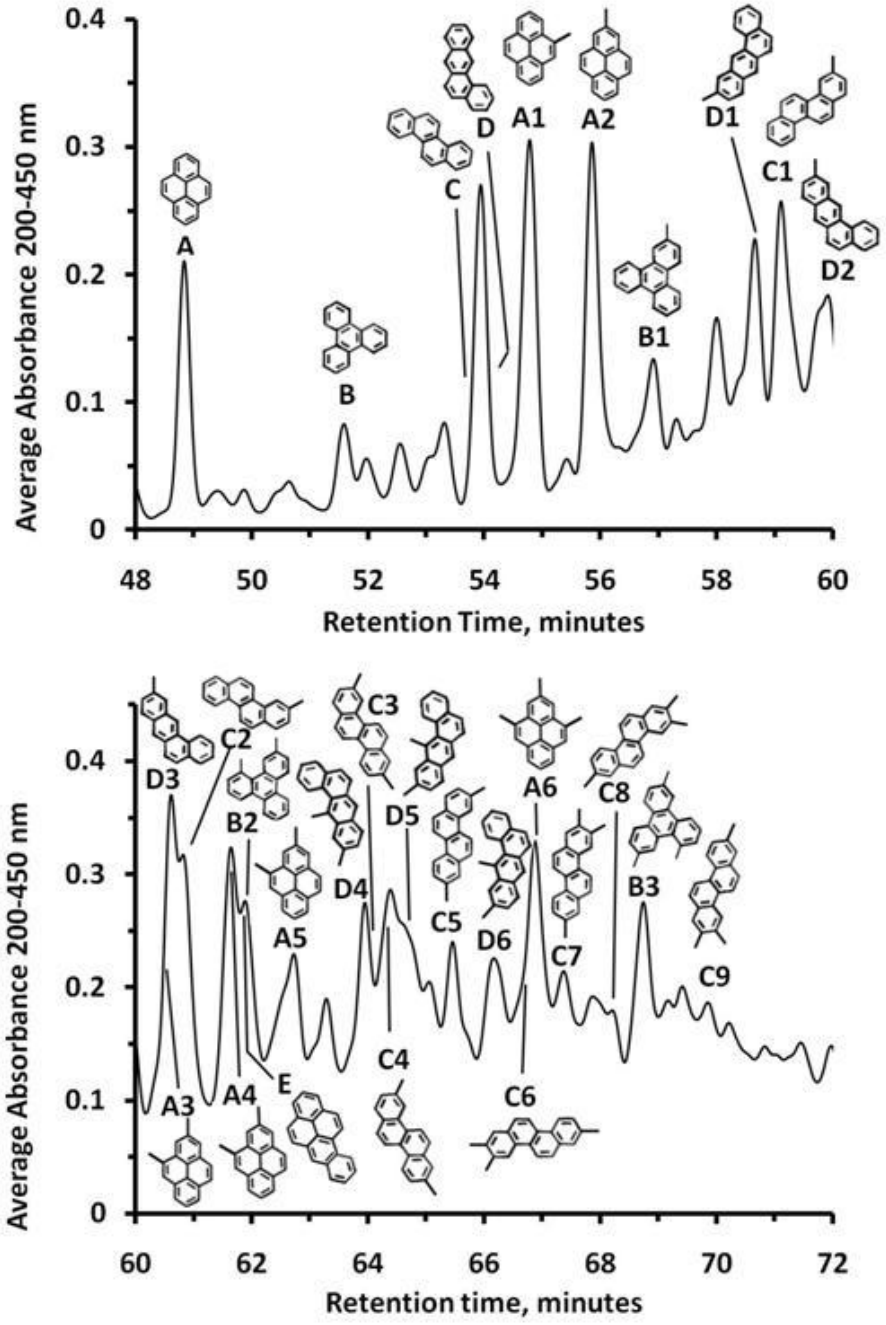

Figure 4.6. HPLC chromatogram for DGE Pitch Cut 1. Results are plotted against average UV-Vis absorption from 200 to 450 nm. All molecules corresponding to peaks in the "A series" have pyrene (mol wt 202) backbones with varying degrees of alkylation. The aromatic backbones of species in the B, C, and D peak series are triphenylene, chrysene, and benz[a]anthracene (all of mol wt 228), respectively. Species E is benzo[a]pyrene (mol wt 252).

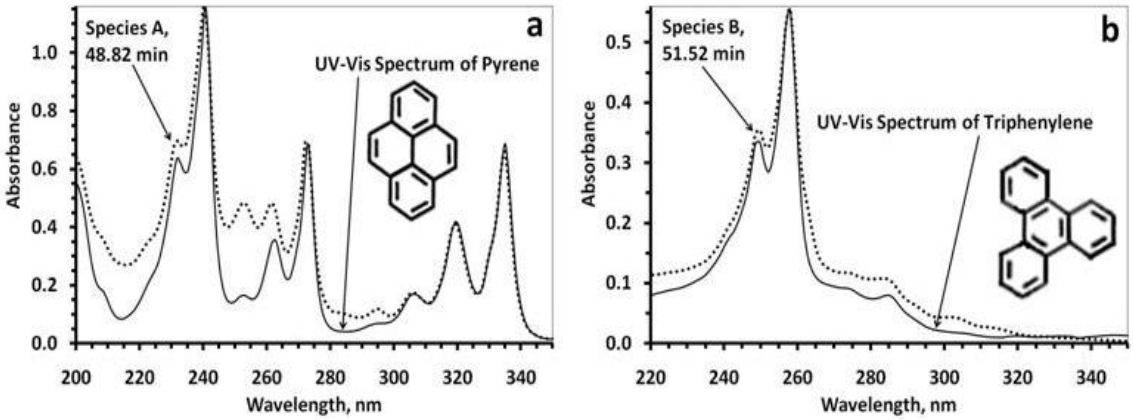

Figure 4.7. UV spectral matches, obtained by HPLC/PDA, of (a) species A with pyrene and (b) species B with triphenylene reference standards.

Another sharply absorbing peak in Fig. 4.6 is peak A4, obtained at an elution time of 61.62 min. Its UV-Vis spectrum also bears a strong similarity to that of pyrene. Considering that the major peak in the MALDI spectrum for the HPLC fraction collected between 61.50 and 61.83 min has a mol wt of 230 Da (see Fig. 4.8f), we conclude that peak A4 is a dimethylpyrene. The additional MALDI peaks in Fig. 4.8f at 252 and 256 Da are, based on both HPLC elution times and UV absorbance behavior, believed to be benzo[a]pyrene and dimethyltriphenylene, respectively.

As shown in Fig. 4.6, other dimethylpyrenes (species A3 and A5), as well as trimethylpyrene (species A6) were also detected in DGE Pitch Cut 1. Thus, it is now clear that the "blue rectangle" signal distribution of Fig. 4.2, originally tentatively identified as a series of benzo[b]fluorene (mol wt 216) and alkylbenzo[b]fluorenes,[3] is composed primarily of pyrene and alkylpyrenes. On the other hand, the "yellow ring" signal distribution in Fig. 4.2 consists mainly of triphenylene, chrysene, benz[a]anthracene, and their alkylated derivatives (species B1-B3, C1-C9, and D1-D6 in

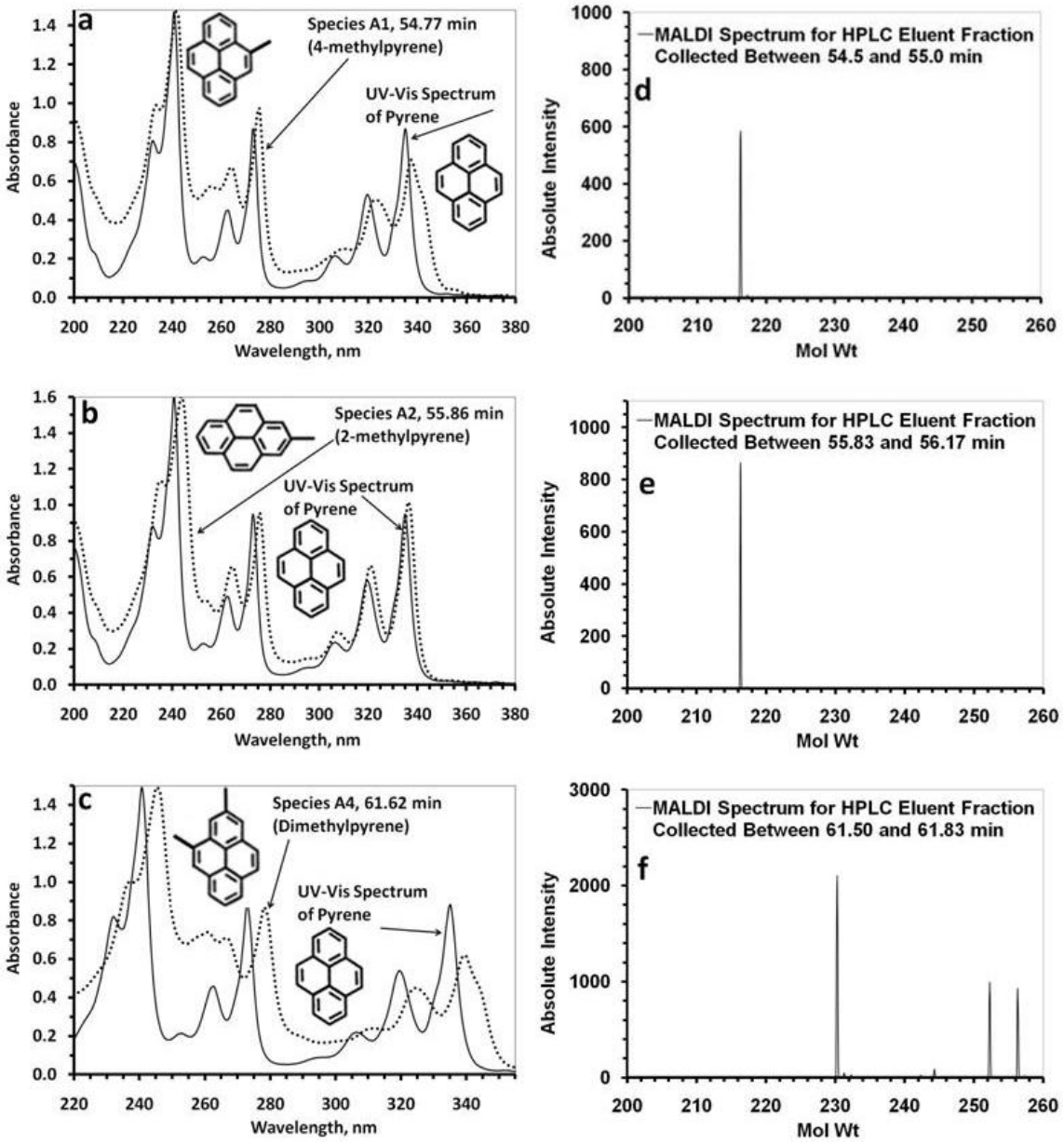

Figure 4.8. UV-Vis spectra for alkylpyrenes (panels a-c) are similar to those for the reference standard for pyrene, with a slight bathochromic shift. The MALDI spectra in panels d-f give the mol wts of the respective alkylpyrenes.

Fig. 4.6, respectively). Here, triphenylene is a species that was not previously identified. The exact locations of the methyl groups on all but 2-methylpyrene and 4-methylpyrene are unknown. Therefore, based on our previous results,[3] in Figs. 4.6 and 4.8c we have placed the majority of methyl groups on aromatic carbons located at a position β from an "inner" aromatic carbon atom that bonds with 3 other carbon atoms.

HPLC/PDA Analysis of GPC Fractions 6 and 7 from DGE Pitch Cut 2

In order to identify the specific components that comprise the "orange circle" and "red triangle" signal distributions in the monomer fraction of M-50 pitch (see Fig. 4.2), GPC Fractions 6 and 7 (see Fig. 4.3) were subjected to reversed-phase HPLC analysis. The MALDI spectrum for Fraction 6 (Fig. 4.9b) shows the presence of major species at 266, 280, and 290 Da, while Fraction 7 (Fig. 4.9a) includes major species at 252, 266, and 276 Da. GPC Fractions 6 and 7 are particularly suitable for HPLC analysis because only a few species are present; therefore, co-eluting peaks were less likely to interfere in the HPLC chromatograms for these fractions.

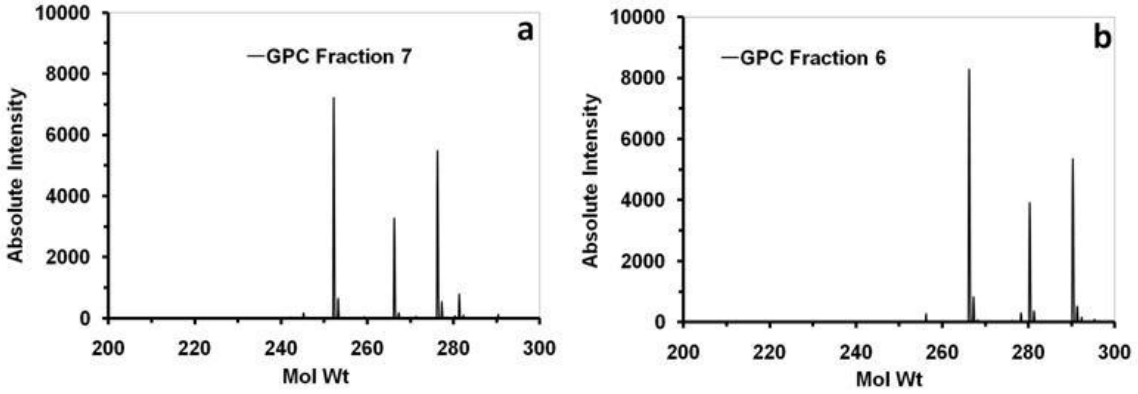

Figure 4.9. MALDI spectra for (a) GPC Fractions 7 and (b) 6, from prep-scale GPC.

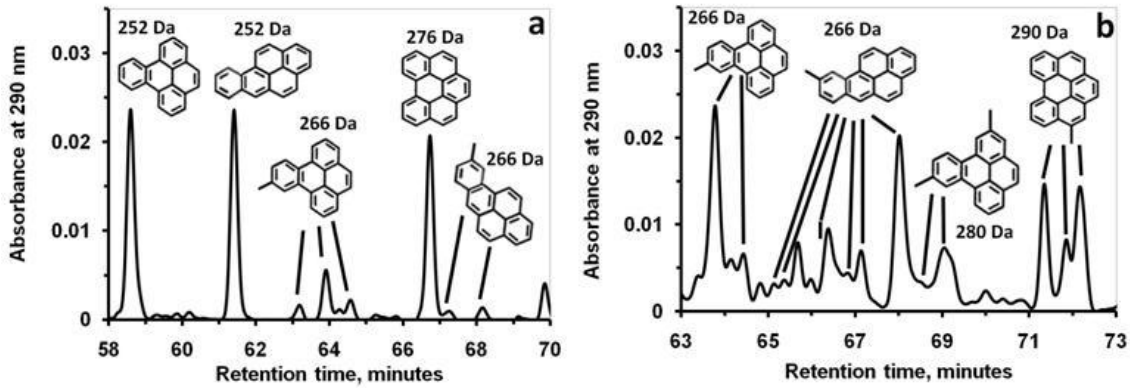

Figure 4.10. HPLC chromatograms for (a) GPC Fractions 7 and (b) 6.

HPLC chromatograms for GPC Fractions 7 and 6 are given in Figs. 4.10a and 4.10b, respectively. For Fraction 7 (Fig. 4.10a), the component eluting at 58.58 min is identified as benzo[e]pyrene (mol wt 252) in Fig. 4.11a. Similarly, the species eluting at 61.38 min is identified as benzo[a]pyrene (mol wt 252) in Fig. 4.11b, and the third prominent peak in Fraction 7 (Fig. 4.10a) at 66.72 min is identified as benzo[ghi]perylene (mol wt 276) in Fig. 4.11c. Also shown at 68.02 min and 63.73 min, and identified by their UV-Vis spectra in Figs. 4.11d and 4.11e, are two methylbenzopyrenes. The PAHs perylene (mol wt 252), and anthanthrene (mol wt 276) are also present, albeit at lower levels (in both cases, the maximum absorbance values measured were ~ 0.010). The PAHs benzo[b]fluoranthene and benzo[k]fluoranthene (both of mol wt 252 Da), each of which contain a 5-membered ring, are also present in trace amounts.

Referring next to the HPLC chromatogram for Fraction 6 (Fig. 4.10b), it is interesting to note that the UV-Vis spectra obtained at an elution time of 63.73 min are virtually identical for both GPC Fractions 6 and 7 (Fig 4.10a and 4.10b), although the magnitude of response is noticeably greater in the case of GPC Fraction 6. These UV-

Vis spectra are very similar to that of benzo[e]pyrene (mol wt 252; see Fig. 4.11a), with a bathochromic shift of 1-2 nm being observed. Furthermore, the only major peak appearing in the MALDI spectra for both fractions (see Figs. 4.9a and 4.9b) has a mol wt of 266 Da. Therefore, the species in question must be a methylated benzo[e]pyrene. However, it is not possible to deduce the location of the alkyl substituent because of the lack of UV-Vis reference spectra for the benzo[e]pyrene isomers.

Another peak, occurring at an elution time of 68.02 min, also appears in the HPLC chromatograms for both GPC Fractions 7 and 6 (Figs. 4.10a and 4.10b). The resulting UV-Vis spectra are virtually identical and are very similar to benzo[a]pyrene, with a light bathochromic shift of 1-2 nm being observed (Fig. 4.11e). Again, the only major peak that appears in the MALDI spectra for both fractions corresponds to 266 Da, so the eluting component must be a methylbenzo[a]pyrene.

Based on the results in Fig. 4.11, then, we conclude that the "orange circle" signal distribution for the monomer fraction in Fig. 4.2 consists primarily of the benzopyrenes and their alkylated derivatives. Perylene and its alkylated derivatives are also present, but in significantly lower quantities.

The final peaks of interest in the HPLC chromatogram of GPC Fraction 6 occur in the 71-72.5 min range, with the UV-Vis spectrum for the peak at 71.33 min being virtually identical to that of the reference standard for benzo[ghi]perylene (Fig. 4.11f). Furthermore, we have a MALDI peak in Fraction 6 (Fig. 4.9b) at 290 Da, so the compound must be a methylbenzo[ghi]perylene. In addition, the HPLC chromatogram peaks at 71.89 and 72.22 min also exhibit UV-Vis spectra that are virtually identical to

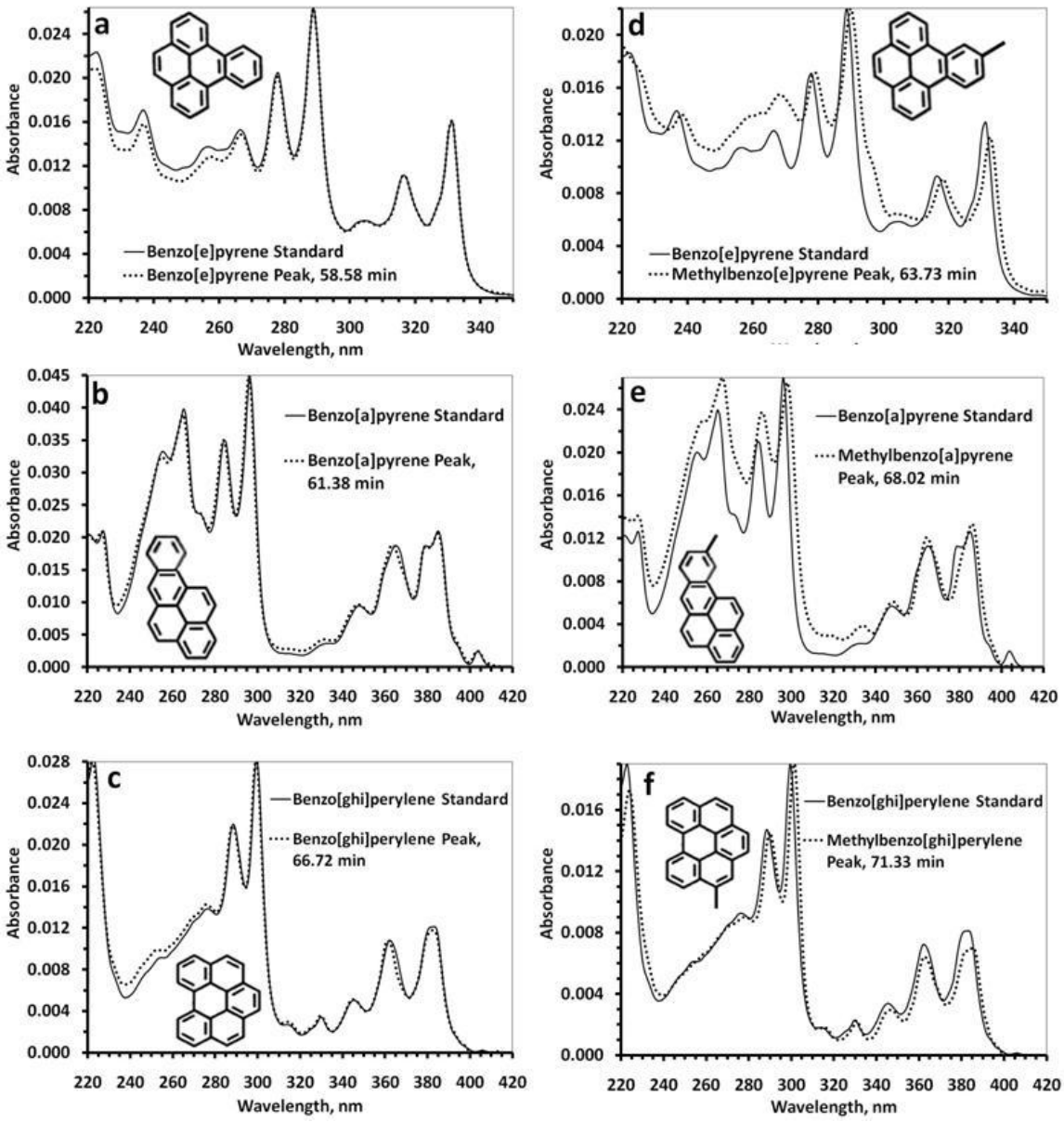

Figure 4.11. UV-Vis spectra indicate that the PAHs (a) benzo[e]pyrene, (b) benzo[a]pyrene, and (c) benzo[ghi]perylene are predominant in GPC Fraction 7, while these same aromatic backbones, albeit with methyl substitution, are predominant in GPC Fraction 6.

benzo[ghi]perylene. Thus, we conclude that there are 3 distinguishable isomers of methylbenzo[ghi]perylene present in this mixture, all with a mol wt of 290 Da. Methylanthanthrene, eluting at ~ 73.3 min, was also detected in trace amounts.

In summary, considering both the UV-Vis results above and the PSD results in Figs. 4.4f-j, we can now unambiguously identify the "red triangle" series in Fig. 4.2 as benzo[ghi]perylene and its alkylated (primarily methylated) derivatives.

UV-Vis Analysis of GPC Fraction 11 from DGE Pitch Cut 3

HPLC/PDA analysis of the GPC fractions isolated from DGE Pitch Cut 3 (see Fig. 4.3) were not carried out because of the scarcity of reference UV-Vis standards for these higher mol wt species that make up the "high end" of the monomer fraction of M-50 pitch (see Fig. 4.2). Thus, having only conventional UV-Vis spectrophotometry available for analysis, we selected a fraction containing one dominant species. As shown in Fig. 4.12a, the MALDI spectrum for GPC Fraction 11 exhibits a major peak at m/z 340. Based on the PSD analysis for the "white square" series in Fig. 4.2, we would expect the peak at m/z 340 (Fig. 4.4l) to denote a species containing one methyl group.

Of the multitude of possible PAH backbone structures that exist for a molecular weight of 326 Da, only a handful of UV-Vis reference standards exist. None of these are a fingerprint match for the spectrum given in Fig. 4.12b. Nevertheless, the characteristic features of the spectrum are somewhat surprising, as there are none of the strong absorption peaks that are observed above 300 nm for the larger PAHs with mol wts near 326 Da, such as peropyrene (326), the dibenzoperylenes (326 or 352), anthanthrene

(276), and the dibenzoanthanthrenes (376).[33] (One exception might be naphtho[8,1,2-bcd]perylene (326), which, because of the presence of peaks at 440 and 470 nm in Fig. 4.12b, may be present in small amounts.) Instead, the UV-Vis spectrum for GPC Fraction 11 exhibits a strong drop-off in absorption above 300 nm and weak absorbance at higher wavelengths.

Such characteristics are much more consistent with the UV-Vis spectra for fluoranthenoids,[33-34] that is, those PAHs containing one five-membered ring[27] (those containing only 6-membered aromatic rings are known as benzenoid PAHs). Examples of fluoranthenoid PAHs with mol wts at or near 326 for which reference spectra are available include 2.3-o-phenylene-4.5-benzopyrene (mol wt 326), 2,3-o-phenylenepyrene (276), 2.3,5.6-dibenzofluoranthene (302), and naphtho-(2'.3':10.11)-fluoranthene (302). Unfortunately, none of these are a particularly good match for the UV-Vis spectrum shown in Fig. 4.12b, but that could be partly because GPC Fraction 11 contains species other than the 340 Da moiety.

Another possibility is that the PAH backbone molecule at 326 Da is actually a dimer created by the condensation reaction of pyrene (mol wt 202) and naphthalene (mol wt 128), joined together by a 5-membered ring. Although naphthalene is not present in M-50 monomer, it has been shown by Eser and co-workers[18-19] to be a component of FCC decant oil, the starting material used for M-50 pitch. However, no reference UV-Vis spectrum exists for examination of this hypothesis. In summary, while it is highly probable that the PAH backbone for the "white square" distribution of Fig. 4.2 is a fluoranthenoid PAH, the actual structure cannot be identified.

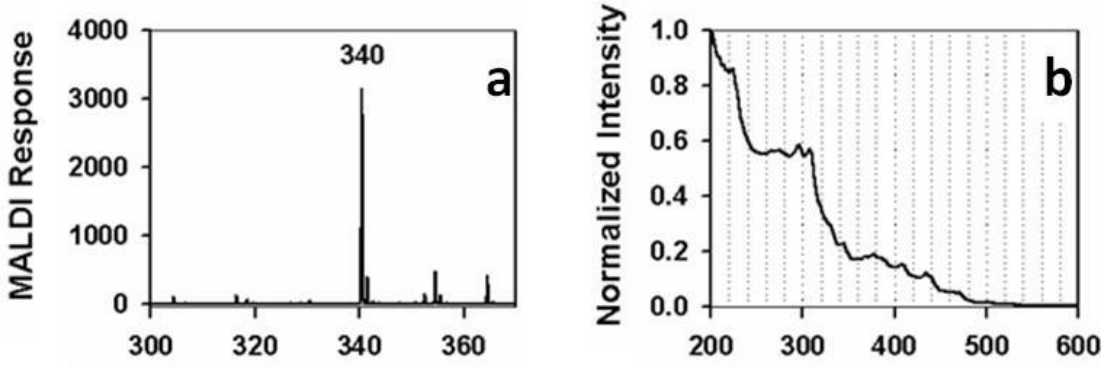

Figure 4.12. (a) MALDI spectrum and (b) UV-Vis spectrum for GPC Fraction 11.

The Molecular Composition of the Monomer Fraction of M-50 Pitch

The results of this study are summarized in Table 4.1 and Fig. 4.13. In Table 4.1, we list the compounds that make up each of the PAH series distributions given in Fig. 4.2 for the monomer fraction of M-50 pitch (except for the "white square" series, for which positive identification of the PAH backbone(s) was not achieved). In Fig. 4.13, we give the specific PAH backbones comprising each of the distributions. Estimates of species concentrations, in both wt % and mol %, as a percentage of the M-50 monomer range investigated, are also given in Table 4.1. These estimates were obtained by (1) determining the monomer area under the MALDI spectrum between 216 and 318 Da, (2) assuming that area fraction and mol fraction are approximately equal for each species (in Chapter 5, this approximation is somewhat reliable for PAHs of mol wt > 250 Da, but alkylated PAHs are overcounted relative to non-alkylated PAHs), (3) calculating a number average mol wt (M_n = 280) for the above mol wt range, and (4) calculating a wt % for the species mol wts investigated in this study. Results indicate that we are identifying more than 40 wt % of the individual pitch species present in the monomer in the 216-318 mol wt range.

Table 4.1. Major species present in the monomeric fraction of M-50 pitch, their concentrations in the entire pitch, and their associated signal distributions (see Fig. 4.2).

Compound	Wt % in Monomer	Mol % in Monomer	Mol Wt (Da)	Signal Distribution
Methylpyrenes (A1, A2)	0.16	0.20	216	Blue rectangle
Dimethylpyrenes (A3, A4, A5)	1.28	1.56	230	Blue rectangle
Trimethylpyrene (A6)	2.16	2.48	244	Blue rectangle
Triphenylene, chrysene, benz[a]anthracene (B, C, D)	0.11	0.14	228	Yellow ring
Methylated triphenylene, chrysene, and benz[a]anthracene (B1, C1, C2, D1, D2, D3)	1.02	1.18	242	Yellow ring
Dimethylated triphenylene, chrysene, and benz[a]anthracene (B2, C3, C4, C5, D4, D5, D6)	2.69	2.94	256	Yellow ring
Trimethylated triphenylene and chrysene (B3, C6, C7, C8, C9)	3.30	3.42	270	Yellow ring
Benzopyrenes	0.18	0.20	252	Orange circle
Methylbenzopyrenes	4.20	4.42	266	Orange circle
Dimethylbenzopyrenes	8.45	8.45	280	Orange circle
Trimethylbenzopyrenes	7.88	7.51	294	Orange circle
Methylbenzo[ghi]perylenes	2.68	2.59	290	Red triangle
Dimethylbenzo[ghi]perylenes	4.15	3.83	304	Red triangle
Trimethylbenzo[ghi]perylenes	3.74	3.30	318	Red triangle
Totals	42.0	42.2	-------	----------

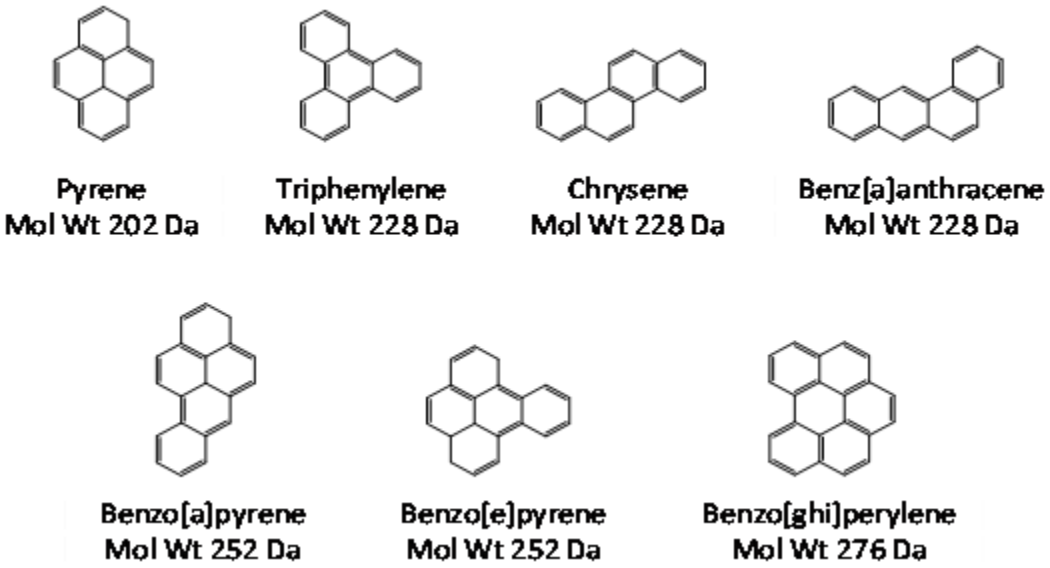

Figure 4.13. The dominant PAH backbones comprising the signal distributions in the monomer fraction of M-50 pitch (see Fig. 4.2 and Table 4.1).

Conclusions

By combining our macroscopic dense-gas extraction (DGE) process with conventional analytical-scale fractionation and characterization techniques, we have been able to obtain a high degree of separation between M-50 pitch components, such that individual species can be unambiguously identified. Thus, we now have a fairly complete picture of the dominant molecular species that comprise the monomer fraction of a representative petroleum pitch. In each of 5 series that were identified, the first molecule was found to be a bare PAH backbone, with the succeeding molecules in each series having increasing degrees of methyl substitution. The dominant PAH backbones include pyrene (mol wt 202); chrysene, benz[a]anthracene, and triphenylene (mol wt

228); benzo[a]pyrene and benzo[e]pyrene (mol wt 252); and benzo[ghi[perylene (mol wt 276). Composition estimates were also obtained and indicate that the most abundant species are those with from one to three methyl groups. Only when a high level (i.e., > 3) of methyl substitution was already present on a molecule was any evidence of ethyl substitution observed.

As FCC decant oil is the starting material for producing petroleum pitch, one would expect similarities in the molecular composition of the monomer fraction and of decant oil. To a significant extent, this assumption is correct. However, several PAHs identified in our work, including the relatively abundant triphenylene, benz[a]anthracene, and their alkylated derivatives, have not been reported in decant oil. In addition, M-50 monomer contains neither naphthalene nor its alkylated derivatives, which have been detected in decant oil.[18-19]

Finally, the fact that species with mol wts as high as those observed in the "white square" series distribution in Fig. 4.2 (mol wt 326-382) have not been reported in decant oil indicates that this series may not be monomeric at all, but the result of the condensation of naphthalene and pyrene to form a small dimer. The elucidation of the structure of the dimer and trimer species in M-50 pitch is the subject of Chapter 6.

References

[1]Malone, D. P.; Moore, H. F.; Kiser, M. D. Method of Producing High Softening Point Pitch. U. S. Patent 7220348, 2007.

[2]Hanks, R. S.; Friley, B. K. Pitch Precursor Production by Distillation. U. S. Patent 5429739, 1995.

[3]Cristadoro, A.; Kulkarni, S. U.; Burgess, W. A.; Cervo, E. G.; Räder, H. J.; Müllen, K.; Bruce, D. A.; Thies, M. C. Structural Characterization of the Oligomeric Constituents of Petroleum Pitches. *Carbon* **2009**, *47*, 2358-2370.

[4]Kershaw, J. R.; Black, K. J. T. Structural Characterization of Coal-Tar and Petroleum Pitches. *Energy Fuels* **1993**, *7(3)*, 420-25.

[5]Greinke, R. A. Kinetics of Petroleum Pitch Polymerization by Gel Permeation Chromatography. *Carbon* **1986**, *24(6)*, 677-86.

[6]Edwards, W. F.; Jin, L.; Thies, M. C. MALDI-TOF Mass Spectrometry: Obtaining Reliable Mass Spectra for Insoluble Carbonaceous Pitches. *Carbon* **2003**; *41*, 2761-68.

[7]Greinke, R. A.; Lewis, I. C. Carbonization of Naphthalene and Dimethylnaphthalene. *Carbon* **1984**, *22(3)*, 305-314.

[8]Lewis, I. C. Thermal Polymerization of Aromatic Hydrocarbons. *Carbon* **1980**, *18(3)*, 191-196.

[9]Beauharnois, M. E.; Edie, D. D.; Thies, M. C. Carbon Fibers from Mixtures of AR and Supercritically Extracted Mesophases. *Carbon* **2001**, *39*, 2101-2111.

[10]Schulz, D. A. Fuel Cell Electrode. U. S. Patent 3960601, 1976.

[11]Mochida, I.; Kawano, S. Capture of Ammonia by Active Carbon Fibers Further Activated with Sulfuric Acid. *Ind. Eng. Chem. Res.* **1991**, *30*, 2322-2327.

[12]Kim, M. C.; Eom, S. Y.; Ryu, S. K.; Edie, D. D. Reformation of Naphtha Cracking Bottom Oil for the Preparation of Carbon Fiber Precursor Pitch. *Korean Chem. Eng. Res.* **2005**, *43*, 745.

[13]Tzeng, S.-S.; Pan, J.-H. Densification of Two-Dimensional Carbon/Carbon Composites by Pitch Impregnation. *Mater. Sci. Eng. A* **2001**, *316*, 127-134.

[14]Mochida, I.; Yoon, S. H.; Korai, Y.; Kanno, K.; Sakai, Y.; Komatsu, M. Carbon Fibers from Aromatic Hydrocarbons. *CHEMTECH* **1995**, *25*, 29-37.

[15]MSDS for M-50 Pitch. <http://www.mapllc.com/MSDS/0275MAR019.pdf>

[16]Fetzer, J. C.; Kershaw, J. R. Identification of Large Polycyclic Aromatic Hydrocarbons in a Coal Tar Pitch. *Fuel* **1995**, *74(10)*, 1533-36.

[17]Basova, Y. V.; Edie, D. D.; Lee, Y. S.; Reid, L. K.; Ryu, S. K.; Effect of Precursor Composition on the Activation of Pitch-Based Carbon Fibers. *Carbon* **2004**, *42*, 485-495.

[18]Wang, G.; Eser, S. Molecular Composition of the High-Boiling Components of Needle Coke Feedstocks and Mesophase Development. *Energy Fuels* **2007**, *21*, 3563-72.

[19]Eser, S.; Wang, G. A Laboratory Study of a Pretreatment Approach to Accommodate High-Sulfur FCC Decant Oils as Feedstocks for Commercial Needle Coke. *Energy Fuels* **2007**, *21*, 3573-82.

[20]Edwards, W. F.; Thies, M. C. Fractionation of Pitches by Molecular Weight Using Continuous and Semibatch Dense-Gas Extraction. *Carbon* **2006**, *44(2)*, 243-52.

[21]Cervo, E. G.; Thies, M. C. Control of Molecular Weight Distribution of Petroleum Pitches via Multistage Supercritical Extraction. *J. Supercrit. Fluids* **2010**, *51*, 345-52.

[22]Cervo, E. G.; Thies, M. C. Isolating Petroleum Pitch Oligomers by Continuous, Countercurrent Dense Gas Extraction. Submitted for publication to *J. Supercrit. Fluids*, 2010.

[23]Hutchenson, K. W.; Roebers, J. R.; Thies, M. C. Fractionation of Petroleum Pitch by Supercritical Fluid Extraction. *Carbon* **1991**, *29(2)*, 215-223.

[24]Geiculescu, A. C. Preparation of Petroleum Pitch Pseudocomponents by Gel Permeation Chromatography. Master Thesis, Clemson University, Clemson, SC, 1994.

[25]Dauché, F. M.; Bolaños, G.; Blasig, A.; Thies, M. C. Control of Mesophase Pitch Properties by Supercritical Fluid Extraction. *Carbon* **1998**, *36(7-8)*, 953-961.

[26]Somers, M. L.; Wornat, M. J. UV Spectral Identification of Polycyclic Aromatic Hydrocarbon Products of Supercritical 1-Methylnaphthalene Pyrolysis. *Polycyclic Arom. Compd.* **2007**, *27*, 261-80.

[27]McClaine, J. W.; Oña, J. M.; Wornat, M. J. Identification of a New $C_{28}H_{14}$ Polycyclic Aromatic Hydrocarbon as a Product of Supercritical Fuel Pyrolysis: Tribenzo[cd,ghi,lm]perylene. *J. Chromatogr. A* **2007**, *1138*, 175-183.

[28]Fetzer, J. C. The Chemistry and Analysis of Large PAHs. *Polycyclic Arom. Compd*. **2007**, *27*, 143-162.

[29]Oña, J. O.; Wornat, M. J. Identification of the $C_{30}H_{16}$ Polycyclic Aromatic Hydrocarbon Benzo[cd]naphtha[1,2,3-lm]perylene as a Product of the Supercritical Pyrolysis of a Synthetic Jet Fuel. *Polycyclic Arom. Compd*. **2007**, *27*, 165-183.

[30]CAS SciFinder. <http://www.cas.org/products/scifindr/index.html>

[31]McLafferty, F. W. *Interpretation of Mass Spectra*, 3rd ed.; University Science Books: Mill Valley (CA), 1980; p. 187.

[32]Friedel, R. A.; Orchin, M. *Ultraviolet Spectra of Aromatic Compounds*; John Wiley and Sons: New York, 1951.

[33]Clar, E. *Polycyclic Hydrocarbons*; Academic Press: London, 1964.

[34]Jacquignon, P.; Perin-Roussel, O.; Perin, F.; Chalvet, O.; Lhoste, J. M.; Mathieu, A.; Saperas, B.; Viallet, P.; Zajdela, F. Oxidation of Dibenzo[a,e]fluoranthene by Osmium Tetroxide. *Can. J. Chem.* **1975**, *53*, 1670-1676.

CHAPTER 5

ADDITIONAL DISCUSSIONS CONCERNING THE STRUCTURAL IDENTIFICATION OF THE MONOMERIC CONSTITUENTS OF PETROLEUM PITCH

This section contains additional information concerning methods used in the fractionation, identification, and quantification of the most prevalent polycyclic aromatic hydrocarbons (PAHs) in M-50 monomer. In addition, recommendations concerning the optimization of equipment performance and lifetime are made.

Extending the Lifetime of the Preparatory-Scale Gel Permeation Chromatography (Prep-Scale GPC) Fractionation Equipment

Extending Prep-Scale Column Lifetime

While performing prep-scale GPC, several precautions are taken in order to maximize column lifetime. First, in order to prevent clogging of the prep-scale columns (and subsequent column and system damage resulting from the excessive backpressure encountered in such situations), the mobile phase 1,2,4-trichlorobenzene (TCB) was filtered twice – first with a 10 micron filter at the interface between the solvent reservoir and the solvent intake line, and then with a 2 micron filter at the mobile phase pump outlet. Second, Dauché et al.[1] have observed significant loss in column efficiency after performing analytical-scale GPC experiments on petroleum pitches for only a matter of weeks. We, too, observed that the prep-scale fractionation of pitch cuts rich in the

heavier M-50 oligomers prepared at 50 mg/mL eventually results in peak tailing (after a couple dozen such fractionation experiments had been performed). Therefore, in order to maximize column lifetime, we recommend minimizing the amount of pitch fractionated in the first place. Thus, samples prepared at relatively low concentrations (~ 10 mg/mL) were typically injected into the prep-scale GPC column. As the volume of the sample injection loop used was 1.080 mL, just over 10 mg pitch were fractionated per prep-scale GPC run. Utilization of concentrations in this range results in the collection of fractions with concentrations sufficient to make feasible their subsequent characterization using matrix-assisted, laser desorption and ionization, time-of-flight mass spectrometry (MALDI), MALDI-post source decay (PSD), high performance liquid chromatography with photodiode array detection (HPLC/PDA), and stand-alone UV-Visible spectrophotometry (UV-Vis).

Modification of Alliance GPCV2000 System for Prep-Scale Applications

With the prep-scale GPC columns installed, it is necessary to bypass the viscometer, as flow rates of greater than 1.5 mL/min damage the viscometer pressure transducer. In addition, bypassing the solvent preheater loop lowers the pump backpressure. With these changes to the system, it was feasible to set the mobile phase flow rate at 2.50 mL/min at an operating temperature of 140° C. A higher flow rate is not feasible, as the pump piston seals fail and cause solvent to leak from the pump. Also, at a flow rate of > 3 mL/min, the refractive index (RI) detector flow cell could crack.

Optimizing PSD Results

It should be noted that the ability of the Bradbury-Nielsen ion gate to isolate ions of a desired mol wt may be limited if there are peaks of comparable intensity within m/z ±5-10 of each other. If there are two peaks of comparable intensity within m/z ±2 of each other, it is seldom possible to obtain a good PSD spectrum of either one without the presence of "pollution" peaks arising because of the ion gate's inability to filter out ions and fragments arising due to the other species. Because the species distributions in M-50 dimer and trimer are more uniform, with fewer peaks that are dominant with respect to their nearest neighbors, it becomes increasingly difficult to isolate the MALDI signals for a particular dimer or trimer species. Usually, in order to perform PSD on dimer and trimer species, a prep-scale GPC fractionation step is necessary in order to obtain less uniform fractions (see Fig. 4.5, Chapter 4) in which the MALDI response for the desired species is sufficiently strong (at least twice as intense) with respect to its nearest neighbors.

Procedure for Collecting Reference UV-Vis Spectra for PAHs

For the UV-Vis spectral identification of M-50 monomer compounds discussed in Chapter 4, reference UV-Vis spectra for PAHs were obtained using a Spectral Instruments model 400 series spectrophotometer. The PAH reference standards pyrene (CAS 129-00-0, > 99.0 % purity) and triphenylene (CAS 217-59-4, 98.5 % purity) were obtained from Fluka, while the PAHs anthracene (CAS 120-12-7, 99.9+ % purity),

phenanthrene (CAS 85-01-8, 99.5+ % purity), benzo[b]fluorene (CAS 243-17-4, 98 % purity), chrysene (CAS 218-01-9, 98 % purity), benz[a]anthracene (CAS 56-55-3), benzo[a]pyrene (CAS 50-32-8, 97 % purity), perylene (CAS 198-55-0, 99+ % purity), and benzo[ghi]perylene (CAS 191-24-2, 98 % purity) were obtained from Aldrich. Benzo[e]pyrene (CAS 192-97-2, neat) was supplied by Supelco.

UV-Vis spectra are obtained by dissolving the standard of interest in a solvent at low (on the order of 0.1 mg/mL) concentration. Reference spectra for such PAHs are readily available.[2,3] However, as indicated in Fig. 5.1, the choice of solvent impacts the location of the absorption peaks on the UV-Vis spectrum. The peak maxima in the UV-Vis spectrum for pyrene in an 80:20 (by volume) mixture of acetonitrile (ACN) and water (with a mixture refractive index of 1.34) occur at absorption wavelengths of 320 and 335 nm. Using TCB (refractive index 1.57) as the UV-Vis solvent instead of the ACN/water mixture causes the peak maxima to shift in the direction of higher wavelengths, to 326 and 342 nm.

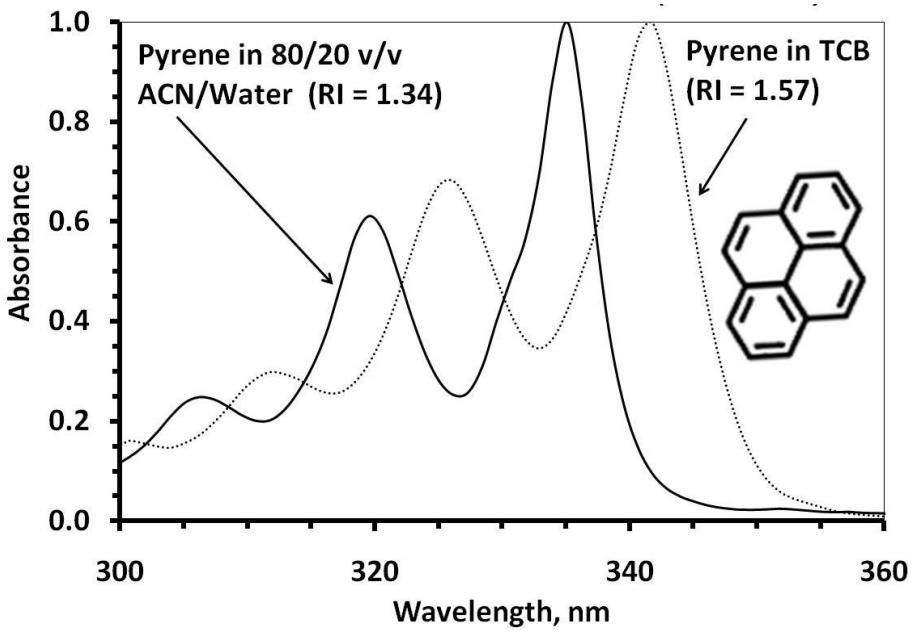

Figure 5.1. Comparison of UV-Vis spectra for pyrene in 80:20 (by volume) ACN:water, and in TCB. An increase in the refractive index of the solvent utilized shifts the peak maxima in the direction of higher wavelength.

Therefore, we adhered to the following procedure in the identification of PAHs eluting from the HPLC column. In Chapter 4, we noted that Species A elutes at 48.82 min, at the point where the mobile phase is approximately 80:20 (by volume) ACN:water. Next, we noted that the shape of the instantaneous UV-Vis spectrum for the eluent stream taken at this time is similar to that of pyrene. Therefore, we obtained the UV-Vis spectrum for a reference standard of pyrene in an ACN/water solution of this concentration. Finally, we matched the two UV-Vis spectra in order to unequivocally confirm the presence of pyrene in M-50 pitch.

Additional MALDI and UV-Vis Spectral Justifications for Identification of Prevalent Monomer Species

In Chapter 4, we demonstrated that unsubstituted aromatics can be identified by matching the UV-Vis spectra of unknown PAHs (from the HPLC analysis of DGE Pitch Cut 1, which is shown again in Fig. 5.2) with those of known reference standards for the PAHs pyrene and triphenylene. In Fig. 5.3, additional spectral matches confirming the identities of species 1, 2, 4, and C in Fig. 5.2 are given. These unsubstituted PAHs are anthracene and phenanthrene (both mol wt 178), benzo[b]fluorene (mol wt 216), and chrysene (mol wt 228), respectively.

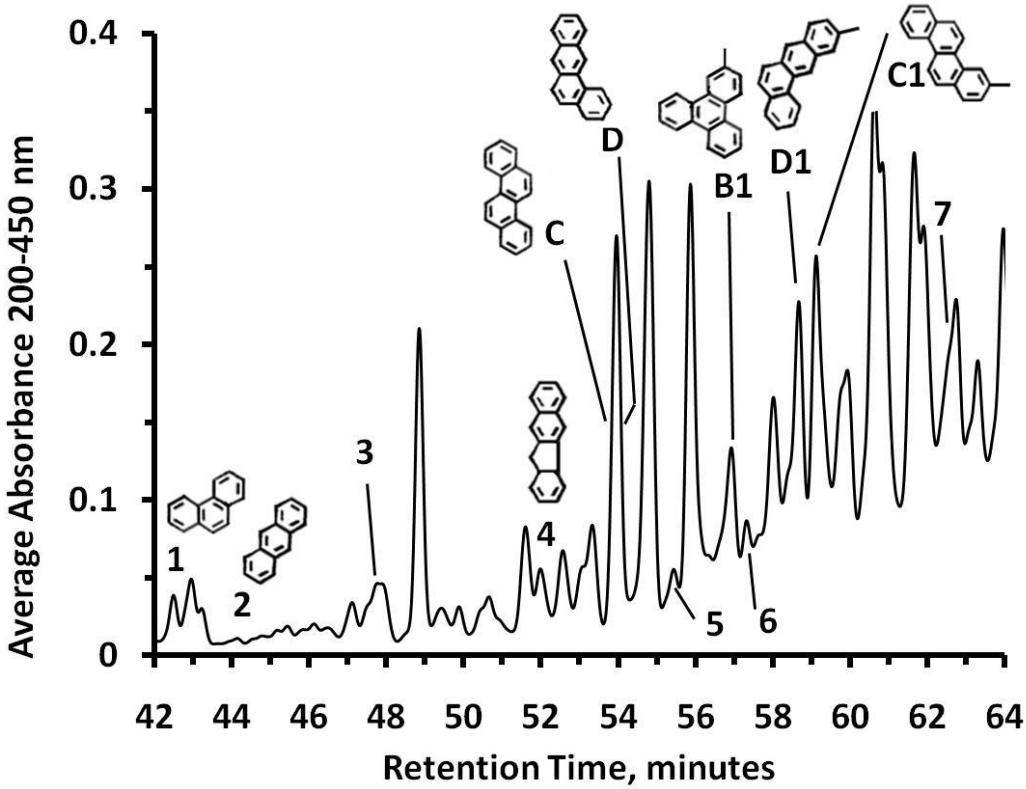

Figure 5.2. HPLC chromatogram of DGE Pitch Cut 1, with selected peaks labeled. Results are plotted against average UV-Vis absorption from 200 to 450 nm. Peaks labeled 1-7 represent M-50 monomeric constituents not appearing on Fig. 4.6 in Chapter 4; peaks labeled B1, C, C1, D, and D1 appear in both cases.

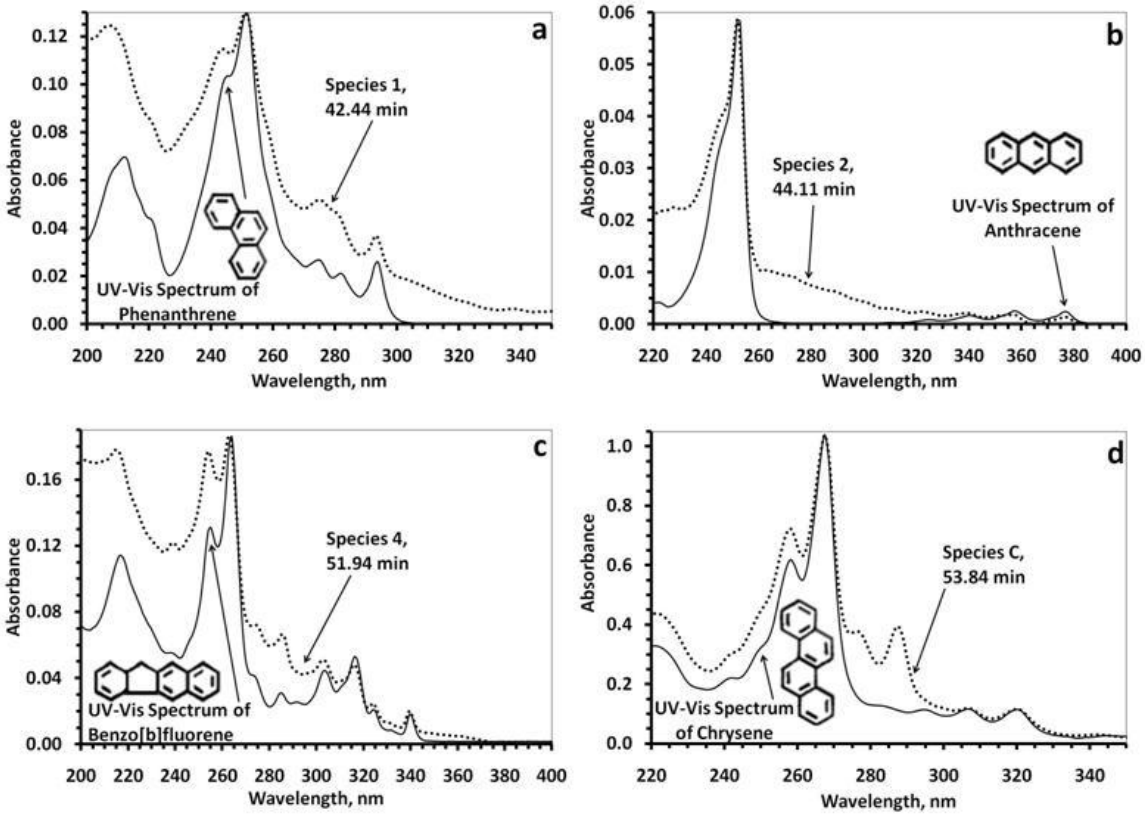

Figure 5.3. UV-Vis spectral matches indicate the presence of: (a) phenanthrene, (b) anthracene, (c) benzo[b]fluorene, and (d) chrysene in DGE Pitch Cut 1.

Meanwhile, UV-Vis spectra for PAHs containing substituent groups are similar in form to that of the unsubstituted PAH.[3,4] Each of the UV-Vis spectra in Figs. 5.4a-d, representing the peaks labeled 3, 5, 6, and 7 in Fig. 5.2, are similar to that of unsubstituted phenanthrene, but with a slight shift of the peak maxima in the direction of higher wavelengths. Unfortunately, MALDI analyses of the collected eluent fraction associated with the elution time of Species 3, 5, and 6 (see Figs. 5.4a-c) did not conclusively reveal the presence of any major peak (possibly because these fractions are dominated by phenanthrene derivatives, which exhibit little to no light absorption at 337

nm, the frequency of the MALDI N_2 laser). However, the similarity of these UV-Vis spectra with that of unsubstituted phenanthrene, along with our knowledge that M-50 monomer is composed primarily of PAH backbones possessing varying degrees of methyl (and to a limited extent, ethyl) substitution, we conclude that the UV-Vis spectra in Figs. 5.4a-c likely represent alkylphenanthrenes.

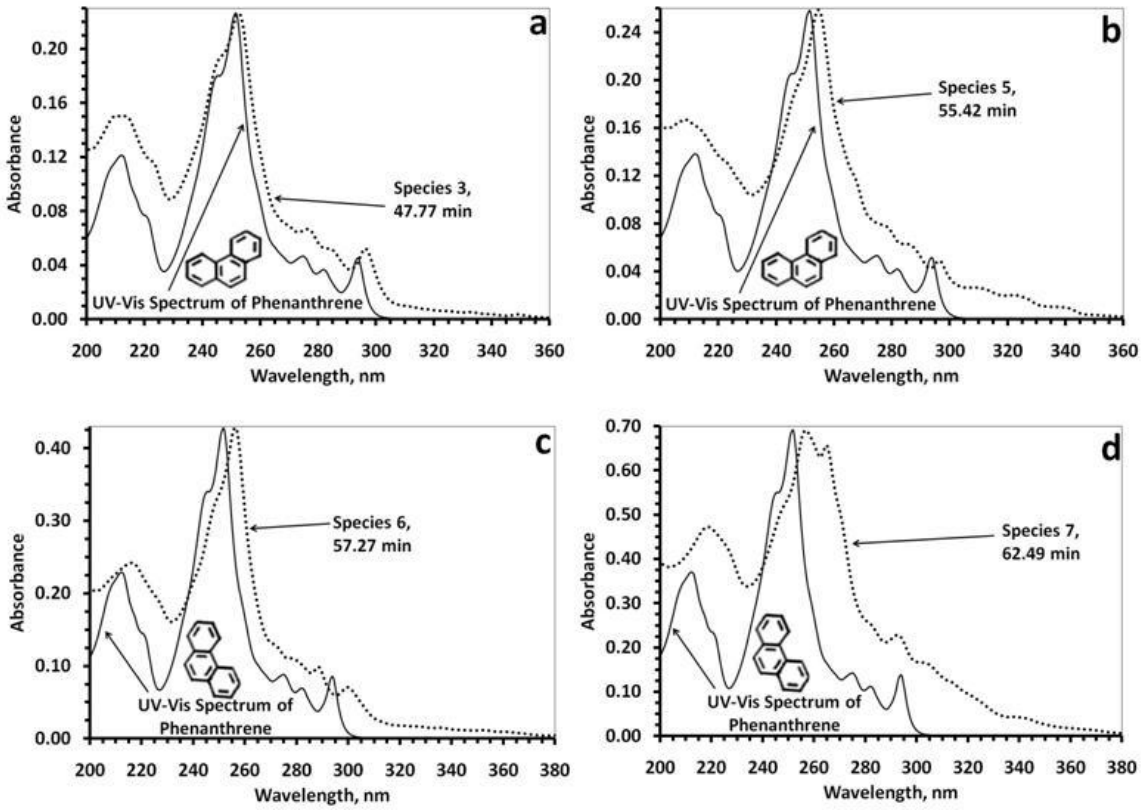

Figure 5.4. UV-Vis spectral results indicate the presence of molecules with a phenanthrene backbone in DGE Pitch Cut 1.

Meanwhile, the MALDI spectrum for the HPLC eluent fraction collected from 62.17 to 62.50 min (during which time Species 7 elutes), given in Fig. 5.5, indicates that

this fraction is comprised primarily of species of mol wt 234, 244, 250, and 256. This fraction includes the species eluting at 62.49 min that give rise to the UV-Vis spectrum in Fig. 5.4d. This UV-Vis spectrum exhibits strong absorption peaks at 257 and 265 nm, values which are similar to the wavelengths at which unsubstituted phenanthrene (mol wt 178) and benzo[b]fluorene (mol wt 216) exhibit their max UV-Vis absorbances (251 and 263 nm respectively; see Figs. 5.3a and 5.3c). Because the presence of alkyl substituent groups shifts the wavelength of maximum absorption in the direction of higher wavelengths, the major eluents at 62.49 min are likely tetramethylphenanthrene (mol wt 234) and dimethylbenzo[b]fluorene (mol wt 244). In Fig. 5.5, the MALDI response for the phenanthrene derivative of mol wt 234 is comparatively weak despite the fact that UV-Vis spectrum at 62.49 min, shown in Fig. 5.4d, is dominated by it. The weak MALDI response is likely because phenanthrene and its derivatives would not be expected to strongly absorb light (or even absorb light at all!) at 337 nm, the frequency of the MALDI laser. Notably, it was not possible to conclusively verify the presence and mol wts of phenanthrene derivatives in other HPLC eluent fractions by MALDI.

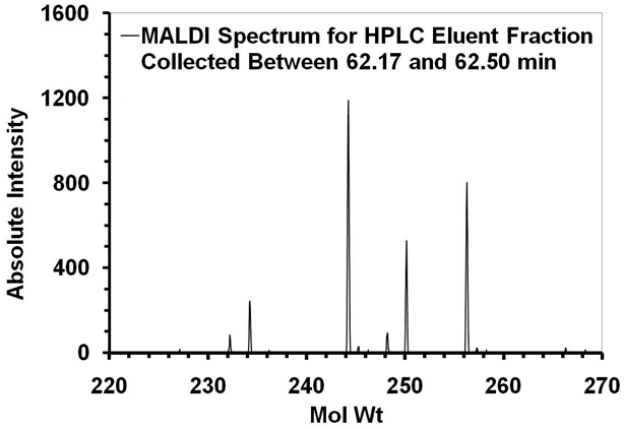

Figure 5.5. MALDI spectrum for HPLC eluent fraction containing Species 7; peak at m/z = 234 corresponds to mol wt of phenanthrene molecule containing 4 methyl groups.

More alkylated PAHs are identified in Fig. 5.6. The UV-Vis spectrum, collected at the maximum for peak B1 (see Fig. 5.2), shown in Fig. 5.6a is very similar to that of triphenylene. A bathochromic shift of 1-2 nm relative to that of the unsubstituted triphenylene is observed. The MALDI spectrum in Fig. 5.6d indicates that this species has a mol wt of 242 Da. Therefore, this species is methyltriphenylene.

The UV-Vis spectrum for the peak labeled D1 (see Fig. 5.2), eluting at 58.66 minutes, is given in Fig. 5.6b. It is similar to that of benz[a]anthracene, while the baseline elevation in the range 250-260 nm is due to the presence of a co-eluting species. Again, a bathochromic shift of 1-2 nm is observed, relative to the absorption spectrum of unsubstituted benz[a]anthracene. The MALDI spectrum given in Fig. 5.6e indicates that the fraction collected between 58.50 and 58.83 minutes contains species of mol wt 230 and 242. A species of 242 Da corresponds to a methylated benz[a]anthracene.

The UV-Vis spectrum given in Fig. 5.6c is similar to that of chrysene, but shifted ~ 2 nm in the direction of higher wavelengths. The peak at 290 nm is due to the presence of the co-eluting species benzo[e]pyrene, which absorbs UV-Vis radiation strongly at this wavelength. Continuing the trend observed for species B1 and D1, the UV-Vis spectrum taken at the max of peak C1 (see Fig. 5.2) exhibits a bathochromic shift of 1-2 nm relative to that of the unsubstituted chrysene. The MALDI mass spectrum given in Fig. 5.6f indicates the presence of species of 242 Da and 252 Da in the fraction collected from 58.83 to 59.17 min elution time. The species corresponding to peak C1 is therefore methylchrysene. Benzo[e]pyrene (mol wt 252) absorbs strongly at 290 nm; this is the identity of the co-eluent.

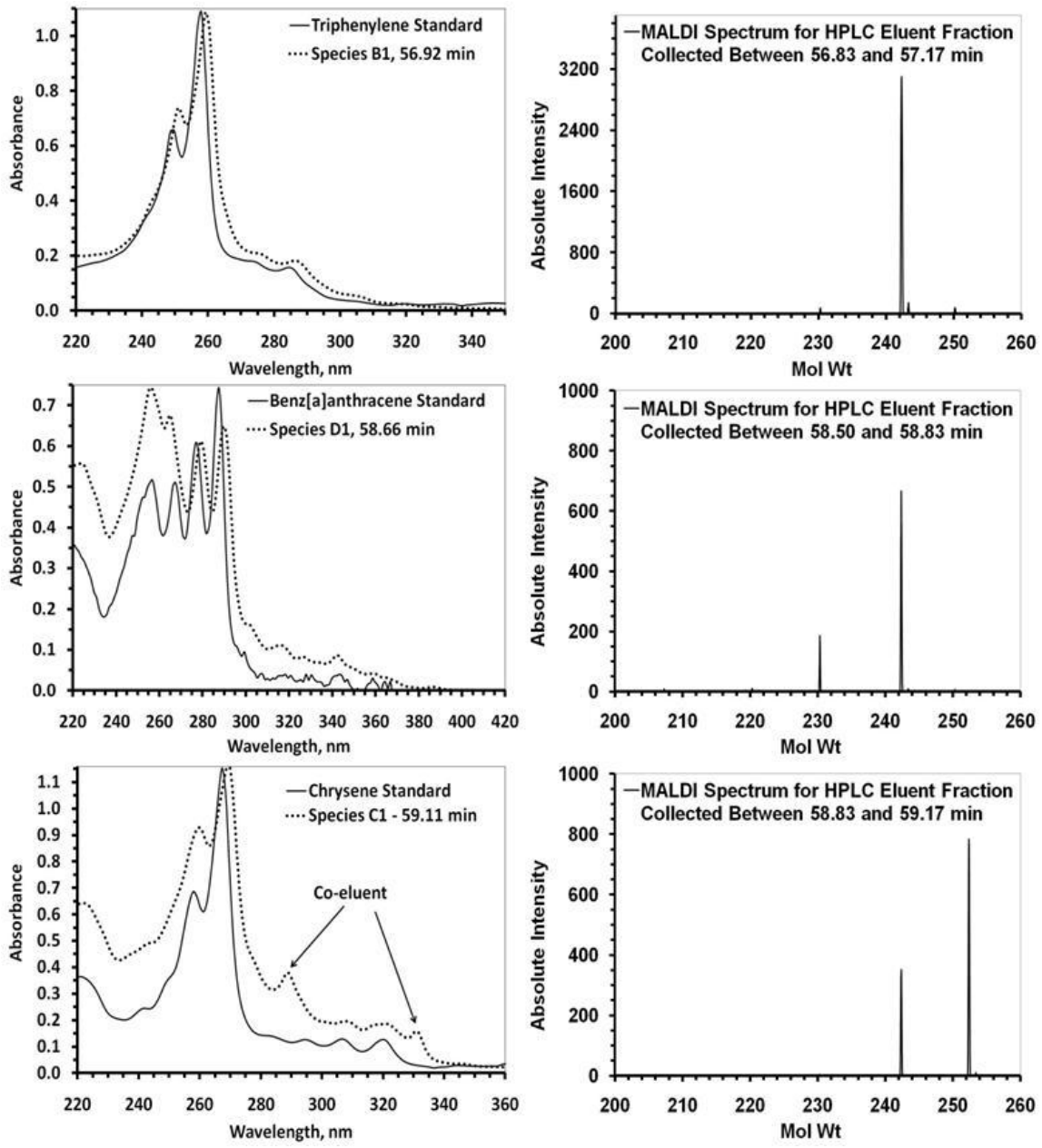

Figure 5.6. UV-Vis and MALDI spectral identification of alkylated PAHs in the HPLC eluent stream. UV-Vis spectra for methylated triphenylene, benz[a]anthracene, and chrysene (panels a-c, respectively) are similar in form to those of the respective unsubstituted PAH, with the spectra of the eluting species shifted in the direction of higher wavelengths. MALDI spectra in panels d-f indicate the mol wt(s) of the eluent(s).

Finally, spectral evidence indicating the presence of perylene in GPC Fraction 7 from Chapter 4 (see Fig. 5.7) is given.

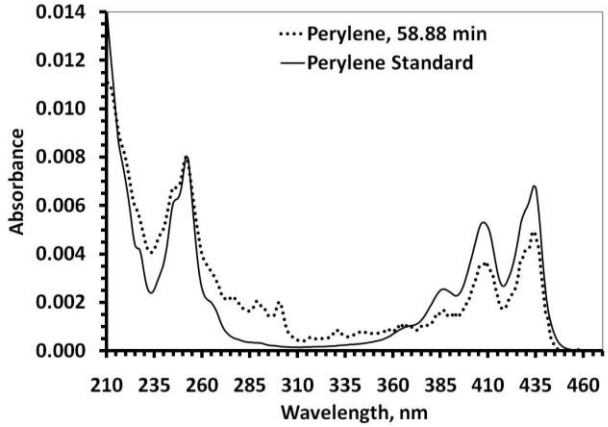

Figure 5.7. UV-Vis spectral match indicating the presence of perylene in GPC Fraction 7. The peaks at ~ 280, 290 and 300 nm are a result of the co-eluting species benzo[b]fluoranthene.

Comparison of MALDI and HPLC/PDA Characterization Results for DGE Pitch Cut 1

As indicated in Chapter 4 (see Figs. 4.1b and 4.6 from that chapter), MALDI and HPLC/PDA yield conflicting results as to the mol wts of the most prevalent species in DGE Pitch Cut 1. MALDI analyses suggest that the species comprising the "orange circle" signal distribution, particularly those at m/z 266, 280, and 294, are the most dominant in DGE Pitch Cut 1. However, HPLC analysis of DGE Pitch Cut 1 indicates that the components comprising the "orange circle" distribution (originating at 252 Da) are not among the most prevalent species in this pitch cut. Indeed, only one species of mol wt 252 Da, benzo[a]pyrene, was determined to be present in DGE Pitch Cut 1 (it is likely that other species comprising the "orange circle" signal distribution are indeed present, but that their peaks are obscured by those of more strongly-UV absorbing species

that are also present in greater amounts). This observation contradicts the result observed in the MALDI spectrum for DGE Pitch Cut 1 given in Fig. 4.1b in Chapter 4.

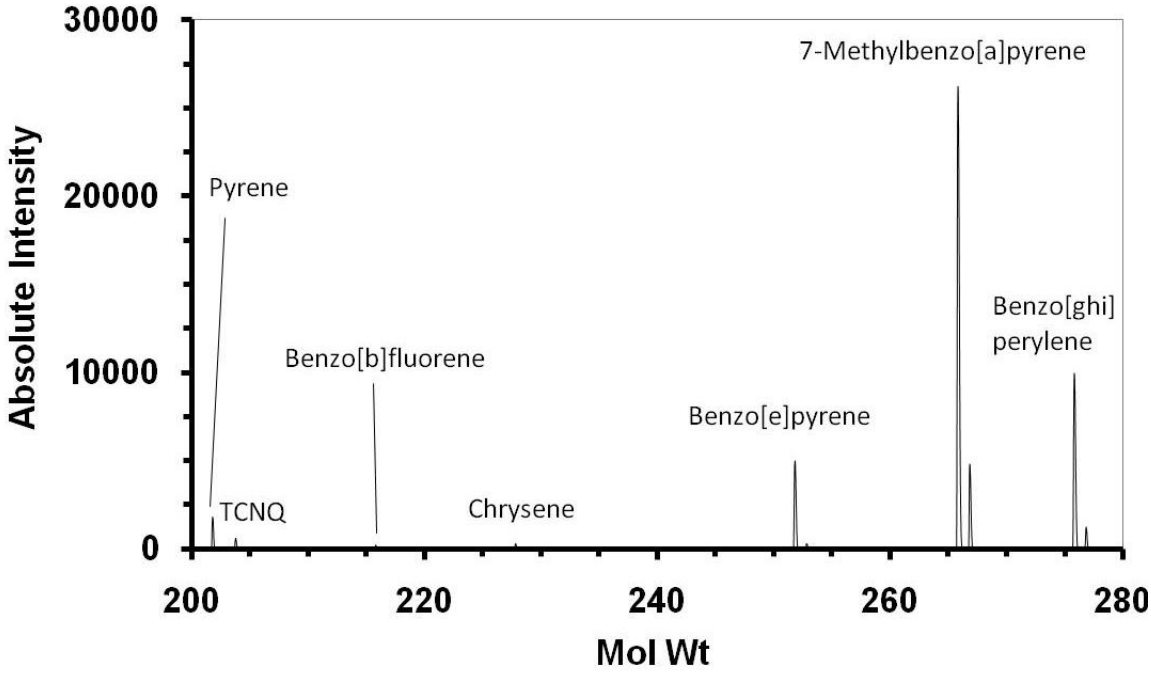

Figure 5.8. MALDI spectrum for an equimolar mixture of PAHs ranging in mol wt from 202 to 276.

We considered the possibility that relatively few of the heavier PAHs (particularly those in the "orange circle" signal distribution) were detected using HPLC/PDA because of solubility limitations – that is, the heavier species in DGE Pitch Cut 1 were less soluble in the relatively weak (for nonpolar molecules) solvent acetonitrile than the lighter species, such as pyrene (202 Da). Investigating further, we examined the MALDI mass spectrum for an equimolar mixture containing the PAHs pyrene, benzo[b]fluorene, chrysene, benzo[e]pyrene, 7-methylbenzo[a]pyrene, and benzo[ghi]perylene (in order to determine if MALDI could be overpredicting the presence of the species in the "orange circle" signal distribution and other species of similar mol wt). Using a ball mill (Wig-L-

Bug model, Thermo Electron), the prepared mixture was then mixed with the MALDI matrix TCNQ at a matrix:PAH mixture mass ratio of 20:1. A water spotting method, described in detail elsewhere[5], was used to apply the mixture to the MALDI target.

The results of the MALDI analysis (see Fig. 5.8) indicate: (1) PAHs with mol wt > 250 g/mol are greatly over-represented in the MALDI spectrum and (2) the MALDI response for 7-methylbenzopyrene is far stronger than that of any of the unsubstituted molecules. From these observations, we draw two conclusions. First, it is likely that MALDI underpredicts the presence of species with a mol wt below ~ 250 Da, which are more likely to volatilize within the high-vacuum MALDI environment (on the order of 10^{-9} bar). Indeed, to this end, Edwards et al.[5] recommend that MALDI not be used in the analysis of species with a mol wt of less than 250 Da. Second, the prevalence of aromatics possessing alkyl substituent groups relative to that of unsubstituted aromatics is overestimated in MALDI. This phenomenon has been previously documented by Cristadoro et al.,[6] who theorized that its cause was twofold. First, the π electrons of the alkylated PAHs associate more weakly with the π electrons of neighboring PAHs than do the π electrons of their non-alkylated counterparts, with weaker π–π interactions leading to an increased probability of desorption. Second, the ionization energy of the PAH analyte is reduced by the presence of alkyl substituents.

Because of these results, we concluded a major source of the discrepancy between the MALDI and HPLC results for DGE Pitch Cut 1 is that MALDI significantly underpredicts the presence of species with a mol wt less than ~ 250 Da. We recommend minimizing the amount of time that the MALDI target plate is in the instrument, in order

to limit volatilization of the TCNQ matrix and other pitch species of mol wt less than ~ 250 Da.

The solubility of DGE Pitch Cut 1 in the initial HPLC mobile phase (comprised of 30% acetonitrile and 70% water on a pre-mixed volume basis) is also likely to be of concern. Because it was prepared at a concentration of 7 mg/mL in acetonitrile (a very high injection concentration to use for HPLC analysis), not all of the injected sample elutes from the HPLC column, with some sticking to the packing instead (when this occurs, it is necessary to flush the column for several hours afterward in order to ensure that all of the injected sample has eluted). Because larger PAHs, such as benzo[a]pyrene (mol wt 276) would be expected to have lower solubilities than smaller PAHs such as pyrene (mol wt 202), these larger PAHs may precipitate out of solution to a greater extent than the smaller ones. Finally, because DGE Pitch Cuts 2 and 3 were prepared at significantly lower concentrations (on the order of 0.1 mg/mL), solubility concerns should not be a big issue.

An Additional Note Concerning Figs. 4.8c and 4.8f in Chapter 4

In Chapter 4, the UV-Vis spectrum given in Fig. 4.8c in Chapter 4 (for the HPLC eluent stream at 61.62 min) bears a strong resemblance to that of pyrene, indicating that the most prevalent species in this mixture is a molecule with a pyrene backbone. The MALDI spectrum of the eluent fraction eluting between 61.50 and 61.83 min (given in Fig. 4.8f in Chapter 4) indicates that this fraction is comprised of species of mol wts 230,

252, and 256 Da. A pyrene molecule substituted with two methyl groups has a mol wt of 230 Da; thus, dimethylpyrene is the likely identity of the species of mol wt 230 Da. The peak at 252 Da in Fig. 4.8f in Chapter 4 is attributed to the minor component benzo[a]pyrene, which has a peak maximum at 61.9 minutes and would not be expected to have begun eluting at 61.62 minutes. Triphenylene (mol wt 228 Da) absorbs UV radiation strongly at 260 nm. Therefore, the identity of the co-eluent is dimethyltriphenylene (mol wt 256 Da).

Method of Determining Concentrations of Major Species Present in M-50 Pitch Monomer

With the work presented thus far herein, we are now able to unambiguously identify the specific molecular structures that comprise the major species in the monomeric fraction of M-50 pitch. Our final objective in this work is to estimate the concentration of these species in M-50 monomer based on the HPLC results for DGE Pitch Cut 1 (in Chapter 4, we put forth a method to estimate the concentrations of M-50 monomer-range species based on MALDI; see Table 4.1). In MALDI mass spectrometry, the "default" assumption is that the area of the peaks in a MALDI mass spectrum is proportional to the molar concentration.[7] However, the methods used in this work provided us with an alternative, independent method for estimating species concentration in the monomer. To show how we calculated the concentration of a given species in the M-50 monomer, we take pyrene as an illustrative example. Referring to Fig. 4.6 in Chapter 4, we note peak A is for pyrene, with the peak maximum at 48.82

min. The maximum absorbance at 48.82 min was 1.15 at 240 nm (Fig. 4.7a in Chapter 4), and ε_{max}, the maximum extinction coefficient, was found to be ~ 80,000[3] (ε_{max} values obtained from reference spectra found in the literature are useful here; work conducted in our laboratory indicates that solvent choice has no discernible effect on ε_{max}. Assuming that the absorbance peaks are symmetrical triangles so that the average absorbance equals one-half the maximum absorbance, we used the Beer-Lambert law (A = elc) to calculate a concentration of 7.19×10^{-6} μmol/μL (with the optical path length l = 1.0 cm). The wt % of pyrene in DGE Pitch Cut 1 (0.91) was then obtained by multiplying the above concentration times the peak width (0.44 min) times the mobile phase flow rate (1000 μL/min) times the molecular weight (202) of pyrene, all divided by the mass of DGE Pitch Cut 1 injected (70 μg). The wt % values for other constituents of DGE Pitch Cut 1 are given in Table 5.1.

Table 5.1. Predicted Composition of DGE Pitch Cut 1, for major PAHs present in DGE Pitch Cut 1. Compound designations (such as A1) refer to peaks on the HPLC chromatogram of DGE Pitch Cut 1, given in Fig. 4.6 in Chapter 4.

Compound	A_{max}	ε_{max}	c_{avg}, mol/L	Mol Wt, g/mol	Eluting Mass, μg	Wt % of DGE Pitch Cut 1
Pyrene (A)	1.15	80000	0.0029	202	0.64	0.91
4-methylpyrene (A1)	1.45	71000	0.0044	216	0.97	1.39
2-methylpyrene (A2)	1.6	96000	0.0036	216	0.79	1.13
Dimethylpyrene 1 (A3)*	0.58	45000	0.0030	230	0.65	0.93
Dimethylpyrene 2 (A4)*	0.62	45000	0.0032	230	0.70	1.00
Dimethylpyrene 3 (A5)*	0.41	45000	0.0021	230	0.46	0.66
Trimethylpyrene (A6)*	0.45	45000	0.0025	244	0.54	0.77
Triphenylene (B)	0.56	150000	0.0008	228	0.19	0.27
Methyltriphenylene (B1)	1.08	150000	0.0020	242	0.38	0.55
Dimethyltriphenylene (B2)	0.8	150000	0.0016	256	0.30	0.43
Trimethyltriphenylene (B3)	0.6	150000	0.0011	270	0.24	0.34
Chrysene (C)	1.04	150000	0.0015	228	0.35	0.50
Methylchrysene 1 (C1)	1.16	150000	0.0022	242	0.41	0.59
Methylchrysene 2 (C2)	1.45	150000	0.0028	242	0.51	0.74
Dimethylchrysene 1 (C3)	0.5	150000	0.0010	256	0.19	0.27
Dimethylchrysene 2 (C4)	0.3	150000	0.0012	256	0.11	0.16
Dimethylchrysene 3 (C5)	0.6	150000	0.0012	256	0.23	0.32
Trimethylchrysene 1 (C6)	0.3	150000	0.0006	270	0.12	0.17
Trimethylchrysene 2 (C7)	0.6	150000	0.0012	270	0.24	0.34
Trimethylchrysene 3 (C8)	0.4	150000	0.0008	270	0.16	0.23
Trimethylchrysene 4 (C9)	0.4	150000	0.0008	270	0.16	0.23
Benz[a]anthracene (D)	0.69	80000	0.0020	228	0.43	0.62
MBAA 1 (D1)	0.65	80000	0.0020	242	0.43	0.62
MBAA 2 (D2)	0.4	80000	0.0012	242	0.27	0.38
MBAA 3 (D3)	0.6	80000	0.0018	242	0.40	0.57
DMBAA 1 (D4)	0.4	80000	0.0013	256	0.28	0.40
DMBAA 2 (D5)	0.3	80000	0.0010	256	0.21	0.30
Totals					10.36	

ε_{max} values were obtained by reading off of the UV-Vis spectra for the unsubstituted species A, B, C, and D as presented by Friedel.[3] Except for species A1-A6, alkylated species were assumed to have the same ε_{max} as nonsubstituted aromatics.

*In determining ε_{max} and A_{max} for species A3-A6, only values obtained at absorption wavelengths of 300 nm and higher were considered.

MBAA = methylbenz[a]anthracene, DMBAA = dimethylbenz[a]anthracene

Finally, we know that the overhead comprising DGE Pitch Cut 1 represents 12.5 wt % of the entire pitch.[8] We show that, for the "blue rectangle" and "yellow ring" signal distributions (see Fig. 4.2 in Chapter 4), approximately equal amounts of the species in question are present in the top and bottoms fractions. Note that, in the MALDI spectrum for M-50 pitch in Fig. 5.9, the MALDI response at m/z = 230, R_{230}, is equal to 665 units, while the MALDI response at m/z = 468, R_{468}, is 2114 units. Meanwhile, the MALDI spectrum (see Fig. 5.10) for the remaining 87.5% of M-50 pitch (that is, M-50 minus DGE Pitch Cut 1) indicates that the ratio R_{230}/R_{468} = 358/2114 when scaled to the value of R_{468} for M-50 pitch in Fig. 5.9. 358 is just over half of 665; assuming that MALDI response is proportional to concentration, just under half of the species of mol wt 230 are extracted in DGE Pitch Cut 1. This assumption is true for the species comprising both the "blue rectangle" and "yellow ring" signal distributions. Thus, we estimate that pyrene (determined to be a member of the "blue rectangle" distribution) comprises 0.23 wt % of the M-50 feed pitch.

Analogous steps to those described above were used to calculate the concentration of benzo[a]pyrene in M-50 pitch. However, for every molecule of mol wt 280 extracted (and generally for all members of the "orange circle" distribution, including unsubstituted benzo[a]pyrene), approximately 3 remain in the bottom phase (see values for R_{280} and R_{468} in both Figs. 5.9 and 5.10). Using this methodology, the concentration of benzo[a]pyrene present in the M-50 feed pitch was determined to be 0.18 wt % (0.31 mol %). Based on trends observed for the "blue rectangle" and "yellow ring" signal distributions, the methylbenzo[a]pyrenes are thus predicted to outnumber unsubstituted

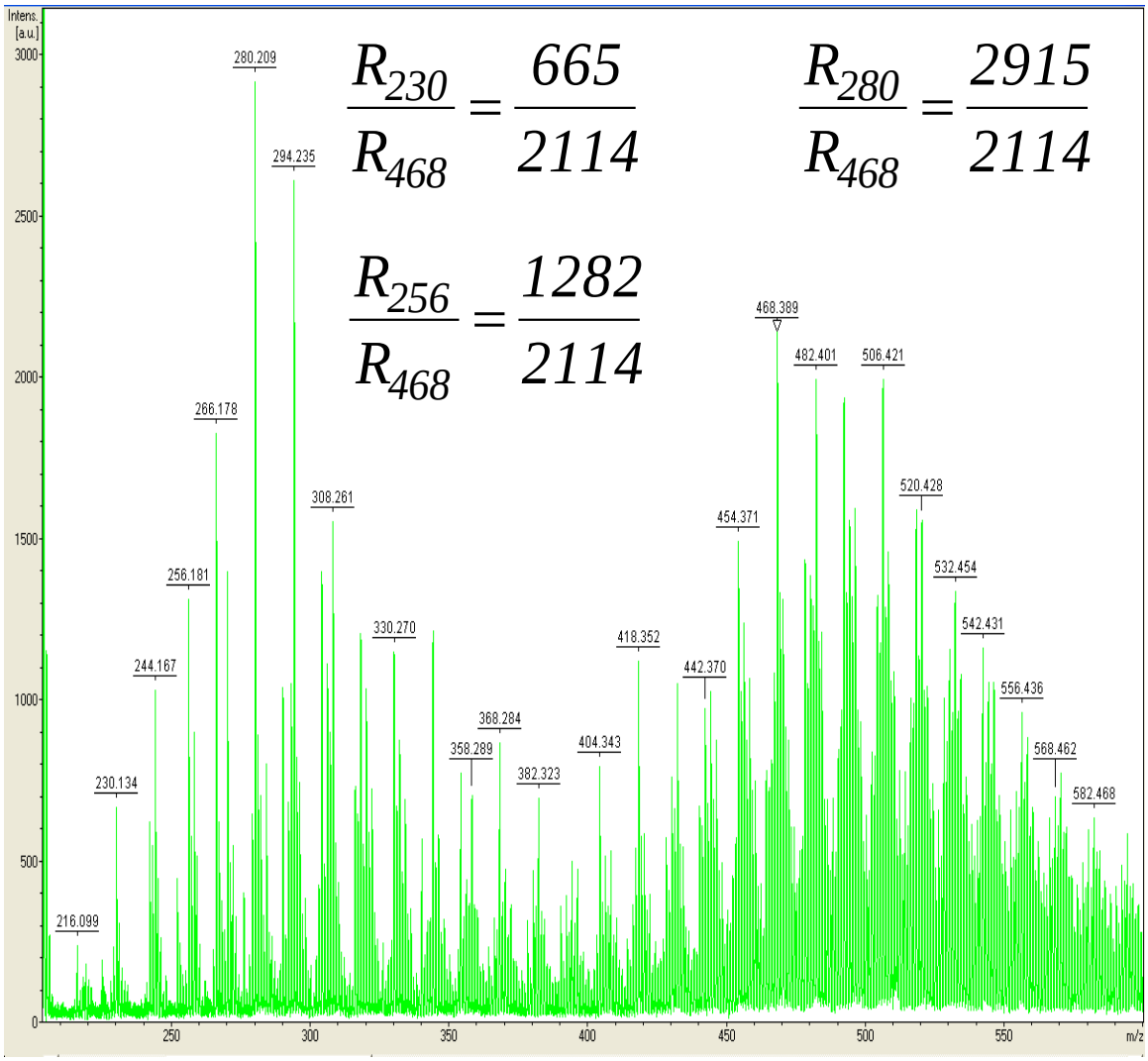

Figure 5.9. MALDI spectrum for M-50 pitch, with mol wt value labels above the most prominent peaks. The terms R_{230}, R_{256}, R_{280}, and R_{468} denote the MALDI response at m/z = 230, 256, 280, and 468 respectively.

benzo[a]pyrene ~ 2.5:1 (and, therefore, a total methylbenzo[a]pyrene mass fraction of 0.45 wt %). Similarly, we predicted that the total dimethylbenzo[a]pyrene and trimethylbenzo[a]pyrene presences were 2 (0.36 wt %) and 1.5 (0.27 wt %) times that of the unsubstituted benzo[a]pyrene, respectively.

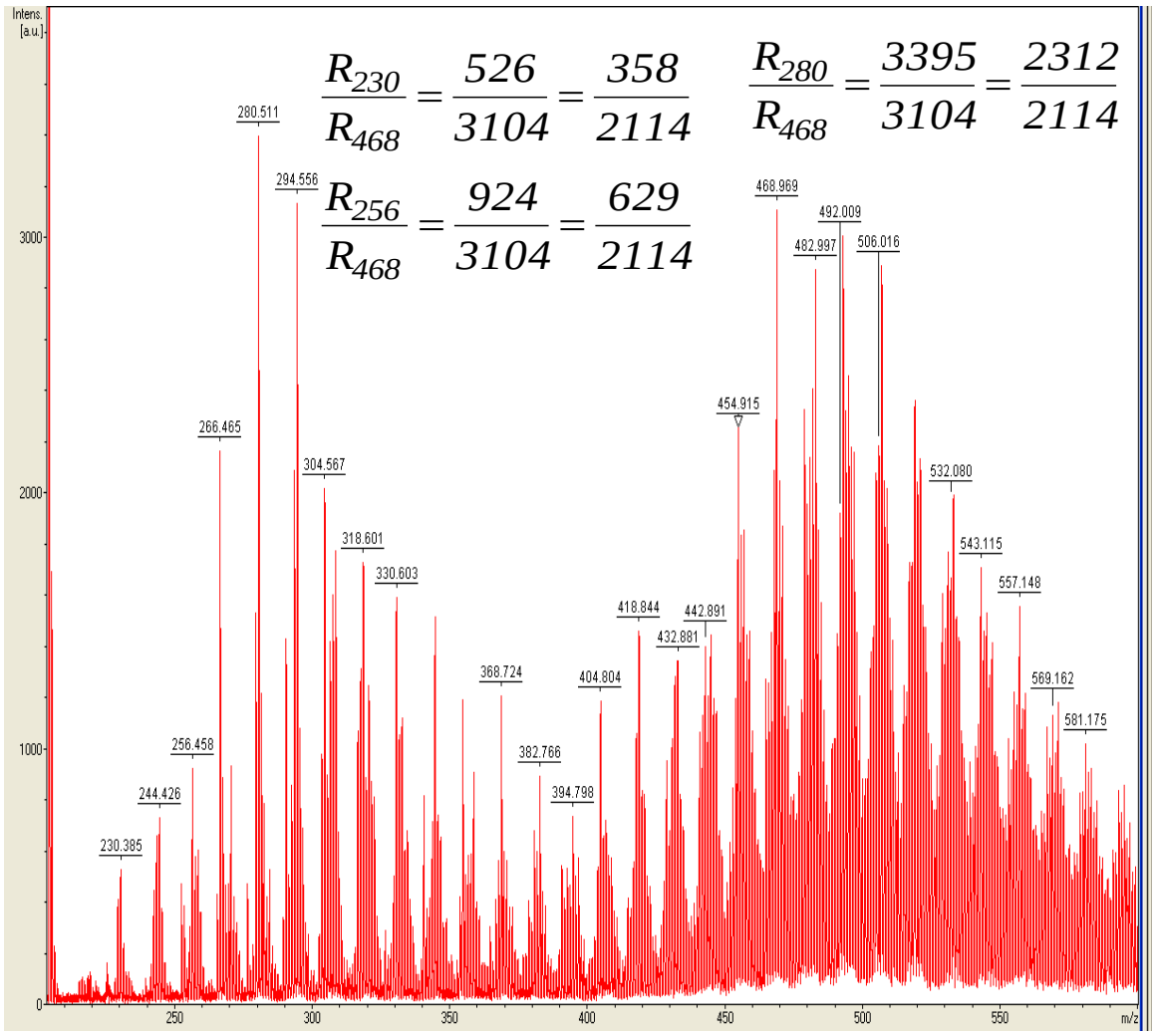

Figure 5.10. MALDI spectrum for the residue remaining after DGE Pitch Cut 1 is extracted from M-50 pitch, with mol wt value labels above the most prominent peaks. The terms R_{230}, R_{256}, R_{280}, and R_{468} denote the MALDI response at m/z = 230, 256, 280, and 468 respectively.

As benzo[e]pyrene and benzo[ghi]perylene are not detected in DGE Pitch Cut 1, extra steps are required to estimate their presence in M-50 pitch. However their approximate compositions can be estimated because the approximate amount of benzo[a]pyrene in M-50 pitch has already been determined. The UV-Vis spectra for the

3 major PAH constituents of GPC Fraction 7 were examined in greater detail in order to provide a rough estimate of the concentration of these two species in the whole M-50 pitch. The Beer-Lambert Law ($A = \varepsilon lc$) can be rearranged in order to solve for the molar concentration ($c = A/\varepsilon l$), and the molar ratio for the concentration of compound 2 to that of compound 1, c_2/c_1 (this molar concentration ratio is equal to the mole fraction ratio, x_2/x_1). Because path length is constant, $l_1 = l_2$, the molar ratio $c_2/c_1 = x_2/x_1 = A_2\varepsilon_1/ A_1\varepsilon_2$.

Defining compound 2 as benzo[e]pyrene and compound 1 as benzo[a]pyrene, one can proceed to estimate the concentration of benzo[e]pyrene present in M-50 pitch. An important assumption is that the relative concentrations of the species in GPC Fraction 7 are indicative of the pitch as a whole. We define the variables as follows:

A_2 = maximum absorption value for benzo[e]pyrene, 0.026
A_1 = maximum absorption value for benzo[a]pyrene, 0.045
ε_2 = maximum extinction coefficient observed for benzo[e]pyrene, 52480[3]
ε_1 = maximum extinction coefficient observed for benzo[a]pyrene, 57540[3]
x_2 = mole fraction of benzo[e]pyrene
x_1 = mole fraction of benzo[a]pyrene, 0.0031

In this manner, the mole fraction of benzo[e]pyrene present is determined to be 0.0020. Similarly, the mole fraction of benzo[ghi]perylene present is 0.0019. The mass fractions of these two compounds present was determined with a knowledge of the MALDI-determined mol wt of M-50 pitch (436 g/mol); the mass fractions of their alkylated derivatives were estimated by applying the same assumptions used to estimate the presence of the alkylated benzo[a]pyrene derivatives. All mass and mole fractions of major M-50 constituents are given to Table 5.2.

Table 5.2. Estimated concentrations of major M-50 monomeric constituents in M-50.

Compound	Wt % in M-50	Mol % in M-50	Mol Wt (Da)	Signal Distribution
Pyrene (A)	0.23	0.50	202	Blue rectangle
4-methylpyrene (A1)	0.35	0.71	216	Blue rectangle
2-methylpyrene (A2)	0.28	0.57	216	Blue rectangle
Dimethylpyrenes (A3, A4, A5)	0.65	1.23	230	Blue rectangle
Trimethylpyrene (A6)	0.19	0.34	244	Blue rectangle
Triphenylene (B)	0.07	0.13	228	Yellow ring
Methyltriphenylene (B1)	0.14	0.25	242	Yellow ring
Dimethyltriphenylene (B2)	0.11	0.19	256	Yellow ring
Trimethyltriphenylene (B3)	0.09	0.15	270	Yellow ring
Chrysene (C)	0.13	0.25	228	Yellow ring
Methylchrysenes (C1, C2)	0.33	0.59	242	Yellow ring
Dimethylchrysenes (C3, C4, C5)	0.19	0.32	256	Yellow ring
Trimethylchrysenes (C6, C7, C8, C9)	0.24	0.39	270	Yellow ring
Benz[a]anthracene (D)	0.16	0.31	228	Yellow ring
Methylbenz[a]anthracenes (D1, D2, D3)	0.39	0.70	242	Yellow ring
Dimethylbenz[a]anthracenes (D4, D5, D6)	0.23	0.39	256	Yellow ring
Benzo[a]pyrene	0.18	0.31	252	Orange circle
Methylbenzo[a]pyrenes	0.45	0.74	266	Orange circle
Dimethylbenzo[a]pyrenes	0.36	0.56	280	Orange circle
Trimethylbenzo[a]pyrenes	0.27	0.40	294	Orange circle
Benzo[e]pyrene	0.11	0.20	252	Orange circle
Methylbenzo[e]pyrenes	0.28	0.46	266	Orange circle
Dimethylbenzo[e]pyrenes	0.23	0.35	280	Orange circle
Trimethylbenzo[e]pyrenes	0.17	0.25	294	Orange circle
Benzo[ghi]perylene	0.12	0.19	276	Red triangle
Methylbenzo[ghi]perylenes	0.31	0.46	290	Red triangle
Dimethylbenzo[ghi]perylenes	0.24	0.35	304	Red triangle
Trimethylbenzo[ghi]perylenes	0.18	0.25	318	Red triangle
326 Da backbone	There is not enough data to estimate concentrations of species comprising the "white square" signal distribution.		326	White square
326 Da backbone + methyl group			340	White square
326 Da backbone + 2 methyl groups			354	White square
326 Da backbone + 3 methyl groups			368	White square
326 Da backbone + 4 methyl groups			382	White square
Totals	6.68	11.54		

Advantages and Disadvantages of MALDI- and HPLC-Derived Methods to Determine Concentration of M-50 Monomeric Species

In summary, the HPLC-derived method for determining the concentrations of the major M-50 oligomers is good for determining the concentrations of the light monomeric species with molecular weights less than ~ 250 Da. In this molecular weight range, the HPLC-derived method is superior to the MALDI-derived method for determining species concentration discussed in Chapter 4, because these species volatilize to a large extent in the high-vacuum environment of MALDI and are therefore under-represented when the MALDI-derived method is used to determine species concentrations. Because this portion of the monomer contains fewer different molecular structures than that above 250 Da, a well-resolved HPLC chromatogram for species with molecular weights in this range is achievable.

However, for determining concentrations of the species above 250 Da, the MALDI-derived method is recommended (as these species are not volatile, even in the high-vacuum environment of MALDI). Mass spectrometry is superior to chromatography in that the former results in better peak resolution than the latter (the MALDI peaks for all species differing in mol wt by ~ 1 Da are fully resolved from each other. In addition, MALDI can be used on either a solvent-based or a solvent-free basis, while solubility of the sample in the HPLC mobile phase is a must.

References

[1]Dauché, F. M.; Bolaños, G.; Blasig, A.; Thies, M. C. Control of Mesophase Pitch Properties by Supercritical Fluid Extraction. *Carbon* **1998**, *36(7-8)*, 953-961.

[2]Clar, E. *Polycyclic Hydrocarbons.* Academic Press, London (1964).

[3]Friedel, R. A.; Orchin, M. *Ultraviolet Spectra of Aromatic Compounds.* John Wiley and Sons, New York (1951).

[4]Somers, M. L.; Wornat, M. J. UV Spectral Identification of Polycyclic Aromatic Hydrocarbon Products of Supercritical 1-Methylnaphthalene Pyrolysis. *Polycyclic Aromatic Compounds*, **2007**, *27*, 261-80.

[5]Edwards W. F.; Jin, L; Thies, M. C. MALDI-TOF Mass Spectrometry: Obtaining Reliable Mass Spectra for Insoluble Carbonaceous Pitches. *Carbon*, **2003**; *41*, 2761-68.

[6]Cristadoro, A.; Räder, H. J.; Müllen, K. Clustering of Polycyclic Aromatic Hydrocarbons in Matrix-Assisted Laser Desorption/Ionization and Laser Desorption Mass Spectrometry and LD Mass Spectrometry. *Rapid Commun. Mass Spectrom.* **2007**, *21*, 2621-28.

[7]Kulkarni, S. U.; Thies, M. C. Solvent-Based vs. Solvent-Free MALDI-TOF-MS Sample Preparation Methods for the Quantitative Analysis of Petroleum Macromolecules. Preprints - American Chemical Society, Division of Petroleum Chemistry **2010**, *55(1)*, 108-11.

[8]Cristadoro, A.; Kulkarni, S. U.; Burgess, W. A.; Cervo, E. G.; Räder, H. J.; Müllen, K.; Bruce, D. A.; Thies, M. C. Structural Characterization of the Oligomeric Constituents of Petroleum Pitches. *Carbon*, **2009**, *47*, 2358-2370.

CHAPTER 6

MOLECULAR STRUCTURES FOR THE OLIGOMERIC CONSTITUENTS OF PETROLEUM PITCH

Introduction

Petroleum pitches are inexpensive raw materials that can be processed into a wide range of carbon products, including high thermal conductivity (HTC) carbon fibers,[1] carbon electrodes,[2] activated carbon fibers,[3,4] and the matrix phase of carbon-carbon composites.[5] As shown in Fig. 6.1, these materials have a broad molecular weight (mol wt) distribution, ranging from about 200 to more than 1000 Daltons (Da).[6,7] Petroleum pitches are oligomeric in nature; previous work[8,9] has shown that the monomer species (202-388 Da) consist of a polycyclic aromatic hydrocarbon (PAH) backbone substituted with from 0 to 4 methyl groups (with an occasional ethyl group being observed). The dimer (388 to 645 Da), trimer (645 to 890 Da), and tetramer (890 to 1120 Da) species are believed to be formed via condensation reactions of the lower mol wt oligomers.[10,11]

As early as the 1970s, [4,7,12] researchers recognized that the mol wt of the precursor pitch has a significant impact on the material properties of the final carbon product. For example, the pitch precursor for HTC carbon fibers must have a high enough mol wt to form a liquid crystalline phase, or mesophase. However, a fundamental understanding of the effect of the mol wt distribution of pitches, or of the molecular structures of the pitch species themselves, on both pitch and final product properties is still lacking. A key impediment to obtaining such information has been the difficulty in isolating either

individual species or even narrow mol wt fractions of pitch for characterization. Thus, most of the past work has reported on the characterization of broad cuts of pitch, obtained by extraction/precipitation with selected solvents and solvent mixtures[13,14,15] (e.g., cyclohexane/acetone mixtures, toluene, pyridine, or quinoline).

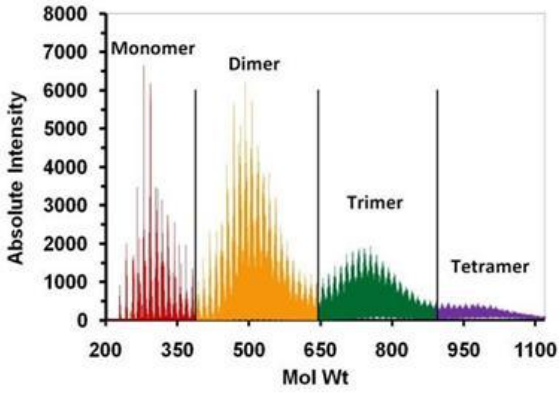

Figure 6.1. MALDI spectrum for M-50 pitch, with the oligomeric peaks (monomer 202-388 Da, dimer 388-645 Da, trimer 645-890 Da, and tetramer 890-1120 Da) indicated. Adapted from Cervo and Thies.[16]

Some progress has been made in determining actual molecular structures for pitch components. In particular, Mochida et al.[15,17] applied field desorption mass spectrometry (FD-MS) to the benzene-soluble portion of both isotropic and mesophase pitches derived via the catalytic and thermal polymerization of anthracene. From FD-MS, the mol wts of the major species present in these fractions, including dimers, trimers, and tetramers, were obtained. However, because the benzene-soluble fractions had a broad mol wt distribution (MWD), that is, from 200 to over 1000 Da, ^{1}H NMR and ^{13}C NMR spectra of these fractions were for only "average" hydrogen and carbon atoms. Thus, the proposed molecular structures were based on definitive mol wt, but only average structural information.

Recent work by our group[9] has demonstrated how the characterization of pitches in terms of their constituent species is facilitated by separation into narrow mol wt fractions. In particular, narrow mol wt cuts of the monomer and dimer portions of Marathon M-50 pitch were isolated by the sequential application of dense-gas extraction (DGE), followed by high-temperature, preparative-scale gel permeation chromatography (prep-scale GPC). The resultant fractions of this 2-step process were then subjected to a battery of characterization methods, including matrix-assisted laser desorption, time-of-flight mass spectrometry (MALDI), molecular fragmentation analysis via MALDI-post source decay (PSD), and high-performance liquid chromatography with photodiode array detection (HPLC/PDA). A key finding of these works was that the M-50 monomeric species are divided into well-defined Gaussian distributions, with each distribution consisting of an aromatic backbone species possessing from 0 to 4 methyl (and occasionally ethyl) substituent groups. The aromatic backbone structures were unequivocally identified using HPLC/PDA. MALDI analyses of the dimer-rich cuts indicated that the formation of major dimer species was consistent with condensation reactions between major monomer species, with a loss of 4-6 hydrogen atoms. However, the arrangement of the bonds between monomer units was not determined.

The objective of this study was the determination of the major molecular species present in the dimer and higher oligomers of two pitches produced by thermal polymerization (also called "heat-soaking" in industry): (1) an anthracene pitch and (2) a representative petroleum pitch, Marathon M-50.[18] In particular, we sought to build upon our recently obtained knowledge[9] of the dominant molecular structures present in M-50

monomer to predict structures for the dimer, trimer, and tetramer constituents of thermally soaked pitches. Recent work in our laboratory[19] has shown that mesophase pitch, the pitch precursor of greatest commercial interest, consists almost exclusively of mixtures of these oligomers. However, definitive molecular structures for actual (vs. average) species present in petroleum-based mesophase pitch have heretofore not been reported.

In order to accomplish the above objectives, M-50 pitch was first fractionated into narrow mol wt cuts rich in a single oligomer. These cuts, and the anthracene pitch, were further fractionated by prep-scale GPC into subfractions, with many consisting of well-separated individual species encompassing a mol wt range of less than 50 Da. These GPC fractions were subsequently characterized by MALDI to determine mol wt and by PSD to determine molecular structure information, particularly the degree of alkylation. Next, UV-Vis spectra of the fractions were used to determine the types of bonds connecting monomer units to form the oligomers. Finally, this new information was combined with our previous knowledge of the most prevalent monomers in M-50 pitch[9] to propose actual molecular structures for the major oligomeric species comprising M-50 pitch.

Experimental

Materials

M-50 pitch (CAS number 68187-58-6; see Fig. 6.1) was obtained from Marathon Petroleum Company LLC. As discussed in Section 2.2, DGE was used to produce three

narrow mol wt pitch cuts from M-50 pitch, which are referred to hereafter as DGE Pitch Cuts 1-3 (with two of these cuts rich in dimer, and the third rich in trimer and tetramer). The anthracene pitch (see Fig. 6.2a) was provided to us by Conoco, Inc. It was produced via the thermal polymerization of anthracene at 475 °C for 2 h in a nitrogen environment. Additional details concerning its production are provided elsewhere.[6]

The DGE solvent toluene (HPLC grade, 99.9% purity, CAS number 108-88-3) was obtained from Fisher Scientific. For the prep-scale GPC experiments, the mobile phase TCB (1,2,4-trichlorobenzene; GPC grade, 99% min. purity, CAS number 120-82-1) was purchased from J. T. Baker. For the MALDI and MALDI-PSD analyses, the matrix 7,7,8,8,-tetracyanoquinodimethane (TCNQ; 98% min. purity) was supplied by TCI America. The UV-Vis solvent cyclohexane (99+% purity, CAS number 110-82-7) was obtained from Sigma-Aldrich. All chemicals were used as supplied without further purification.

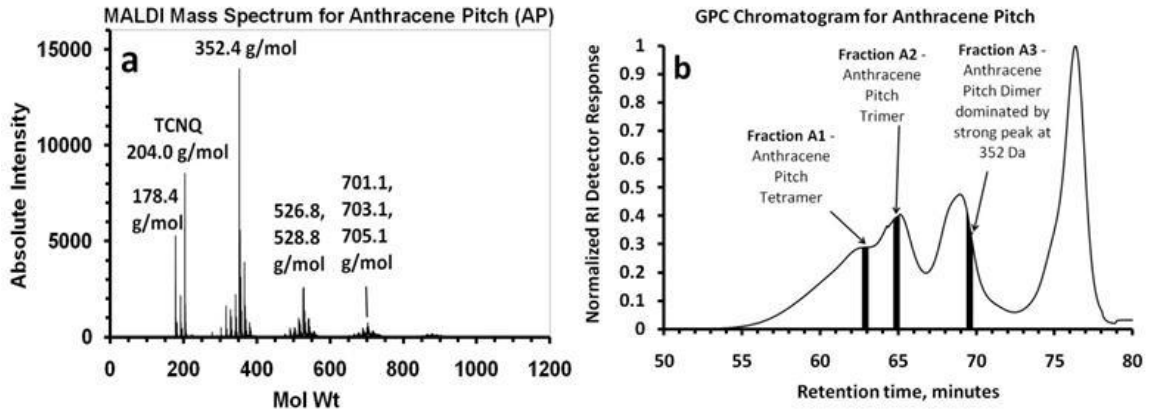

Figure 6.2. (a) MALDI spectrum for anthracene pitch produced via thermal polymerization of anthracene at 475 °C. (b) GPC chromatogram for this anthracene pitch. The black bars indicate the 20-s time intervals over which the fractions of interest were collected.

Production of DGE Pitch Cuts

DGE Pitch Cuts 1 and 2 (see Figs. 6.3a and 6.4a) were produced from M-50 pitch using a two-step process. First, a two-column, continuous DGE process, as developed by Cervo and Thies,[16] was used to obtain a dimer-rich cut also containing some heavy monomer and light trimer species; they refer to this cut as "Dimer-Rich B." For the second step, and the actual production of DGE Cuts 1 and 2, ~ 1.5 g of the dried, Dimer-Rich B cut were subjected to a one-column, semibatch DGE process, which is described in detail elsewhere.[8] For the production of DGE Pitch Cut 1, a positive temperature gradient was employed such that the bottom of the column was held at 330 °C, the middle at 350 °C, and the top at 380 °C. Collection of DGE Pitch Cut 1 as the extracted top product commenced as soon as the column reached the desired operating pressure of 29 bar and continued thereafter for 40 min. The column pressure was then raised to 42 bar, and collection of DGE Pitch Cut 2 as overhead product began 2.25 h later and lasted for 40 min thereafter.

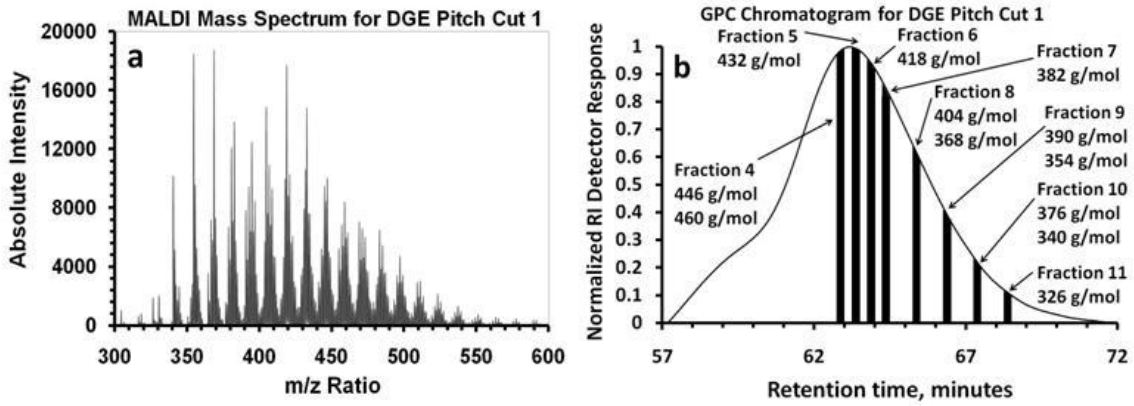

Figure 6.3. (a) MALDI spectrum for DGE Pitch Cut 1, rich in light M-50 dimer species. (b) GPC chromatogram for DGE Pitch Cut 1, with the black bars indicating the 15-s time intervals over which the fractions of interest were collected. The mol wts listed with the fraction numbers indicate the species to which PSD was subsequently applied.

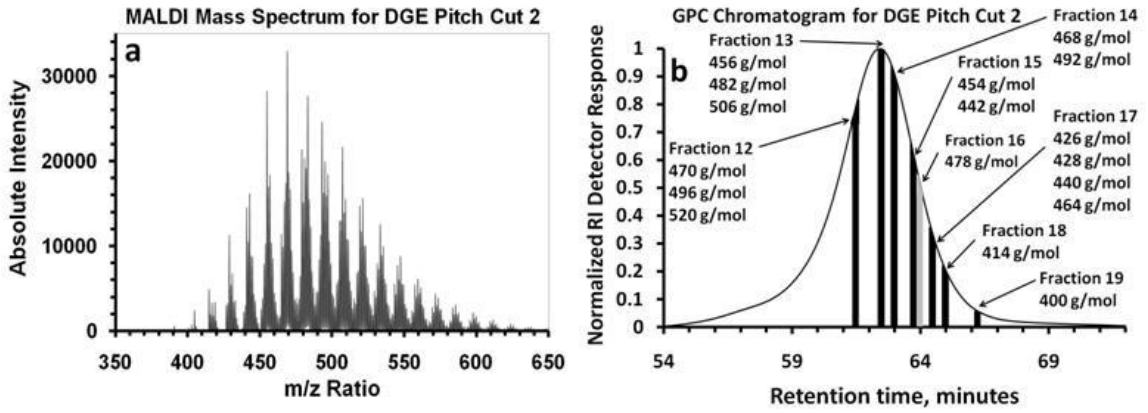

Figure 6.4. (a) MALDI spectrum for DGE Pitch Cut 2, rich in M-50 dimer species. (b) GPC chromatogram for DGE Pitch Cut 2, with 15-s time intervals being used for fraction collection. The mol wts listed with the fraction numbers indicate the species to which PSD was subsequently applied.

DGE Pitch Cut 3 (see Fig. 6.5a), rich in M-50 trimer and tetramer, was also produced via a two-step process. First, M-50 pitch was subjected to a one-column, continuous DGE process (column pressure 49.3 bar, with the column temperature constant at 330 °C) to produce a heavy pitch cut (bottoms product) rich in trimer and tetramer. Next, 1.5 g of this pitch cut was subjected to a one-column, semibatch DGE process. First, dimer was removed as top product by setting the column pressure to 56.2 bar (column temperatures were identical to those used for DGE Pitch Cuts 1 and 2 above). After a period of 2 h, the pressure was raised to 111.8 bar. Collection of DGE Pitch Cut 3 began at this point, and lasted for 40 min thereafter.

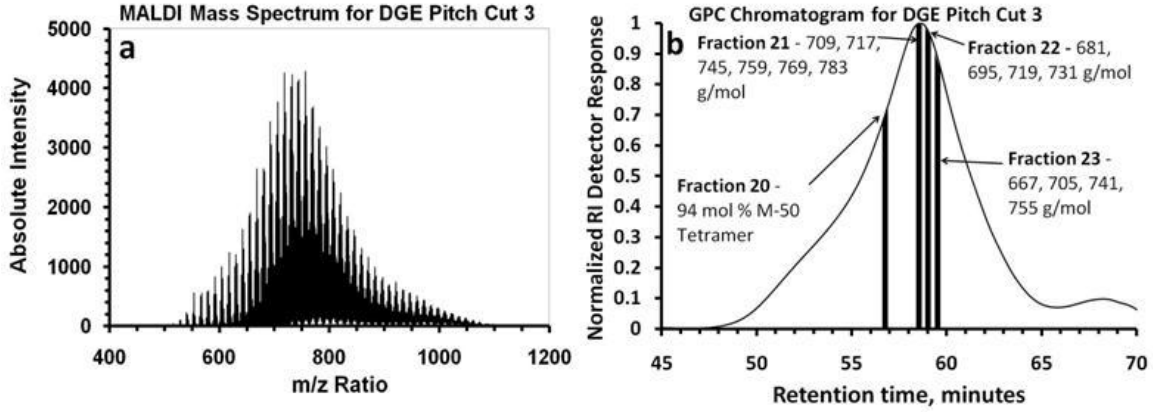

Figure 6.5. (a) MALDI spectrum for DGE Pitch Cut 3, rich in M-50 trimer and tetramer species. (b) GPC chromatogram for DGE Pitch Cut 3, with 15-s time intervals being used for fraction collection. The mol wts listed with the fraction numbers indicate the species to which PSD was subsequently applied.

Production of Narrow Mol Wt Pitch Fractions via Prep-Scale GPC

Prep-scale GPC was used to produce narrow mol wt fractions of the anthracene pitch (GPC Fractions A1-A3; see Fig. 6.2b) and of DGE Pitch Cuts 1-3 (GPC Fractions 4-23; see Figs. 6.3b-6.5b). A Waters Alliance GPCV 2000 was adapted[9] so that it could be operated on a preparative scale, with the mobile-phase flow rate set to 2.50 mL/min at an operating temperature of 140 °C. The soluble portion (~ 80 wt % at room temperature) of the anthracene pitch and the fully-TCB soluble DGE Pitch Cuts 2 and 3 were prepared for GPC fractionation at a concentration of 10 mg/mL. Because of its scarcity, DGE Pitch Cut 1 (fully soluble in TCB) was prepared at a concentration of only 3 mg/mL. Because it was necessary to collect several micrograms of M-50 trimer and tetramer for FT-IR analyses (much more than what was required for MALDI, PSD, and UV-Vis), a second fractionation of DGE Pitch Cut 3 was conducted at a much higher injected sample concentration of 50 mg/mL. For all samples fractionated, an injection

volume of 1.080 mL was used. The M-50 trimer and tetramer fractions collected as a result of this second fractionation of DGE Pitch Cut 3 are referred to as GPC Fractions 24 and 25. GPC Fraction 24 was collected from 55.9 to 57.4 min, and GPC Fraction 25 was collected from 58.4 to 59.9 min.

GPC Fractions A1-A3 and 4-25 were collected by diverting the column eluent stream to a Waters Fraction Collector (model 1). For the fractionation of the anthracene pitch, the time interval for each fraction collected was 20 s; for DGE Pitch Cuts 1-3, it was 15 s. The refractive index detector of the GPCV 2000 was used to produce the GPC chromatogram.

Analytical Characterization of Collected Fractions

UV-Vis analyses of the collected GPC fractions were carried out using a Spectral Instruments 400 Series spectrophotometer. GPC fractions subjected to UV-Vis analysis were either run directly, or were dried for 2 hours at 120 °C and a pressure of 25 torr to remove the TCB mobile phase before re-dissolving in cyclohexane, the UV cutoff wavelength of which is ~110 nm less than that of TCB. Typically, cyclohexane was used as the UV-Vis solvent for the dimer-range GPC fractions, while for the trimer and tetramer fractions TCB had to be used because of the poor solubility of these heavier fractions in cyclohexane. In all cases, the concentrations of the GPC fractions analyzed were adjusted by adding solvent until the maximum light absorbance value measured was less than 2.0.

Both MALDI and PSD analyses were performed on GPC Fractions A1-A3 and 4-23. All MALDI and PSD analyses were obtained using a Bruker Daltonics Autoflex (model 1) MALDI mass spectrometer with a 337 nm nitrogen laser. We have previously described both the sample preparation method[6,8] and the operating parameters for the two techniques[8] in detail elsewhere.

A Nicolet Magna 550 Fourier Transform IR (FT-IR) spectrometer equipped with a Thermo-Spectra Tech Nic-Plan FT-IR microscope was used to perform all FT-IR analyses, in transmission mode, on thin films of the dried GPC Fractions 24 and 25. (The film method of IR analysis was chosen because only a few micrograms of sample are required per analysis.) Prior to FT-IR analysis, each GPC fraction analyzed was dried for 2 h at a temperature of 140 °C and 25 torr to remove the TCB mobile phase. Next, each sample was subjected to a second drying at a temperature of 200 °C and a relatively low pressure of 1.5 torr, in order to remove any residual TCB that was still present. For each pitch fraction characterized, a stainless steel rolling tool was used to deposit a small portion of sample into a thin film on the zinc selenide IRTran plates (the sample analysis surface).

Results and Discussion

Structural Characterization of Anthracene Pitch Oligomers

Isolating Anthracene Pitch Oligomers by GPC

Because the goal of the GPC fractionations was to obtain fractions containing only a single oligomer, the time intervals for collection (see Fig. 6.2b) were chosen with

this objective in mind. Of the 51 GPC fractions collected during the fractionation of the anthracene pitch, GPC Fractions A1-A3 were the purest fractions collected, and thus were the ones selected for further analysis. As the number of species in anthracene pitch is considerably lower than for M-50 pitch, prep-scale GPC alone was sufficient to prepare the desired fractions, so no DGE fractionation step was necessary.

Anthracene Pitch Dimer

MALDI analysis (see Fig. 6.6a) reveals that GPC Fraction A3 (see Fig. 6.2b) is primarily composed of a species of mol wt 352.4, suggesting that the anthracene pitch dimer forms via a condensation reaction between two anthracene (mol wt 178) monomer units, accompanied by the loss of 4 hydrogen atoms. PSD analysis of the peak at m/z = 352.4 indicates no fragment peaks, a mass spectrum result[20] consistent with this hypothesis. The absence of strong fragment peaks also indicates that the species possesses no naphthenic rings. The UV-Vis spectrum for GPC Fraction A3 (see Fig. 6.6b, thin black line) was subsequently compared to reference spectra[21] for two isomers of mol wt 352, either of which could possibly be a dimer of anthracene. For 2.3-benzonaphtho-(2".3":11.12)-fluoranthene (BNF: thick black line), the two anthracene monomer units are situated such that the two intermolecular bonds form a five-membered ring (such species are known as nonalternant PAHs). The other possible anthracene dimer, 1.2,7.8-dibenzoperylene (DBP; thick gray line), is comprised solely of six-membered aromatic rings (such species are known as alternant, or benzenoid, PAHs). Clearly, the UV-Vis spectrum for the nonalternant PAH provides a much better match to

GPC Fraction A3 than does the alternant PAH. Furthermore, we note that fully alternant PAHs of this mol wt exhibit strong light absorption above 400 nm,[21] a feature noticeably absent in GPC Fraction A3. Thus, we conclude that BNF is a major component of anthracene pitch dimer, and that most of the remaining species in this dimer are also nonalternant PAHs containing a five-membered "connecting" ring.

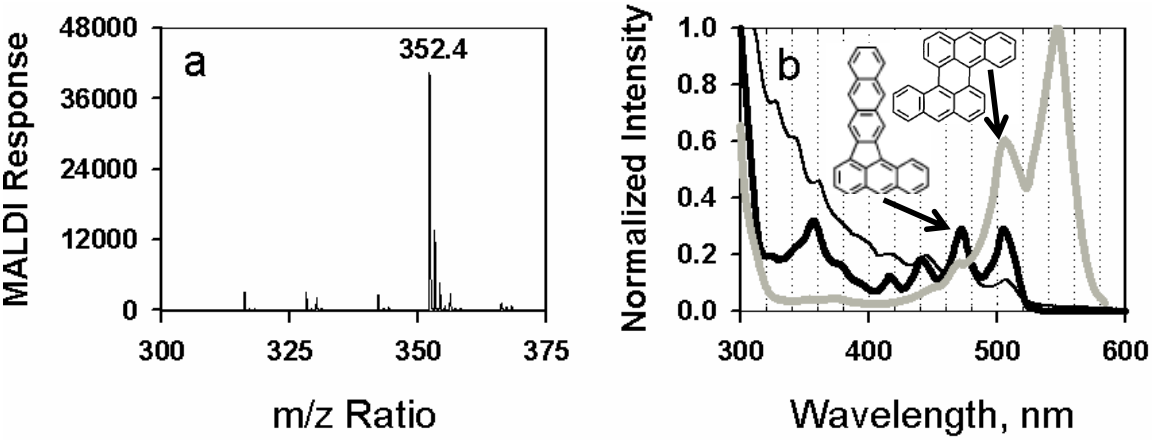

Figure 6.6. (a) MALDI spectrum for GPC Fraction A3 (see Fig. 6.2b). (b) The UV-Vis spectrum for GPC Fraction A3 (thin black line) is compared to that of BNF (thick black line) and DBP (thick gray line). Reference spectra are adapted from Clar.[21]

Anthracene Pitch Trimer

MALDI analysis (see Fig. 6.7a) of the trimer-rich GPC Fraction A2 (Fig. 6.2b) indicates that the most prevalent peak occurs at m/z = 526.8. This suggests that this trimer forms via condensation between anthracene pitch monomer (178.4 Da) and the most common anthracene pitch dimer, BNF, again with an accompanying loss of 4 hydrogen atoms. The PSD spectrum for this peak does not reveal the presence of any fragment peaks, an observation consistent with the suggested structure shown in Fig. 6.7a, and with the absence of any naphthenic content.

Besides the peak at m/z = 526.8, the MALDI spectrum of anthracene pitch trimer contains approximately a dozen other peaks. PSD spectra for two of these peaks, arising at m/z = 528.8 and 530.9, indicate the presence of fragment peaks possessing m/z ratios of 15 and 28 less than that of the parent species. Such behavior is consistent with that observed for the dihydroanthracenes (mol wt 180),[20] which possess 2 naphthenic carbon atoms. Scaroni[10] proposed that, upon heating of anthracene to 465-525 °C, free-radical dihydroanthracenes are formed, with these species then reacting with anthracene and/or each other to create dimers and higher oligomers. Therefore, it is likely that this trimer consists of a combination of anthracene and dihydroanthracene "monomer" units. PSD analysis for the peak at m/z = 540.9 reveals a spectrum in which there are no fragment peaks, a result consistent with the mass spectrum of the species at m/z = 526.8 if a single methyl group was added to that base PAH backbone.[20,22]

The UV-Vis spectrum for GPC Fraction A2 (see Fig. 6.7b, thin black line) does not exhibit any sharp peaks because of the presence of multiple species. Instead, it exhibits a uniform decrease in light absorption with respect to increasing wavelength. Comparison of the spectrum for GPC Fraction A2 was made to reference spectra for two of the few PAH trimers available in the literature: the fully alternant 7.8-benzoterrylene (see Fig. 6.7b, thick gray line) and the nonalternant 1.2,3.4-di(peri-naphthylene)anthracene (thick black line). Each of these trimers consists of the same three monomer units: two naphthalenes and one anthracene molecule.

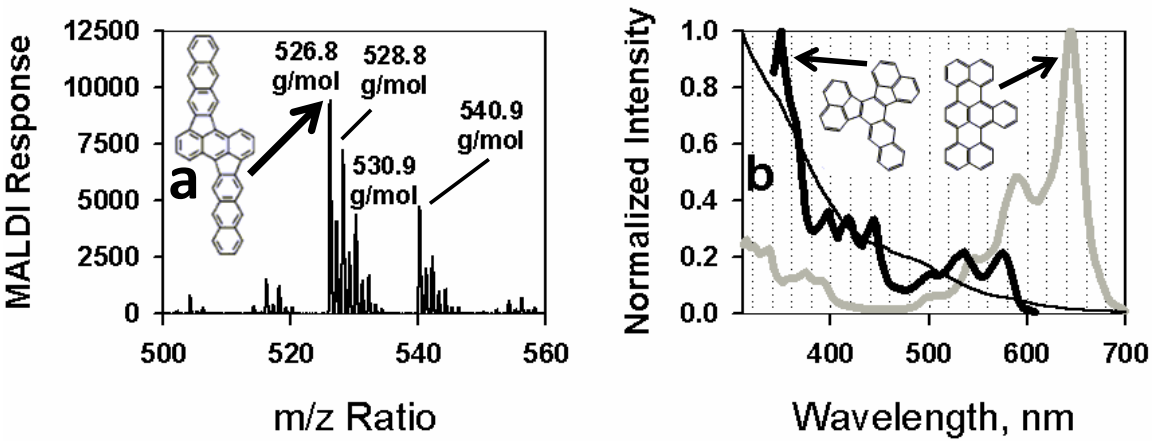

Figure 6.7. (a) MALDI spectrum for GPC Fraction A2, composed of anthracene pitch trimer, along with a proposed structure for m/z = 526.8. (b) The UV-Vis spectrum for GPC Fraction A2 (thin black line) is much more similar to that of the nonalternant 1.2,3.4-di(peri-naphthylene) anthracene (thick black line) than to that of the alternant 7.8-benzoterrylene (thick gray line). Reference spectra are adapted from Clar.[21]

Results clearly indicate that the UV-Vis spectrum for the nonalternant PAH is the better match for GPC Fraction A2. Particularly striking is the fact that 7.8-benzoterrylene exhibits its maximum absorption at a wavelength of 643.5 nm – a wavelength where the light absorption by GPC Fraction A2 is virtually nil. Thus, while we cannot positively identify the molecular structures present in anthracene pitch trimer, we can conclude that the vast majority of the species present in the trimer must be nonalternant PAHs with their characteristic five-membered rings.

The above results are in significant contrast to those of Mochida et al.[15] and of Edwards and Thies,[23] who proposed structures for anthracene pitch trimers composed only of alternant PAHs with their six-membered rings. In the case of Mochida et al.,[15] their isotropic anthracene pitch was produced catalytically using HF/BF_3 (with the mesophase pitch subsequently being produced from this isotropic pitch by thermal polymerization). On the other hand, five-membered connecting rings are in agreement

with the work of Sasaki et al.,[24] who predicted that the high-temperature (480 °C) carbonization of anthracene results in the formation of large, two-dimensional, discotic molecules consisting of anthracene monomers bonded via five-membered rings.

Anthracene Pitch Tetramer

MALDI analysis of tetramer-rich GPC Fraction A1 (see Fig. 6.8a) reveals that the most prevalent peaks occur at m/z = 701.1, 703.1, and 705.1. Consistent with our previous analysis, the peak at m/z = 701.1 is likely due to the condensation reaction of an anthracene molecule (mol wt 178) with the trimeric species of mol wt 526.8 (Fig. 6.7a), and the accompanying loss of 4 hydrogens. The peak at m/z = 703.1 is likely due to the reaction of the anthracene trimer of mol wt 528.8 (Fig. 6.7a) with anthracene, while the peak at m/z = 705.1 could arise from either the reaction of the anthracene trimer of mol wt 528.8 with dihydroanthracene (mol wt 180), or from the reaction of the anthracene trimer of mol wt 530.9 (Fig. 6.7a) with anthracene. Unfortunately, it was not feasible to perform PSD analyses on these peaks, as it was not possible to isolate the ions (parent and fragments) arising from each respective species from those arising from neighboring species.

The UV-Vis spectrum of tetramer (see Fig. 6.8b, thin black line) is quite similar to that of trimer, as it exhibits a uniform decrease in light absorption with respect to increasing wavelength. The UV-Vis spectrum for GPC Fraction A1 was compared to reference spectra for two large PAHs available in the literature[21] that are the closest match to our most likely species: (i) quaterrylene (see Fig. 6.8b; thick gray line), which

can be visualized as a tetramer of naphthalene and (ii) 1.2,3.4,5.6,7.8-tetra(peri-naphthylene)anthracene (Fig. 6.8b; thick black line), a large PAH that contains four five-membered rings. Once again, the UV-Vis spectrum for the nonalternant PAH provides a much better match to the UV-Vis spectrum for the GPC fraction. Thus, all characterization data observed for the three oligomeric fractions of anthracene pitch are consistent with the formation of oligomers by joining monomers via a five-membered ring.

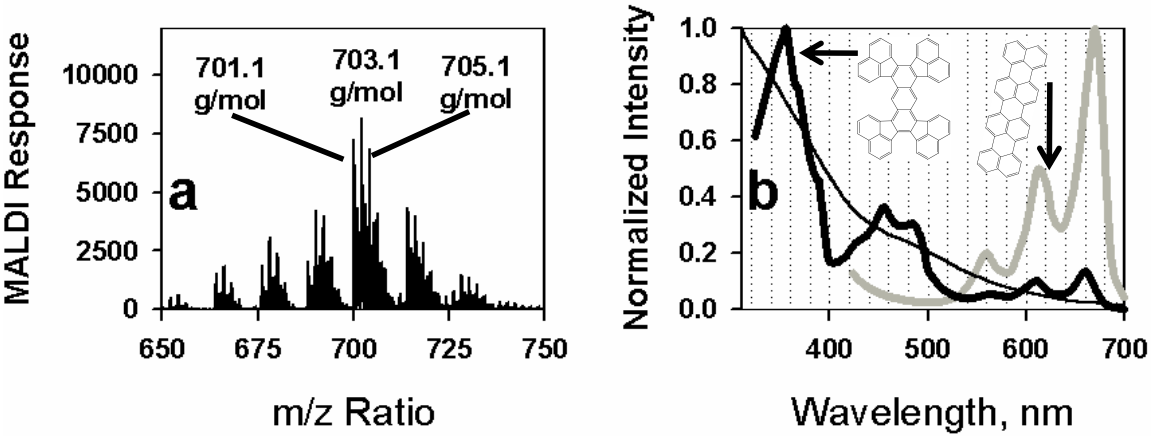

Figure 6.8. (a) MALDI spectrum for GPC Fraction A1, composed of anthracene pitch tetramer. (b) The UV-Vis spectrum for GPC Fraction A1 (thin black line) is much more similar to that of the nonalternant PAH (thick black line) than to that of the alternant PAH quaterrylene (thick gray line). Reference spectra are adapted from Clar.[21]

Structural Characterization of M-50 Pitch Oligomers

M-50 Pitch Dimer

The MALDI spectrum of M-50 pitch, focused in on the heavy monomer and dimer region, is given in Fig. 6.9. Previous work[8,9] has established that the species present in M-50 monomer can be resolved into a number of Gaussian signal distributions, with their constituent species being separated by increments of 14 Da. Such distributions

are created by methyl groups on a base PAH backbone of given mol wt. Like M-50 monomer, the major constituents of M-50 dimer can also be resolved into signal distributions separated by increments of 14 Da. For example, the "black square" signal distribution, originating at m/z = 376.4, is comprised of species of mol wts of 376.4, 390.5, 404.5, 418.5, 432.6, 446.5, and 460.5 Da. Three other major signal distributions present in M-50 dimer shown in Fig. 6.9 are (1) the "black triangle" distribution, originating at m/z = 400.4, (2) the "white circle" distribution, originating at m/z = 426.2, and (3) the "white triangle" distribution, originating at m/z = 450.6.

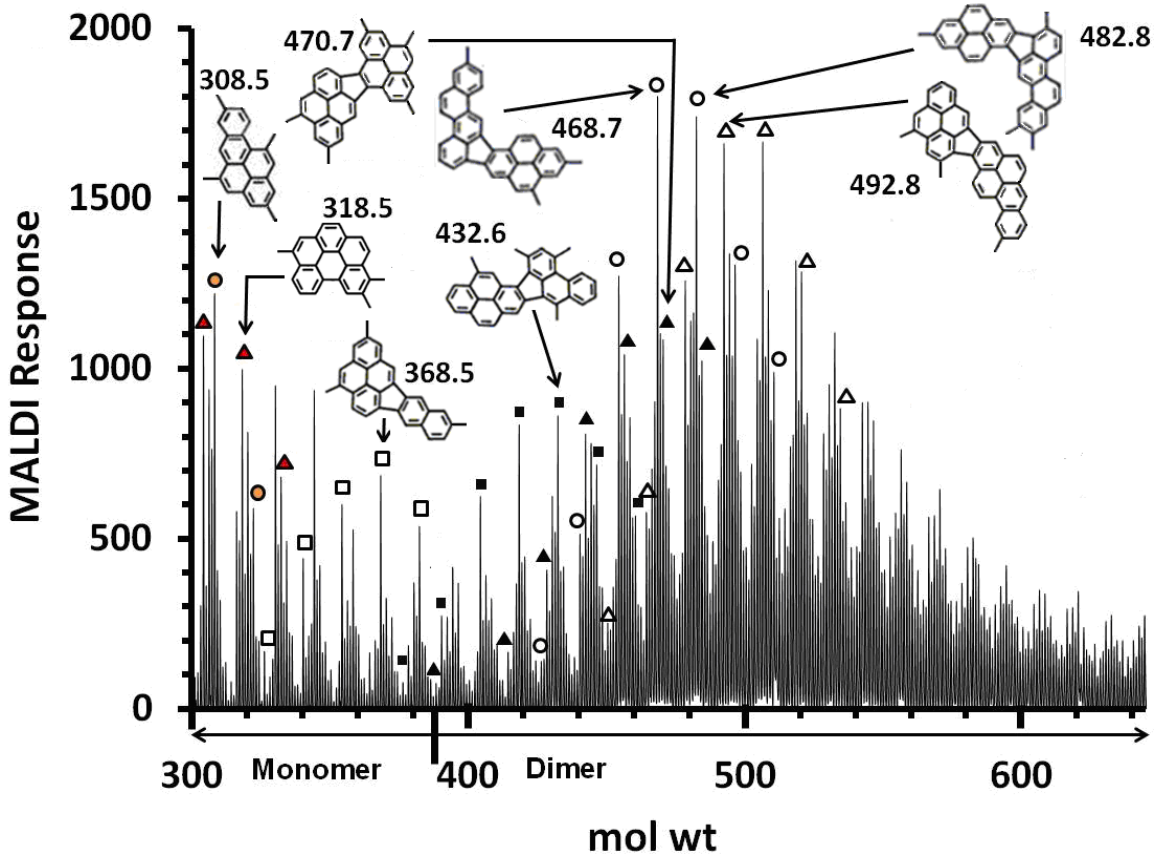

Figure 6.9. MALDI of M-50 pitch, focused in on the mol wt range of the heavy monomer and dimer. Major signal distributions are highlighted. Molecular structures of major and notable components, based on the structural characterization results discussed later in this section, are also shown.

The orange circles and red triangles shown in Fig. 6.9 are the tail end of the monomer distributions that were previously identified.[9] The "white square" signal distribution, originating at m/z = 326.5, was previously identified by our group.[9] However, the parent aromatic backbone was not established.

In preparation for PSD analyses, prep-scale GPC was applied to DGE Pitch Cuts 1-3 to produce GPC fractions rich in M-50 dimer, and in trimer and tetramer (see Figs. 6.3-6.5). Up to 45 GPC fractions per DGE pitch cut were obtained, with each cut being collected over a time interval of 15 s. MALDI analysis was performed on these fractions, and 16 of them exhibited prominent, well-isolated peaks such that they could be readily analyzed for molecular structure by PSD. Mol wts of the species in dimer-rich GPC Fractions 4-19 that were subjected to PSD analysis are given below the respective fraction numbers in Figs. 6.3b and 6.4b. We have previously discussed the capabilities and limitations of PSD elsewhere.[9]

In Figs. 6.10 and 6.11, MALDI-PSD fragmentation analyses are shown for the species in each of the aforementioned distributions. The PSD fragmentation patterns for the first two species in the "black square", "black triangle", and "white circle" signal distributions exhibit no fragment peaks, an observation that is in agreement with reference mass spectra[20] for unsubstituted and single-methylated PAHs. However, PSD spectra for all other species constituting these signal distributions exhibit a sharp fragment peak at a mol wt 15 Da less than that of the parent species, indicating a species that has lost a methyl group (e.g., 454.5 and 439.5 in Fig. 6.11i). In addition, PSD spectra for some of the heavier and all of the heaviest species in each distribution exhibit

fragment peaks at a mol wt 29 Da less than that of the parent species, indicating a species that has lost an ethyl group (e.g., 446.5, 431.5, and 417.6 in Fig. 6.10k). Notably, these trends are similar to those observed in PSD spectra for the species comprising M-50 monomer.[9] Also notable is the fact that none of the observed PSD spectra are consistent with mass spectra for molecules containing naphthenic groups.[20]

For none of GPC Fractions 4-19 was it feasible to perform MALDI-PSD analyses on the species of mol wt 450.6 Da, because of interference from closely neighboring species with stronger MALDI responses. However, we consider it likely that the "white triangle" signal distribution (see Figs. 6.9 and 6.11m-r) begins at 450.6 Da. Similarly, PSD could not be applied to the portion of M-50 dimer above ~520 Da, as prep-scale GPC was not able to adequately isolate individual species for PSD analysis in this mol wt region.

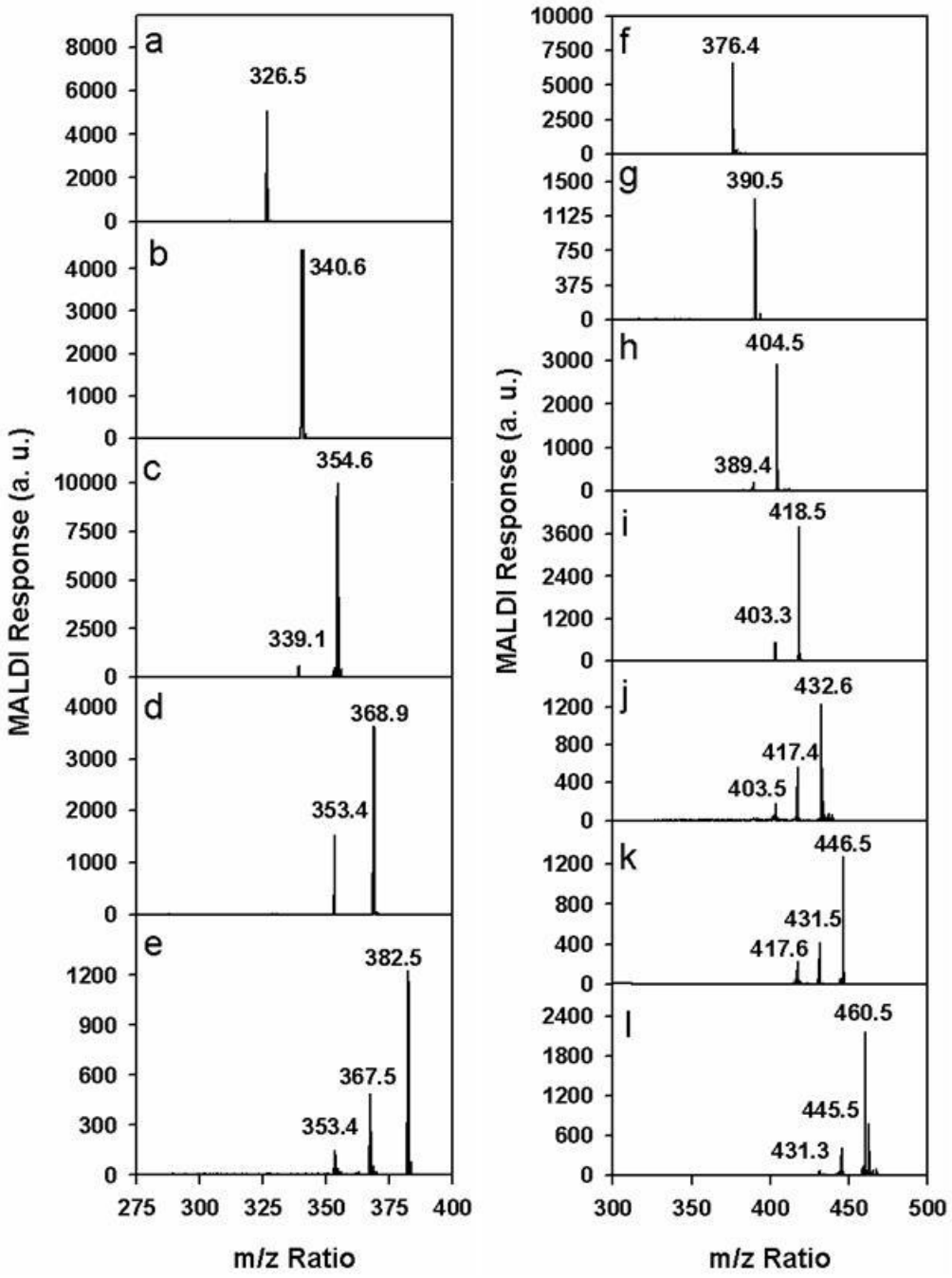

Figure 6.10. MALDI-PSD fragmentation analyses for the "white square" (a-e) and "black square" (f-l) signal distributions given in Fig. 6.9. PSD spectra are from GPC Fractions 4-11 (see Fig. 6.3b). Note that more than one PSD spectra was obtained from a given GPC fraction in many instances. For example, GPC Fraction 10 was the source of spectra for the parent species at both 340.6 (b above) and 376.4 (f above) Da.

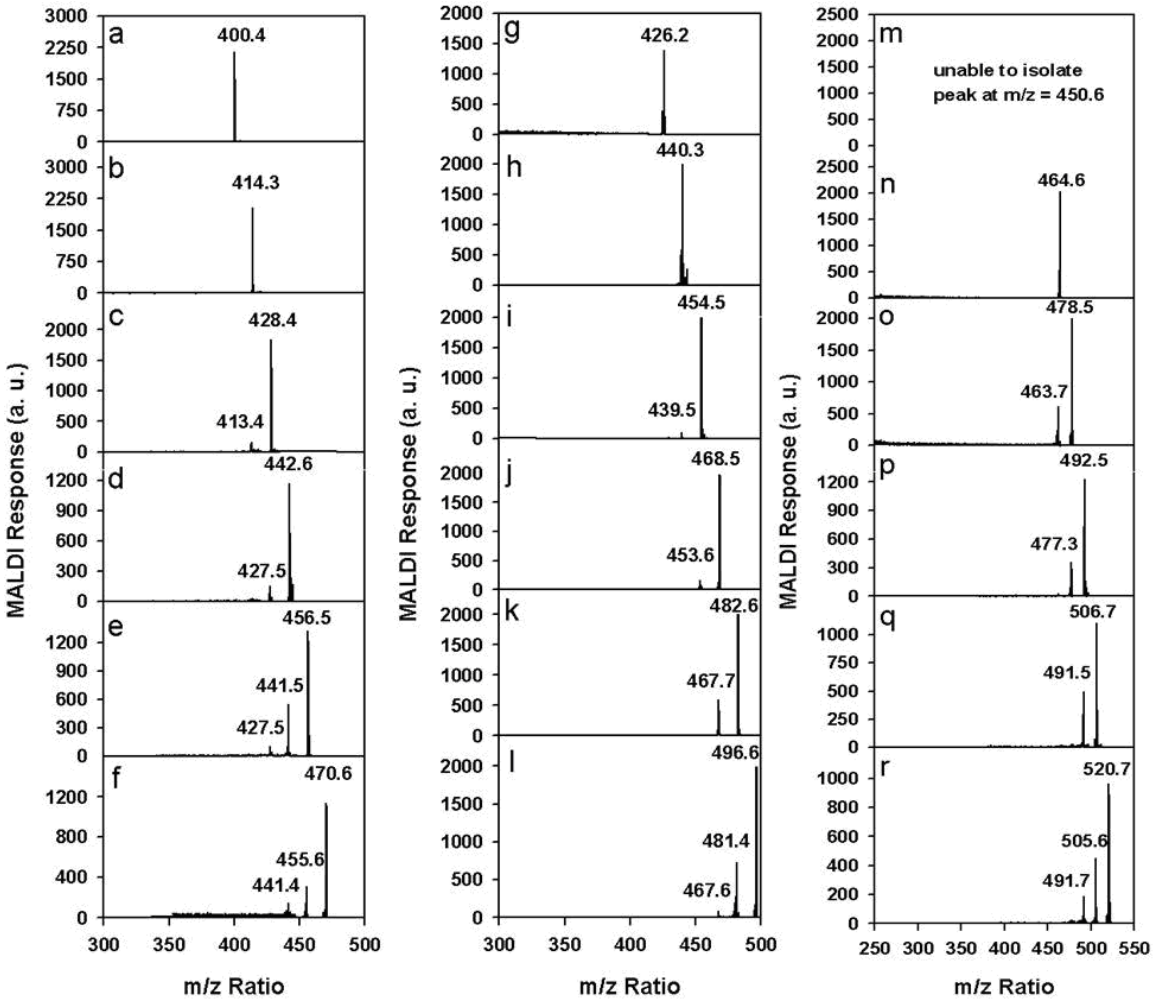

Figure 6.11. MALDI-PSD fragmentation patterns for the "black triangle" (a-f), "white circle" (g-l), and "white triangle" (m-r) distributions depicted in Fig. 6.9. PSD spectra were generated from GPC Fractions 12-19 (see Fig. 6.4b).

The next step in our work was the determination of the arrangement of bonds between the monomer units comprising the dimers. GPC Fractions 5, 10, and 14 were selected for UV-Vis analysis because of their relatively high purity, with each containing only one major species (see Fig. 6.12). The dominant peak in GPC Fraction 10 at m/z = 340.6 (Fig. 6.12a) corresponds to the second species in the "white square" distribution (see Figs. 6.9 and 6.10b), while in GPC Fraction 5 (Fig. 6.12c) the dominant species at

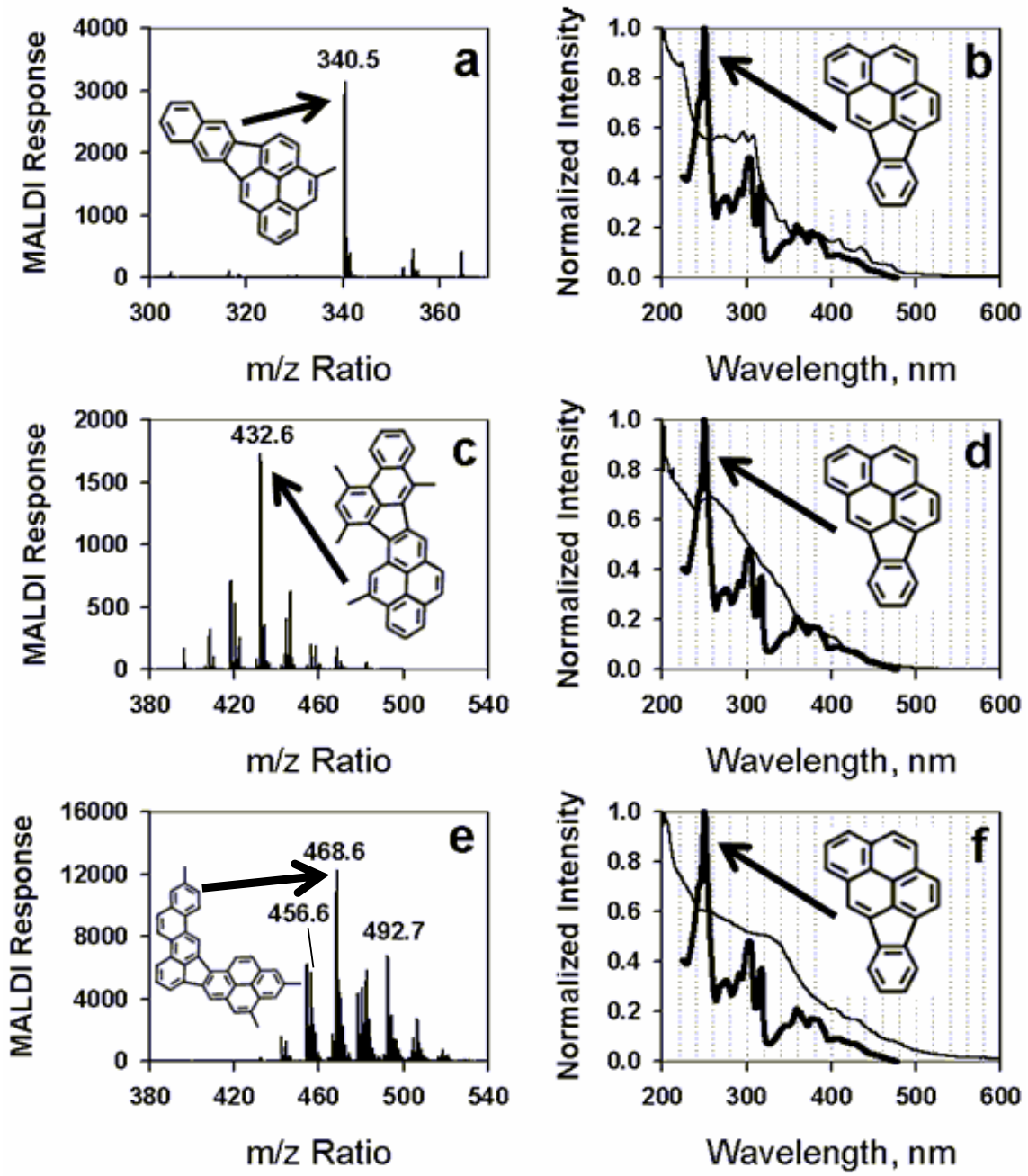

Figure 6.12. MALDI and UV-Vis spectra for dimer-rich GPC Fractions 10 (panels a and b), 5 (panels c and d), and 14 (panels e and f). The similarity of these UV-Vis spectra to that of the reference standard 2.3-o-phenylenepyrene (adapted from Clar[21]) indicates that these dimers are formed by joining the monomer precursors via a 5-membered ring. Depicted on the MALDI spectra are the molecular structures of the most prevalent dimer species for the signals at m/z = 340.5, 432.6, and 468.6.

m/z = 432.6 belongs to the "black square" signal distribution (Figs. 6.9 and 6.10j). Finally, GPC Fraction 14 (Fig. 6.12e) is rich in species that belong to the "white circle" (m/z = 468.6; Figs. 6.9 and 6.11j), "white triangle" (m/z = 492.5; Figs.6. 9 and 6.11p), and "black triangle" (m/z = 456.6; Figs. 6.9 and 6.11e) signal distributions.

The UV-Vis spectra (see Figs. 6.12b, 6.12d, and 6.12f) for these three GPC fractions exhibit common features: strong light absorption at wavelengths below 350 nm, with particularly strong absorption below 300 nm, and essentially nonexistent light absorbance at and above 500 nm. UV-Vis spectra for the other M-50 dimer-rich fractions are similar in appearance to those described above. Thus, all of these UV-Vis spectra differ significantly from those of fully alternant, benzenoid PAHs, such as the benzenoid dimers of phenanthrene and of pyrene presented by Clar.[21] They are much more similar to those of nonalternant PAHs,[21] such as 2.3-o-phenylenepyrene. Thus, the prevailing evidence indicates that M-50 dimer is primarily comprised of nonalternant PAHs containing a five-membered ring.

The next issue to be resolved was whether any significant structural change in the monomer precursors occurred in the formation of dimers. As shown in Figs. 6.10 and 6.11, the PSD fragmentation patterns indicate the absence of both naphthenic content and single biphenyl linkages in the dimer species analyzed. Thus, we concluded that the only structural change in the monomer precursors upon forming a dimer was the loss of two aromatic hydrogen atoms/monomer and subsequent formation of the 5-membered connecting ring. Furthermore, as was the case for the monomer distributions,[9] PSD

fragmentation patterns in Figs. 6.10 and 6.11 indicate that that the first species in each signal distribution is unsubstituted.

Taking into account the above information, we then proposed molecular structures for the most prevalent M-50 dimers by assuming that they form from the condensation reaction of two of the most common monomeric species, with the accompanying loss of 4 hydrogens and the formation of a five-membered "connecting" ring. Using this method, we were able correctly predict the mol wts for the most prevalent dimer species shown in Fig. 6.9. For example, the "white square" peak at m/z = 340.6 is a dimer of pyrene (m/z = 202) and naphthalene (m/z = 128) with one methyl substituent, while the "black square" peak at 432.6 is a dimer of pyrene and phenanthrene (178) with 4 methyl substituents. At 468.7, the "white circle" peak is a tri-methylated dimer of pyrene with a monomer of m/z = 228. Here the monomer could be chrysene, triphenylene, or benz[a]anthracene, as all of these were found in significant amounts in the monomer of M-50 pitch. A summary of the most prevalent dimers, their mol wts, and their monomer precursors, is given in Table 6.1.

M-50 Pitch Trimer

M-50 trimer was also prepared for characterization by using the two-step fractionation technique employed in the previous section. Specifically, DGE Pitch Cut 3 (see Fig. 6.5) was subjected to prep-scale GPC to yield GPC Fractions 20-23, on which MALDI, PSD, and UV-Vis analyses were then performed.

The MALDI spectrum of GPC Fraction 22, which encompasses most of the mol wt range for trimer in M-50 pitch (see Fig. 6.1), is given in Fig. 6.13. Analogous to what has previously been observed for the monomer and dimer portions of M-50 pitch, the highest-intensity peaks in the spectrum can be seen to belong to Gaussian-type signal distributions, with each peak separated by increments of 14 Da. For the "red triangle", "green square", and "blue circle" distributions shown in Fig. 6.13, PSD analysis (see Fig. 6.14) demonstrates that these increments are created by methyl substituent groups, again consistent with what we have previously reported for both monomers[8,9] and, above, for dimers. Because of signal interference from closely neighboring peaks, PSD analysis could only be performed on a limited number of the species within these signal distributions (and, in fact, on none of the species in the "purple rectangle" distribution).

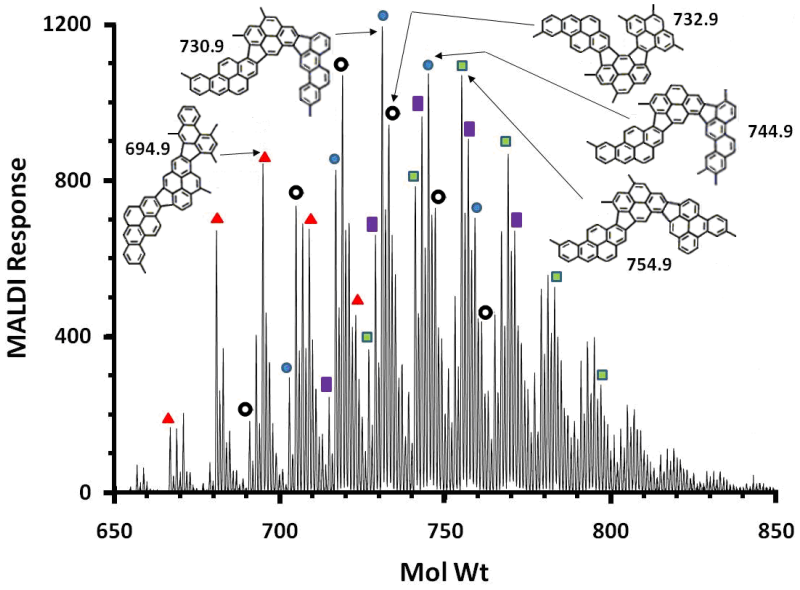

Figure 6.13. MALDI spectrum for trimer-rich GPC Fraction 22 (see Fig. 6.5b). Major species distributions are highlighted; molecular structures of the most prevalent trimers are depicted.

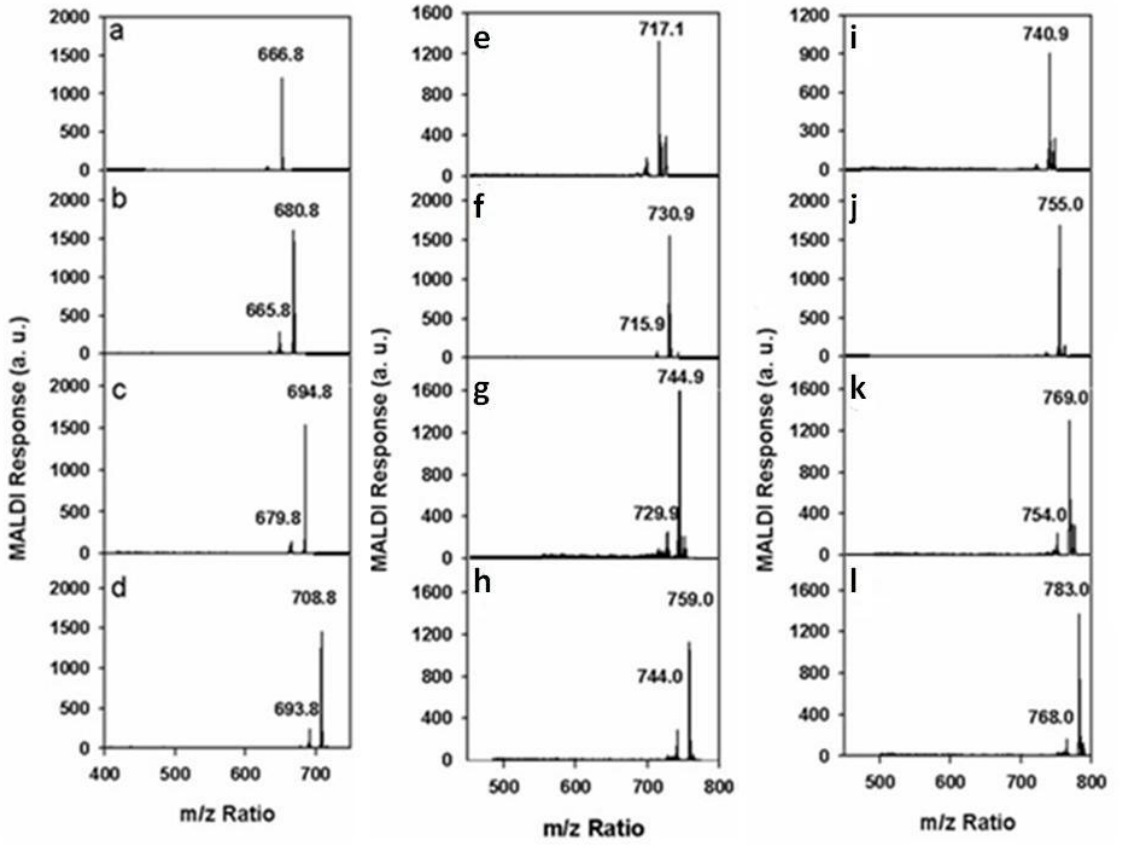

Figure 6.14. MALDI-PSD fragmentation patterns for selected species comprising various signal distributions in M-50 trimer: "red triangle" distribution (a-d), "green square" distribution (e-h), and "blue circle" distribution (i-l). PSD spectra were generated from GPC Fractions 21-23.

As was the case for M-50 dimer, none of the PSD spectra in Fig. 6.14 are consistent with reference mass spectra for molecules possessing either naphthenic content or single biphenyl linkages.[20] The weak intensity of the de-methylation peaks (and the total lack of any de-ethylation peaks) in Fig 6.14 occurred because a lower laser power had to be used for PSD analyses (thus reducing fragmentation) in order to reduce the total number of ions that had to be screened out by the ion gate. A higher ion count would have overloaded the ion gate, making all but impossible the task of isolating peaks in the more "crowded" GPC fractions containing the trimer species.

The UV-Vis absorption spectrum for GPC Fraction 22 is given in Fig. 6.15, as is the spectrum for trimer-rich, anthracene pitch GPC Fraction A2. The two spectra are quite similar, with both exhibiting the weak absorption at higher wavelengths characteristic of mixtures comprised primarily of nonalternant PAHs with their five-membered rings. These results thus continue the trend observed above for the dimers and/or trimers of anthracene and M-50 pitches: that is, M-50 pitch trimers consist of a dimer and a monomer joined via a five-membered ring.

Trimer structures for the most prominent signals in the MALDI spectrum for GPC Fraction 22 (see Fig. 6.13) were then constructed by assuming that some of the most prevalent dimer structures in M-50 pitch (e.g., the species of mol wts 432.6, 470.7, 482.8, and 492.8 in Fig. 6.9) undergo a condensation reaction with two of the most abundant monomer species in M-50, for example, methylbenzo[a]pyrene and methylbenzo[e]pyrene.[9] Once again, this procedure was successful in predicting the mol wts of some of the most prominent trimer signals in Fig. 6.13. Note that many variations on the reactions proposed above are possible. In fact, any species from the "black square", "black triangle", "white circle", or "white triangle" signal distributions in Fig. 6.9 could react with an alkylated benzopyrene to produce the trimer structures shown in Fig. 6.13, as long as the total number of methyl substituent groups on the final trimer in question remained unchanged. Finally, we note that, unlike the dimer distributions shown in Fig. 6.9, the first trimer in a series distribution in Fig. 6.13 does not consist of a bare PAH backbone, as these precursors were not among the most abundant ones. A

summary of the most prevalent trimers, their mol wts, and their monomer precursors, is given in Table 6.1.

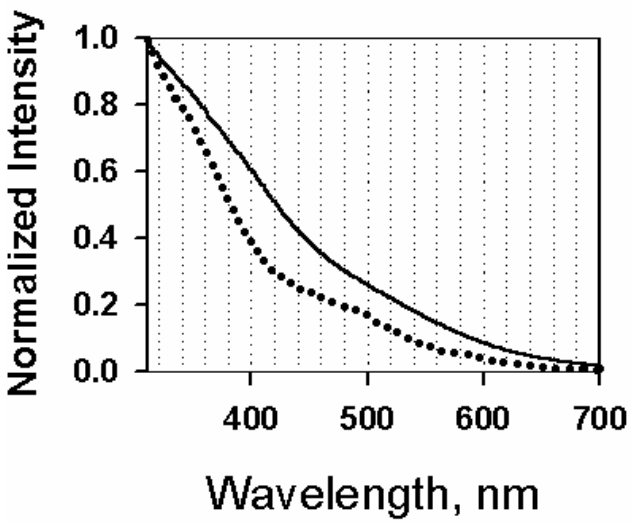

Figure 6.15. UV-Vis spectra for trimer-rich GPC Fraction 22 (solid black line) and for trimer-rich, anthracene pitch GPC Fraction A2 (dotted black line) are compared.

M-50 Pitch Tetramer

M-50 tetramer was isolated for characterization by subjecting DGE Pitch Cut 3 to prep-scale GPC. The heaviest fraction, GPC Fraction 20 (see Fig. 6.5b) was found to contain more than 90% tetramer and was thus selected for analysis by both MALDI and UV-Vis analysis. PSD could not be performed because the tetramer peaks were too close to each other for any to be isolated.

The MALDI spectrum for tetramer-rich GPC Fraction 20 is given in Fig. 6.16. Applying the analogous methods to what was previously applied to M-50 dimers and trimers, we can classify many of the most prevalent constituents of M-50 tetramer as belonging to one of three signal distributions, denoted in Fig. 6.16 by white rectangles, white diamonds, and black circles, with the peaks in each distribution being separated by

increments of 14 Da. Although the more continuous nature of the mol wt distribution of the M-50 tetramer makes the application of PSD for fragmentation analysis impractical, there is no reason to believe that the increments of 14 Da described above could be anything but increasing levels of methylation on a base PAH backbone, analogous to what was definitively determined for the dimer and trimer oligomers.

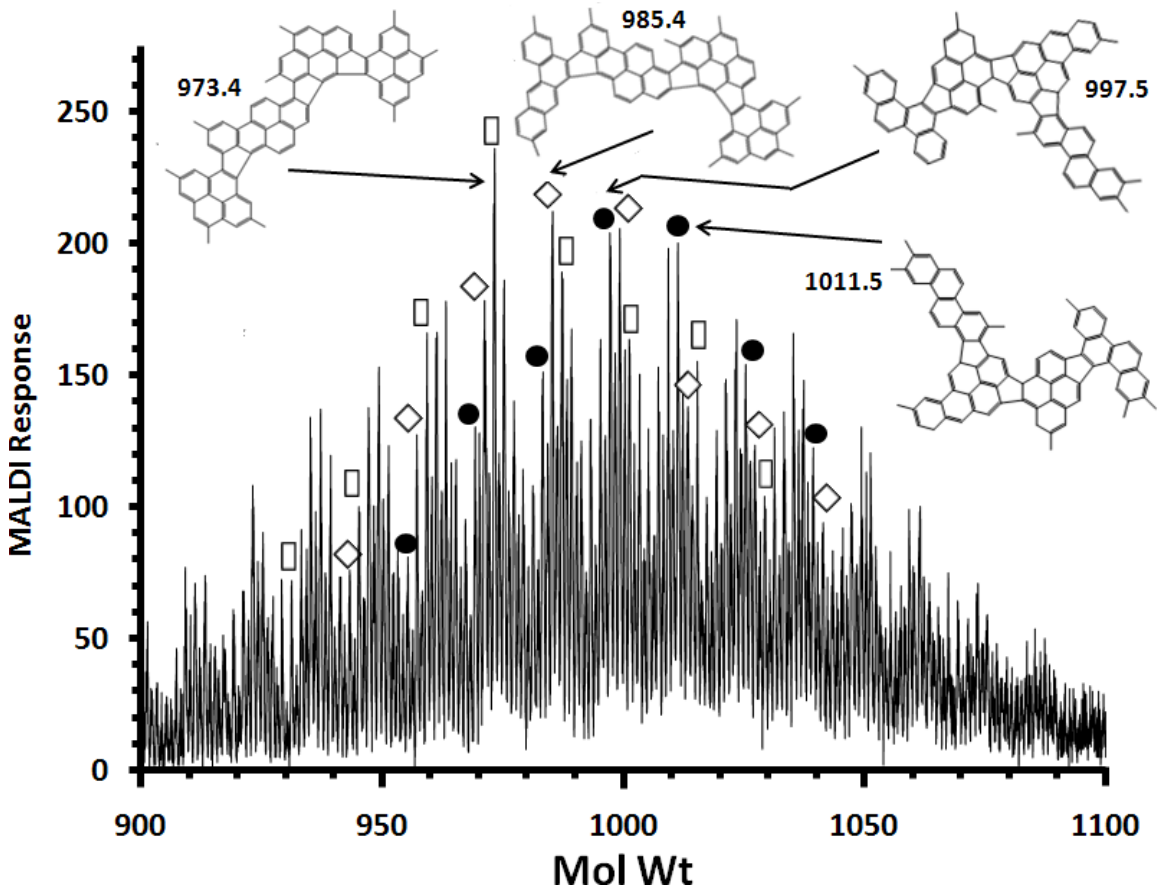

Figure 6.16. MALDI spectrum for tetramer-rich GPC Fraction 20 (see Fig. 6.5b). Major signal distributions are highlighted, and the molecular structures of some of the most prevalent tetramer species are depicted.

The UV-Vis absorption spectrum for GPC Fraction 20 is given in Fig. 6.17, along with the spectrum of tetramer-rich, anthracene pitch GPC Fraction A1. As before, the weakness of absorption at higher wavelengths suggests that M-50 tetramer is formed by

the condensation reaction of lower mol wt oligomeric units such that five-membered rings connect the reacting monomeric or oligomeric species. Proposed molecular structures for the major M-50 tetramer species, which are consistent with the condensation reaction of two common dimers, or with the reaction of a common monomer and trimer, are given in Fig. 6.16. The mol wts of these species, and their monomeric constituent units, are summarized in Table 6.1.

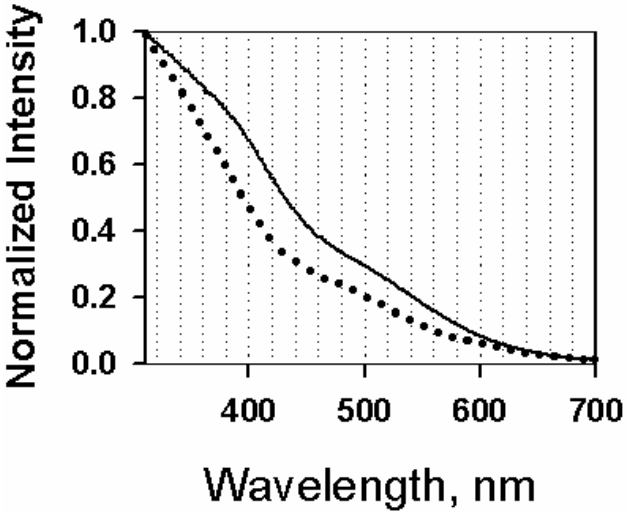

Figure 6.17. UV-Vis absorption spectra for GPC Fraction 20 (solid black line) and anthracene pitch, tetramer-rich GPC Fraction A1 (dotted black line) are compared.

Table 6.1. Molecular weights of both the precursor monomer units[b] and the resultant major oligomers that comprise M-50 pitch.

Oligomer Type	Monomer Reactant 1	Monomer Reactant 2	Monomer Reactant 3	Monomer Reactant 4	H Atom Loss[a]	Mol Wt of Oligomer Product (g/mol)
Dimer	220[i]	216[ii]	------	------	4	432.6
Trimer	220[i]	216[ii]	266[iii]	------	8	694.9
Dimer	244[iv]	230[v]	------	------	4	470.7
Trimer	244[iv]	230[v]	266[iii]	------	8	732.9
Tetramer	244[iv]	230[v]	266[iii]	244[iv]	12	973.4
Tetramer	244[iv]	230[v]	266[iii]	256[vi]	12	985.4
Dimer	230[v]	242[vii]	------	------	4	468.7
Trimer	230[v]	242[vii]	266[iii]	------	8	730.9
Tetramer	230[v]	242[vii]	266[iii]	270[viii]	12	997.5
Dimer	270[h]	216[ii]	------	------	4	482.8
Trimer	270[h]	216[ii]	266[iii]	------	8	744.9
Tetramer	270[h]	216[ii]	266[iii]	270[viii]	12	1011.5
Dimer	266[iii]	230[v]	------	------	4	492.8
Trimer	266[iii]	230[v]	266[iii]	------	8	754.9

[a]Four hydrogen atoms are lost for each condensation reaction between monomeric units as a five-membered connecting ring is formed.
[b]Likely identities for the monomer units are proposed based on our previous results:[9]
[i]Trimethylphenanthrene; [ii]Methylpyrene; [iii]Methylbenzo[a]pyrene, methylbenzo[e]pyrene; [iv]Trimethylpyrene; [v]Dimethylpyrene; [vi]Dimethylchrysene, dimethylbenz[a]anthracene, dimethyltriphenylene; [vii]Methylchrysene, methylbenz[a]anthracene, methyltriphenylene;
[viii]Trimethylchrysene, trimethylbenz[a]anthracene, trimethyltriphenylene.

FT-IR Spectroscopy of M-50 Pitch Oligomers

For FT-IR analyses, two GPC fractions of higher concentration than those described above were also collected: GPC Fraction 25, a trimer-rich fraction collected from 58.4 to 59.9 min, and GPC Fraction 24, a tetramer-rich fraction collected from 55.9 to 57.4 min. The FT-IR absorption spectra for these trimer- and tetramer-rich fractions of M-50 pitch, along with spectra for monomer- and dimer-rich fractions of M-50 pitch, are shown in Figs. 6.18a-d. Of particular interest to us is the fact that all fractions of M-50

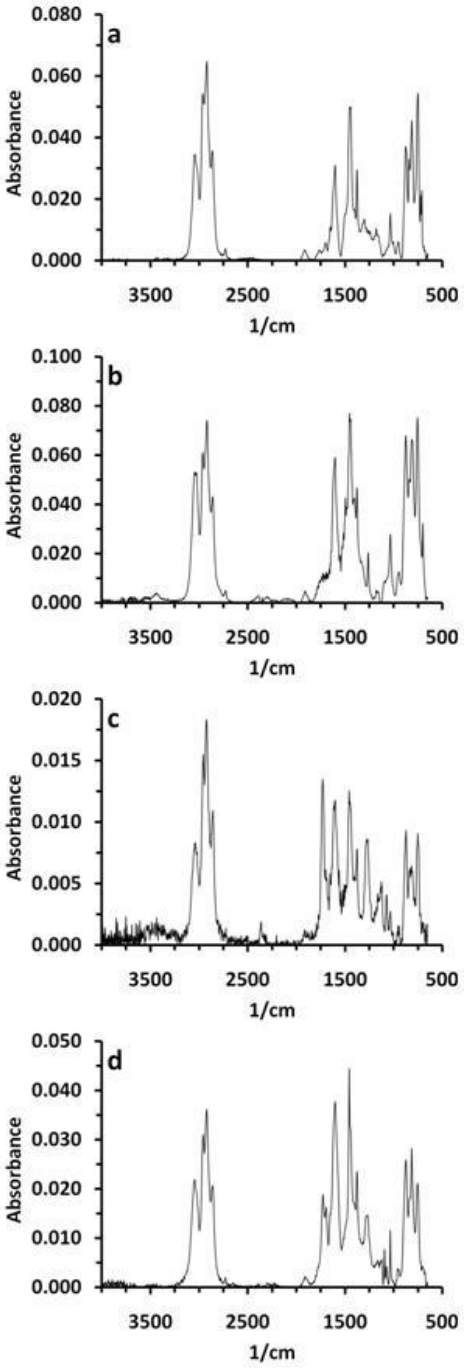

Figure 6.18. Transmission FT-IR analysis for (a) a pitch cut containing 98% M-50 monomer, (b) a pitch cut containing 97% M-50 dimer, (c) a trimer-rich cut (GPC Fraction 25), and (d) a tetramer-rich cut (GPC Fraction 24). The monomer and dimer cuts were prepared as described by Cristadoro et al.[8] Significant aryl content (note peaks from 900 to 700 cm^{-1} indicating out-of-plane bending vibrations of aryl C-H groups) are observed for all fractions.

pitch have significant aryl content, as exhibited by the strong absorption between 900 and 700 cm^{-1} in all cases. The fact that the aryl content does not significantly decrease with increasing oligomeric size is consistent with our structural observations thus far: that is, linkage between monomer units does not occur by large-scale condensation or significant rearrangement of monomer units to form highly condensed, graphitic structures, but by the loss of only four hydrogen atoms and the formation of a single, five-membered ring.

Conclusions

Although characterization of the mesophase-forming constituents (i.e., mesogens) in pitches has been a subject of interest for many years, identification of their actual molecular structures has met with limited success. By applying our two-step, sequential fractionation process (i.e., DGE followed by prep-scale GPC) to M-50 petroleum pitch, we have been able to isolate individual oligomeric constituents for subsequent analysis and identification. A key finding of our work is that the dimer, trimer, and tetramer oligomers present in petroleum pitch are formed by the joining of monomer "building block" units via a nonalternant, 5-membered connecting ring – and not by the alternant, 6-membered connecting ring that is typically proposed in the literature.[8,25,26] Furthermore, the monomer precursors are seen to undergo essentially no structural change and minimal loss of alkyl substituent groups as they link up to form oligomers. Because this oligomer formation occurs via a condensation reaction in which only a total of 4 hydrogens are lost as the connecting, nonalternant ring is created between two monomer units, no large-scale condensation occurs. This is in significant contrast to the

highly condensed nature of the higher mol wt species that are found in coal-tar pitches,[27] and may have significant implications for the formation of mesophase pitch from each of these starting materials.

Finally, we note that M-50 pitch and the mesogenic oligomers therein are typically produced by the thermal polymerization of FCC decant oil. Whether similar formation mechanisms and molecular structures occur when catalytic polymerization is used to produce isotropic and mesophase pitches will require further investigation.

References

[1]Beauharnois, M. E.; Edie, D. D.; Thies, M. C. Carbon Fibers from Mixtures of AR and Supercritically Extracted Mesophases. *Carbon,* **2001**, *39*, 2101-2111.

[2]Schulz, D. A. Fuel Cell Electrode. U. S. Patent 3960601, 1976.

[3]Mochida, I.; Kawano, S. Capture of Ammonia by Active Carbon Fibers Activated with Sulfuric Acid, *Ind. Eng. Chem. Res.*, **1991**, *30*, 2322-2327.

[4]Kim, M. C.; Eom, S. Y.; Ryu, S. K.; Edie, D. D. Reformation of Naphtha Cracking Bottom Oil for the Preparation of Carbon Fiber Precursor Pitch. *Korean Chem. Eng. Res.* **2005**, *43*, 745-750.

[5]Edie, D. D. The effect of processing on the structure and properties of carbon fibers, *Carbon*, **1998**, *36(4)*, 345-362.

[6]Edwards WF, Jin L, Thies MC. MALDI-TOF mass spectrometry: Obtaining reliable mass spectra for insoluble carbonaceous pitches, *Carbon,* 2003; **41**, 2761-2768.

[7]Greinke, R. A. Kinetics of petroleum pitch polymerization by gel permeation chromatography, *Carbon* **1986**, *24(6)*, 677-686.

[8]Cristadoro, A.; Kulkarni, S. U.; Burgess, W. A.; Cervo, E. G.; Räder, H. J.; Müllen, K.; Bruce, D. A.; Thies, M. C. Structural characterization of the oligomeric constituents of petroleum pitches. *Carbon,* **2009**, *47,* 2358-2370.

[9]Burgess, W. A.; Thies, M. C. Structural Identification of the Monomeric Constituents of Petroleum Pitch. *Energy Fuels,* in press.

[10]Scaroni, A. W.; Jenkins, R. G.; Walker, P. L. Carbonization of Anthracene in a Batch Reactor, *Carbon* **1991**, *29(7)*, 969-980.

[11]Mochida, I.; Oyama, T.; Korai, Y.; Fei, Y. O. Study of Carbonization Using a Tube Bomb; Evaluation of Lump Needle Coke, Carbonization Mechanism, and Optimization. *Fuel* **1988**, *67*, 1171-1181.

[12]Lewis, I. C.; Petro, B. A. Molecular Weight Analysis of Pitches and Polymeric Pitches by Gel Permeation Chromatography. *J. Polym. Sci., Polym. Chem. Ed.* **1976**, *14*, 1975-1985.

[13]Dickinson, E. M. Average Structures of Petroleum Pitch Fractions by $^{1}H/^{13}C$ N.M.R. Spectroscopy. *Fuel* **1985**, *64*, 704-706.

[14]Kershaw, J. R.; Black, K. J. T. Structural Characterization of Coal-Tar and Petroleum Pitches, *Energy Fuels*, **1993**, *7(3)*, 420-25.

[15]Mochida, I.; Shimizu, K.; Korai, Y.; Sakai, Y; Fujiyama, S. Mesophase Pitch Derived from Isotropic Anthracene Pitch Produced Catalytically with HF/BF_3, *Bull. Chem. Soc. Jpn.* **1990**, *63*, 2945-2950.

[16]Cervo, E. G.; Thies, M. C. Control of Molecular Weight Distribution of Petroleum Pitches via Multistage Supercritical Extraction, *J. Supercrit. Fluids*, **2010**, *51*, 345-352.

[17]Korai, Y.; Yoon, S.-H.; Oka, H.; Mochida, I.; Nakamura, T.; Kato, I.;Sakai, Y. The Properties of Co-Oligomerized Mesophase Pitch from Methylnaphthalene and Naphthalene Catalyzed by HF/BF_3. *Carbon* **1998**, *36(4)*, 369-375.

[18]MSDS for M-50 Pitch. <http://www.mapllc.com/MSDS/0275MAR019.pdf>

[19]Cervo, E. G.; Thies, M. C. Controlling the Oligomeric Composition of Carbon-Fiber Precursors by Dense-Gas Extraction. *J. Am. Ceram. Soc.*, **2008**, *91*, 1416-1422.

[20]CAS SciFinder. <http://www.cas.org/products/scifindr/index.html>

[21]Clar, E. *Polycyclic Hydrocarbons.* Academic Press, London (1964). pp. 43, 55, 58, 231, 266, 267, 284, 328, 330, 361, 370.

[22]McLafferty, F. W. *Interpretation of Mass Spectra*, 3rd ed.; University Science Books: Mill Valley (CA), 1980; p. 187.

[23]Edwards, W. F.; Thies, M. C. Dense Gas Fractionation and MALDI Characterization of Carbonaceous Pitches. *Energy & Fuels* **2005**, *19*, 984-991.

[24]Sasaki, T.; Jenkins, R. G.; Eser, S.; Schobert, H. H. Carbonization of Anthracene and Phenanthrene. 2. Spectroscopy and Mechanisms, *Energy Fuels* **1993**, *7*, 1047-1053.

[25]Greinke, R. A.; Lewis, I. C. Carbonization of Naphthalene and Dimethylnaphthalene. *Carbon* **1984**, *22(3)*, 305-314.

[26]Lewis, I. C. Thermal Polymerization of Aromatic Hydrocarbons. *Carbon* **1980**, *18(3)*, 191-196.

[27]Herod, A. A.; Bartle, K. D.; Kandiyoti, R. Characterization of Heavy Hydrocarbons by Chromatographic Mass Spectrometric Methods: An Overview. *Energy Fuels* **2007**, *21(4)*, 2176-2203.

CHAPTER 7

ADDITIONAL DISCUSSIONS CONCERNING THE STRUCTURAL IDENTIFICATION OF THE OLIGOMERIC CONSTITUENTS OF PETROLEUM PITCH

Effect of Reaction Mechanism on Bonding Arrangement Between Monomers

The lack of understanding of the bonding arrangement between the monomer units comprising pitch oligomers is an impediment to determining accurate molecular structures for the components of mesophase pitch. Previous work suggests that the reaction conditions (that is, whether the reaction proceeds by a thermal, or catalytic polymerization mechanism) largely determines the number and arrangement of the bonds. For example, reaction of naphthalene in the presence of $AlCl_3$ results in the formation of perylene,[1] a dimer of naphthalene in which the monomer units are joined via a six-membered ring. Similar results are observed when the reactant is pyrene or coronene. Therefore, we studied two pitches which were produced at similar conditions: M-50 pitch (the residue produced by the thermal polymerization of FCC decant oil) and an anthracene pitch produced by reacting anthracene at high temperature with no catalyst.[2,3] In this work, we seek to use our knowledge of the structures present in M-50 monomer to determine molecular structures for the heavier, mesophase-forming trimer and tetramer oligomers of M-50 pitch. The objectives of this work, then, were twofold: (i) determining the number and arrangement of the bonds in the prominent species comprising the oligomers of anthracene and M-50 pitches, and (ii) using this information

in predicting molecular structures for the major oligomers in both anthracene and M-50 pitches.

Optimizing the Quality of UV-Vis Spectra

UV Cutoff Wavelength

The UV cutoff wavelength indicates the lowest wavelength for which absorbance values can be measured for a particular compound. All light of lower wavelength incident on the sample solution is absorbed by the solvent. The UV cutoff wavelengths for cyclohexane and 1,2,4-trichlorobenzene (TCB) are 200 and 308 nm, respectively. Clearly, a solvent with a lower UV cutoff is desirable, as such a choice would allow for the collection of a UV-Vis spectrum over a greater range of wavelengths. However, pitch cuts of higher molecular weights (trimer-range and higher) are typically insoluble in such solvents. For pitches, aromatic solvents such as benzene, toluene, and TCB possess greater solvating power than cyclohexane and other common UV-Vis solvents. However, there is a trade-off as aromatic solvents have relatively high UV cutoff wavelengths.

Effect of Concentration

Lower concentrations which lead to max absorbances below 2.0 (using the Spectral Instruments 400 Series spectrophotometer) result in better, well-resolved UV-Vis spectra.

Note Concerning the Mol Wt at Which the Monomer/Dimer Boundary Occurs

Because of the similarity in the overall form of the UV-Vis spectra in Figs. 12b, 12d, and 12f in Chapter 6, it is likely that a number of "heavy monomer" species, such as those comprising the "white square" signal distribution, are actually dimers. Thus, there is no clear point where monomer ends and dimer begins (note the overlap in Fig. 6.9 in Chapter 6 between the "red triangle" distribution in M-50 monomer with the "white square" distribution in M-50 dimer). Rather, the species within a mol wt range of 326 and 388 Da are comprised of both monomer and dimer.

UV-Vis Spectra for Benzenoid Dimers

In this section, we give additional UV-Vis spectral justification for our conclusion that benzenoid (that is, aromatic molecules containing only 6-membered rings) dimers are not present in M-50 pitch in significant amounts. In Fig. 7.1, the UV-Vis spectra for phenanthrene dimer (see panel a) and pyrene dimer (see panel b) are given. Each of these dimers has an isomer, the UV-Vis spectrum of which is similar in form to those displayed in Fig. 7.1. The UV-Vis spectra shown in this figure were adapted from Clar (1964).[4]

Unlike the UV-Vis spectra for the GPC Fractions introduced in Chapter 6, the peaks at absorption wavelengths above 400 nm are very strong. Hence we conclude that dimer molecules in which the monomer units are joined via a six-membered ring are not prevalent in M-50 dimer.

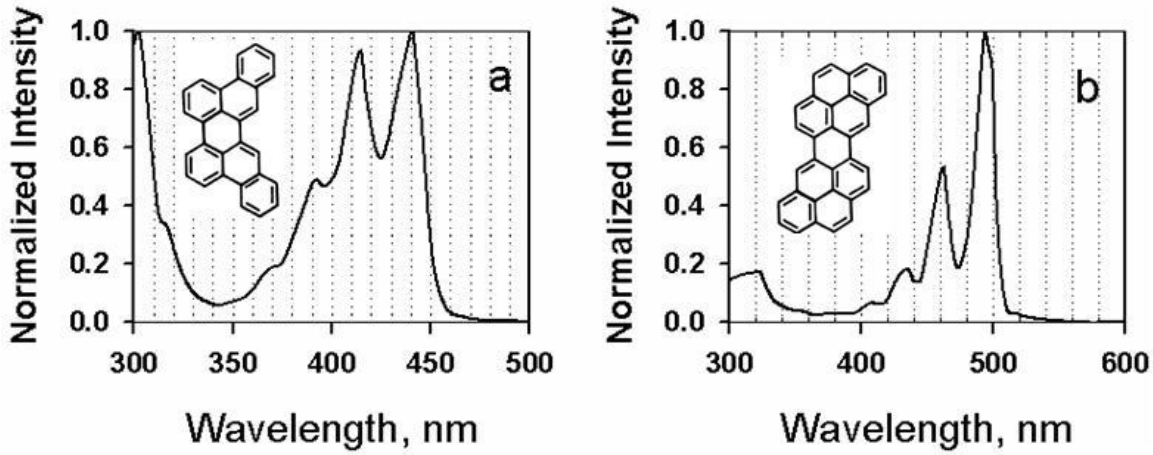

Figure 7.1. UV-Vis spectra for selected benzenoid dimers of phenanthrene (panel a), and pyrene (panel b). Adapted from Clar.[4]

Additional Discussions Concerning IR Spectral Analyses of Pitches

M-50 and coal-tar pitches are similar in that both classes of pitch are residues remaining after the high-temperature distillation of carbonaceous feeds (FCC decant oil and coal-tar, respectively). Herod et al.[5] have reported IR spectra indicating that the heaviest species of coal-tar pitch are structurally very dissimilar to the lighter ones (acetonitrile-soluble), postulating that while light PAHs such as pyrene and the benzopyrene isomers are present in the pitch, the largest species have a structure that is 3-D, with very few aromatic C-H bonds present. Specifically, IR spectra for light fractions of coal-tar pitch exhibit sharp, strong peaks in the fingerprint region of the spectrum between 900 and 700 cm^{-1}. These peaks indicate out-of-plane bending vibrations of aryl C-H groups. However, IR spectra for the heaviest fractions of coal-tar pitch exhibit weak absorption in this area, suggesting that there are very few aryl C-H sites present in these fractions.

Because of the marked differences in the IR spectra of the light and heavy fractions of coal-tar pitch, the IR spectra for oligomeric fractions of M-50 monomer, dimer, trimer, and tetramer were compared (see Fig. 6.18, Chapter 6). For all M-50 pitch fractions characterized, there is a sizable presence of peaks in the region 900-700 cm^{-1}. From this result we can conclude that there are an appreciable number of aryl C-H sites present in M-50 monomer, dimer, trimer, and tetramer, a conclusion markedly different to that observed for the coal-tar pitch. This conclusion differs from that observed for the coal-tar pitch in that the light coal-tar pitch fractions exhibited strong peaks in this region, while the heavy ones did not. Therefore, for M-50, the hypothesis that molecules in this mol wt range consist of monomers connected via condensation reactions appears accurate.

References

[1]Fetzer, J. C. The Chemistry and Analysis of Large PAHs. *Polycyclic Arom. Compd*. **2007**, *27(2)*, 143-162.

[2]MSDS for M-50 Pitch. http://www.mapllc.com/MSDS/0275MAR019.pdf

[3]Edwards, W. F.; Jin, L.; Thies, M. C. MALDI-TOF Mass Spectrometry; Obtaining Reliable Mass Spectra from Insoluble Carbonaceous Pitches. *Carbon* **2003**, *41*, 2761.

[4]Clar, E. *Polycyclic Hydrocarbons.* Academic Press, London (1964). pp. 58, 266.

[5]Herod, A. A.; Bartle, K. D.; Kandiyoti, R. Characterization of Heavy Hydrocarbons by Chromatographic Mass Spectrometric Methods: An Overview. *Energy Fuels* **2007**, *21(4)*, 2176-2203.

CHAPTER 8

CONCLUSIONS AND RECOMMENDATIONS

The work of the Carbon group has been focused on both controlling and characterizing the molecular composition of carbonaceous pitches, with a longer-term goal of producing molecularly optimized precursors for high-performance carbon molecules. To this end, this dissertation had two major goals: (i) development of an equation of state for predicting the global phase behavior of carbonaceous pitches over a wide range of temperatures and pressures, both in the presence and absence of solvents. (ii) identification of the molecular structures of the major components in a representative petroleum pitch.

The success of this work is illustrated by 3 major achievements:

(1) The Statistical Associated-Fluid Theory (SAFT) equation of state was combined with the liquid crystal theory of Maier and Saupe[1,2,3] (as expanded to multicomponent mixtures by Humphries, James, and Luckhurst[4,5,6]) to produce the SAFT-liquid crystal (SAFT-LC) equation, which can be used to predict both isotropic phase equilibria and mesophase content in pitch and pitch-solvent mixtures.

(2) Matrix-assisted, laser desorption and ionization, time-of-flight mass spectrometry-post source decay (MALDI-PSD, or PSD) was applied to narrow molecular

weight (mol wt) fractions of M-50 pitch to determine molecular structure information (primarily alkyl substituent information) for the species therein.

(3) A two-step separation technique, consisting of dense-gas extraction (DGE) followed by high-temperature, preparatory-scale gel permeation chromatography (prep-scale GPC), was used to produce narrow pitch fractions in quantities sufficient to allow for the further, successful characterization of said fractions using high-performance liquid chromatography with photodiode array detection (HPLC/PDA), ultraviolet-visible spectrophotometry (UV-Vis), MALDI, PSD, and thin films transmission Fourier Transform-Infrared (FT-IR) spectroscopy.

Achievements (2) and (3) above are the most complete structural characterization to date of the most prominent individual species comprising M-50 pitch.

Conclusions

SAFT-LC Equation

SAFT-LC is a potentially powerful tool for predicting the optimum DGE operating conditions for producing pitch fractions of a desired mol wt distribution (MWD) and mesophase content. For the first time, an equation of state that can predict both the isotropic phase equilibrium (e. g., both vapor-liquid equilibrium and liquid-liquid equilibrium) and mesophase content of pitch and pitch-solvent mixtures at near-critical and super-critical conditions is available. So far, this equation has been used to

predict phase equilibrium and mesophase content only for single-stage extraction processes, but it could also be extended to multistage DGE separations using packed columns (such multistage calculations would be aided by the use of a simulation package such as ASPEN or HYSYS).

However, the accuracy of SAFT in predicting the oligomeric composition of pitch fractions obtained via DGE processing remains an open question. Recall that the experimental phase-equilibrium data used in Chapters 2 and 3 to fit SAFT-LC parameters was incomplete, as only the solvent content of each phase during DGE, plus the mesophase content after solvent drying, were available for fitting SAFT-LC parameters (the MALDI technique was nascent at that time, and no such instrumentation existed at Clemson University).

PSD

PSD has shown itself to be a useful technique for the characterization of pitches, as a pitch species of a given mol wt that has been insufficiently isolated can be can be analyzed to obtain a molecular fragmentation pattern (which yields information concerning the molecular structure, such as naphthenic content and the nature of substituent groups present). Unlike other mass spectrometry techniques, the PSD technique can be applied to nonvolatile species. The unique ability of our group to obtain oligomeric cuts by DGE, and then to isolate pitch species from these DGE cuts by high-temperature GPC, was a key factor in the success of this work.

The quality of the PSD spectra obtained was maximized through proper selection of the instrument operating parameters. In the FlexControl MALDI operating software, separate methods have been prepared to yield crisp, neat spectra (featuring well-defined peaks with a minimum of baseline elevation), depending on the mol wt of the pitch species to be characterized. These methods include pre-programmed values of the laser power and microchannel plate detector gain to be used for each segment of the PSD spectrum obtained (see Appendices E and F). However, it is necessary to reassess these parameters based on the age of the detector. This issue is discussed in greater detail later in this chapter.

Prep-scale GPC

Prep-scale GPC was successfully used to fractionate up to 10 mg of pitch (during a single chromatographic run) into oligomeric fractions of narrow MWD without observing any deterioration in column performance. In Chapter 4, M-50 monomer-rich pitch cuts produced from both continuous and semibatch DGE were subjected to prep-scale GPC to yield fractions encompassing a mol wt range of 60 Da or less. This two-step separation method was essential for adequately isolating pitch fractions for subsequent PSD analysis. It is not feasible to perform PSD on the whole M-50 pitch, as for most, if not all species in the whole pitch the MALDI response is overshadowed or interfered with by those of neighboring monomer species (within a range of at least ±2 g/mol). That is, when we attempted to perform PSD on such species, we find that the ion gate is not able to fully screen out neighboring species for which the mol wt of the parent

compound is within a range of at least ±2 g.mol of the species of interest (leading to unreliable PSD spectra). As we saw from the work in Chapter 4, DGE/prep-scale GPC sequential separation solved the problem to a large extent for the monomeric portion of M-50 pitch.

In Chapter 5, the combination of DGE and prep-scale GPC continued to be an essential means for separation, as fractions of dimer and higher oligomers were generated that were narrower in mol wt than any produced in this laboratory to date. For example, semibatch DGE was used to produce pitch cuts of 100% dimer spanning a mol wt range of just over 200 g/mol. When these DGE cuts were subjected to prep-scale GPC, dimer-rich fractions encompassing a mol wt range of less than 100 g/mol were isolated. In a similar manner, semibatch DGE was used to produce a pitch cut containing nearly 90 mol % M-50 trimer, with the remainder consisting of M-50 tetramer. The subsequent fractionation of this pitch cut via prep-scale GPC resulted in the collection of two fractions: one containing 100% M-50 trimer and spanning a range of about 200 g/mol and a second containing 94% M-50 tetramer and spanning a range of ~ 300 g/mol.

It is only necessary to inject ~ 10 mg of pitch into the GPC column in order to collect pitch fractions of concentrations sufficient to make feasible their subsequent characterization by UV-Vis, MALDI, PSD, and HPLC/PDA. Key to the development of the MALDI and PSD work was the use of a sample preparation technique developed in our laboratory (see Chapter 4) that requires that only one drop of the collected fraction be spotted onto a thin film of matrix on the MALDI target.

HPLC/PDA

HPLC/PDA has proven to be a useful tool for unequivocally identifying prevalent polycyclic aromatic hydrocarbon (PAH) backbones present in M-50 monomer, which include pyrene, chrysene, benz[a]anthracene, triphenylene, chrysene, benzo[a]pyrene, benzo[e]pyrene, and benzo[ghi]perylene. Again, the DGE/prep-scale GPC separation technique described above was essential in allowing us to separate pitch species adequately such that HPLC could be applied. Typically, the narrower the pitch fraction analyzed, the higher the quality of the results, as it became increasingly possible to resolve the chromatographic peaks from each other.

Recommendations

Improving the SAFT-LC Equation

In order to improve the SAFT-LC equation so that it gives accurate quantitative predictions for the MWDs of the top and bottom phases associated with the DGE process, the following course of action is recommended. Efforts need to be made to modify the pure-component parameters of the SAFT-LC equation of state so that they are appropriate for carbonaceous pitches, such as petroleum pitch (the parameters that we have been using to date were developed using equations developed for bitumen, a much more aliphatic and less PAH-condensed material than our pitches are). First, it will be

necessary to obtain phase equilibrium data for the M-50 pitch/toluene system over a range of temperatures, pressures, and solvent-to-pitch ratios. This task could be accomplished by performing DGE experiments without any packing material in the column; however, measures must also be taken (e. g., preheating and mixing) to ensure that true equilibrium is obtained. Next, the adjustable SAFT-LC parameters A, B, C, a, and b must be re-calculated by fitting the parameters to the above equilibrium data. The objective function could be developed to minimize the differences in experimental and calculated values for pseudocomponents (PCs) – or for selected "key species" in each oligomeric cut. The mesophase content of the dried bottom phase may (or may not) be included as desired.

If the above procedure does not produce a SAFT-LC model with acceptable predictive capabilities, then the method of calculating the pure-component SAFT parameters v^{00}, m, and u^0/k for our pitch PCs or species should be re-evaluated. For all SAFT-LC work discussed in this dissertation, SAFT parameters were generated using correlations developed by Huang and Radosz[7] for PCs of bitumen. Huang and Radosz developed these correlations based on their knowledge of SAFT parameters for aliphatic compounds (of mol wts from 16 to 619 g/mol) and aromatic compounds (of mol wts from 78 to 228 g/mol). A necessary input to the correlations was the PC aromaticity, which was determined from knowledge of the PC mol wt and its atomic carbon/hydrogen (C/H) ratio. The bitumen PCs of Huang and Radosz have atomic C/H ratios ranging from 0.55 to 0.72, indicating a relatively high aliphatic content. Notably, these C/H ratio values are significantly lower than those for pitch PCs, which are PAHs (e.g., in Chapter 3 C/H

ratios of pitch PCs ranged from 1.14 to 2.19). As noted above, Huang and Radosz only considered aromatic compounds up to mol wt 228 g/mol (triphenylene) in developing their correlations. Furthermore, their correlations were based primarily on an aliphatic database used because of the relative paucity of data for aromatic compounds. In addition, all but 2 of the pitch PCs used in Chapters 2 and 3 possessed mol wts significantly greater than 228 g/mol. To our knowledge, no SAFT parameter data exist in the literature for PAHs containing more than 4 rings. Thus, it is difficult to confirm that the calculated values for the pure-component SAFT parameters for PCs are reliable.

Clearly, another method of predicting the three pure-component SAFT parameters m, v^{00}, and u^0/k is desirable. One such method was put forth recently by Tamouza et al,[8,9] who used a group contribution method to express each pure-component SAFT parameter as a function of several group contribution parameters reflecting the nature (that is, whether the carbon is part of a methylene group, methyl group, etc.) of the various carbon atoms comprising the molecule. Therefore, use of such a method requires the knowledge of the molecular structure of the molecule.

Subsequently, Huynh et al.[10] used the method of Tamouza et al. to calculate group contribution parameters for various types of carbon atoms present in PAHs (examples of such are the 10 outer aromatic ring carbons in pyrene that are bonded to two carbon atoms and a hydrogen atom, and the 6 inner aromatic carbon atoms in pyrene that are bonded to three other carbon atoms). This task was completed by regressing to PVT data available for seven PAHs (the largest being triphenylene, with a mol wt of 228 Da). The group contribution parameters thus calculated for the various carbon atoms present in

PAHs could be used to predict SAFT parameters for pitch constituents with mol wt values significantly greater than 228 Da. However, in order to successfully extend the group contribution theory of Tamouza et al. to PAHs, it was necessary to add another Helmholtz energy term to the SAFT equation in order to account for quadrupolar interactions. Another deficiency is that this group contribution theory does not create a separate classification for carbon atoms that are part of a five-membered ring.

As altering the current SAFT program file currently in use at Clemson University would be a time-consuming task, an alternate course of action may be worthy of investigation. One idea is to follow the general approach used by Hutchenson et al.[11] in determining the pure-component Peng-Robinson parameters a_C, b, and κ for pitch PCs. Hutchenson et al. then showed that each of these characteristic constants could be expressed a linear function of the most statistically relevant molecular structure parameters. In order to apply this method to the current problem, it would first be necessary to compile a list of literature values for the pure-component SAFT parameters for as many PAHs as feasible. The next step would be to develop a new set of equations expressing each of these parameters as a function of the most statistically significant structural parameters. This set of parameters could include, but not be limited to, the numbers of the different types of carbon atoms present in the molecule of interest (for example, it could also include mol wt and the number of carbon atoms that are part of a five-membered ring). It is recommended that a number of sets of structural parameters be investigated as the variables in which terms the pure-component SAFT parameters are expressed.

Troubleshooting long-term variations in PSD spectra

In order to successfully conduct PSD analyses, it is necessary to account for the factors that cause long-term variation in the PSD spectra. One problem encountered is that of long-term variability in the laser power and detector gain necessary to achieve well-resolved spectra with high signal-to-noise ratios, without inducing baseline elevation.

An example in the long-term variability in the laser power and detector gain (i. e., the voltage across the microchannel plate detector; higher detector gains result in stronger secondary electron currents arising from the incident ions on the walls of the detector microchannels and thus, stronger MALDI responses) necessary to achieve roughly identical PSD spectra is shown in Table 8.1 for two different time periods: May 2008 (when the reflector detector was still relatively new) and March 2010. Values for laser power and detector gain for the first 3 segments (see Appendices E and F for detailed information on how PSD spectra are obtained) in the composite PSD spectrum are shown, as these are typically the only ones in which fragment peaks occur (for constituents of M-50 pitch). The values labeled May 2008 are taken from the MALDI FlexControl software operating method FAST_May_2008.psm. The values labeled March 2010 are taken from the method FAST_March_2010.psm. From Table 8.1, it is apparent that increasing the values for both laser power and detector gain is necessary as time passes and the channels of the microchannel plate detector become clogged with matrix and analyte materials. To make up for the loss of detector sensitivity that occurs due to this aging process, the operator can increase laser power and/or detector gain. It

has been the experience of this researcher that the larger ion counts produced from higher laser powers tend to "overload" the Bradbury-Nielsen ion gate, increasing the likelihood that undesired species will not be prevented from reaching the detector. Therefore, it is recommended that the current MALDI method utilized in the collection of PSD spectra be updated periodically (that is, a new method with updated parameters that result in a PSD spectrum with peak heights similar to those obtained using the original method) in order to account for the detector aging. The loss of detector sensitivity observed because of aging should be counteracted by creating a new operating method in which the detector gain is increased as necessary, while keeping increases in the laser powers for each segment to a minimum.

Table 8.1. Variation, with respect to time, of the detector gain and laser power necessary to achieve similar PSD spectra.

Segment Number	Laser Power (% of Maximum)		Detector Gain	
	May 2008	March 2010	May 2008	March 2010
1	26	31	6.10	12.20
2	29	29	8.10	26.00
3	30	30	10.20	36.00

Modifying the prep-scale GPC apparatus to allow for higher mobile-phase flow rates

The maximum flow rate that the Alliance GPCV2000 model is designed to handle is 1.5 mL/minute. If the mobile phase flow rate is higher than this value, the result will be damage of the pressure transducer in the viscometer. If the viscometer and solvent preheater loop are bypassed, then the solvent pump can deliver a maximum flow rate of 2.5 mL of the mobile-phase 1,2,4-trichlorobenzene (TCB) per minute (because of the relatively high viscosity of TCB relative to that of other common GPC mobile phases, it is possible that the maximum flow rate will rise other, less viscous mobile phases are used). For TCB, if flow rates higher than 2.5 mL/min are used, then the pump piston seal begins to leak.

The disadvantage of the low maximum allowable mobile phase flow rate is that the run times are relatively long. A pitch fractionation experiment typically requires a run time of 70-80 minutes. Using a mobile phase flow rate of 10.0 mL/min would cut the necessary run time to one quarter of the current value, with comparable peak resolution. In order to increase the flow rate above 2.5 mL/min without damaging the apparatus, several parts of the system must be altered, including the solvent pump, the solvent degasser, and the refractometer unit, as follows:

1. In order to deliver mobile-phase flow rates greater than 2.5 mL/min without damaging the equipment, it would be necessary to procure a new solvent pump that can deliver the desired flow rates. It would be necessary to bypass the current GPC pump in order to accomplish this task, with the discharge side of the new

pump connected to the Alliance GPCV 2000 apparatus at the inlet to the solvent in-line filter.

2. Relying on the current degassing unit to degas a mobile-phase pumped by a new, stronger pump is not advised by the Alliance GPCV2000 manufacturer Waters Inc. Thus, it would be necessary to manually degas the solvent prior to use. The degassing operation is important because this is the process by which dissolved oxygen is removed from the mobile phase. If this operation is not performed, then one runs the risk of starving the pump of solvent, leading to a messy baseline.
3. Eluent stream (with TCB as the mobile-phase) flow rates of greater than 3 mL/min within the refractometer risk cracking the refractometer flow cell. Replacing the refractometer would cost a minimum of $10,000. Therefore, when the flow rate of mobile phase is above this value, it will be necessary to install a flow splitter at the column outlet, so that only a portion of the effluent enters and passes through the refractometer. The installation of such a device would allow the GPC operator to vary the percentage of the total eluent stream entering the refractometer (with the rest of the eluent stream bypassing the refractometer). One could adjust the flow splitter such that most of the column effluent bypasses the refractometer, being sent straight to the fraction collector instead.

Purging TCB from refractometer when changing to another mobile phase

Special care must be taken to fully purge all TCB from the Alliance GPCV 2000 system (particularly the refractometer) when changing the GPC mobile phase. If the refractometer is not fully purged of TCB, its sensitivity will be greatly weakened (sometimes the signal-to-noise ratio is so low that it is difficult to distinguish the GPC response from baseline noise). TCB is particularly difficult to purge from the refractometer because it is significantly more viscous than many other common GPC mobile phases.

It was often necessary to switch from operating in prep-scale mode (in which TCB was used as the mobile phase) to analytical-scale mode (in which tetrahydrofuran was used as the mobile phase). The prep-scale columns were first removed. Because TCB and tetrahydrofuran are immiscible, it was necessary to first switch the GPC mobile phase from TCB to toluene (normal boiling point 110° C); many common GPC mobile phases, including both TCB and THF, are fully miscible with toluene. In order to effectively purge TCB from the refractometer, we set the column compartment temperature to 80° C and allowed it to reach equilibrium (this process takes approximately an hour). The toluene flow rate was set to 1.0 mL/min, with a purge time of 60 minutes (the procedure for purging the refractometer is given in the Alliance GPCV2000 system software operating manual, Section 3.4.3, Purging the Refractometer). When the purge is complete, check the refractometer LED current (from Diagnostics Mode of the Alliance GPCV 2000 system operating software, click Diagnostics, click on Service Diagnostics login, enter the password, and click Detector

Diagnostics). The reading should be less than 40 mA. If it is significantly higher than this number, then the refractometer has not been completely purged of TCB. When the reading for the LED current was below 40 mA, the temperatures of the column, carousel, and injector compartments were programmed to 40° C and allowed to reach equilibrium. At that point, the mobile phase was switched over to tetrahydrofuran.

Maximizing GPC Column Lifetime

Prep-scale GPC column lifetime is maximized by limiting the amount of pitch injected onto the column. At an injection volume of 1.080 mL, we recommend that the injection concentration be no greater than 10 mg/mL (that is, no more than 10 mg pitch fractionated per run) in order to avoid pore clogging and buildup of pitch on the column-packing particles. Our experience in this laboratory has been that such factors greatly reduce the efficiency of the prep-scale columns by causing peak tailing effects, particularly when the species fractionated are primarily heavy (that is, trimer-range and higher) oligomers.

HPLC/PDA identification of dimer and higher-order oligomers

Based on the success of HPLC/PDA in identifying the most prevalent monomer species present in M-50 pitch from pitch, this technique is recommended for use in the unequivocal identification of the lower mol wt species in all kinds of pitches (including synthetic pitches produced via the catalytic or thermal polymerization of a single

molecule, such as naphthalene, anthracene or pyrene). Reference UV-Vis spectra for a wide range of unsubstituted aromatics of mol wt < 450 Da (and selected substituted aromatics) are available in the open literature, so analysis of both monomer and dimer species will be possible. Because many dimer species have mol wt < 450 Da (for example, in Chapter 5, the chief component of anthracene pitch dimer is shown to have a mol wt of 352 Da), HPLC/PDA analysis of narrow dimer fractions is also recommended. HPLC/PDA analyses of higher oligomeric fractions are possible, but unequivocal identification of the species present in such fractions is hindered by the scarcity of reference UV-Vis spectra in the literature for PAHs with a mol wt over 450 Da.

It is the view of this researcher that HPLC/PDA would be particularly effective for the unequivocal molecular characterization of oligomeric fractions derived from synthetic pitches (which would enable future researchers to relate the molecular structures of said pitches to their processibility and the properties of the final carbon products into which they are fabricated). As indicated in Chapter 6, anthracene pitch (Fig. 6.2a) is comprised of relatively few species compared to M-50 petroleum pitch (Fig. 6.1). Thus, it was possible to isolate oligomeric fractions from this synthetic pitch with much narrower mol wt ranges than for M-50. Because the anthracene dimer and trimer fractions are comprised of relatively few species, HPLC/PDA analysis should yield chromatograms with well-resolved peaks, allowing for the collection of UV-Vis spectra for each eluting compound, and thus making unequivocal compound identification possible if the respective reference UV-Vis spectra are present.

In order to separate dimer and higher pitch oligomers via HPLC, it will be necessary to alter the mobile-phase program from that put forth in Chapter 4 for the HPLC/PDA analyses for various M-50 petroleum pitch fractions containing M-50 monomer. As was reported by Fetzer and Kershaw,[12] pure acetonitrile (ACN: a highly polar solvent that nevertheless can dissolve some low mol wt PAHs because of the presence of a methyl group in its molecular structure) is too polar to cause larger, highly nonpolar, dimer-range PAHs (mol wt 300 to 424 Da) in coal-tar pitch to elute from the HPLC column. Similar trends have been noted in other works.[13,14,15,16] Therefore, we recommend using a solvent gradient from ACN to a chemical such as methylene chloride (as did Fetzer and Kershaw[12]) or chlorobenzene. Both of these solvent gradients have been used with success by previous researchers in the HPLC analyses of PAHs above mol wt 300 Da.[13,14,15,16] However, methylene chloride causes plastic polyether ethyl ketone (PEEK) tubing to swell. Because this type of tubing is used in many HPLC systems, we recommend the use of an ACN-to-chlorobenzene solvent gradient.

HPLC column lifetime is maximized by greatly limiting the amount of pitch injected onto the column. We recommend a small injection volume (10 μL) and injection concentration (on the order of 0.1 mg/mL) in order to avoid buildup of pitch on the column-packing particles. Such buildup has the end result of distorting the chromatogram baseline as the excessive pitch material belatedly elutes from the HPLC column during subsequent analyses.

Where Does This Work Fit Into the Big Picture?

The analytical methods presented in this dissertation have yielded a means to determine actual molecular structures present in petroleum pitches and related materials. Where, then, does the interested researcher go from here? How could the methods presented in this chapter aid the pursuits of future researchers?

A current objective of the Carbon research group at Clemson is the design of precursor materials that are suitable for a given application. In order to accomplish this objective, it is necessary to consider three important variables: the precursor viscosity, softening point and mesophase content. Mesophase pitches produced by DGE or related techniques often have high softening points. Such pitches are difficult to spin, as the high temperatures required for spinning of such fibers causes them to oxidize upon exposure to air. The fibers then become brittle and break easily, resulting in low fiber yields per unit mass of precursor supplied.

Currently, the design of suitable pitch precursor materials is more of an art than a science, because investigators cannot relate the molecular structures of the precursor materials to mesophase content, precursor processibility and properties of the final carbon product in anything but a general sense. For example, what molecular structures must be present to form mesophase? What makes a good plasticizer (that is, a material that lowers the softening point (and thus, the minimum processing temperature necessary) of the precursor while having little to no effect on its mesophase content)? Does the presence of a five-membered ring in the molecular structure have a noticeable effect on

the tendency of molecules within a certain mol wt range to act as a mesogen or a plasticizer?

The molecular structures present in the precursor can also be related to final carbon product properties such as porosity, tensile and compressive strengths, tensile (Young's) modulus, and thermal conductivity. In so doing, the investigator can glean clues concerning the graphitizabilities of stabilized fibers produced from various precursors (graphitization is a high-temperature reaction in which a stabilized fiber is converted to thin sheets of graphite). Specifically, does the presence of a large proportion of 5-membered rings in a given precursor have a noticeable effect on its ability to form the highly graphitic microstructure necessary to achieve high tensile strength, tensile modulus and thermal conductivity in the final carbon product?

References

[1]Maier, V. W.; Saupe, A. Eine Einfache Molekulare Theorie des Nematischen Kristallinflüssigen Zustandes. *Z. Naturforschg.* **1958**, *13a*, 564-566.

[2]Maier, V. W.; Saupe, A. Eine Einfache Molekular-Statistische Theorie der Nematischen Kristallinflüssigen Phase. Teil I. *Z. Naturforschg.* **1959**, *14a*, 882-889.

[3]Maier, V. W.; Saupe, A. Eine Einfache Molecular-Statistische Theorie der Nematischen Kristallinflüssigen Phase. Teil II. *Z. Naturforschg*. **1960**, *15a*, 287-292.

[4]Humphries, R. L.; James, P. G.; Luckhurst, G. R. A Molecular Field Treatment of Liquid Crystalline Mixtures. *Symp. Faraday Soc.* **1971**, *5*, 107-118.

[5]Humphries, R. L.; James, P. G.; Luckhurst, G. R. Molecular Field Treatment of Nematic Liquid Crystals. *J. Chem. Soc. Faraday Trans. II* **1972**, *68*, 1031-1044.

[6]Humphries, R. L.; Luckhurst, G. R. A Statistical Theory of Liquid Crystalline Mixtures: Phase Separation. *Proc. R. Soc. Lond., Ser. A* **1976**, *352*, 41-56.

[7]Huang, S. H.; Radosz, M. Phase Behavior of Reservoir Fluids V: SAFT Model of CO_2 and Bitumen Systems. *Fluid Phase Equilib.* **1991**, *70*, 33-54.

[8]Tamouza, S.; Passarello, J.-P.; Tobaly, P.; De Hemptinne, J.-C. Group Contribution Method with SAFT EOS Applied to Vapor Liquid Equilibria of Various Hydrocarbon Series. *Fluid Phase Equilib.* **2004**, *222-223*, 67-76.

[9]Tamouza, S.; Passarello, J.-P.; Tobaly, P.; De Hemptinne, J.-C. Application to Binary Mixtures of a Group Contribution SAFT EOS (GC-SAFT). *Fluid Phase Equilib*. **2005**, *228-229*, 409-419.

[10]Huynh, D. N; Benamira, M.; Passarello, J.-P.; Tobaly, P.; De Hemptinne, J.-C. Application of GC-SAFT EOS to Polycyclic Aromatic Hydrocarbons. *Fluid Phase Equilib*. **2007**, *254*, 60-66.

[11]Hutchenson, K. W.; Roebers, J. R.; Thies, M. C. Fractionation of Petroleum Pitch by Supercritical Fluid Extraction. *Carbon* **1991**, *29(2)*, 215-223.

[12]Fetzer, J. C.; Kershaw, J. R. Identification of Large Polycyclic Aromatic Hydrocarbons in a Coal Tar Pitch. *Fuel* **1995**, *74(10)*, 1533-36.

[13]Somers, M. L.; Wornat, M. J. UV Spectral Identification of Polycyclic Aromatic Hydrocarbon Products of Supercritical 1-Methylnaphthalene Pyrolysis. *Polycyclic Arom. Compd.* **2007**, *27*, 261-80.

[14]McClaine, J. W.; Oña, J. M.; Wornat, M. J. Identification of a New $C_{28}H_{14}$ Polycyclic Aromatic Hydrocarbon as a Product of Supercritical Fuel Pyrolysis: Tribenzo[cd,ghi,lm]perylene. *J. Chromatogr. A* **2007**, *1138*, 175-183.

[15]Fetzer, J. C. The Chemistry and Analysis of Large PAHs. *Polycyclic Arom. Compd.* **2007**, *27(2)*, 143-162.

[16]Oña, J. O.; Wornat, M. J. Identification of the $C_{30}H_{16}$ Polycyclic Aromatic Hydrocarbon Benzo[cd]naphtho[1,2,3-lm]perylene as a Product of the Supercritical Pyrolysis of a Synthetic Jet Fuel. *Polycyclic Arom. Compd*. **2007**, *27(3)*, 165-183.

APPENDICES

APPENDIX A

EXTENSION OF THE MAIER-SAUPE THEORY TO MIXTURES OF HARD DISKS

The Maier-Saupe theory was originally derived to model the nematic interaction between long, rod-like molecules.[1,2,3] This theory can be expressed as a Helmholtz energy of orientation which quantifies the tendency of these molecules form a liquid-crystalline phase, or mesophase. An example of such a molecule, 4,4'-di-*n*-methoxy-azoxybenzene (otherwise known as *p*-azoxyanisole) is shown as Species I (R = CH_3) in Fig. A.1 below. Derivatives of this molecule, such as 4,4'-di-*n*-heptyloxy-azoxybenzene (Species II: R = C_7H_{15}) also exhibit the tendency to form a liquid-crystalline phase.

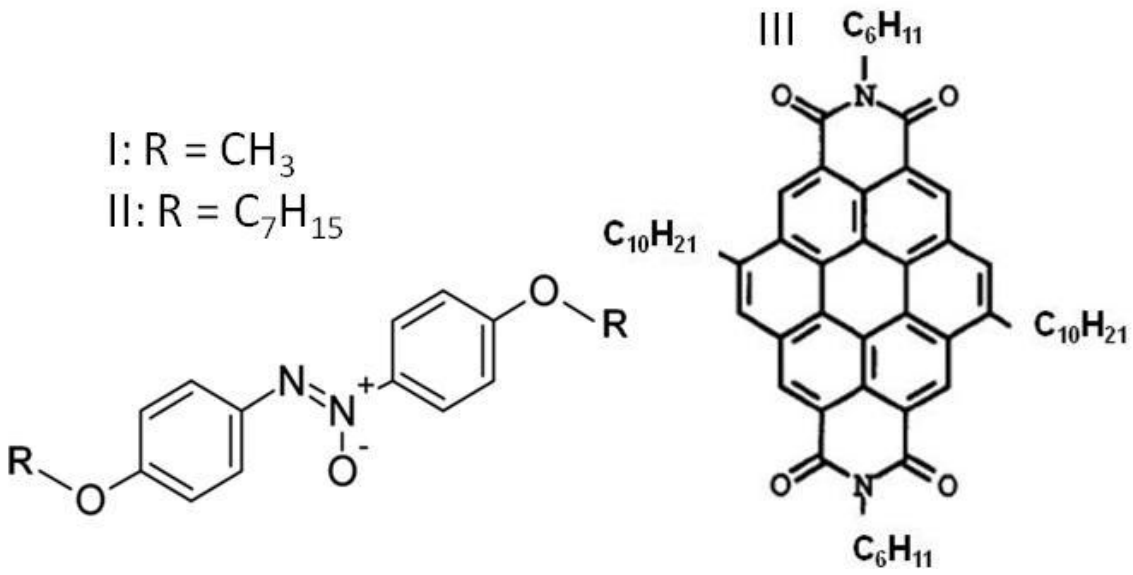

Figure A.1. Mesophase-forming molecules 4,4'-dimethoxy-azoxybenzene (I),[3] 4,4'-di-*n*-heptyloxy-azoxybenzene (II);[3] in the structure of (III),[4] the coronene-3,4:9,10-bis(dicarboximide) backbone is substituted with alkyl chains.

In this appendix, the applicability of the Maier-Saupe theory to disk-like molecules, such as the polycyclic aromatic hydrocarbons that comprise pitch, will be

investigated. First, we note a key assumption made by Maier and Saupe[2] in the derivation of their theory. They assumed that the liquid crystalline phase forms solely as a result of general, Coulombic dispersion interactions (even if the nematogen, such as p-azoxyanisole, does in fact possess a permanent dipole moment, interactions between the permanent dipole moments of two such molecules are not assumed to play an appreciable role in the formation of nematic order and are thus neglected), with only the dipole-dipole term of the dispersion forces being considered. Higher-order terms, such as quadrupole-quadrupole and octopole-octopole terms, are shorter in range and would be expected to be negligible.[5] It is notable that nonpolar, carbonaceous pitches, the discotic mesophase-forming materials in which we are interested, do not even possess permanent dipoles.

We note that the structures of discotic nematogens are similar to the rod-like nematogens in that they are both highly rigid molecules with a highly conjugated system of double bonds. Because of the similarities (i. e., aromatic content, a two-dimensional core structure substituted with alkyl chains of varying length) in the molecular properties of rod-like (Fig. A.1, structures I and II) and disk-like nematogens (Fig. A.1, structure III) , the Maier-Saupe theory will be derived for disk-like molecules using the same initial assumptions previously set out by Maier and Saupe.

Determination of the Nematic Interaction Energy Between A Molecule and the Mean Field Generated by its Neighbors

Note: In performing this derivation, the nomenclature used by Maier and Saupe was used. Therefore, it differs from the nomenclature used in the presentation of the SAFT-LC equation in Chapters 2 and 3.

Using these assumptions, Maier and Saupe arrive at the following expression:

$$U_i(\theta_l,\theta_k)=\sum_k\sum_{\mu\upsilon}\frac{1}{E_{00}-E_{\mu\upsilon}}\left\{f_{0\mu}f_{0\upsilon}\frac{A(R_{lk})}{R_{lk}^6}+\left[f_{0\mu}\delta_{0\upsilon}\left(1-\frac{3}{2}\sin^2\theta_l\right)+f_{0\upsilon}\delta_{0\mu}\left(1-\frac{3}{2}\sin^2\theta_k\right)\right]\frac{B(R_{lk})}{R_{lk}^6}\right. \quad (A.1)$$
$$\left.+\delta_{0\mu}\delta_{0\upsilon}\left(1-\frac{3}{2}\sin^2\theta_l\right)\left(1-\frac{3}{2}\sin^2\theta_k\right)\frac{C(R_{lk})}{R_{lk}^6}\right\}$$

Here, $f_{0\mu}$ and $f_{0\nu}$ are measures of the isotropy of the 0-μ and 0-ν transitions, while the terms $\delta_{0\mu}$ and $\delta_{0\nu}$ are measures of the anisotropy of the 0-μ and 0-ν transitions (i.e., the transitions from the ground state 0 to energy state μ or ν). The term E_{00} represents the combined ground state energies for molecule l and molecule k, while $E_{\mu\nu}$ represents the combined energies of molecules l and k in energy states μ and ν, respectively. The angle θ_l represents the angle between the long axis of molecule l and a fixed, laboratory-based axis. Similarly, θ_k represents the angle between the long axis of molecule k and the laboratory-based axis. The term R_{lk} represents the distance between the centers of gravity of molecule l and molecule k (this step is not derived herein). $A(R_{lk})$, $B(R_{lk})$ and $C(R_{lk})$ are functions of the molecular coordinates X, Y, and Z (where $R^2 = X^2 + Y^2 + Z^2$),

which denote the centers of gravity of the molecules. Maier and Saupe do not explicitly define these terms. However, De Jeu[6] states that they can be written as:

$$A(R) = 6 \tag{A.2}$$

$$B(R) = 3\frac{Z^2}{R^2} - 1 \tag{A.3}$$

$$C(R) = 1 - 8\frac{Z^2}{R^2} + 9\frac{Z^4}{R^4} \tag{A.4}$$

Here, the subscripts are dropped from the R terms, for the sake of simplicity. The right hand side of Equation A.1 is composed of three terms, the first of which is dependent solely upon isotropic transitions. The second term is dependent on both isotropic and nematic transitions, and the final term is dependent only upon nematic transitions.

The next step in the development of Maier-Saupe theory is the alteration of Equation A.1 so that it predicts the intermolecular potential between a particular molecule l and the mean field generated by its neighbors. This average is obtained by first assuming that the average orientation angle for all molecules (other than molecule l) in the system at any particular instant in time is a constant value, θ. The average value of θ_k (the angle of orientation for molecule k over an infinitely long period of time), is assumed to be equal to θ. For any ergodic system, this is a good assumption to make. Therefore,

$$\overline{\sin^2\theta_k} = \overline{\sin^2\theta} \tag{A.5}$$

While it is not fully accurate in the immediate vicinity of molecule k, it considerably simplifies the problem of deriving the theory. By converting the $\sin^2 \theta_k$ term on the right hand side of Equation A.1 to an average (and then by substituting Equation A.5 into Equation A.1), an equation for the intermolecular potential between molecule l and the mean field generated by its neighbors is created in the form of Equation A.6.

$$\bar{U}_i(\theta_l,\theta) = \sum_k \sum_{\mu\upsilon} \frac{1}{E_{00}-E_{\mu\upsilon}} \left\{ f_{0\mu} f_{0\upsilon} \sum_k \frac{A(R_{lk})}{R_{lk}^6} + \left[f_{0\mu}\delta_{0\upsilon}\left(1-\frac{3}{2}\sin^2\theta_l\right) + f_{0\upsilon}\delta_{0\mu}\left(1-\frac{3}{2}\overline{\sin^2\theta}\right)\right]\sum_k \frac{B(R_{lk})}{R_{lk}^6} \right. \quad \text{(A.6)}$$
$$\left. + \delta_{0\mu}\delta_{0\upsilon}\left(1-\frac{3}{2}\sin^2\theta_1\right)\left(1-\frac{3}{2}\overline{\sin^2\theta}\right)\sum_k \frac{C(R_{lk})}{R_{lk}^6} \right\}$$

Equation A.6 is still quite complicated. However, it can be shown that the middle term is equal to zero when the central molecule l is assumed to be spherically symmetric. Even though the assumption that the central molecule l is spherically symmetric is strictly incorrect for both rod-like and discotic nematogens, it must be made in order to reduce Equation A.6 to a simpler equation, in which the average energy of a central molecule l is divided into an isotropic component independent of nematic order, and a second component dependent upon the angle of molecular orientation θ_l. This task is carried out by determination of the average value of the term $B(R_{lk})/R_{lk}^6$ on the right hand side of Equation A.6, expressed as follows:

$$\sum_k \frac{B(R_{lk})}{R_{lk}^6} = 3\sum_k \frac{Z^2}{R_{lk}^8} - \sum_k \frac{1}{R_{lk}^6} \quad \text{(A.7)}$$

where

$$\sum_k \frac{Z^2}{R^8} \approx N\iiint \frac{Z^2}{R^8} d\tau = 4\pi N \iiint \frac{Z^2}{R^8} r dr dz \tag{A.8}$$

Using a cylindrical coordinate system, τ is equal to the volume outside the central molecule, while $d\tau$ is equal to the surface area of a cylindrical shell. To begin, it is assumed that the central molecule is spheroidal (approximately rodlike), with a short axis (in the plane of the equator of the spheroid) of length b and a long axis of length a. Equation A.8 is integrated in the following manner, in which the spheroidal volume occupied by the molecule is excluded from integration:

$$\sum_k \frac{Z^2}{R^8} \approx 4\pi N \left[\int_0^a z^2 dz \int_{r_0}^{\infty} \frac{r dr}{\left(r^2 + z^2\right)^4} + \int_a^{\infty} z^2 dz \int_0^{\infty} \frac{r dr}{\left(r^2 + z^2\right)^4} \right] \tag{A.9}$$

$$\sum_k \frac{Z^2}{R^8} \approx 4\pi N \left[\int_0^a z^2 dz \left| \frac{-1}{6\left(r^2 + z^2\right)^3} \right|_{r_0}^{\infty} + \int_a^{\infty} z^2 dz \left| \frac{-1}{6\left(r^2 + z^2\right)^3} \right|_0^{\infty} \right] \tag{A.10}$$

$$\sum_k \frac{Z^2}{R^8} \approx 4\pi N \left[\int_0^a z^2 dz \left(\frac{1}{6\left(r_0^2 + z^2\right)^3} \right) + \int_a^{\infty} z^2 dz \left(\frac{1}{6z^6} \right) \right] \tag{A.11}$$

The quantity r_0 is in the plane of the equator of the spheroid. It ranges from 0 to b, the length of the short axis of the spheroid. When at a point in the plane of the equator, $r_0 = b$. When at a point at the poles, $r_0 = 0$. De Jeu[6] makes the following substitution for r_0,

$$r_0^2 = b^2 + e^2 z^2 - z^2 \tag{A.12}$$

in which the excentricity e of the spheroid is given by:

$$e = 1 - \frac{b^2}{a^2} \tag{A.13}$$

Substitution of Equation A.12 into Equation A.11 yields Equation A.14.

$$\sum_k \frac{Z^2}{R^8} \approx 4\pi N \left[\int_0^a z^2 dz \left(\frac{1}{6\left(b^2 + e^2 z^2\right)^3} \right) + \int_a^\infty z^2 dz \left(\frac{1}{6z^6} \right) \right] \tag{A.14}$$

In the limit of a spherically symmetric excluded volume (which is assumed to represent the volume occupied by the molecule), the long axis and the short axis become indistinguishable, b = a, and the eccentricity e equals zero. Equation A.14 simplifies to:

$$\sum_k \frac{Z^2}{R^8} \approx 4\pi N \left[\int_0^a z^2 dz \left(\frac{1}{6b^6} \right) + \int_a^\infty z^2 dz \left(\frac{1}{6z^6} \right) \right] \tag{A.15}$$

Integration with respect to z yields:

$$\sum_k \frac{Z^2}{R^8} \approx 4\pi N \left[\left| \frac{z^3}{18b^6} \right|_0^a + \left| \frac{-1}{18z^3} \right|_a^\infty \right] \tag{A.16}$$

$$\sum_k \frac{Z^2}{R^8} \approx 4\pi N \left[\frac{a^3}{18b^6} + \frac{1}{18a^3} \right] \tag{A.17}$$

In the limit of spherical symmetry of the excluded volume, b = a, and the above equation simplifies to:

$$\sum_k \frac{Z^2}{R^8} \approx 4\pi N \left[\frac{1}{18a^3} + \frac{1}{18a^3} \right] = \frac{4\pi N}{9a^3} \tag{A.18}$$

Meanwhile,

$$\sum_k \frac{1}{R^6} \approx 4\pi N\left[\int_0^a dz \int_{r_0}^{\infty} \frac{r dr}{\left(r^2+z^2\right)^3} + \int_a^{\infty} dz \int_0^{\infty} \frac{r dr}{\left(r^2+z^2\right)^3}\right] \tag{A.19}$$

$$\sum_k \frac{1}{R^6} \approx 4\pi N\left[\int_0^a dz \left|\frac{-1}{4\left(r^2+z^2\right)^2}\right|_{r_0}^{\infty} + \int_a^{\infty} dz \left|\frac{-1}{4\left(r^2+z^2\right)^2}\right|_0^{\infty}\right] \tag{A.20}$$

$$\sum_k \frac{1}{R^6} \approx 4\pi N\left[\int_0^a dz \left(\frac{1}{4\left(r_0^2+z^2\right)^2}\right) + \int_a^{\infty} dz\left(\frac{1}{4z^4}\right)\right] \tag{A.21}$$

Substituting for r_0, and setting e = 0, the following equation is obtained.

$$\sum_k \frac{1}{R^6} \approx 4\pi N\left[\int_0^a dz\left(\frac{1}{4b^4}\right) + \int_a^{\infty} dz\left(\frac{1}{4z^4}\right)\right] \tag{A.22}$$

Integration with respect to z yields:

$$\sum_k \frac{1}{R^6} \approx 4\pi N\left[\left|\frac{z}{4b^4}\right|_0^a + \left|\frac{-1}{12z^3}\right|_a^{\infty}\right] \tag{A.23}$$

$$\sum_k \frac{1}{R^6} \approx 4\pi N\left[\frac{1}{4a^3} + \frac{1}{12a^3}\right] = \frac{4\pi N}{3a^3} \tag{A.24}$$

Substituting the results of Equations A.18 and A.24 into Equation A.7,

$$\sum_k \frac{B\left(R_{lk}\right)}{R_{lk}^6} = 3\sum_k \frac{Z^2}{R_{lk}^8} - \sum_k \frac{1}{R_{lk}^6} = 3\left(\frac{4\pi N}{9a^3}\right) - \frac{4\pi N}{3a^3} = 0 \tag{A.25}$$

Therefore, in all cases in which the central molecule l is assumed to be spherically symmetric, Equation A.6 reduces to Equation A.26 (as indicated in Equation A.25, in

such a scenario the term in Equation A.6 containing $\Sigma B(R_{lk})/(R_{lk})^6$ goes to zero), which represents the mean energy of interaction for molecule l, with the first term on the right hand side of Equation A.26 arising from isotropic effects and the latter term arising from anisotropic effects.[2]

$$\overline{U_i} = \sum_{\mu\upsilon} \frac{f_{0\mu} f_{0\upsilon}}{E_{00} - E_{\mu\upsilon}} \sum_k \frac{A(R_{lk})}{R_{lk}^6} + \left(1 - \frac{3}{2}\sin^2\theta_1\right)\left(1 - \frac{3}{2}\overline{\sin^2\theta}\right) \sum_{\mu\upsilon} \frac{\delta_{0\mu}\delta_{0\upsilon}}{E_{00} - E_{\mu\upsilon}} \sum_k \frac{C(R_{lk})}{R_{lk}^6} \quad \text{(A.26)}$$

Maier and Saupe abbreviate the latter term as shown in Equation A.27, in order to yield an equation for D_1, the mean energy of interaction, due entirely to anisotropic interactions, for molecule l in the nematic phase,

$$D_l = -\frac{A}{V^2} S\left(1 - \frac{3}{2}\sin^2\theta_l\right) \quad \text{(A.27)}$$

with

$$\frac{A}{V^2} = \sum_{\mu\upsilon} \frac{\delta_{0\mu}\delta_{0\upsilon}}{E_{\mu\upsilon} - E_{00}} \sum_k \frac{C(R_{lk})}{R_{lk}^6} \quad \text{(A.28)}$$

and

$$S = \left(1 - \frac{3}{2}\overline{\sin^2\theta}\right) \quad \text{(A.29)}$$

The term S denotes the average order parameter, which defines the average state of nematic order for all the molecules in a mixture. Meanwhile, the term V represents molar volume. Maier and Saupe[2] assert that the anisotropic energy parameter A is temperature-independent because the "liquid lattice" symmetry will not be greatly affected as a result of a temperature change.

Because an assumption implicit in the derivation of Equation A.27 is that the central molecule l is spherically symmetric, it is plausible that it will also predict, with reasonable accuracy, the formation of mesophase within species that are modeled as hard disks, rather than rods (because of the success of the Maier-Saupe theory, under this implicit assumption, in modeling the nematic interactions for molecules that are modeled as hard rods).

In order to determine ΔA_{ori}, the molar Helmholtz energy of orientation resulting from the isotropic-nematic phase transition, the molar internal energy of orientation ΔU_{ori} and molar entropy of orientation ΔS_{ori} must first be calculated (see Equation A.30).

$$\Delta A_{ori} = \Delta U_{ori} - T\Delta S_{ori} \qquad \text{(A.30)}$$

$\Delta U_{ori} = U_{ori,\,n} - U_{ori,\,i}$ where $U_{ori,\,n}$ is the internal energy of orientation of the nematic phase, and $U_{ori,\,i}$ is the molar internal energy of orientation of the isotropic phase (an analogous relation holds for the molar Helmholtz energy of orientation, $\Delta S_{ori} = S_{ori,\,n} - S_{ori,\,i}$.

For the isotropic phase, the average order parameter for all molecules, S, is equal to 0. Therefore, $U_{ori,\,i} = 0$, and $\Delta U_{ori} = U_{ori,\,n}$. Starting with Equation A.27, $U_{ori,\,n}$ is obtained by first summing to yield the average orientation of molecule l, and then multiplying by N/2 pairs of molecules, where N is Avogadro's number. Thus,

$$U_{ori} \equiv \Delta U_{ori,\,n} = -\frac{NAS^2}{2V^2} \qquad \text{(A.31)}$$

The molar entropy of orientation ΔS_{ori} is then calculated. According to the equation put forth by McQuarrie,[7] the entropy S_i of a single molecule i would be given by

Equation A.32. Substitution of Equation A.27 into Equation A.32 yields an expression for the orientational entropy of one molecule i. To obtain the average entropy of one molecule i, $\langle S_i \rangle$, an average must be taken over all possible orientation angles θ_l for molecule l in Equation A.33, leading to Equation A.34.

$$S_i \equiv -k \ln Pr_i = -k \ln \frac{e^{-\frac{D_i}{kT}}}{Z} = \frac{D_i}{T} + k \ln Z \tag{A.32}$$

$$S_i \equiv -\frac{AS}{TV^2}\left(1 - \frac{3}{2}\sin^2 \theta_l\right) + k \ln Z \tag{A.33}$$

The average entropy of molecule i is given by:

$$\langle S_i \rangle \equiv \frac{\langle U_i \rangle}{T} + k \ln Z \equiv -\frac{AS^2}{TV^2} + k \ln Z \tag{A.34}$$

Therefore, the molar entropy of orientation S_{ori} for all N molecules is obtained by multiplying Equation A.34 by N.

$$S_{ori} = N\langle S_i \rangle \equiv N\left(\frac{\langle U_i \rangle}{T} + k \ln Z\right) \equiv -\frac{NAS^2}{TV^2} + Nk \ln Z \tag{A.35}$$

where Z is the orientational partition function. It is given by

$$Z \equiv \sum_{i=1}^{n} \exp^{\frac{-D_i}{kT}} \equiv \int_0^{2\pi} \int_0^{\pi} \exp^{\frac{-D_i}{kT}} \sin\theta_i \, d\theta_i \, d\varphi_i \tag{A.36}$$

The orientational partition function Z represents a summation of the different energy states which arise because of the anisotropic interactions between molecule l and the mean nematic field generated by its neighbors. Thus, this is an intermolecular (vs. the

classic intramolecular) partition function. Assuming that the distribution of these possible orientational energy states is continuous, Z can be expressed as an integral as shown in Equation A.36 (by integrating over θ and the azimuthal angle ϕ). The observed energy state of a nematogen is dependent upon the angle θ_1 at which it is oriented relative to the fully oriented, preferred state denoted by the director. This is a representation of a laboratory-based coordinate system (see Chapter 2, pp. 44-45).

Note that this orientational partition function is not the same as the rotational partition function, which is based upon a summation of rotational energy states within a particular molecule; these rotational energy states do not depend upon interactions with another molecule. Also, the rotational energy states are calculated using a molecular-based coordinate system instead of our laboratory-based coordinate system.

By integrating Equation A.36 with respect to the azimuthal angle ϕ, the above expression is simplified:

$$Z \equiv 2\pi \int_0^{\pi} \exp^{\frac{-D_i}{kT}} \sin\theta_i d\theta_i \qquad \text{(A.37)}$$

Substituting for the energy D_i yields

$$Z \equiv 2\pi \int_0^{\pi} \exp^{\frac{AS}{kTV^2}\left(1-\frac{3}{2}\sin^2\theta_1\right)} \sin\theta_i d\theta_i \qquad \text{(A.38)}$$

Next, substitution of Equation A.38 into Equation A.35 yields

$$S_{ori} \equiv -\frac{NAS^2}{TV^2} + Nk\ln\left(2\pi\int_0^{\pi} \exp^{\frac{AS}{kTV^2}\left(1-\frac{3}{2}\sin^2\theta_l\right)} \sin\theta_i d\theta_i\right) \quad \text{(A.39)}$$

The value for ΔS_{ori}, the difference in the entropy between the isotropic and nematic states, is given by:

$$\Delta S_{ori} \equiv S_{ori,n} - S_{ori,i} \quad \text{(A.40)}$$

Where the terms $S_{n,ori}$ and $S_{i,ori}$ represent the orientational entropies of the nematic and isotropic phases, respectively. Because the value for the average order parameter S is zero throughout the isotropic phase, the determination of $S_{ori,i}$ is academic. Substitution of S = 0 into Eq. A.38 yields Z = 4π. Substitution of this result into Eq. A.35 yields Eq. A.41 below.

$$S_{ori,i} \equiv NklnZ \equiv Nkln\left(2\pi\int_0^{\pi} \sin\theta_i d\theta_i\right) \equiv Nkln4\pi \quad \text{(A.41)}$$

Meanwhile, the orientational entropy of the nematic phase is given by

$$S_{ori,n} \equiv -\frac{NAS^2}{TV^2} + Nk\ln\left(2\pi\int_0^{\pi} \exp^{\frac{AS}{kTV^2}\left(1-\frac{3}{2}\sin^2\theta_l\right)} \sin\theta_i d\theta_i\right) \quad \text{(A.42)}$$

It can be shown that

$$\int_0^{\pi} \exp^{\frac{AS}{kTV^2}\left(1-\frac{3}{2}\sin^2\theta_l\right)} \sin\theta_i d\theta_i = 2\int_0^{\pi/2} \exp^{\frac{AS}{kTV^2}\left(1-\frac{3}{2}\sin^2\theta_l\right)} \sin\theta_i d\theta_i \quad \text{(A.43)}$$

because $\sin^2\theta$ is symmetric about $\theta = \pi/2$. Therefore,

$$S_{ori,n} \equiv -\frac{NAS^2}{TV^2} + Nk \ln 4\pi + Nk \ln \left(\int_0^{\pi/2} \exp^{\frac{AS}{kTV^2}\left(1-\frac{3}{2}\sin^2\theta_l\right)} \sin\theta_i d\theta_i \right) \quad \text{(A.44)}$$

Substitution of Equations A.41 and A.44 into Equation A.40 yields ΔS_{ori}.

$$\Delta S_{ori} \equiv -\frac{NAS^2}{TV^2} + Nk \ln \left(\int_0^{\pi/2} \exp^{\frac{AS}{kTV^2}\left(1-\frac{3}{2}\sin^2\theta_l\right)} \sin\theta_i d\theta_i \right) \quad \text{(A.45)}$$

Subsequent substitution of Equations A.31 and A.45 into Eq. A.30 yields an equation for the orientational Helmholtz energy.

$$\Delta A_{ori} = \frac{NAS^2}{2V^2} - NkT \ln \left(\int_0^{\pi/2} \exp^{\frac{AS}{kTV^2}\left(1-\frac{3}{2}\sin^2\theta_l\right)} \sin\theta_i d\theta_i \right) \quad \text{(A.46)}$$

Maier and Saupe[3] show, that for the nematic to isotropic phase transition at constant volume, $A/V^2 = 4.541$. This equation holds for both hard disks and hard rods. At the clearing temperature, S is predicted to be 0.4292. This model provides results that match closely with the experimentally observed order parameter of p-azoxyanisole.[1]

This equation can also be expressed in the nomenclature used in Chapters 2 and 3, as indicated in Equation A.47.

$$\Delta A_{ori} = -\frac{N\varepsilon\bar{P}^2}{2} - NkT \ln \left(\int_0^{\pi/2} \exp^{-\frac{\varepsilon\bar{P}}{kT}\left(\frac{3}{2}\cos^2\theta_i - \frac{1}{2}\right)} \sin\theta_i d\theta_i \right) \quad \text{(A.47)}$$

The term inside the parentheses on the right hand side of Equation A.47 is equivalent to the partition function Z if the simplifying assumptions of Humphries et al.[8] and Shishido et al.[9] are used to simplify Equation A.36 to eliminate the ϕ dependence of

Z, and to change the limits of integration from $\theta = 0$ to π, to $\theta = 0$ to $\pi/2$. In that case, Equation A.47 simplifies to Equation A.48. It can be shown that Equation A.48 is equivalent to the result obtained by Humphries et al.[8]

$$\Delta A_{ori} = -\frac{N\varepsilon\bar{P}^2}{2} - NkTlnZ \qquad \text{(A.48)}$$

References

[1]Maier, V. W.; Saupe, A. Eine Einfache Molekulare Theorie des Nematischen Kristallinflüssigen Zustandes. *Z. Naturforschg.* **1958**, *13a*, 564-566.

[2]Maier, V. W.; Saupe, A. Eine Einfache Molekular-Statistische Theorie der Nematischen Kristallinflüssigen Phase. Teil I. *Z. Naturforschg.* **1959**, *14a*, 882-889.

[3]Maier, V. W.; Saupe, A. Eine Einfache Molecular-Statistische Theorie der Nematischen Kristallinflüssigen Phase. Teil II. *Z. Naturforschg*. **1960**, *15a*, 287-292.

[4]Rohr, U.; Schlichting, P.; Böhm, A.; Gross, M.; Meerholz, K.; Bräuchle, C.; Müllen, K. Liquid Crystalline Coronene Derivatives with Extraordinary Fluorescence Properties. *Angew. Chem. Int. Ed.* **1998**, *37(10)*, 1434-1437.

[5]Parsonage, N. G.; Scott, R. L. Contribution of Octopole-Octopole Interactions to the Excess Properties of Mixtures of Tetrahedral Molecules. *J. Chem. Phys.* **1962**, *37*, 304-306.

[6]De Jeu, W. H. On the Role of Spherical Symmetry in the Maier-Saupe Theory. *Mol. Cryst. Liq. Cryst.* **1997**, *292*, 13-24.

[7]McQuarrie, D. A.; Simon, J. D. *Molecular Thermodynamics*. University Science Books: Sausalito, California, 1999, Chapter 6.

[8]Humphries, R. L.; James, P. G.; Luckhurst, G. R. A Molecular Field Treatment of Liquid Crystalline Mixtures. *Symp. Faraday Soc.* **1971**, *5*, 107-118.

[9]Shishido, M.; Inomata, H.; Arai, K.; Saito, S. Application of Liquid Crystal Theory to the Estimation of Mesophase Pitch Phase Transition Behavior. *Carbon* **1997**, *35*, 797-799.

APPENDIX B

DERIVATION OF AN EQUATION FOR THE EFFECT OF MOLECULAR ORIENTATION ON THE FUGACITY COEFFICIENT OF THE NEMATIC PHASE

In his dissertation, Topliss[1] put forth a relationship to calculate the fugacity coefficient ϕ_i for species i in a mixture, with a knowledge of the mixture Helmholtz energy $\tilde{A}$.

$$\ln \phi_i = \tilde{A} + \frac{\partial \tilde{A}}{\partial x_i} - \sum_{j=1}^{n} x_j \frac{\partial \tilde{A}}{\partial x_j} + \rho\theta - \ln(1+\rho\theta) \tag{B.1a}$$

$$\text{where } \theta = \left(\frac{\partial \tilde{A}}{\partial \rho} \right)_{T,x} \tag{B.1b}$$

Substitution of Equation B.1b into Equation B.1a yields

$$\ln \phi_i = \tilde{A} + \frac{\partial \tilde{A}}{\partial x_i} - \sum_{j=1}^{n} x_j \frac{\partial \tilde{A}}{\partial x_j} + \rho \frac{\partial \tilde{A}}{\partial \rho} - \ln\left(1 + \rho \frac{\partial \tilde{A}}{\partial \rho} \right) \tag{B.1c}$$

where

ϕ_i = Fugacity coefficient of component i

ρ = Density of the mixture of n components

$\tilde{A}$ = Dimensionless Helmholtz energy

x_i = Mole fraction of component i

Humphries et al.[2] extended Maier-Saupe theory to cover multicomponent mixtures; below in Equation B.2a is the definition for the orientational molar Helmholtz energy of the mixture, a_{orient}. It is given in Equation 2.23 of their work. This definition was used by Hurt and Hu[3] in subsequent experiments. It is given in Equation 9 of that work.

$$a_{orient} = -\frac{N_{AV}}{2}\sum_{i=1}^{n}\sum_{j=1}^{n} x_i x_j \varepsilon_{ij} \overline{P_i}\,\overline{P_j} - RT\sum_{i=1}^{n} x_i \ln Z_i \qquad \text{(B.2a)}$$

or

$$a_{orient} = -\frac{N_{AV}}{2}\sum_{i=1}^{n}\sum_{j=1}^{n} x_i x_j \varepsilon_{ij} \overline{P_i}\,\overline{P_j} - N_{AV} kT\sum_{i=1}^{n} x_i \ln Z_i \qquad \text{(B.2b)}$$

N_{AV} = Avogadro's number, 6.022×10^{23}

x_i, x_j = Mole fractions of two different components i and j

ε_{ij} = Anisotropic energy parameter between two molecules i and j

$\bar{P}_i$, $\bar{P}_j$ = Ensemble average order parameter for components i and j

Z_i = Orientational partition function for component i

The ε_{ij} term is dependent on mole fraction, so it needs to be defined. It is defined as shown below.

$$\varepsilon_{ij} = -\left(\sqrt{\varepsilon_{ii}\varepsilon_{jj}}\right)\left(\frac{\sqrt{V_i V_j}}{\sum_{k=1}^{n} x_k V_k}\right) \qquad \text{(B.3a)}$$

The pure component molar volume V_i of component i is related to the pure component density as follows:

$$V_i = \frac{MW_i}{\rho_i} \tag{B.3b}$$

Meanwhile, the pure-component energy parameters ε_{ii} and ε_{jj} represent anisotropic potentials between two like molecules, and are defined as follows.

$$\varepsilon_{ii} = -4.542kT_{cl,i} \tag{B.4a}$$

$$\varepsilon_{jj} = -4.542kT_{cl,j} \tag{B.4b}$$

Substituting Eqs. B.4a and B.4b into Equation B.3a, the following expression for ε_{ij} is obtained:

$$\varepsilon_{ij} = -4.542k\left(\frac{\sqrt{T_{cl,i}T_{cl,j}V_iV_j}}{\sum_{k=1}^{n} x_k V_k}\right) \tag{B.4c}$$

The a_{orient} term is made dimensionless by dividing each side of Equation B.2a by $N_{AV}kT$, yielding

$$\tilde{A}_{orient} = -\frac{1}{2}\sum_{i=1}^{n}\sum_{j=1}^{n} x_i x_j \left(\frac{\varepsilon_{ij}}{kT}\right)\bar{P}_i\bar{P}_j - \sum_{i=1}^{n} x_i \ln Z_i \tag{B.5}$$

where the dimensionless anisotropic pair potential is given by

$$\frac{\varepsilon_{ij}}{kT} = \bar{\varepsilon}_{ij} = -4.542\left(\frac{\sqrt{T_{cl,i}T_{cl,j}V_iV_j}}{T\sum_{k=1}^{n} x_k V_k}\right) \tag{B.6a}$$

or

$$\bar{\varepsilon}_{ij} = \left(\frac{C_{ij}}{\sum_{k=1}^{n} x_k V_k} \right) \tag{B.6b}$$

where

$$C_{ij} = -4.542 \left(\frac{\sqrt{T_{cl,i} T_{cl,j} V_i V_j}}{T} \right) \tag{B.6c}$$

A breaking down of the terms constituting ε_{ij} reveals that there is no dependence of ε_{ij} on ρ, the overall mixture density.

Next, the ensemble average order parameter, $\bar{P}_k$, is defined. The $\bar{P}_k$ for all component k molecules in the mixture is given in Equation 2.18 in Humphries, et al.[2] It was also employed in the work of Hurt and Hu[3] and is given in Equation 15 of their paper.

$$\bar{P}_k = \frac{\int_0^{\pi/2} P_k \exp\left\{ -\sum_{j=1}^{n} x_j \bar{\varepsilon}_{jk} \bar{P}_j P_k \right\} \sin\theta d\theta}{\int_0^{\pi/2} \exp\left\{ -\sum_{j=1}^{n} x_j \bar{\varepsilon}_{jk} \bar{P}_j P_k \right\} \sin\theta d\theta} \tag{B.7}$$

where P_k is the order parameter for a single molecule k.

$$P_k = \frac{3}{2} \cos^2 \theta_k - \frac{1}{2} \tag{B.8}$$

and θ_k is the angle of orientation of molecule k.

We want to learn if the macroscopic quantity $\bar{P}_k$ is dependent on ρ or x_i. This task requires taking two derivatives, so I will start by differentiating with respect to a hypothetical property M.

$$\left(\frac{\partial \bar{P}_k}{\partial M}\right) = \frac{\left(\int_0^{\pi/2} \exp\{DP_k\}\sin\theta d\theta\right)\int_0^{\pi/2} P_k\left(\left(\frac{\partial}{\partial M}\right)(DP_k)\right)\exp\{DP_k\}\sin\theta d\theta}{\left(\int_0^{\pi/2} \exp\{DP_k\}\sin\theta d\theta\right)^2} \tag{B.9a}$$

$$- \frac{\left(\int_0^{\pi/2} P_k \exp\left\{-\sum_{j=1}^{n} x_j \bar{\varepsilon}_{jk} \bar{P}_j P_k\right\}\sin\theta d\theta\right)\int_0^{\pi/2}\left(\left(\frac{\partial}{\partial M}\right)(DP_k)\right)\exp\{DP_k\}\sin\theta d\theta}{\left(\int_0^{\pi/2} \exp\{DP_k\}\sin\theta d\theta\right)^2}$$

where $D = -\sum_{j=1}^{n} x_j \bar{\varepsilon}_{jk} \bar{P}_j$ (B.9b)

$$\left(\frac{\partial \bar{P}_k}{\partial M}\right) = \frac{\int_0^{\pi/2} P_k\left(\left(\frac{\partial}{\partial M}\right)\left(-\sum_{j=1}^{n} x_j \bar{\varepsilon}_{jk} \bar{P}_j P_k\right)\right)\exp\left\{-\sum_{j=1}^{n} x_j \bar{\varepsilon}_{jk} \bar{P}_j P_k\right\}\sin\theta d\theta}{\left(\int_0^{\pi/2} \exp\left\{-\sum_{j=1}^{n} x_j \bar{\varepsilon}_{jk} \bar{P}_j P_k\right\}\sin\theta d\theta\right)} \tag{B.9c}$$

$$- \frac{\bar{P}_k \int_0^{\pi/2}\left(\left(\frac{\partial}{\partial M}\right)\left(-\sum_{j=1}^{n} x_j \bar{\varepsilon}_{jk} \bar{P}_j P_k\right)\right)\exp\left\{-\sum_{j=1}^{n} x_j \bar{\varepsilon}_{jk} \bar{P}_j P_k\right\}\sin\theta d\theta}{\left(\int_0^{\pi/2} \exp\left\{-\sum_{j=1}^{n} x_j \bar{\varepsilon}_{jk} \bar{P}_j P_k\right\}\sin\theta d\theta\right)} \tag{B.9d}$$

The value P_k can come outside the summation sign because the summation is with respect to j.

$$\left(\frac{\partial \bar{P}_k}{\partial M}\right) = \frac{\int_0^{\pi/2} (P_k)^2 \left(\left(\frac{\partial}{\partial M}\right)\left(-\sum_{j=1}^{n} x_j \bar{\varepsilon}_{jk} \bar{P}_j\right)\right) \exp\left\{-\sum_{j=1}^{n} x_j \bar{\varepsilon}_{jk} \bar{P}_j P_k\right\} \sin\theta d\theta}{\left(\int_0^{\pi/2} \exp\left\{-\sum_{j=1}^{n} x_j \bar{\varepsilon}_{jk} \bar{P}_j P_k\right\} \sin\theta d\theta\right)} \tag{B.9e}$$

$$- \frac{\bar{P}_k \int_0^{\pi/2} P_k \left(\left(\frac{\partial}{\partial M}\right)\left(-\sum_{j=1}^{n} x_j \bar{\varepsilon}_{jk} \bar{P}_j\right)\right) \exp\left\{-\sum_{j=1}^{n} x_j \bar{\varepsilon}_{jk} \bar{P}_j P_k\right\} \sin\theta d\theta}{\left(\int_0^{\pi/2} \exp\left\{-\sum_{j=1}^{n} x_j \bar{\varepsilon}_{jk} \bar{P}_j P_k\right\} \sin\theta d\theta\right)} \tag{B.9f}$$

Now we need to examine the terms within the following derivative:

$$\left(\frac{\partial}{\partial M}\right)\left(-\sum_{j=1}^{n} x_j \bar{\varepsilon}_{jk} \bar{P}_j P_k\right)$$

The integral is a summation that includes all $O(10^{23})$ molecules. The variable of integration θ represents θ_i, the angle of orientation of an individual molecule.

If all of the terms inside the summation sign are independent of θ_k, then this derivative can come outside of the integrals in the equation above. A review of the earlier discussion concerning the energy parameter $\bar{\varepsilon}_{jk}$ will indicate that this variable does not depend on θ_k. It is quite obvious that the mole fraction of a species present in the nematic phase can not be altered simply by changing the order parameter of one of the $\sim 10^{23}$ molecules. By the same reasoning, the ensemble average order parameter $\bar{P}_k$ will be virtually unaffected if the θ_k of a single molecule is altered.

Thus the derivative can come out of the integral.

$$\left(\frac{\partial \bar{P}_k}{\partial M}\right) = \frac{\left(\left(\frac{\partial}{\partial M}\right)\left(-\sum_{j=1}^{n} x_j \bar{\varepsilon}_{jk} \bar{P}_j\right)\right)\int_0^{\pi/2} (P_k)^2 \exp\left\{-\sum_{j=1}^{n} x_j \bar{\varepsilon}_{jk} \bar{P}_j P_k\right\} \sin\theta d\theta}{\left(\int_0^{\pi/2} \exp\left\{-\sum_{j=1}^{n} x_j \bar{\varepsilon}_{jk} \bar{P}_j P_k\right\} \sin\theta d\theta\right)} \tag{B.9g}$$

$$- \frac{\left(\left(\frac{\partial}{\partial M}\right)\left(-\sum_{j=1}^{n} x_j \bar{\varepsilon}_{jk} \bar{P}_j\right)\right)\bar{P}_k \int_0^{\pi/2} P_k \exp\left\{-\sum_{j=1}^{n} x_j \bar{\varepsilon}_{jk} \bar{P}_j P_k\right\} \sin\theta d\theta}{\left(\int_0^{\pi/2} \exp\left\{-\sum_{j=1}^{n} x_j \bar{\varepsilon}_{jk} \bar{P}_j P_k\right\} \sin\theta d\theta\right)} \tag{B.9h}$$

$$\left(\frac{\partial \bar{P}_k}{\partial M}\right) = \left(\left(\frac{\partial}{\partial M}\right)\left(-\sum_{j=1}^{n} x_j \bar{\varepsilon}_{jk} \bar{P}_j\right)\right)\left(\bar{P}_k\right)^2 - \left(\left(\frac{\partial}{\partial M}\right)\left(-\sum_{j=1}^{n} x_j \bar{\varepsilon}_{jk} \bar{P}_j\right)\right)\left(\bar{P}_k\right)^2 \tag{B.9i}$$

$$\left(\frac{\partial \bar{P}_k}{\partial M}\right) = 0 \tag{B.9j}$$

Thus, $\bar{P}_k$ is independent of both density ρ and mole fraction x.

Finally, the orientational partition function is defined. For component k, Z_k is obtained from Equation 2.17, Humphries, et al.[2] This equation differs slightly from that put forth in Equations 2.20 and 3.3 of this work in that the limits of integration with respect to the angle θ are from 0 to $\pi/2$ instead of from 0 to π, and there is no integration with respect to the azimuthal angle ϕ. Humphries et al.[2] justify their choice of not integrating with respect to ϕ by noting that the distribution of possible energy states is independent of ϕ. They do not explicitly state or justify their choice of an integration

range with respect to θ, from 0 to $\pi/2$. However, Shishido et al.,[4] in a later work, justified that choice by reasoning that the head of a discotic mesogen cannot be distinguished from its tail. Thus, the energy states when the molecular axis is oriented at angles θ and $\pi - \theta$ relative to the director would in this case be identical (one notes that, because $\cos^2 \theta = \cos^2 \theta\ (\pi - \theta)$, the orientational order parameter P_i (see Equation 2.16) for mesogen i with the short axis oriented at an angle θ with respect to the director is equal to that calculated for the same molecule oriented at an angle $\pi - \theta$ relative to the director.

For simplicity, we use the partition function defined by Humphries et al.[2] and given in Equation B.10, rather than the one given in Equations 2.20 and 3.3. In the end, either approach yields identical results for the orientational contribution to the Helmholtz free energy (however, the determination of this free energy is much more straightforward when the partition function of Humphries is used). In Appendix A, Equation A.36 for the orientational partition function Z for a single component is equivalent to Equation 2.20 or 3.3 as adapted for a pure species; Equation A.36 is used in the development of Equation A.48 (a somewhat tedious procedure) for the orientational contribution to the Helmholtz free energy ΔA_{ori}. It can be shown that the right hand side of Equation A.48 is equivalent to Equation 2.25 (Humphries et al.[2]) for the orientational Helmholtz free energy of a pure nematic mesophase (provided that in this equation of Humphries et al.,[2] the terms within the summation on the right hand side of the equation are restricted to terms for which L = 2).

$$Z_k = \int_0^{\pi/2} \exp\left\{-\sum_{j=1}^{n} x_j \bar{\varepsilon}_{jk} \bar{P}_j P_k\right\} \sin\theta d\theta \qquad \text{(B.10)}$$

It becomes apparent that none of the terms in Equation B.2a depend on the mixture density ρ. Thus, the last two terms on the right hand side of Equation B.1c are zero and Equation B.1c reduces to

$$\ln \phi_i = \tilde{A} + \frac{\partial \tilde{A}}{\partial x_i} - \sum_{j=1}^{n} x_j \frac{\partial \tilde{A}}{\partial x_j} \qquad \text{(B.11a)}$$

Now, the goal is to find ϕ_i^{orient}, the portion of the fugacity coefficient for component i that is due to anisotropic interactions between molecules. Thus, Equation B.11a is rewritten:

$$\ln \phi_i^{orient} = \tilde{A}^{orient} + \frac{\partial \tilde{A}^{orient}}{\partial x_i} - \sum_{j=1}^{n} x_j \frac{\partial \tilde{A}^{orient}}{\partial x_j} \qquad \text{(B.11b)}$$

In order to make this calculation, the derivative of $\tilde{A}^{orient}$ with respect to mole fraction must be calculated. We start with:

$$\tilde{A}_{orient} = -\frac{1}{2} \frac{\sum_{j=1}^{n}\sum_{k=1}^{n} x_j x_k C_{jk} \overline{P_j}\,\overline{P_k}}{\sum_{=1}^{n} x_k V_k} - \sum_{k=1}^{n} x_k \ln Z_k \qquad \text{(B.12)}$$

The next step is to calculate $\left(\frac{\partial \tilde{A}^{orient}}{\partial x_i}\right)_{T,P,x_j \neq x_i}$. In order to save space, I denote the term

$\sum_{k=1}^{n} x_k V_k$ as V.

$$\left(\frac{\partial \tilde{A}^{orient}}{\partial x_i}\right)_{T,P,x_j} = -\left(\sum_{j=1}^{n} x_j \bar{\varepsilon}_{ij} \overline{P_i} \overline{P_j}\right) + \frac{1}{2}\frac{V_i}{V}\sum_{j=1}^{n}\sum_{k=1}^{n} x_j x_k \bar{\varepsilon}_{jk} \overline{P_j P_k} - \frac{\partial}{\partial x_i}\left(\sum_{k=1}^{n} x_k \ln Z_k\right) \quad \text{(B.13)}$$

$$\left(\frac{\partial \tilde{A}^{orient}}{\partial x_i}\right)_{T,P,x_j} = -\left(\sum_{j=1}^{n} x_j \bar{\varepsilon}_{ij} \overline{P_i} \overline{P_j}\right) + \frac{1}{2}\frac{V_i}{V}\sum_{j=1}^{n}\sum_{k=1}^{n} x_j x_k \bar{\varepsilon}_{jk} \overline{P_j P_k} - \left(\sum_{k=1}^{n} x_k \left(\frac{1}{Z_k}\right)\left(\frac{\partial Z_k}{\partial x_i}\right)\right) - \ln Z_i \quad \text{(B.14)}$$

Next we evaluate the partial derivative of Z_k with respect to component i.

$$\left(\frac{\partial Z_k}{\partial x_i}\right) = \int_0^{\pi/2}\left(\frac{\partial}{\partial x_i}\left(-\sum_{j=1}^{n} x_j \bar{\varepsilon}_{jk} \overline{P}_j P_k\right)\right)\exp\left\{-\sum_{j=1}^{n} x_j \bar{\varepsilon}_{jk} \overline{P}_j P_k\right\}\sin\theta d\theta \quad \text{(B.15)}$$

Substituting Equations B.10 and B.15 into Equation B.14, we obtain

$$\left(\frac{\partial \tilde{A}^{orient}}{\partial x_i}\right)_{T,P,x_j} = -\left(\sum_{j=1}^{n} x_j \bar{\varepsilon}_{ij} \overline{P_i} \overline{P_j}\right) + \frac{1}{2}\frac{V_i}{V}\sum_{j=1}^{n}\sum_{k=1}^{n} x_j x_k \bar{\varepsilon}_{jk} \overline{P_j P_k}$$
$$-\sum_{k=1}^{n} x_k \frac{\int_0^{\pi/2}\left(\frac{\partial}{\partial x_i}\left(-\sum_{j=1}^{n} x_j \bar{\varepsilon}_{jk} \overline{P}_j P_k\right)\right)\exp\left\{-\sum_{j=1}^{n} x_j \bar{\varepsilon}_{jk} \overline{P}_j P_k\right\}\sin\theta d\theta}{\int_0^{\pi/2}\exp\left\{-\sum_{j=1}^{n} x_j \bar{\varepsilon}_{jk} \overline{P}_j P_k\right\}\sin\theta d\theta} - \ln Z_i \quad \text{(B.16)}$$

As determined earlier (see p. 223), the derivative can come outside the integral, yielding

$$\left(\frac{\partial \tilde{A}^{orient}}{\partial x_i}\right)_{T,P,x_j} = -\left(\sum_{j=1}^{n} x_j \bar{\varepsilon}_{ij} \overline{P_i P_j}\right) + \frac{1}{2}\frac{V_i}{V}\sum_{j=1}^{n}\sum_{k=1}^{n} x_j x_k \bar{\varepsilon}_{jk} \overline{P_j P_k}$$

$$-\sum_{k=1}^{n} x_k \frac{\left(\frac{\partial}{\partial x_i}\left(-\sum_{j=1}^{n} x_j \bar{\varepsilon}_{jk} \bar{P}_j\right)\right)\int_0^{\pi/2} P_k \exp\left\{-\sum_{j=1}^{n} x_j \bar{\varepsilon}_{jk} \bar{P}_j P_k\right\}\sin\theta d\theta}{\int_0^{\pi/2} \exp\left\{-\sum_{j=1}^{n} x_j \bar{\varepsilon}_{jk} \bar{P}_j P_k\right\}\sin\theta d\theta} - \ln Z_i \quad \text{(B.17)}$$

Using the definition of $\bar{P}_k$ (Equation B.7), Equation B.17 is simplified.

$$\left(\frac{\partial \tilde{A}^{orient}}{\partial x_i}\right)_{T,P,x_j} = -\left(\sum_{j=1}^{n} x_j \bar{\varepsilon}_{ij} \overline{P_i P_j}\right) + \frac{1}{2}\frac{V_i}{V}\sum_{j=1}^{n}\sum_{k=1}^{n} x_j x_k \bar{\varepsilon}_{jk} \overline{P_j P_k}$$

$$-\sum_{k=1}^{n} x_k \left(\frac{\partial}{\partial x_i}\left(-\sum_{j=1}^{n} x_j \bar{\varepsilon}_{jk} \bar{P}_j\right)\right)\bar{P}_k - \ln Z_i \quad \text{(B.18)}$$

Now the derivative on the right hand side of Equation B.15 must be calculated.

$$\frac{\partial}{\partial x_i}\left(-\sum_{j=1}^{n} x_j \bar{\varepsilon}_{jk} \bar{P}_j\right) = \frac{\partial}{\partial x_i}\left(\frac{-\sum_{j=1}^{n} x_j C_{jk} \bar{P}_j}{\sum_{k=1}^{n} x_k V_k}\right) = \frac{V\left(-C_{ik}\bar{P}_i\right) - \left(-\sum_{j=1}^{n} x_j C_{jk}\bar{P}_j\right)\left(V_i\right)}{V^2} \quad \text{(B.19)}$$

$$\frac{\partial}{\partial x_i}\left(-\sum_{j=1}^{n} x_j \bar{\varepsilon}_{jk} \bar{P}_j\right) = -\bar{\varepsilon}_{ik}\bar{P}_i + \left(\frac{V_i}{V}\right)\left(\sum_{j=1}^{n} x_j \bar{\varepsilon}_{jk} \bar{P}_j\right) \quad \text{(B.20)}$$

Substituting Equation B.20 into Equation B.18,

$$\left(\frac{\partial \tilde{A}^{orient}}{\partial x_i}\right)_{T,P,x_j} = -\left(\sum_{j=1}^{n} x_j \bar{\varepsilon}_{ij} \overline{P_i}\,\overline{P_j}\right) + \frac{1}{2}\frac{V_i}{V}\sum_{j=1}^{n}\sum_{k=1}^{n} x_j x_k \bar{\varepsilon}_{jk} \overline{P_j}\,\overline{P_k}$$
$$-\sum_{k=1}^{n} x_k \overline{P}_k \left(-\bar{\varepsilon}_{ik}\overline{P}_i + \left(\frac{V_i}{V}\right)\left(\sum_{j=1}^{n} x_j \bar{\varepsilon}_{jk}\overline{P}_j\right)\right) - \ln Z_i \qquad \text{(B.21)}$$

$$\boxed{\left(\frac{\partial \tilde{A}^{orient}}{\partial x_i}\right)_{T,P,x_j} = -\frac{1}{2}\frac{V_i}{V}\sum_{j=1}^{n}\sum_{k=1}^{n} x_j x_k \bar{\varepsilon}_{jk}\overline{P_j}\,\overline{P_k} - \ln Z_i} \qquad \text{(B.22)}$$

Substituting into Equation B.11b, we obtain

$$\ln \phi_i^{orient} = -\frac{1}{2}\sum_{j=1}^{n}\sum_{k=1}^{n} x_j x_k \bar{\varepsilon}_{jk}\overline{P_j}\,\overline{P_k} - \sum_{j=1}^{n} x_j \ln Z_j - \frac{1}{2}\frac{V_i}{V}\sum_{j=1}^{n}\sum_{k=1}^{n} x_j x_k \bar{\varepsilon}_{jk}\overline{P_j}\,\overline{P_k} - \ln Z_i$$
$$+\sum_{j=1}^{n}\frac{1}{2}\frac{x_j V_j}{V}\sum_{k=1}^{n}\sum_{m=1}^{n} x_k x_m \bar{\varepsilon}_{km}\overline{P_k}\,\overline{P_m} + \sum_{j=1}^{n} x_j \ln Z_j \qquad \text{(B.23)}$$

$$\ln \phi_i^{orient} = -\frac{1}{2}\sum_{j=1}^{n}\sum_{k=1}^{n} x_j x_k \bar{\varepsilon}_{jk}\overline{P_j}\,\overline{P_k} - \sum_{j=1}^{n} x_j \ln Z_j - \frac{1}{2}\frac{V_i}{V}\sum_{j=1}^{n}\sum_{k=1}^{n} x_j x_k \bar{\varepsilon}_{jk}\overline{P_j}\,\overline{P_k} - \ln Z_i$$
$$+\frac{1}{2}\sum_{j=1}^{n}\sum_{k=1}^{n} x_j x_k \bar{\varepsilon}_{jk}\overline{P_j}\,\overline{P_k} + \sum_{j=1}^{n} x_j \ln Z_j \qquad \text{(B.24)}$$

Thus, $$\boxed{\ln \phi_i^{orient} = \left(\frac{\partial \tilde{A}^{orient}}{\partial x_i}\right)_{T,P,x_j} = -\frac{1}{2}\frac{V_i}{V}\sum_{j=1}^{n}\sum_{k=1}^{n} x_j x_k \bar{\varepsilon}_{jk}\overline{P_j}\,\overline{P_k} - \ln Z_i} \qquad \text{(B.25)}$$

This final expression (Eq. B.25) is identical to the one in the Visual FORTRAN SAFT-LC computer program employed by researchers in the Carbon group at Clemson.

There appears to be no overall mixture density dependence in Equation B.5. The way the equation is set up, the ε_{ij} terms depend on the various V_i values, which in turn depend on the pure component density values ρ_i. So, as it stands, it is safe to say that the a^{orient} term can be decoupled from the SAFT equation (mixture density values calculated by SAFT are the same regardless of whether LC part is added or not).

References

[1]Topliss, R. J. Techniques to Facilitate the Use of Equations of State for Complex Fluid Phase Equilibria. Ph. D. Dissertation, University of California, Berkeley, 1985.

[2]Humphries, R. L.; James, P. G.; Luckhurst, G. R. A Molecular Field Treatment of Liquid Crystalline Mixtures. *Symp. Faraday Soc.* **1971**, *5*, 107-118.

[3]Hurt, R. H.; Hu, Y. Thermodynamics of Carbonaceous Mesophase II. General Theory for Nonideal Solutions. *Carbon* **2001**, *39*, 887-896.

[4]Shishido, M.; Inomata, H.; Arai, K.; Saito, S. Application of Liquid Crystal Theory to the Estimation of Mesophase Pitch Phase Transition Behavior. *Carbon* **1997**, *35*, 797.

APPENDIX C

DIAGNOSTIC TEST OF THE PREDICTIVE ABILITY OF THE SAFT-LC EQUATION TO MODEL THE DENSE-GAS EXTRACTION PROCESS

In this appendix, a diagnostic test of the predictive ability of the Statistical Associated-Fluid Theory – Liquid Crystal (SAFT-LC) equation was performed. The SAFT-LC equation (using the values of the SAFT-LC parameters A, B, C, a, and b given in Chapter 3) was used to predict equilibrium top and bottom phase compositions for M-50 pitch-toluene mixtures at 56.2 bar, 350° C, and a solvent-to-pitch ratio of 5.1:1. A multistage dense-gas extraction (DGE) experiment[1] was also performed on M-50 pitch at these conditions (which are representative of those necessary to produce a DGE bottom product that, upon drying, possesses a high mesophase content[1]), using toluene as the dense-gas solvent. The molecular weight distribution (mol wt distribution, or MWD) for M-50 pitch initially proposed by Cervo[2] was input to the SAFT-LC model, with one alteration. Mass fractions for the 10 pseudocomponents (PCs) present were altered based on subsequent DGE mass balance experiments[3,4] which indicate that M-50 pitch is comprised of 50% monomer, 27% dimer, with the remaining 23% consisting of trimer, tetramer, and pentamer. The altered MWD, mass fractions, and molecular carbon-to-hydrogen (C/H) ratios are given in Table C.1. For the M-50 pitch PCs, the pure-component SAFT parameters m, v^{00}, and u^0/k were predicted using the correlations of Huang and Radosz[5] in a manner identical to that described in Chapter 3. For each PC,

the mol wt and the molecular C/H ratios given by Cervo[2] were used as inputs to these correlations.

Table C.1. The MWD of M-50 pitch, as derived by Cervo;[2,3,4] each pseudocomponent (PC) is assumed to account for half (by mass) of the presence of a given oligomer in the pitch.

Pitch PC data			
PC number	Mol wt	Mass Fraction	C/H Ratio
1	246.4	0.25	1.06
2	334.5	0.25	1.18
3	448.6	0.135	1.25
4	572.8	0.135	1.41
5	696.9	0.06	1.53
6	821	0.06	1.63
7	957.2	0.0275	1.73
8	1067.3	0.0275	1.75
9	1213.5	0.0275	2.02
10	1409.7	0.0275	2.17

The results of this diagnostic test, shown in Fig. C.1, indicate that SAFT-LC overpredicts the extractive capacity of the dense-gas solvent at 56.2 bar and 350° C. That is, the MWD of the dried bottom product predicted by SAFT-LC for a one-phase extraction process (see gray line, Fig. C.1) reveals a residue comprised primarily of molecules with a mol wt of greater than 1000, with virtually all monomer and dimer extracted into the top phase. However, the mass spectrum (see black line, Fig. C.1) obtained for the dried bottom product resulting from the multistage DGE technique indicates that a substantial amount of dimer remains in the bottom phase. Because it is clear from the single-stage SAFT-LC results that the model greatly overpredicts the

extractive capacity of the dense-gas solvent, no multistage SAFT-LC calculations were performed.

From the above results, it is apparent that the SAFT-LC model must be improved. Recommendations as to how to improve the SAFT-LC model are discussed in Chapter 8 (the Conclusions and Recommendations section).

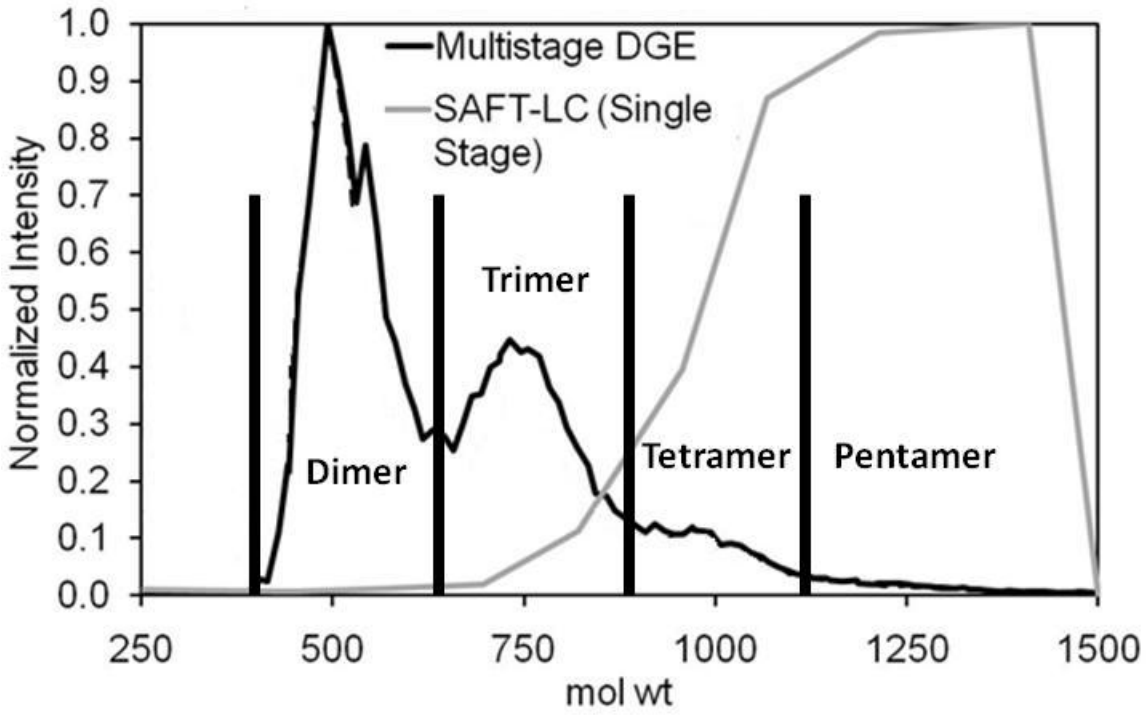

Figure C.1. At 56.2 bar, 800 psig, and S/P ratio = 5.1 (DGE operating conditions utilized in the production of mesophase pitch from isotropic M-50), the SAFT-LC model greatly underpredicts the presence of M-50 dimer and trimer in the dried bottom product. The result labeled "Multistage DGE" indicates the smoothed mass spectrum for the dried bottom product obtained at the stated DGE operating conditions.

References

[1]Cervo, E. G.; Thies, M. C. Controlling the Oligomeric Composition of Carbon-Fiber Precursors by Dense-Gas Extraction. *J. Am. Ceram. Soc.* **2008**, *91*, 1416-1422.

[2]Cervo, E. G.; Thies, M. C. Control of the Molecular Weight Distribution of Petroleum Pitches via Dense-Gas Extraction. *Chem. Eng. Technol*. **2007**, *30*, 742-748.

[3]Cervo, E. G.; Thies, M. C. Isolating Petroleum Pitch Oligomers by Continuous, Countercurrent Dense Gas Extraction. Submitted for publication to *J. Supercrit. Fluids*, 2010.

[4]Cervo, E. G. Isolating Petroleum Pitch Oligomers via Multistage Supercritical Extraction. Ph. D. Dissertation, Clemson University, 2010.

[5]Huang, S. H.; Radosz, M. Phase Behavior of Reservoir Fluids V: SAFT Model of CO_2 and Bitumen Systems. *Fluid Phase Equilib.* **1991**, *70*, 33-54.

APPENDIX D

GPC: PROCEDURES FOR SAMPLE PREPARATION, SYSTEM OPERATION, AND DATA RETRIEVAL

Materials Necessary

1. Waters Alliance GPCV 2000 model (to characterize samples via gel permeation chromatography (GPC)) equipped with 1080 μL sample injection loop when operating in preparatory-scale mode and with a 106 μL sample injection loop when operating in analytical-scale mode. Larger loop volumes are not recommended when fractionating M-50 pitch; the chief use of prep-scale GPC is the preparation of narrow fractions which can then be subjected to analytical techniques that do not require large amounts of sample (such as the methods indicated in Chapters 4-7). For analytical-scale operation, peak resolution is optimized when using the 106 μL loop, but larger volumes (314.5 μL) have also been used with success.
2. 1,2,4-Trichlorobenzene (TCB, GPC grade, 99% min. purity, CAS number 120-82-1, obtained from VWR) mobile phase
3. Balance (M-310 model, Denver Instrument)
4. 2 prep scale GPC columns (PLgel stationary phase, 10 microns particle size, 300 mm long x 25 mm wide, first column pore size 500 Å, second column pore size 100 Å).
5. Filter vial assembly (plunger, seal, and cup; 24/pk – part number 600000186)
6. 0.5 micron filter (100/pk – part number 600000163)
7. 20 mm crimp cap (100/pk; part number 600000138)

8. Crimping tool (part number 700000847)
9. 10 mL volumetric flask with stopper
10. Pitch to be fractionated

Experimental – Following is the sample preparation procedure used to fractionate DGE Pitch Cut 2 in Chapter 4.

1. First, prepare the sample solution. Weigh out 100 mg of pitch (because of this relatively low mass requirement, prep-scale GPC is ideal for further purification of pitch cuts produced via semibatch DGE).
2. Next, in order to produce a solution with a pitch concentration of 10 mg/mL,* place the pitch in a volumetric flask with a volume of 10 mL. Note that the use of higher sample concentrations (particularly with samples containing significant amounts of trimer and higher-order oligomers) is not recommended because such action will cause the column to degrade (because our prep-scale GPC columns have a cross-sectional area that is 10x greater than that of a typical Waters analytical-scale Styragel ® column of inside diameter 7.8 mm, a concentration of no greater than 1 mg/mL is recommended when performing analytical-scale GPC).

*Over time (that is, ~ 30 fractionation runs), the injection of a sample of M-50 pitch containing primarily trimer and tetramer at a concentration of 50 mg/mL was shown to result in column degradation, resulting in significant peak tailing. Separate efficiency tests of each prep-scale GPC column indicated that the column with a pore size of 100 Å exhibited significantly more deterioration than the column with the 500 Å pore size.

3. Fill the flask up to the mark with TCB. Place the stopper over the mouth of the flask.
4. Shake thoroughly and sonicate for 15 minutes.
5. Fill the metal GPC sample vial "cup" with ~ 7 mL of the sample solution (that is, it should be 70-80% full). If an insufficient volume of sample is present, a reduced volume of sample (or none at all) will be injected into the GPC column bank.
6. Prepare the plunger and filter. This assembly, of which the plunger is a part, is used by the Alliance GPCV2000 autosampler to filter particulate matter from the prepared solution before it is injected into the GPC sample loop. Make sure that the open end of the plunger seal is pointing toward the alignment line and away from the end of the plunger. Secure a 0.5 micron filter to this end of the plunger.
7. Secure a 20 mm, sealed crimp cap to the assembly. Use the crimping tool to accomplish this task.
8. Slide the plunger assembly, filter end first, into the sample vial. Slide it to such a depth that the filter and the solution within the vial are barely in contact with one another.
9. If the Alliance GPCV2000 unit is currently ready for use, skip this step and the next three steps and proceed to Step 13. If the unit is ready for use, the messages CAR: 140, INJ: 140, and COL: 140 should appear in green at the bottom of the Interactive Mode window. These messages indicate that the sample carousel, injector, and column temperatures are at the operating temperature of 140° C.
10. If the Alliance GPCV2000 instrument is not currently up and running, start it up (refer to Alliance GPCV2000 system software operating manual, Section 3.1, Starting

the System, pp. 62-64). Upon completion of the steps laid out in this section, the Interactive Mode window appears.

11. Click on **Setup** in the top left corner of the Interactive Mode window. From the menu that appears, click on **Current Instrument Method**. A list of instrument methods will pop up. Double-click on **TCB_0x10_mL_min_140_C**. This instrument method sets the mobile-phase flow rate at 0.10 mL/min, and sets the carousel, injector, and column temperatures to 140° C. Click **OK** to change to the flow rate and temperatures to those programmed in this instrument method.
12. It should take 1-1.5 hours for the carousel, injector, and column temperatures to reach 140° C. Make sure that all temperatures stabilize at 140° C (if they don't stabilize, but continue rising above 140° C unabated, then there is possibly a fused column heater assembly). In such an event, shut the Alliance GPCV2000 system down (to shut down the Alliance GPCV2000, proceed as directed in the manual, Section 3.8, Shutting Down the system, pp. 103-104) immediately and call Waters Technical Service at 1-800-252-4752 for support on identifying and fixing the problem.
13. From Interactive mode, go to Sample Set mode (see manual, Fig. 1-12, p. 21). Click on the **Editor** button (located in the lower left corner of the screen) to open the **Sample Set Method Editor**, which appears as a separate window. This is where the GPC operator programs the operating conditions (run time, column operating temperature, mobile-phase flow rate, etc.) for the GPC fractionation experiment to be conducted. For a detailed tutorial in this area, see manual (Section 3.7, Creating and Running a Sample Set, pp. 97-103).

14. In Row 1, under **Sample**, type Equilibrate. Next, click in Row 1 under the **Method** box. A menu will appear. Select the method **TCB_2x50_mL_min_140_C** from the list. Next, click on the box in Row 1 that is directly under **Function**. A menu will appear; from this menu, select **Equil**. In Row 1, under **Time**, type 90.00 in order to equilibrate the system at the mobile-phase flow rate of 2.50 mL/min for 90 minutes and at a temperature of 140° C (do not use a mobile-phase flow rate higher than 2.50 mL/min, as such action causes the solvent pump piston seals to leak. Operating at a flow rate of greater than 3.00 mL/min may cause the refractometer cells to crack).
15. In Row 2, under **Vial #**, type 1. Under **Sample**, type the sample name (for the fractionation of DGE Pitch Cut 2, the sample name was S_DGE_4_Cut_4). In Row 2, under **Method**, select the method **TCB_2x50_mL_min_140_C**; under Function, select **Broad Unknown**; under **Time**, select 80.00 min in order to record the GPC chromatogram for 80 minutes. Click in Row 2 under the box labeled **Vial Size**. A menu appears. Click on 7.
16. In Row 3, program the system to return to the standby flow rate upon completion of the fractionation run. In Row 3, type Standby under the **Sample** box. Select the method **TCB_0x10_mL_min_140_C** in order to tell the system to return to a resting mobile-phase flow rate of 0.10 mL/min. In Row 3, under **Function**, select **Equil**. Once finished, click **Save As** to save the sample set. Choose a filename (this name should clearly identify the experiment number and the sample fractionated, such as Exp_56_S_DGE_4_Cut_4). In Row 3, under **Time**, type 1.00 min. Click **OK** to exit the **Sample Set Method Editor**.

17. Load this sample vial (with plunger/filter assembly inserted) into the Alliance GPCV2000 sample compartment, at carousel position 1.
18. In Sample Set mode, click on **Run**. The **Start Sample Set** box appears. To ensure that the chromatogram data are sent to the Empower data processing software, make sure that the **Enable** box under **Empower Login** is checked. Enter the Empower user name and password (system and manager, respectively). Make sure that the **Local** box is selected. Click **Browse** to select the Empower project to which you want the chromatographic results to be sent (we sent the results for the GPC fractionation of DGE Pitch Cut 2 to the project Exp_56_S_DGE_4_Cut_4). When finished, click **OK**. The **Save Sample Set** box appears. Give the sample set the same name as that given in Step 16 and click **OK** . The run should start.

Upon completion of the GPC runs, the chromatogram data must be exported so that it can be subsequently plotted in a program such as Microsoft Excel. This procedure follows

1. From the Desktop, double-click the Empower software icon.
2. The Empower Login box pops up. Enter username and password. Click **OK**.
3. A popup box appears. Click **Browse Project**.
4. Open the project to which you sent the chromatographic results in Step 18 above (for the GPC fractionation of DGE Pitch Cut 2, this project is Exp_56_S_DGE_4_Cut_4).
5. On the screen that appears, click on the **Channels** tab.

6. Select the channel with the sample name identical to that specified in Step 15 on the previous pages. Make sure that the label under **Channel Description** is Refractive Index.
7. At the top of the screen, click **Database**.
8. On the menu that appears, click **Export Data**. The **Export** box appears.
9. In the lower left corner of the **Export** box, click **Export Method**.
10. The **Export Method Editor** box appears. In the upper left corner of this box, click the **Raw Data** tab.
11. Type the filename (for DGE Pitch Cut 2, the filename was Exp_56_SDGE_4_cut_4_022809).
12. Specify the location to which the chromatographic data file will be exported. To export to the Desktop, enter C:\Documents and Settings\Administrator\Desktop in the long rectangular box under **Path to File(s)**. Make sure that the small white box immediately to the left of this box is checked.
13. In the upper left corner of the **Export Method Editor** box, click **File**/**Save As**. On the box that appears, enter the filename for the export method, along with remarks indicating the column types, injection loop size, mobile-phase flow rate, etc.
14. Click **Save**.
15. Close **Export Method Editor** box.
16. Back at the **Export** box, click **OK**.
17. The **Project** box appears with the message "Finished exporting." Click **OK**.
18. Retrieve exported file from the desktop.

Purging the detector (the refractometer)

Special care must be taken to fully purge all TCB from the Alliance GPCV 2000 system (particularly the refractometer) when changing the GPC mobile phase. If the refractometer is not fully purged of TCB, its sensitivity will be greatly weakened (sometimes the signal-to-noise ratio is so low that it is difficult to distinguish the GPC response from baseline noise). TCB is particularly difficult to purge from the refractometer because it is significantly more viscous than many other common GPC mobile phases.

It was often necessary to switch from operating in prep-scale mode (in which TCB was used as the mobile phase) to analytical-scale mode (in which tetrahydrofuran was used as the mobile phase). The prep-scale columns were first removed. Because TCB and tetrahydrofuran are immiscible, it was necessary to first switch the GPC mobile phase from TCB to toluene (normal boiling point 110° C); many common GPC mobile phases, including both TCB and THF, are fully miscible with toluene. In order to effectively purge TCB from the refractometer, we set the column compartment temperature to 80° C and allowed it to reach equilibrium (this process takes approximately 3 hours when starting at 140° C, the typical operating temperature when using TCB as the mobile phase). The toluene flow rate was set to 1.0 mL/min, with a purge time of 60 minutes (the procedure for programming a refractometer purge is given in the Alliance GPCV2000 system software operating manual, Section 3.4.3, Purging the Refractometer). When the purge is complete, check the refractometer LED current (from Diagnostics Mode of the Alliance GPCV 2000 system operating software, click

Diagnostics, click on Service Diagnostics login, enter the password, and click Detector Diagnostics). The reading should be less than 40 mA. If it is significantly higher than this number, then the refractometer has not been completely purged of TCB. When the reading for the LED current was below 40 mA, the temperatures of the column, carousel, and injector compartments were programmed to 40° C and allowed to reach equilibrium. At that point, the mobile phase was switched over to tetrahydrofuran.

Note: Procedure for calibrating the GPC is given in the Empower GPC Software guide.

APPENDIX E

MALDI AND PSD PROCEDURES

This section contains procedures pertaining to: (1) maintenance of the MALDI apparatus and (2) the operating procedure for the Fragmentation Analysis and Structural Time-of-Flight (FAST) feature in the FlexAnalysis MALDI operating software, by which post-source decay (PSD) analyses are performed.

Note: All screen snapshots from the FlexAnalysis and FlexControl software in this chapter are reprinted with the permission of Bruker Daltonics.

MALDI Ion Source Cleaning Procedure

The ion source (otherwise known as the IS2 plate) is responsible for initiating the flow of ions toward the detector. Over time, matrix and analyte buildup on the ion source can cause a detraction in its performance. Thus, in order for it to function properly, it must be cleaned periodically.

1. Open Flex Control. Click on the **Status** tab. On the screen that appears, click the **Details** button. A new line of tabs should appear on the upper half of the screen. Click the **Vacuum** tab. On the screen that appears, press the **Vent.** button.
2. Close Flex Control and shut down the MALDI computer. If you do not perform this step, FlexControl will crash later on in the process.
3. There is a keyhole approximately 1 meter above the MALDI sample tray insert/eject port. Using the provided key, turn key to the perpendicular position.
4. Turn the power switch at the rear of the instrument to the **OFF** position. Now all vacuum pumps are turned off.
5. Open the door at the rear of the instrument by loosening the screw near the power switch.
6. Locate the roughing pump (it is about knee-high). Locate the metal hose that leads away from this pump. This hose is connected to the metal cylinder directly above the roughing pump. A screw holds this hose in place; a plastic red fitting is attached to this hose. Loosen the red fitting and remove the screw. Then, remove

the vacuum hose. You should hear some hissing as air is sucked into the instrument, breaking the vacuum.

7. Using an Allen wrench, loosen the 4 screws at the base of the MALDI apparatus that hold the floor of the source compartment in place. You will likely need to lie down on your back in order to perform this task.
8. SLOWLY allow the floor of the source compartment to swing downward as you remove the last screw. A small wire will pop out near the hinge closest to the wall and the electrical outlets. It is important not to open the compartment too fast, lest the wire be damaged.
9. Gently spray methanol on the source in order to wash away TCNQ and any other species that may have accumulated there. Use Kimwipes to wipe clean every reachable surface (such as the walls of the source compartment) without touching sensitive equipment (such as the source plates themselves) that is easy to damage.
10. When the source compartment has been cleaned, replace the small wire that popped out of its moorings when the compartment was opened. Be patient, as you may not accomplish this task on your first try!!
11. Once the wire has been secured, close the source compartment door and replace the four screws on the base of the source compartment.
12. Secure the loose vacuum hose to the vacuum pump by tightening the plastic red fitting.
13. Close the door at the rear of the instrument, and flip the power switch to the **ON** position.

14. Insert the key in the keyhole above the MALDI sample tray insert/eject port, and turn it to the parallel position.
15. Restart the MALDI computer and open FlexControl. Click on the **Status** tab, **Details** button, and **Vacuum** tab as in step 1. This time, however, click on the **Evac.** button.

Wait 1-2 hours for the system to evacuate.

MALDI Roughing Pump Oil Changing Procedure

Bruker Daltonics recommends that the oil for the roughing pump located at the rear of the MALDI apparatus be changed at least once a year. Typically, the spent oil will be a reddish color. In order to maximize the lifetime of the pump, we have utilized the following procedure to change its oil.

1. Open Flex Control. Click on the **Status** tab. On the screen that appears, click the **Details** button. A new line of tabs should appear across the upper half of the screen. Click the **Vacuum** tab. On the screen that appears, press **Vent.** button.
2. Close Flex Control and shut down the MALDI computer. If you do not perform this step, FlexControl will crash later on in the process.
3. There is a keyhole approximately 1 meter above the MALDI sample tray insert/eject port. Using the provided key, turn key to the perpendicular position.
4. Turn the power switch at the rear of the instrument to the **OFF** position. Now all vacuum pumps are turned off.
5. Open the door at the rear of the instrument by loosening the screw near the power switch.
6. Unplug the vacuum pump by removing plug P22 from jack J22.
7. Disconnect the inlet hose to the vacuum pump by removing the metal clamp.
8. Disconnect the cylinder above the roughing pump from the pump by removing the metal clamp. Now the pump is thoroughly disconnected from the MALDI high vacuum system.

9. Remove vacuum pump from the MALDI apparatus.
10. Allow the old pump oil to drain out by removing the fitting on the pump face using an Allen wrench. Once the draining is complete, replace the fitting.
11. Remove red plastic cap on top of pump and pour in the new pump oil (the pump oil and a funnel are stored along the wall behind the MALDI computer). Stop pouring once the water level is ~ 75-80% full height, as indicated on the level viewer.
12. Replace the red cap.
13. Replace the vacuum pump in the MALDI apparatus and replace the inlet hose and the cylinder at the pump outlet. Make sure the clamps are tight. Make sure the manufacturer name Pfeiffer is pointing toward the rear of the instrument.
14. Replace plug P22 in jack P22.
15. Close the door at the rear of the instrument, and flip the power switch to the **ON** position.
16. Insert the key in the keyhole above the MALDI sample tray insert/eject port, and turn it to the parallel position.
17. Restart the MALDI computer and open FlexControl. Click on the **Status** tab, **Details** button, and **Vacuum** tab as in step 1. This time, however, click on the **Evac.** button instead of the **Vent.** Button.

Wait 1-2 hours for the system to evacuate.

Procedure for Obtaining PSD Spectra

In this tutorial, the procedure for obtaining PSD spectra is given. The MALDI matrix material 7,7,8,8-tetracyanoquinodimethane (TCNQ) was chosen for analysis because, unlike the polycyclic aromatic hydrocarbons comprising pitches, it yields a considerable number of fragments upon excessive irradiation by the N_2 laser. Thus, PSD spectra for such materials are relatively easy to obtain, so TCNQ is an ideal material on which beginners can practice the PSD technique. The procedure for obtaining PSD spectra for TCNQ is as follows:

1. From the Desktop, click on the icon labeled **flexControl**. A box, labeled "**Logon Information**", pops up in the middle of the screen. Click **OK**.

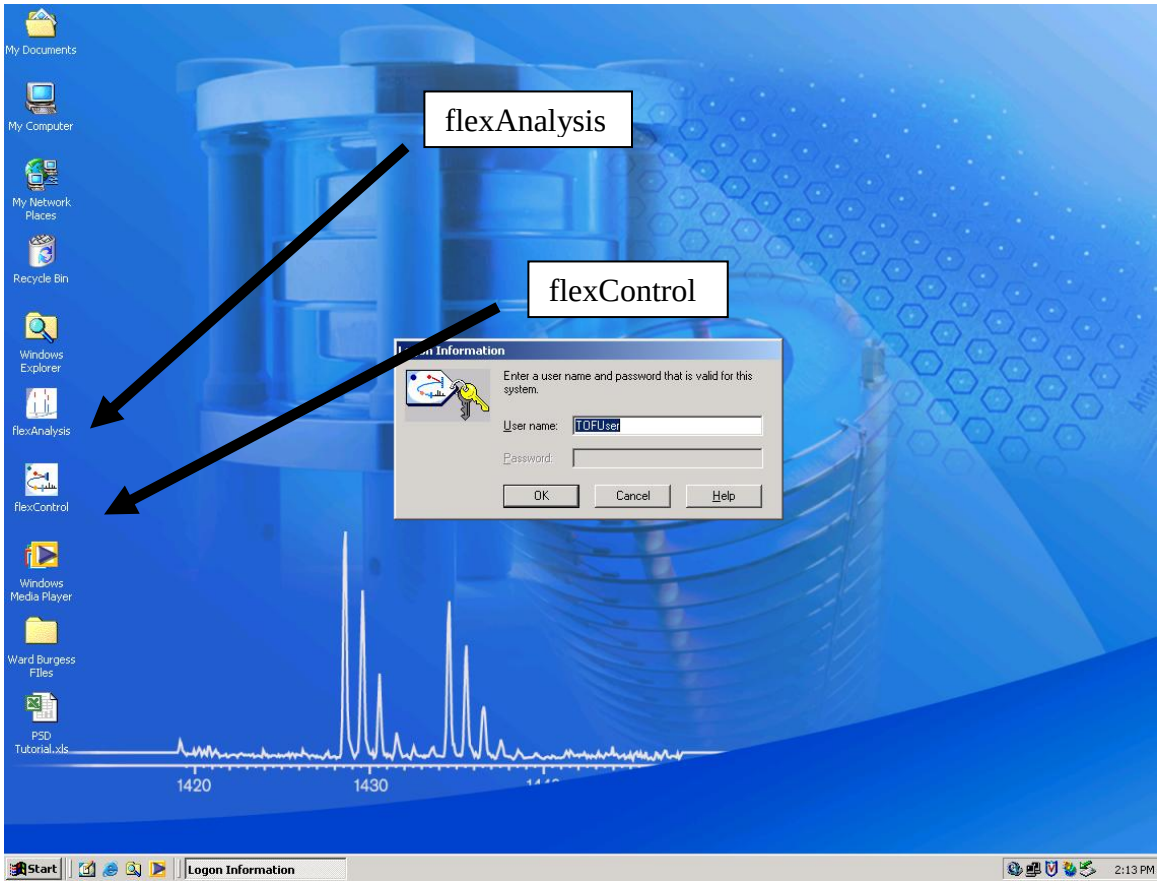

2. The FlexControl program opens, and the **Open flexControl Method** box pops up. Double click on **FAST_low mass.psm**.
3. Click on the Open/Close button, to access the loading tray. Place the MALDI target in the loading tray, and press the Open/Close button a second time to load the target into the instrument.

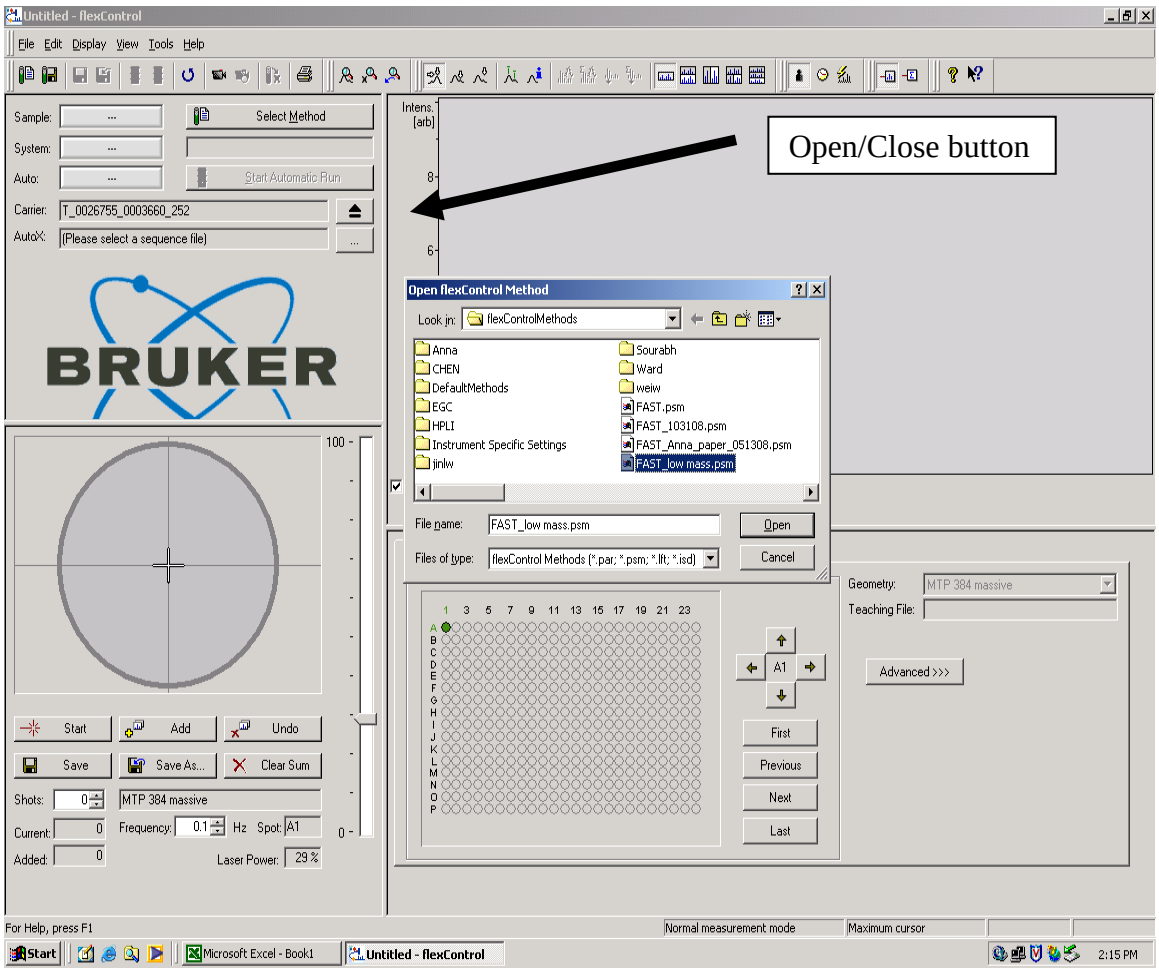

4. In order to perform molecular fragmentation analyses, click on the **FAST** tab. On the screen that appears, make sure that the ion selector is turned on by ensuring that the **Ion Selector** box is checked as indicated below. Set the ion selection **Window Range** from -5 Da to + 5 Da. This step allows only ions for which the molecular weight of the parent molecule ranges from 199 to 209 Da to reach the detector. Set the parent mass to 204.19, the molecular weight of TCNQ. Name the file PSD – TCNQ Standard by typing in the long, white, rectangular box labeled **Sample**. Make sure that the box labeled **Show apparent masses** is not checked.

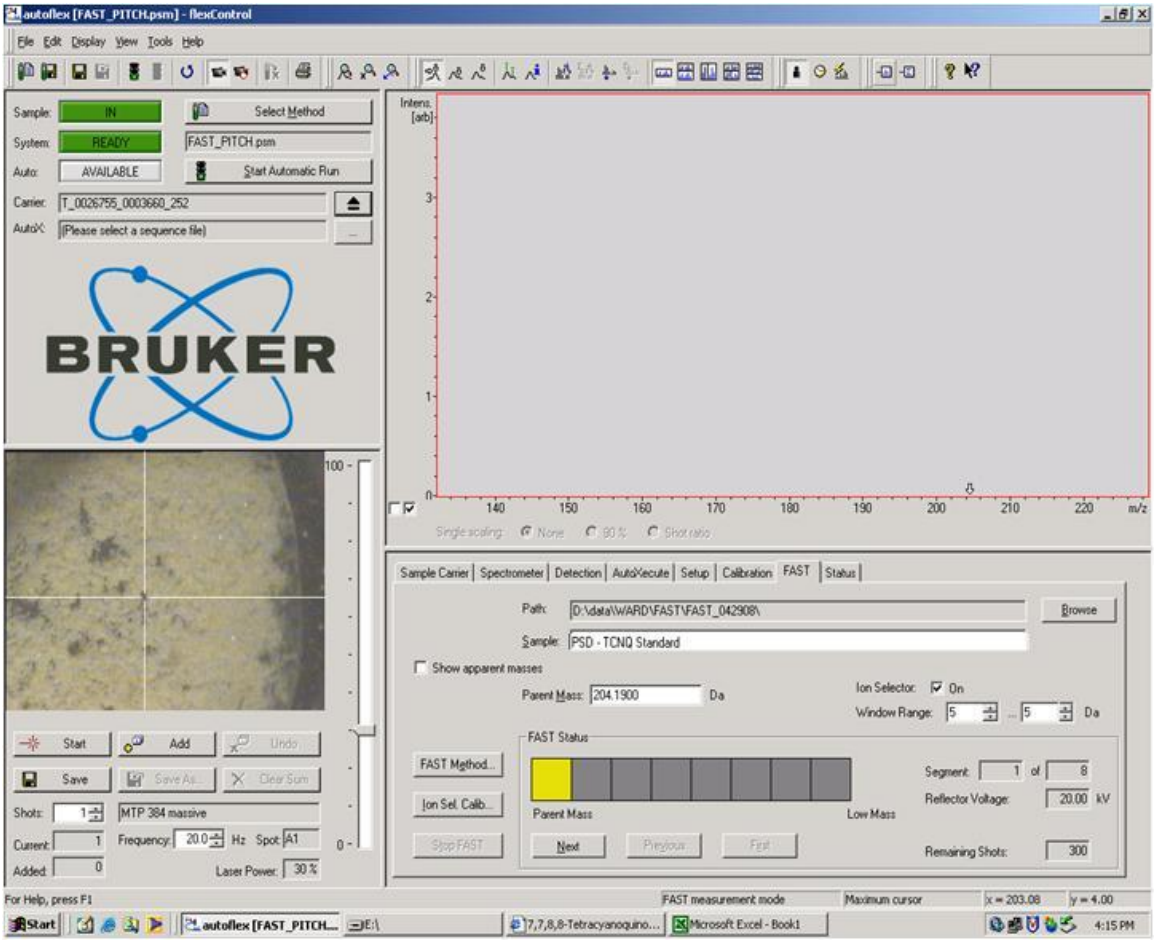

Finally, note that the PSD spectrum will be saved in the location designated in the long, rectangular box next to **Path**; that is, D:\data\WARD\FAST\FAST_042908\

5. To adjust the FAST method parameters, click on the box labeled **FAST Method**. The following screen will appear.

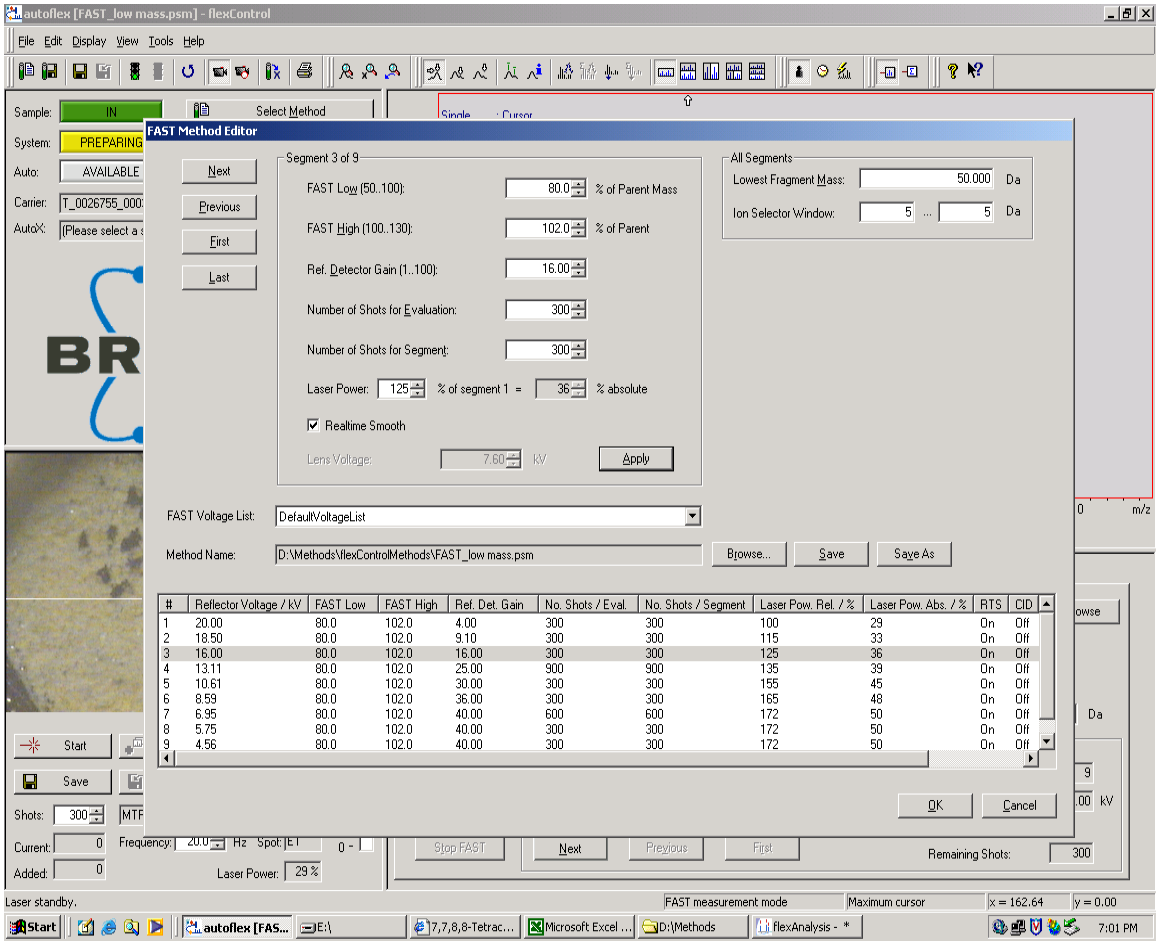

6. At the bottom of the screen that appears will be a list of the parameters for each segment of the PSD spectrum. The voltage at which the reflector is kept is unique for each segment and is successively stepped down with respect to increasing segment number over the course of PSD spectrum acquisition. Relatively high detector voltages (20 kV) are necessary to redirect large ions to the detector (such as the parent ion). However, when subjected to such strong reflecting voltages, medium-range and smaller (fragment) ions miss the detector. Therefore, progressively lower reflector voltages are required to accurately redirect and refocus ions of diminishing molecular weight to the detector. Because of the relative scarcity of fragment ions produced, it is necessary to use increasing laser powers and detector gains to ionize and detect fragments of diminishing size.

   Another factor requiring increases in detector gains and/or laser powers is detector aging (the detector becomes clogged with matrix and analyte). Over a period of time, equivalent numbers of incoming ions will yield diminishing amounts of secondary electron currents in the microchannel plate detector (and, therefore, weaker signals). Therefore, higher detector gains are necessary to generate a response with an acceptable signal-to-noise ratio. After making changes to the parameters for a particular segment, click **Apply** to save the changes. To exit this screen and to return to the previous one, click **OK.**

7. Next, ensure that the ion pre-selector correctly identifies the molecular weight of the peak of interest. The default method was obtained for peptides, all of mol wt > 1000 Da. Add the low-mass TCNQ to the calibration curve by clicking the **Add Mass to Calibration List** button. Click **Calculate** to re-calculate the calibration curve. Click **Apply** to update the calibration curve. Finally, to exit, click **OK**.

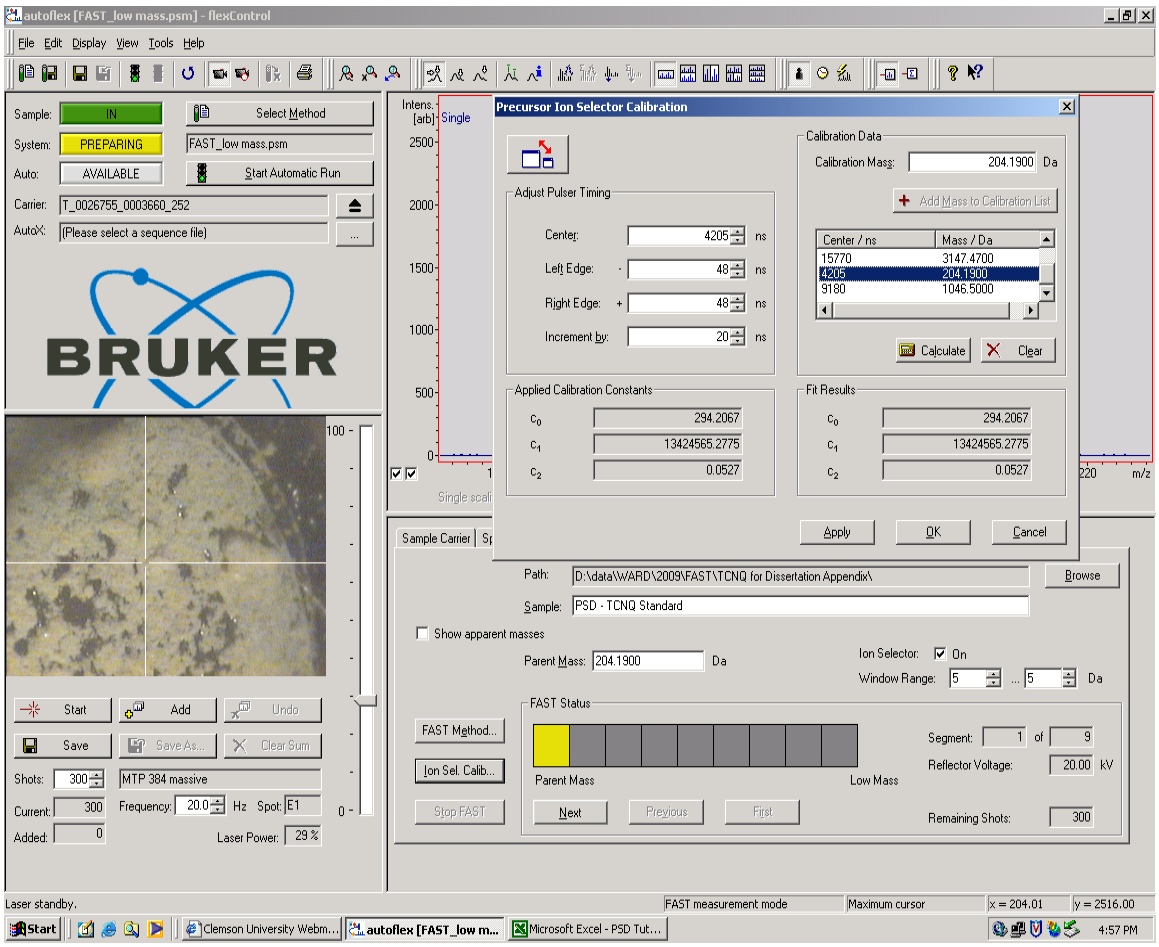

8. Collect the mass spectrum for the first segment. After the required number of shots (300 in this case; see white box next to **Shots** below**)** has been taken, click on the **Add** button. It will add the collected spectrum to the sum buffer. The color of the word 'Add' will turn from black to grey, and the button labeled **Next** will turn green. Click on this button to collect the mass spectrum for the next segment.

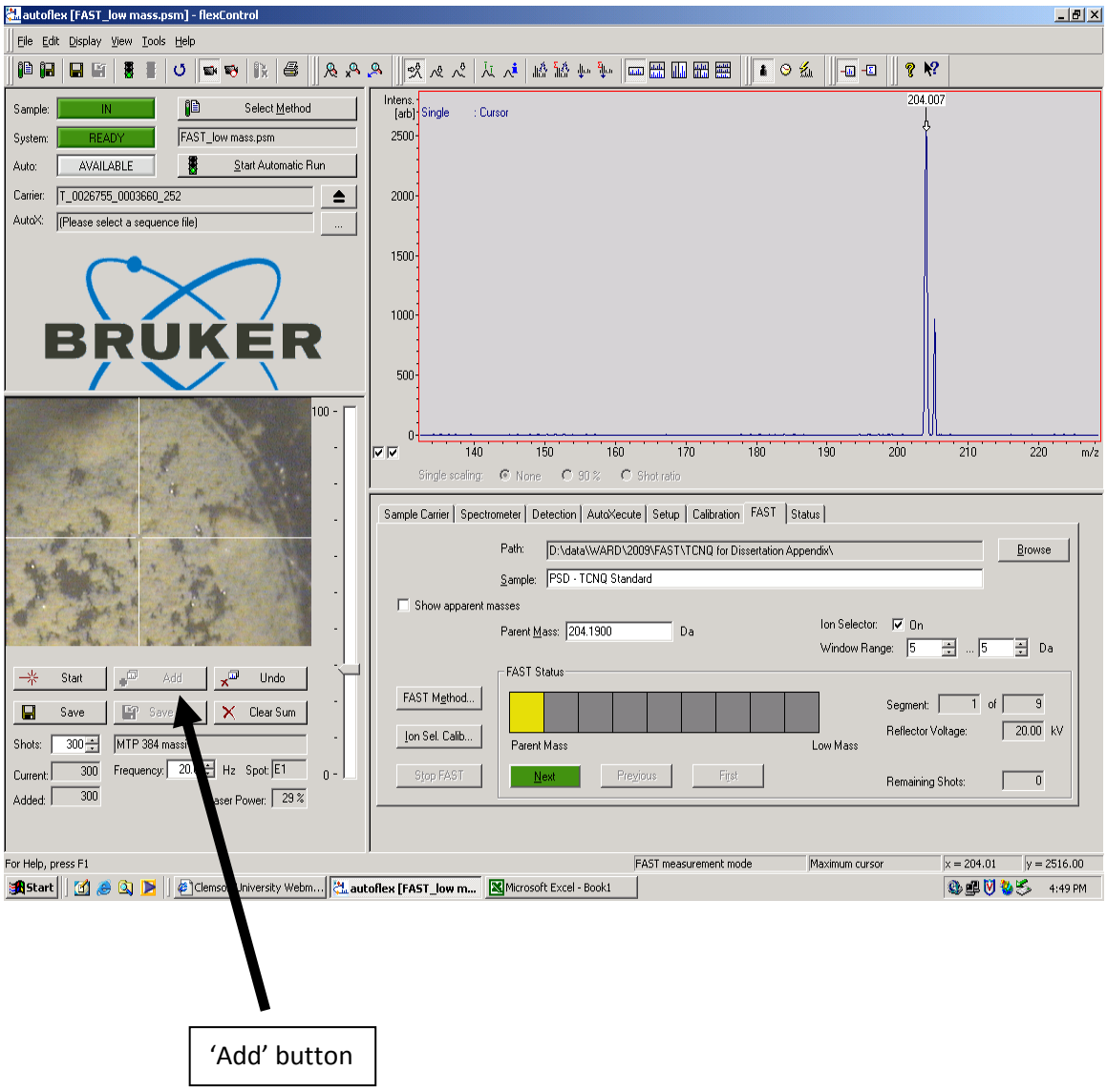

9. Repeat step 8 for the second segment, and all subsequent segments. Note that, in MALDI spectrum for the second segment, a sharp fragment peak is present at 178 Da. This peak was not present at all in the MALDI spectrum for the first segment, illustrating the importance of ion focusing with the optimum reflector voltage.

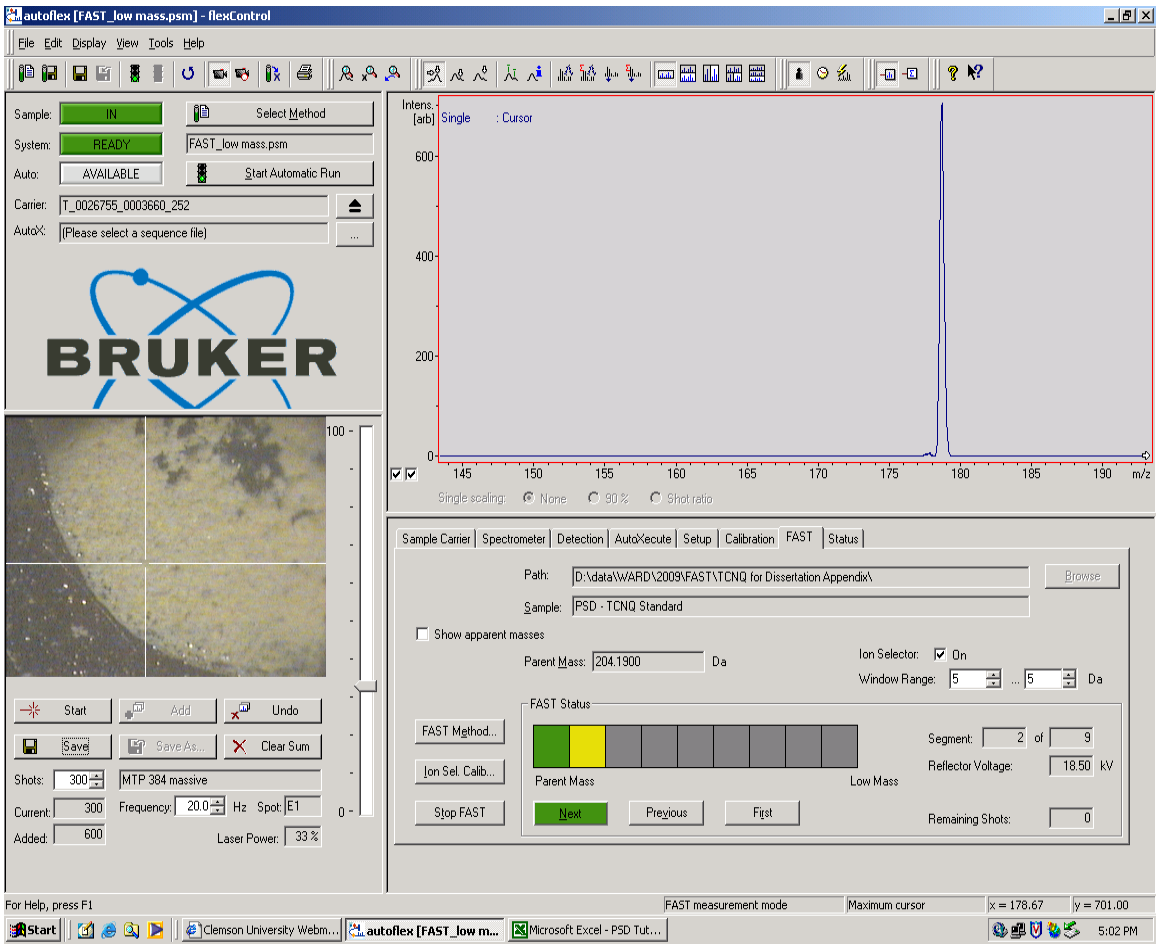

10. Once the last segment spectrum is recorded, open **Flex Analysis** from the Desktop (see desktop illustration on page 7) to view and process the data into a single, composite MALDI spectrum. Open the files containing the desired analysis by following the path shown on page 10. Highlight each individual MALDI spectrum obtained for the sample PSD – TCNQ Standard as shown. Click the **FAST** tab at the top of the screen. A pulldown menu appears. Click on **Paste Segment Spectra** to sum each of the individual MALDI spectra into one, composite MALDI spectrum containing the peaks for the parent TCNQ molecule, as well as those of all of the fragments observed (see below).

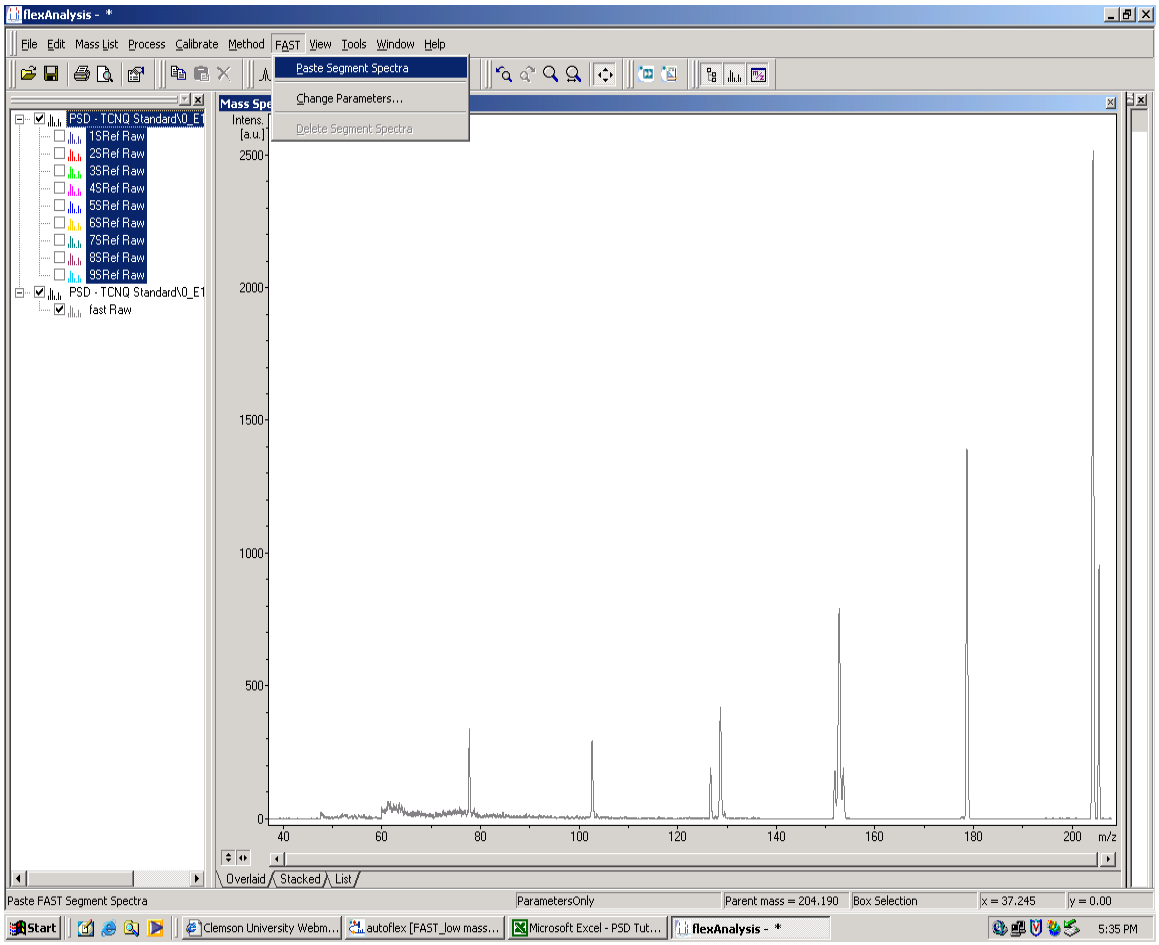

APPENDIX F

OPTIMIZING THE SEGMENT REFLECTOR VOLTAGES FOR PSD

Depending on the fragmentation behavior (that is, the molecular weights, or mol wts, of the ion fragments produced from a particular analyte as a result of laser irradiation) of the species to which the post source decay[1] (PSD) technique is applied, it is necessary to develop suitable operating methods in the FlexControl software which is used to operate the Bruker Daltonics Autoflex mass spectrometer by which matrix-assisted, laser desorption and ionization, time-of-flight mass spectrometric (MALDI-TOF-MS, or MALDI for short) analyses are performed. For M-50 pitch oligomers, this means developing individual, optimized methods to facilitate the PSD analyses of the species comprising a particular oligomer class (that is, monomer, dimer, etc.). For one of these optimized methods, **FAST_M-50_Monomer_051308.psm** (FAST is an abbreviation standing for Fragmentation Analysis and Structural Time-of-Flight Mass Spectrometry; the PSD technique is referred to by this name throughout the FlexControl and FlexAnalysis software programs used to operate the MALDI apparatus and to process the mass spectral data obtained, respectively), used to obtain PSD spectra for species comprising M-50 pitch monomer, the method parameters are shown in Fig. F.1 as they appear on the **FAST Method Editor** screen in the FlexControl software (see page B.10 for instructions on how to get to this screen).

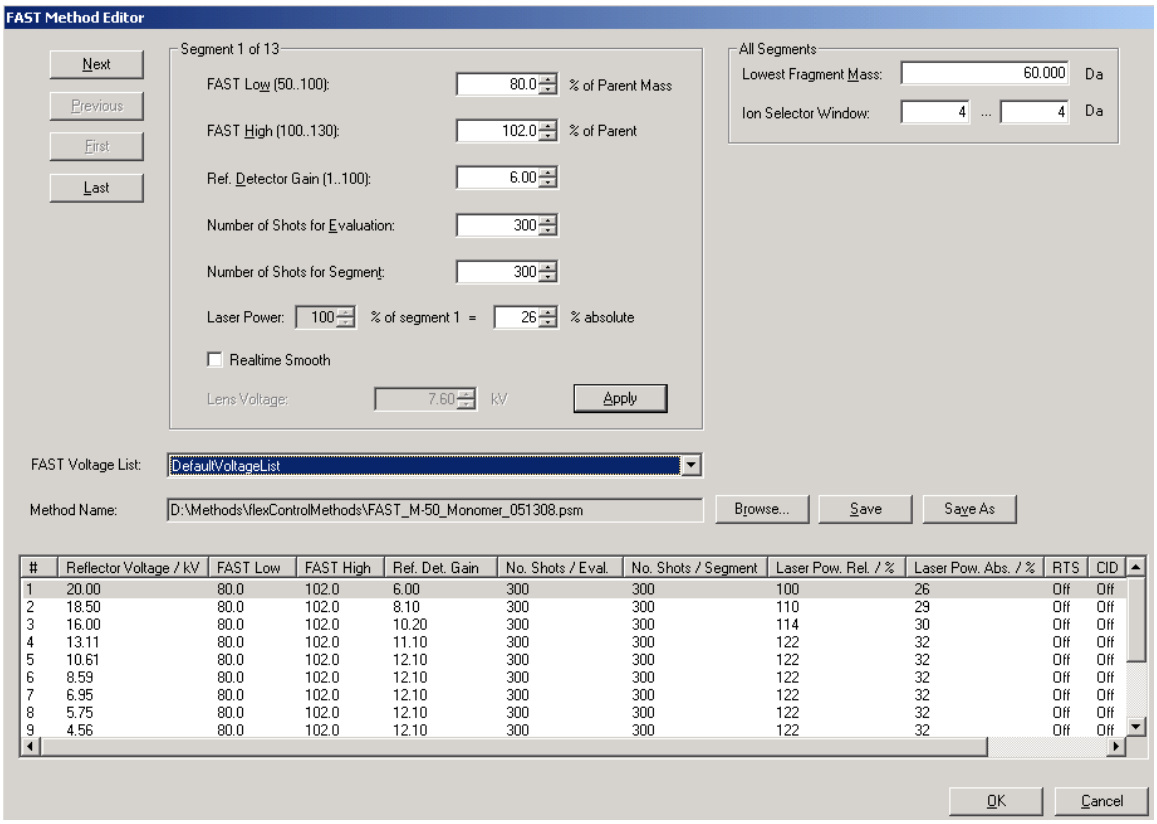

#	Reflector Voltage / kV	FAST Low	FAST High	Ref. Det. Gain	No. Shots / Eval.	No. Shots / Segment	Laser Pow. Rel. / %	Laser Pow. Abs. / %	RTS	CID
1	20.00	80.0	102.0	6.00	300	300	100	26	Off	Off
2	18.50	80.0	102.0	8.10	300	300	110	29	Off	Off
3	16.00	80.0	102.0	10.20	300	300	114	30	Off	Off
4	13.11	80.0	102.0	11.10	300	300	122	32	Off	Off
5	10.61	80.0	102.0	12.10	300	300	122	32	Off	Off
6	8.59	80.0	102.0	12.10	300	300	122	32	Off	Off
7	6.95	80.0	102.0	12.10	300	300	122	32	Off	Off
8	5.75	80.0	102.0	12.10	300	300	122	32	Off	Off
9	4.56	80.0	102.0	12.10	300	300	122	32	Off	Off

Figure F.1. PSD operating parameters for the method **FAST_M-50_Monomer_051308.psm**, optimized for PSD analyses of individual species comprising M-50 monomer.

As specified earlier in Appendix B (the Procedure for Obtaining PSD Spectra section), a PSD spectrum is actually a composite result comprised of several summed MALDI spectra, each obtained at a different ion reflector voltage. Typically, the reflector voltage utilized in the collection of the MALDI spectrum for Segment 1 is the same as that used for the acquisition of a MALDI spectrum in reflectron mode (for the Bruker Autoflex model, when operating in reflectron mode, that value is 20.00 kV). For Segment 1 of the method **FAST_M-50_Monomer_051308.psm**, the values **FAST Low** and **FAST High** denote percentages of the parent ion molecular weight. Thus, for a

parent ion with a mol wt of 230.3 Da (its PSD spectrum, including details concerning the acquisition thereof, is given elsewhere[2]), a **FAST Low** value of 80.0 corresponds to an m/z value of 0.80*230.3 = 184.2. Similarly, a **FAST High** value of 102.0 corresponds to m/z = 1.02*230.3 = 234.8. Such manipulation of these values sets the mol wt range of the MALDI spectrum for Segment 1 of the composite PSD spectrum for the M-50 monomeric species of 230.3 Da (as confirmed in Fig. F.2 below). Fragment ions with m/z ratios falling below the mol wt corresponding to **FAST Low** are very unlikely to be detected (even if they are, the peaks are poorly resolved[1]) because such ions have too little kinetic energy to sufficiently penetrate the grid of a reflector charged to 20.00 kV so as to be accurately reflected to and focused on the detector in detectable quantities.

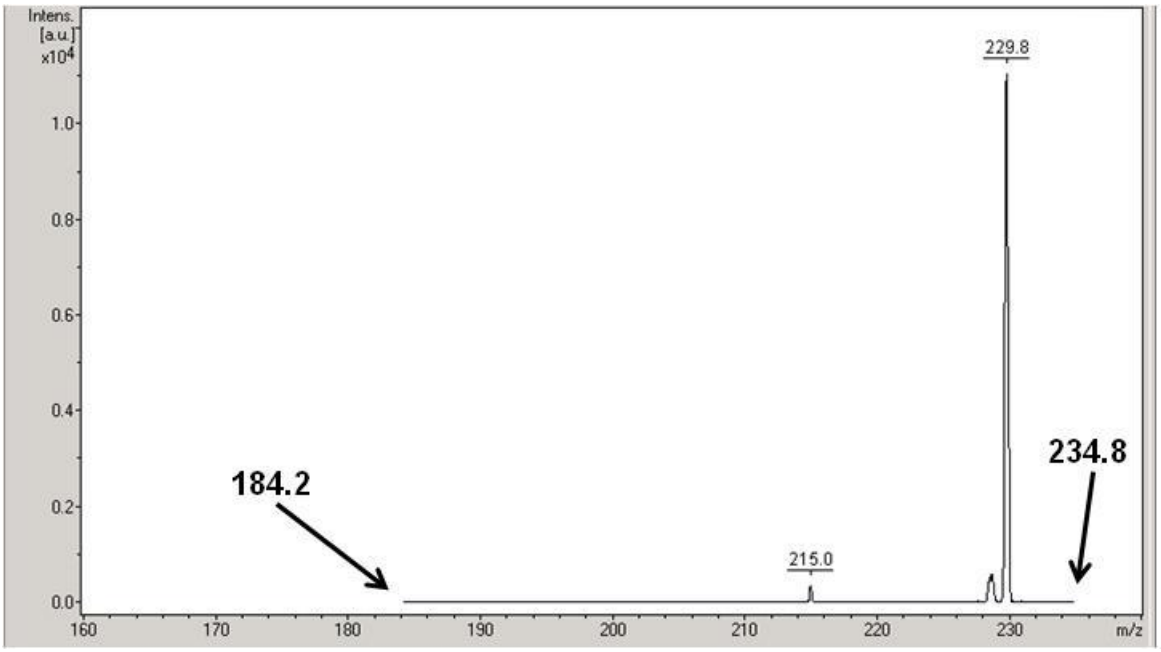

Figure F.2. MALDI spectrum for Segment 1 of the composite PSD spectrum for an M-50 monomeric species of mol wt 230.3 Da, obtained using the MALDI operating method **FAST_M-50_Monomer_051308.psm**.

This concept also applies to weak fragment peaks detected; in the PSD spectrum for Segment 1 shown in Fig. F.2, there is a peak at m/z = 215.0 indicating the presence of a de-methylated species, which is very weak in relation to the parent peak at m/z = 229.8. In Segment 1, this fragment had insufficient kinetic energy to penetrate the reflectron to the optimum depth (as shown in Fig. F.3, this means the incoming ion must stop just short of fully penetrating the reflectron voltage grid before being reflected) and thus a weak response was observed. In order to maximize the height of the peak at m/z = 215.0, it is necessary to optimize the focus of such ions on the detector. By recording an additional, second segment MALDI spectrum (see Fig. F.4), the peak height can be increased considerably through a slight reduction of the reflector voltage (note that while the reflector voltage is the most important parameter to optimize, it is typically also necessary to optimize laser power and detector gain, as indicated in Fig. F.1).

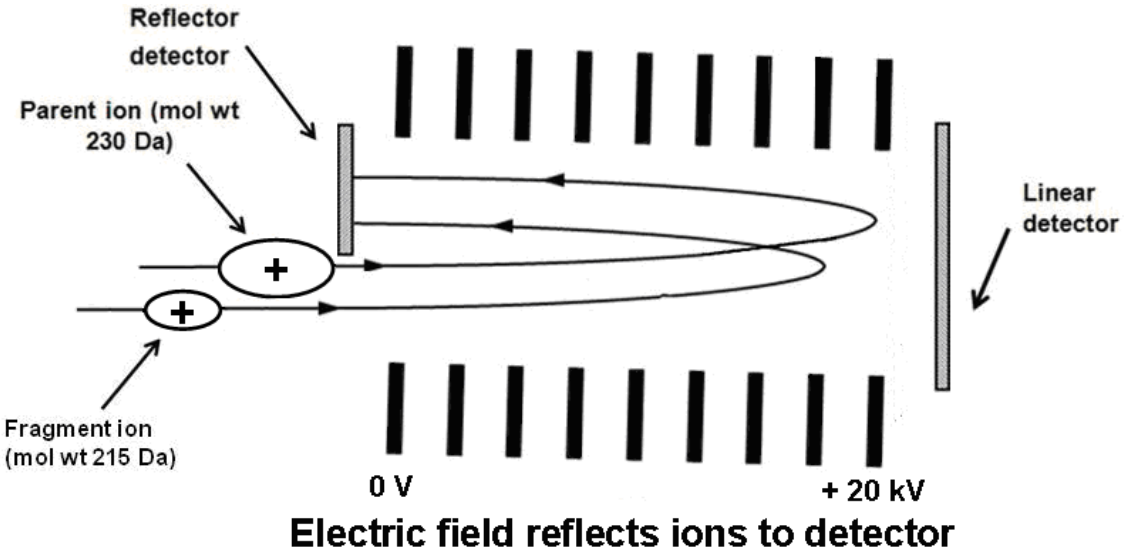

Figure F.3. An almost complete penetration of the reflectron voltage grid, so that the reflecting voltage is just strong enough to redirect the incoming ion to the detector, is desired. For the parent ion, a reflectron voltage of 20 kV is necessary to achieve this condition. The fragment ion of mol wt 215 Da does not penetrate the reflectron as deeply as the parent ion in Segment 1, and so is not as well focused on the detector.

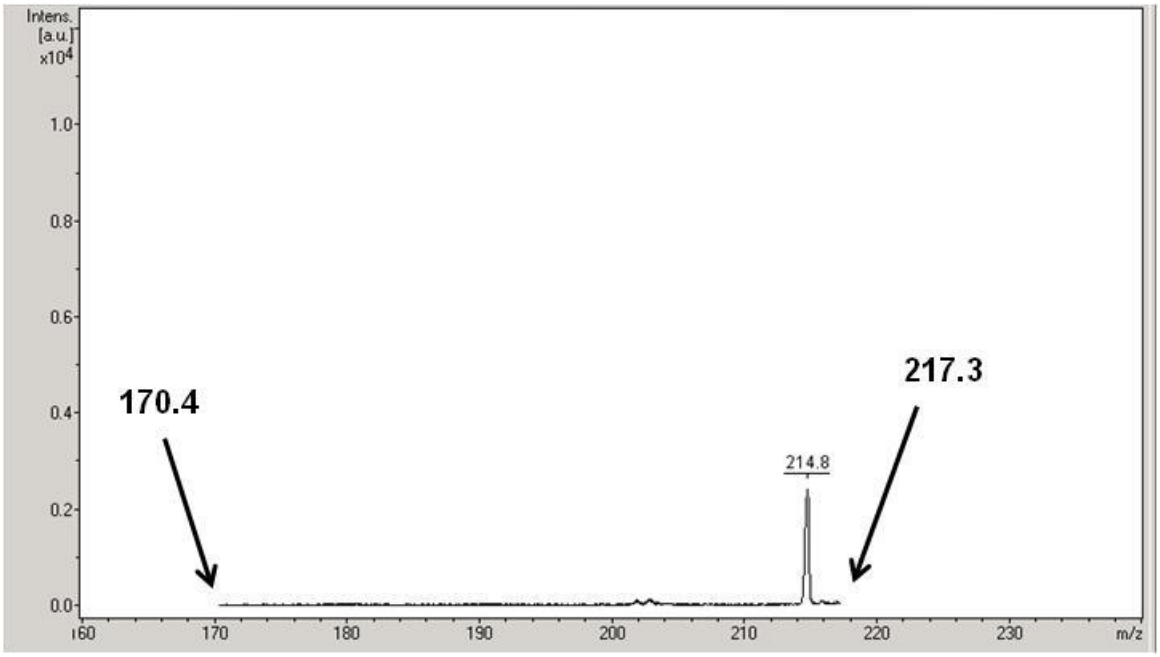

Figure F.4. MALDI spectrum for Segment 2 of the composite PSD spectrum for an M-50 monomeric species of mol wt 230.3 Da, obtained using the MALDI operating method **FAST_M-50_Monomer_051308.psm**.

For segment 2 (and any subsequent segments that comprise a PSD spectrum), **FAST High** and **FAST Low** do not denote a percentage of the actual parent ion molecular weight. Rather, they represent a percentage of the mol wt of the ion that penetrates the reflectron to the ideal depth (in Segment 1, this ion was the parent ion of mol wt 230 Da). In order to preferentially focus the fragment of mol wt 214.8 Da on the detector, it is necessary to examine the relationship between the kinetic energy of the incoming ion and the reflectron voltage necessary in order to optimize the detector response for a particular ion. The initial ion kinetic energy is 19 keV, which is equal to the charge on an ion containing one positive charge multiplied by the accelerating voltage (19.00 kV in our MALDI operating methods which utilize reflectron mode). Because bond energies are more than three orders of magnitude smaller, the metastable ion

fragmentation process can be approximated as elastic, having no noticeable effect on ion velocities. That is, the sum of the kinetic energies of the fragment ions is equal to that of the parent ion prior to fragmentation. Thus, the fragments remain traveling at the same velocity as their parent ion, so that all ions arising from a particular species (such as dimethylpyrene) reach the reflectron at the same time as un-fragmented parent ions of that particular species (dimethylpyrene).

As kinetic energy = ½*ion mass*ion velocity^2, the ion fragment of mol wt 215 Da possesses less kinetic energy than the parent ion of mol wt 230 Da. Therefore, in segment 1, the fragment ion does not penetrate the reflectron to the optimum depth. For Segment 2, it is necessary to lower the reflectron voltage so that the fragment ion can satisfy this condition. The ratio of the reflectron voltages $V_{R,1}$ and $V_{R,j}$ utilized in segments 1 and j should be equal to the ratio of the kinetic energies KE_{parent} and $KE_{fragment}$ of the parent ion, and a particular fragment ion (see Equation F.1). Therefore,

$$\frac{KE_{parent}}{KE_{fragment}} = \frac{V_{R,1}}{V_{R,j}} \qquad \text{(F.1)}$$

Because the velocities v_{parent} and $v_{fragment}$ of the incoming parent and fragment ions are equal, Equation F.1 simplifies to

$$\frac{KE_{parent}}{KE_{fragment}} = \frac{\frac{1}{2} m_{parent} v_{parent}^2}{\frac{1}{2} m_{fragment} v_{fragment}^2} = \frac{m_{parent}}{m_{fragment}} = \frac{V_{R,1}}{V_{R,j}} \qquad \text{(F.2)}$$

By rearranging Equation F.2, it can be shown that in Segment j, the mol wt $m_{fragment}$ of the fragment ion that penetrates the reflectron to the optimum distance (corresponding to 100.0 on the scale between **FAST Low** and **FAST High**) is a function of the reflectron voltages $V_{R,1}$ and $V_{R,j}$ utilized in segments 1 and j, and m_{parent}, the mass of the parent ion.

$$m_{fragment} = \frac{V_{R,j}}{V_{R,1}} m_{parent} \tag{F.3}$$

For Segment 2, when the reflectron voltage is stepped down to 18.50 kV,

$$m_{fragment} = \frac{18.50kV}{20.00kV} 230.3Da = 213.0Da \tag{F.4}$$

Thus, for segment 2, 213.0 Da is mass of the ion fragment that penetrates the reflectron to the optimum distance. At a reflectron voltage of 18.50 kV, the incoming fragment ion has a mol wt (215 Da) less than 1% greater than this value, so it would penetrate the reflectron to approximately the same depth (see Fig. F.5). This minimal difference has no adverse effects on the MALDI response for the fragment, as the peak at m/z = 214.8 in the MALDI spectrum for Segment 2 (see Fig. F.4) is considerably stronger than it is in that for Segment 1 (see Fig. F.2).

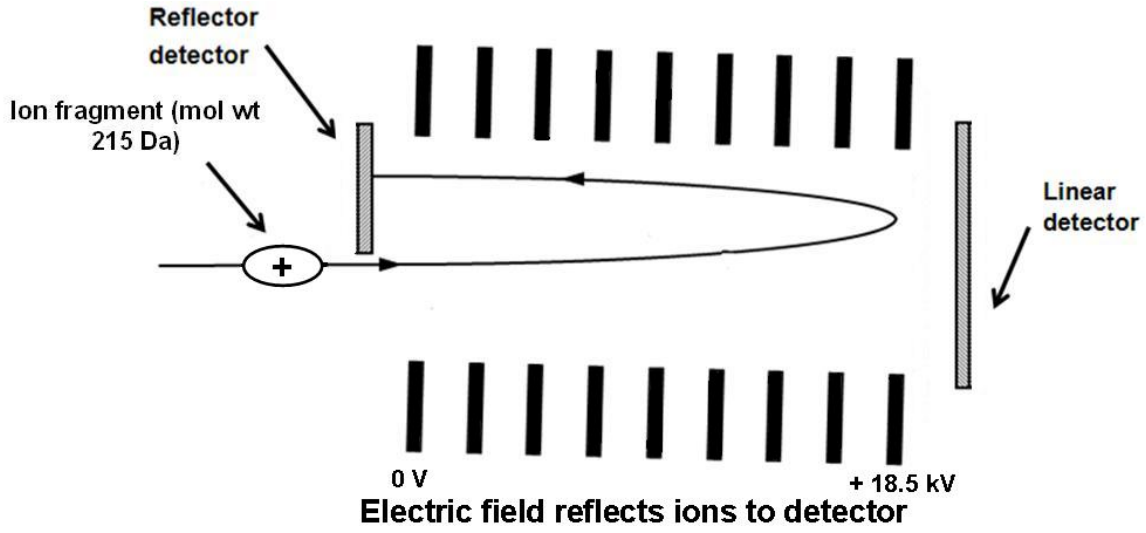

Figure F.5. For the fragment ion (mol wt 215 Da) arising from the parent ion of mol wt 230 Da, a reflectron voltage of 18.5 kV is sufficient to focus it on the detector.

For Segment 2, the m/z value corresponding to **FAST Low** is equal to $(0.80)*m_2$ = 0.80*213.0 = 170.4; similarly, the m/z value corresponding to **FAST High** is determined to be 1.02*213.0 = 217.3 (as confirmed in Fig. F.4).

PSD Spectra for M-50 Dimer Constituents

A key facet of the work presented in Chapter 6 of this dissertation was the collection of PSD spectra for major constituents of M-50 dimer. The **FAST Method Editor** screen indicating the method parameters for the method **FAST_M-50_Dimer_030910.psm** is shown in Fig. F.6. Note that the reflector voltages for segments 2 and 3 are greater than those given for the optimized method **FAST_M-50_Monomer_051308.psm**, developed specifically to obtain PSD spectra for the species comprising M-50 monomer. The reason for these changes is discussed in the following paragraphs.

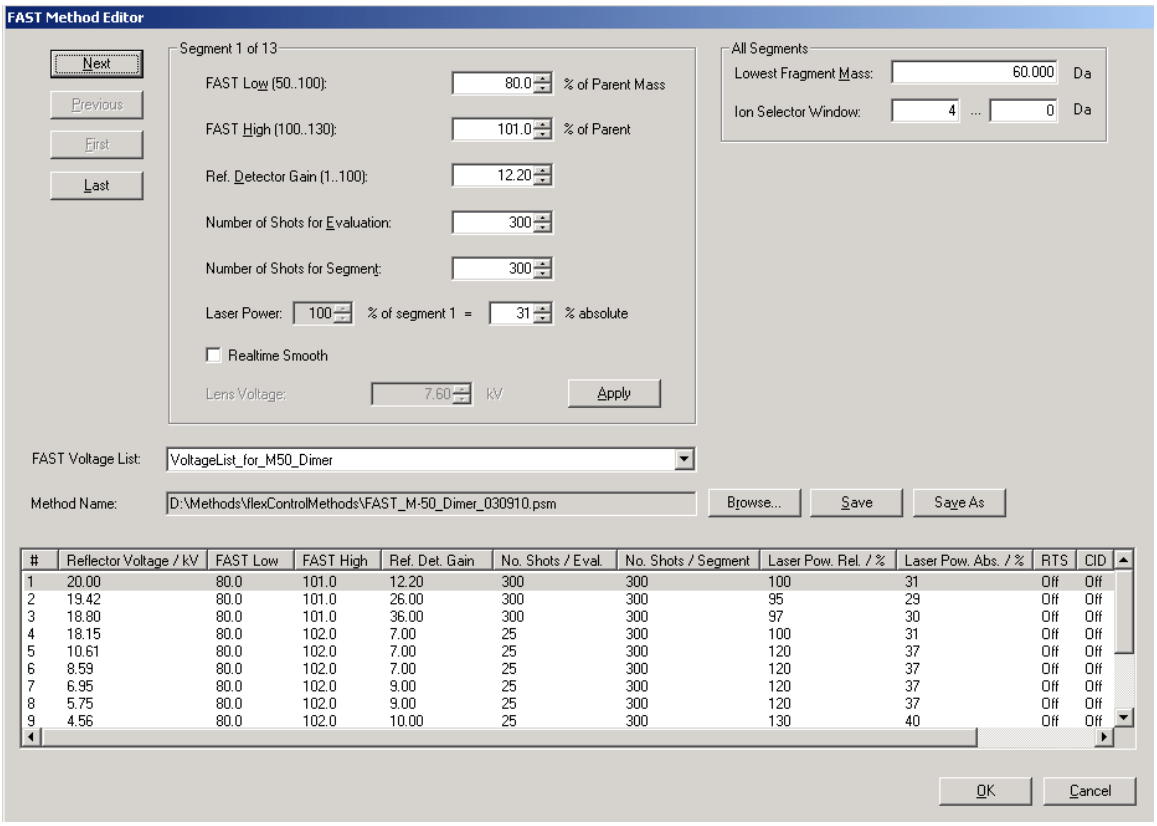

#	Reflector Voltage / kV	FAST Low	FAST High	Ref. Det. Gain	No. Shots / Eval.	No. Shots / Segment	Laser Pow. Rel. / %	Laser Pow. Abs. / %	RTS	CID
1	20.00	80.0	101.0	12.20	300	300	100	31	Off	Off
2	19.42	80.0	101.0	26.00	300	300	95	29	Off	Off
3	18.80	80.0	101.0	36.00	300	300	97	30	Off	Off
4	18.15	80.0	102.0	7.00	25	300	100	31	Off	Off
5	10.61	80.0	102.0	7.00	25	300	120	37	Off	Off
6	8.59	80.0	102.0	7.00	25	300	120	37	Off	Off
7	6.95	80.0	102.0	9.00	25	300	120	37	Off	Off
8	5.75	80.0	102.0	9.00	25	300	120	37	Off	Off
9	4.56	80.0	102.0	10.00	25	300	130	40	Off	Off

Figure F.6. PSD operating parameters for the method **FAST_M-50_Dimer_030910.psm**, optimized for PSD analyses of individual species comprising M-50 dimer.

Based on the molecular structures for the major monomeric structures presented in Chapter 4 of this dissertation, and the appearance of the PSD spectra associated with these species, the most prominent fragment peaks were expected to indicate the loss of a methyl group – that is, with the fragment peak being located at m/z of 15 less than that of the parent species. For a parent species of mol wt 446.7 Da (the PSD spectrum of which is given in Fig. 10k of Chapter 6), the fragment mol wt would be 431.7 Da. Rearranging Equation F.3 (setting j = 2), an expression can be obtained for the minimum second-segment reflector voltage $V_{R,2}$ that will allow for the accurate reflection of the fragment

ion ($m_{fragment}$ = 431.7 Da) to the detector (see Equation F.5). This minimum reflector voltage, 19.33 kV, is significantly greater than the 18.50 kV used in the second segment of the PSD spectra obtained using the FAST method **FAST_M-50_Monomer_051308.psm** developed to obtain PSD spectra for monomeric M-50 pitch species of lower mol wts.

$$V_{R,j} = V_{R,2} = \frac{m_{fragment}}{m_{parent}} V_{R,1} = \frac{431.7 Da}{446.7 Da} * 20.00 kV = 19.33 kV \quad \text{(F.5)}$$

Because the value of the minimum second-segment reflector voltage necessary to detect a de-methylated fragment increases with respect to mol wt of the parent species, a second-segment reflector voltage of 19.42 kV was chosen for the method **FAST_M-50_Dimer_030910.psm**, which was designed for the whole molecular weight range of the M-50 dimer species analyzed in Chapter 6. Such care in setting the second-segment reflector voltage is necessary in obtaining PSD spectra for methylated dimers because, as was the case with the monomeric species, the peak indicating the presence of the de-methylated species is either very weak or not present at all in the PSD spectrum for the first segment of the composite PSD spectrum for the dimeric species of mol wt 446.7 Da (see Fig. F.7). Meanwhile, the PSD spectrum for the second segment confirms the reliability of the method just presented for determining the necessary reflector voltage to use in the second segment (see Fig. F.8), resulting in the observation of a well-defined peak indicating the presence of a de-methylated fragment ion of m/z = 431.5.

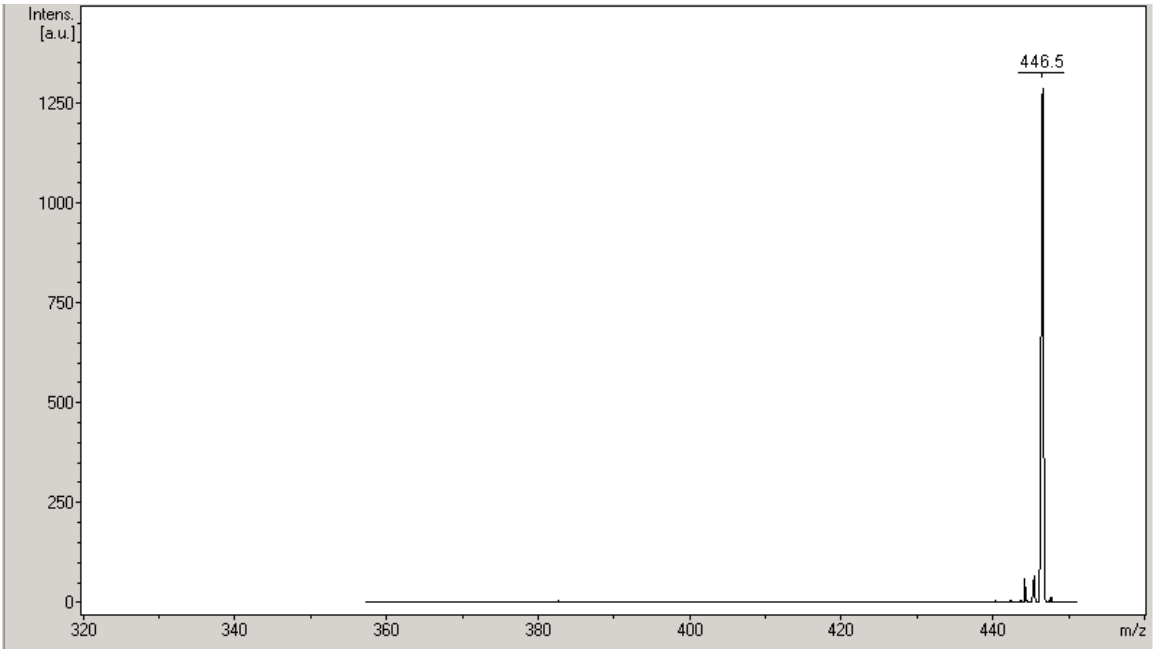

Figure F.7. MALDI spectrum for Segment 1 of the composite PSD spectrum for an M-50 dimeric species of mol wt 446.7 Da, obtained using the MALDI operating method **FAST_M-50_Dimer_030910.psm**.

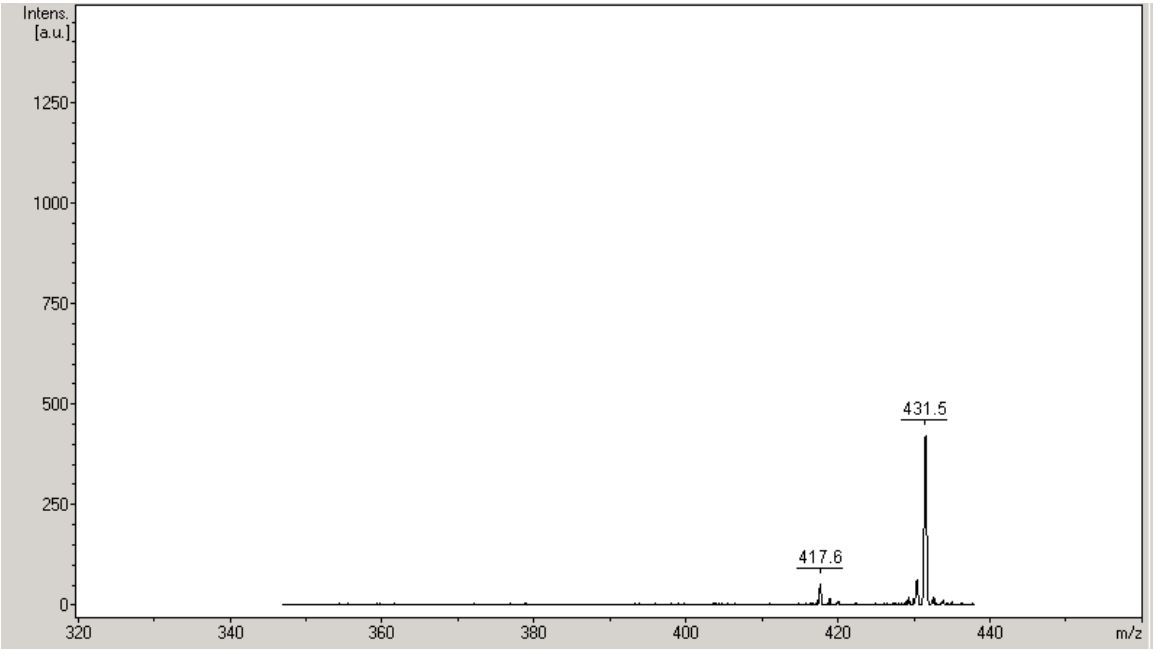

Figure F.8. MALDI spectrum for Segment 2 of the composite PSD spectrum for an M-50 dimeric species of mol wt 446.7 Da, obtained using the MALDI operating method **FAST_M-50_Dimer_030910.psm**.

The peak at m/z = 417.6 in Fig. F.8, which indicates the presence of a de-ethylated fragment ion, is very weak. Its response was increased considerably by optimizing the reflector voltage utilized in obtaining the PSD spectrum for a third segment of this composite PSD spectrum. Using the same method as we did for the second segment of this PSD spectrum, we calculated $V_{R,3}$ (see Equation F.6), the third-segment reflector voltage necessary to preferentially focus this ion on the detector (again, this would be the voltage such that a value of 100.0 on the scale of **FAST Low** to **FAST High** would correspond to a fragment ion of m/z = 417.7 Da).

$$V_{R,j} = V_{R,3} = \frac{m_3}{m_{parent}} V_{R,1} = \frac{417.7 Da}{446.7 Da} * 20.00 kV = 18.70 kV \qquad \text{(F.6)}$$

The use of a reflector voltage of 18.80 kV results in the collection of the third-segment PSD spectrum that is shown in Fig. F.9. Note that the strength of the de-ethylated ion peak is significantly enhanced compared to the strength of the same peak in the PSD spectrum for the second segment, given in Fig. F.8.

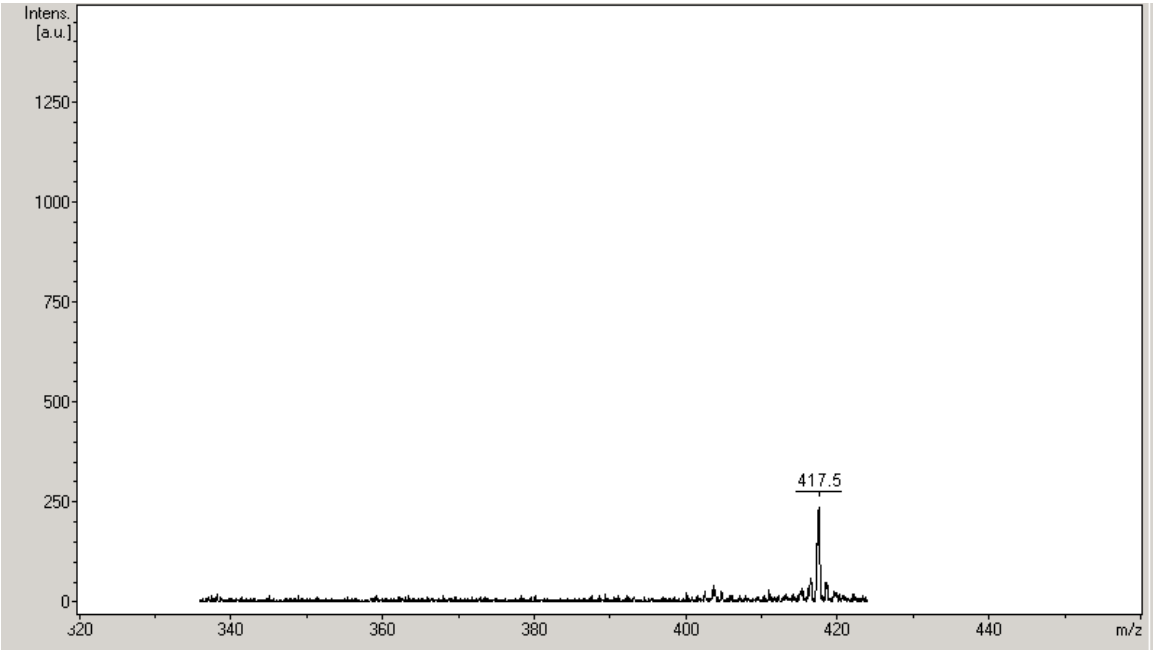

Figure F.9. MALDI spectrum for Segment 3 of the composite PSD spectrum for an M-50 dimeric species of mol wt 446.7 Da, obtained using the MALDI operating method **FAST_M-50_Dimer_030910.psm**.

References

[1]Cotter, R. J. Time-of-Flight Mass Spectrometry: Instrumentation and Applications in Biological Research. American Chemical Society, Washington, DC, 1997, pp. 175-181, 191.

[2]Cristadoro, A.; Kulkarni, S. U.; Burgess, W. A.; Cervo, E. G.; Räder, H. J.; Müllen, K.; Bruce, D. A.; Thies, M. C. Structural Characterization of the Oligomeric Constituents of Petroleum Pitches. *Carbon* **2009**, *47*, 2358-2370.

APPENDIX G

A REFERENCE FOR INTERPRETING POST-SOURCE DECAY (PSD) SPECTRA FOR PITCH CONSTITUENTS

Reference mass spectra for fully aromatic PAHs (such as anthracene), are presented, along with those for species possessing naphthenic content (such as 9,10-dihydroanthracene). At the end of this section, these spectra are used to interpret the PSD spectra for various components of anthracene pitch, in order to determine whether or not said components possess naphthenic content.

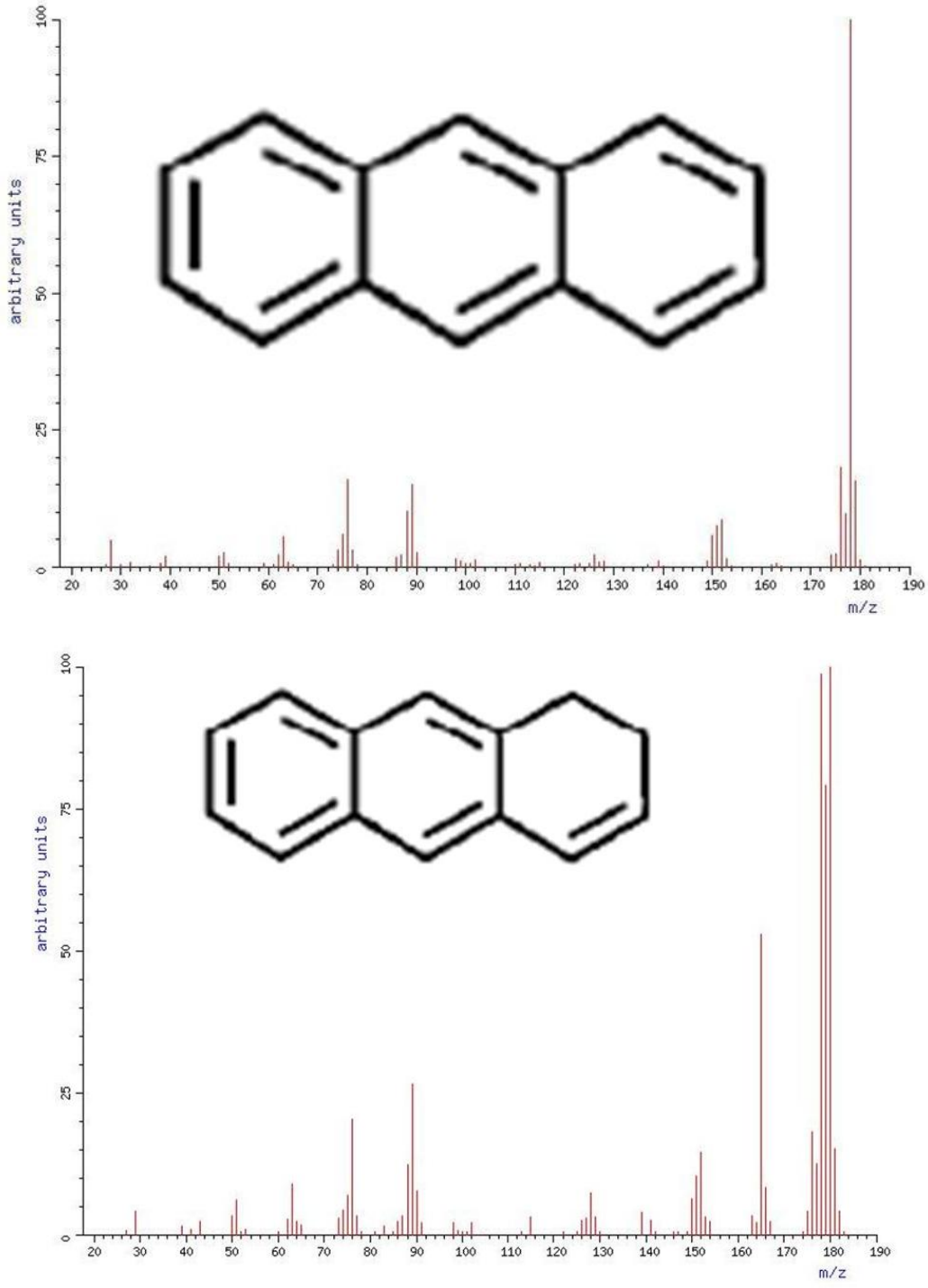

Figure G.1. Electron ionization (EI) mass spectra for anthracene[1] (top) and 1,2-dihydroanthracene[2] (bottom). Reprinted with the permission of the American Chemical Society. Copyright 2010 American Chemical Society (ACS). All rights reserved. For Figs. G.1-G.9, superimposed molecular structures have been generated by the author.

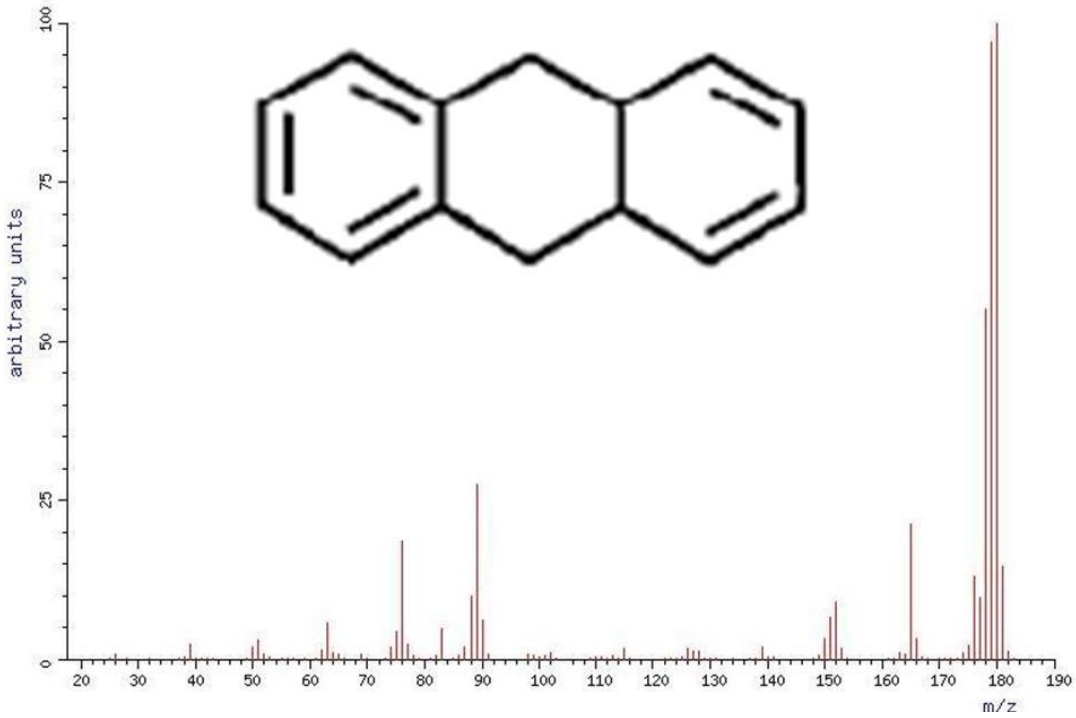

Figure G.2. EI mass spectrum for 9,10-dihydroanthracene.[3] Reprinted with the permission of the American Chemical Society.

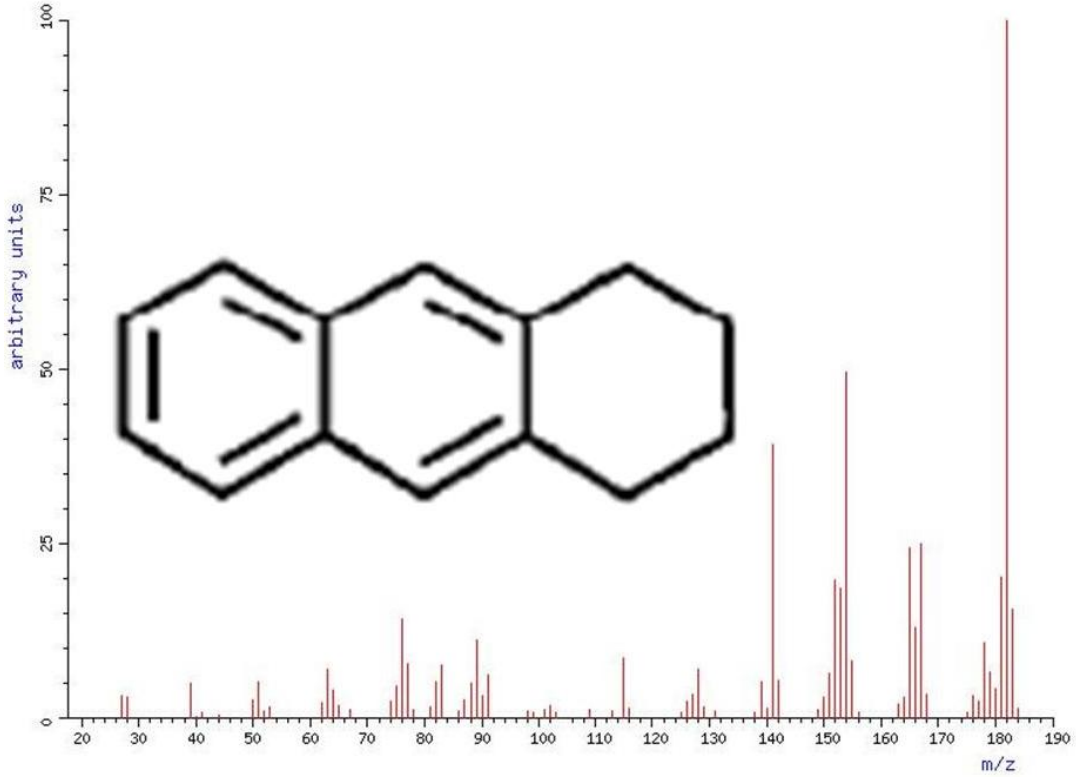

Figure G.3. EI mass spectrum for 1,2,3,4-tetrahydroanthracene.[4] Reprinted with the permission of the American Chemical Society. Copyright 2010 American Chemical Society (ACS). All rights reserved.

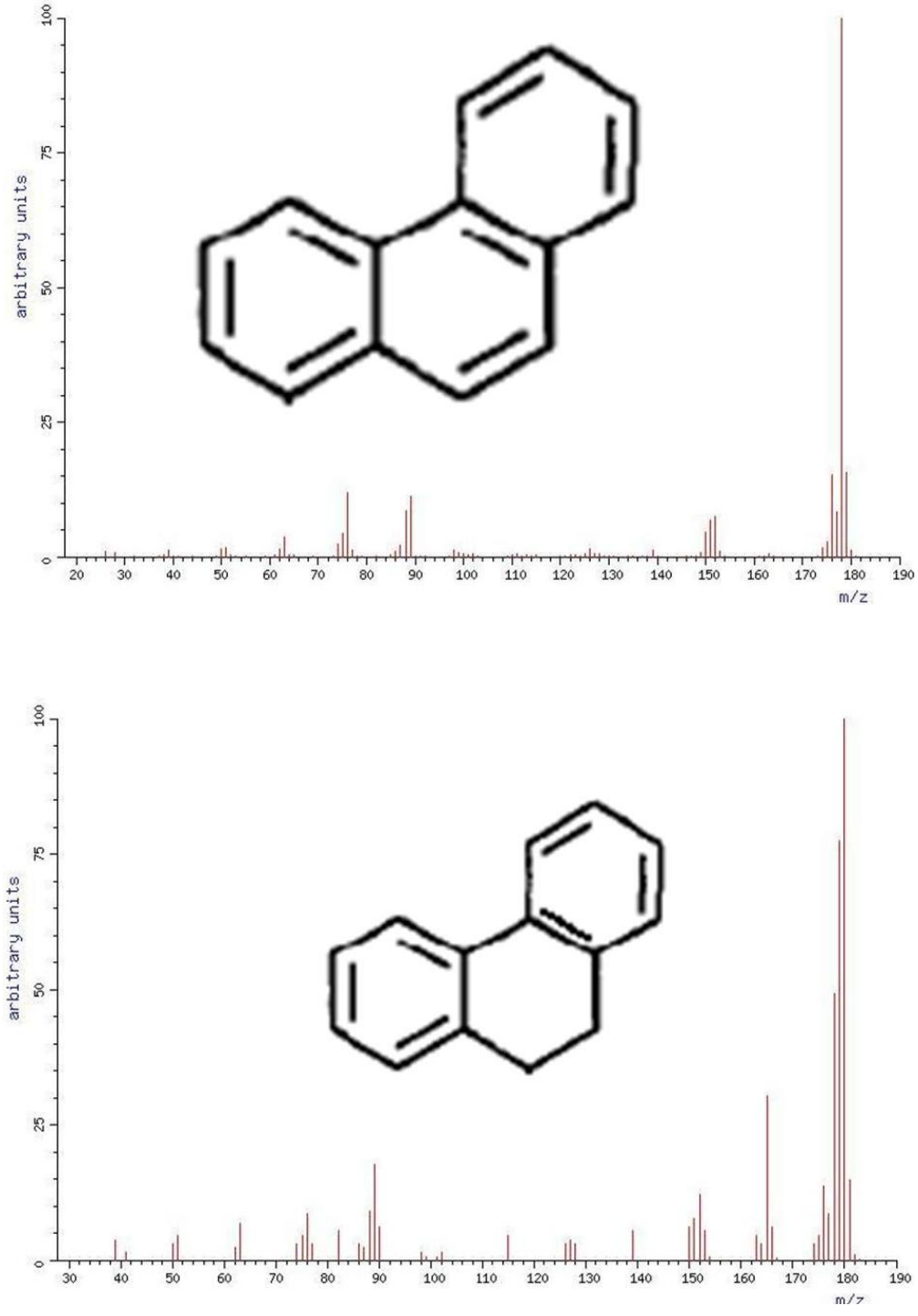

Figure G.4. EI mass spectra for phenanthrene[5] (top) and 9,10-dihydrophenanthrene[6] (bottom). Reprinted with the permission of the American Chemical Society. Copyright 2010 American Chemical Society (ACS). All rights reserved.

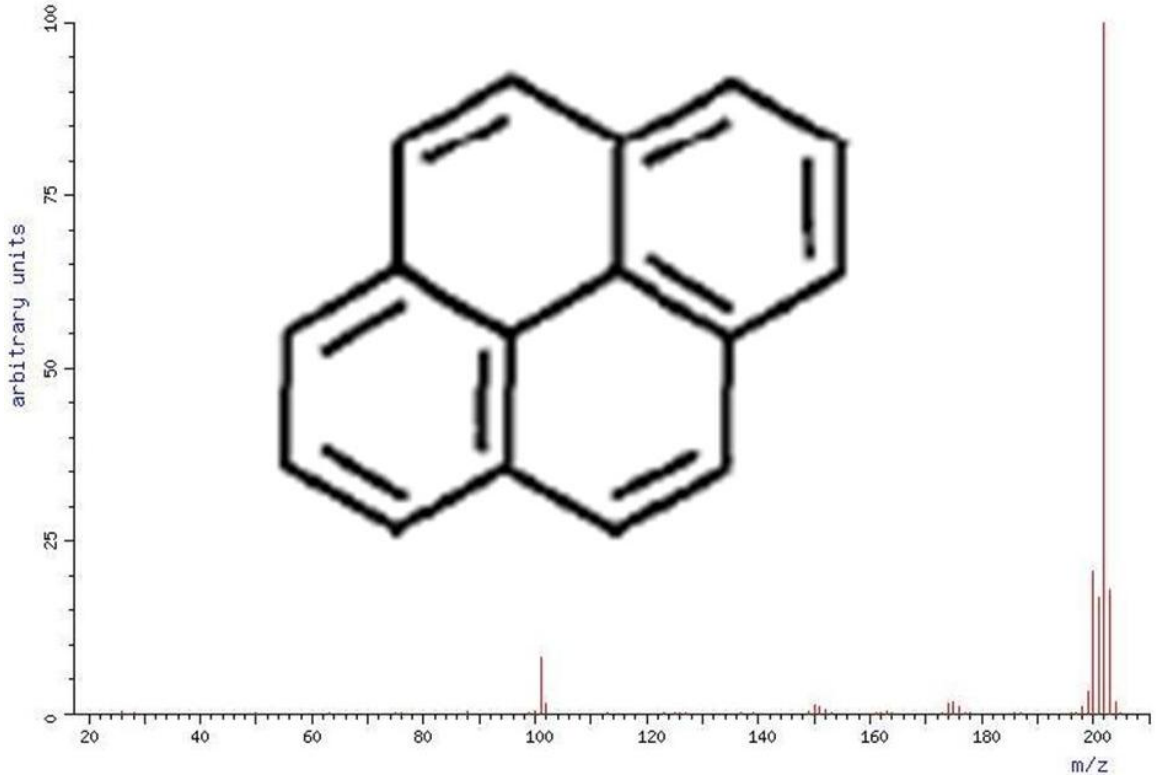

Figure G.5. EI mass spectrum for pyrene.[7] Reprinted with the permission of the American Chemical Society. Copyright 2010 American Chemical Society (ACS). All rights reserved.

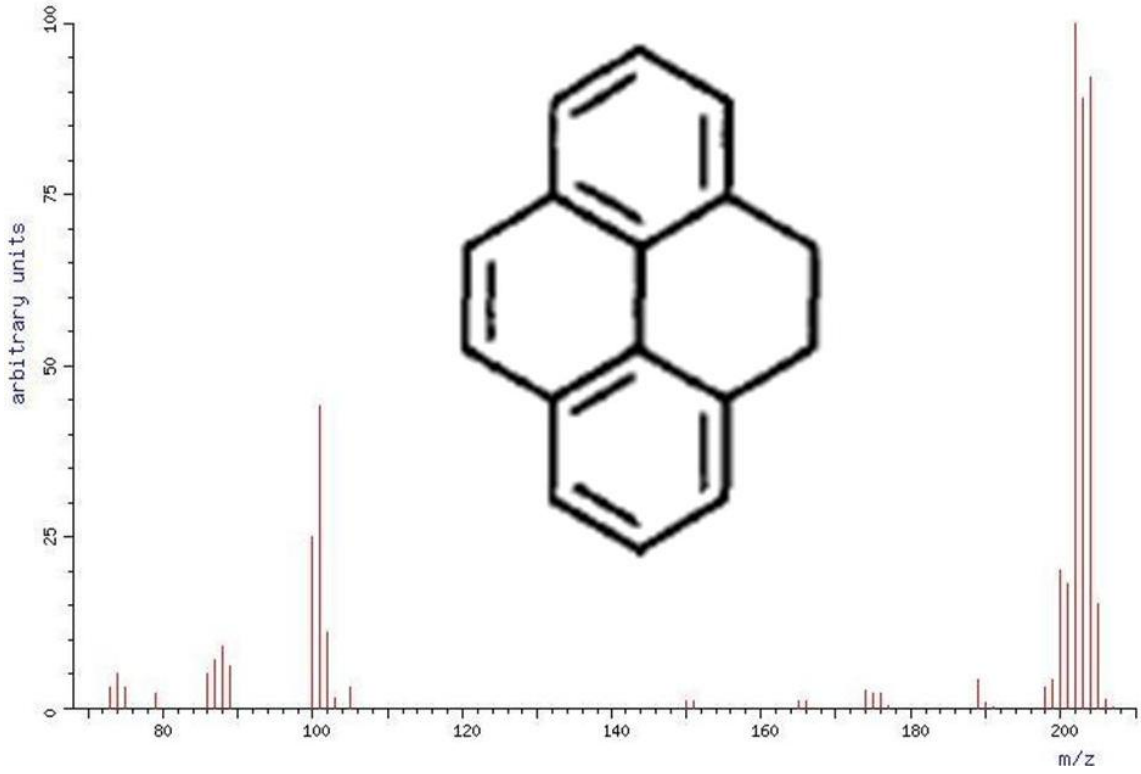

Figure G.6. EI mass spectrum for 4,5-dihydropyrene.[8] Reprinted with the permission of the American Chemical Society. Copyright 2010 American Chemical Society (ACS). All rights reserved.

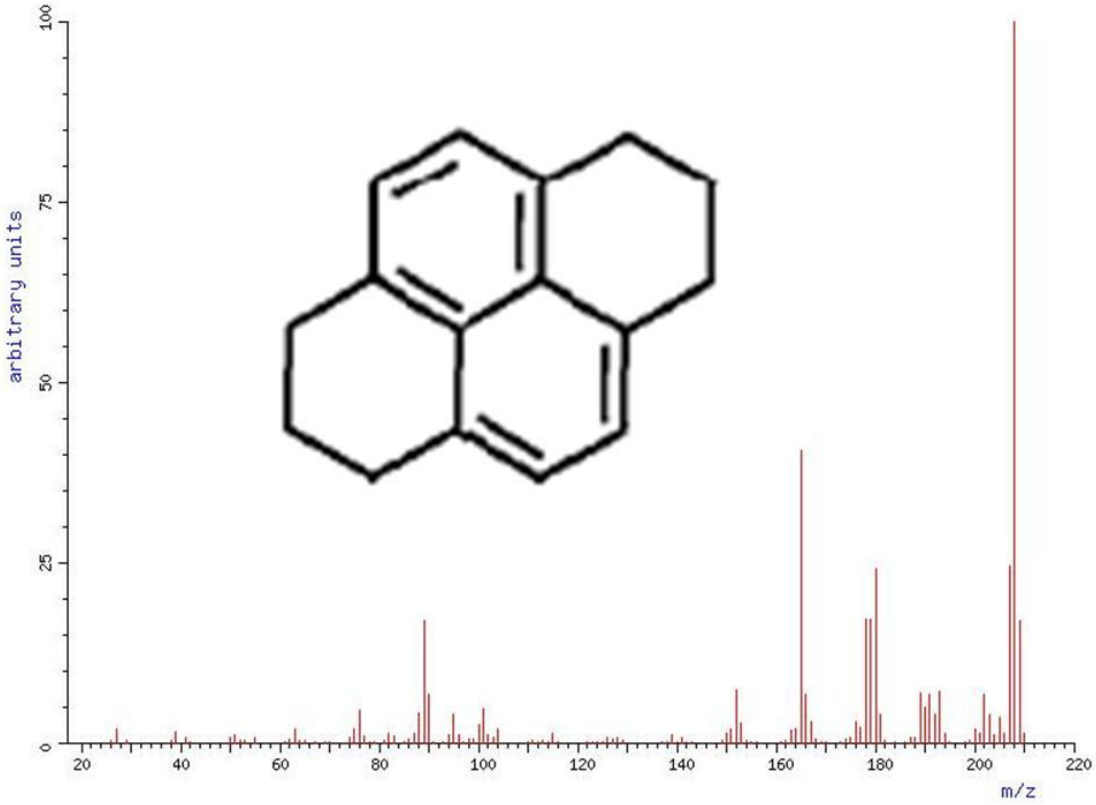

Figure G.7. EI mass spectrum for 1,2,3,6,7,8-hexahydropyrene.[9] Reprinted with the permission of the American Chemical Society. Copyright 2010 American Chemical Society (ACS). All rights reserved.

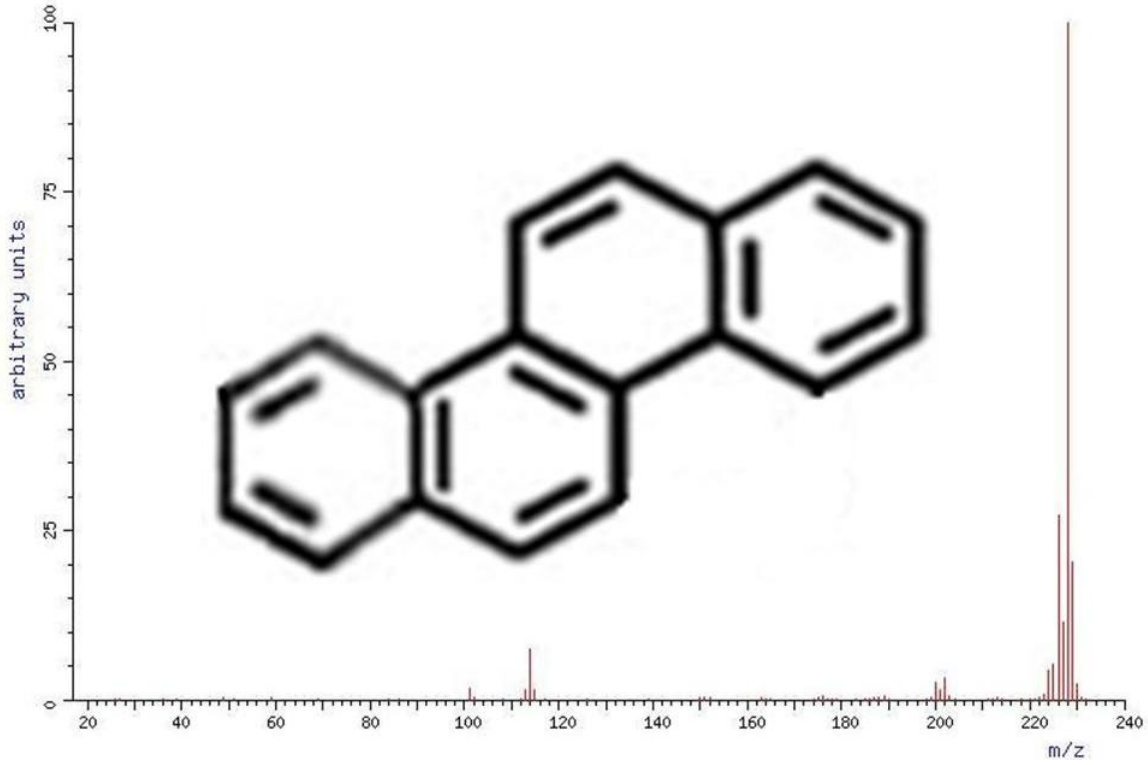

Figure G.8. EI mass spectrum for chrysene.[10] Reprinted with the permission of the American Chemical Society. Copyright 2010 American Chemical Society (ACS). All rights reserved.

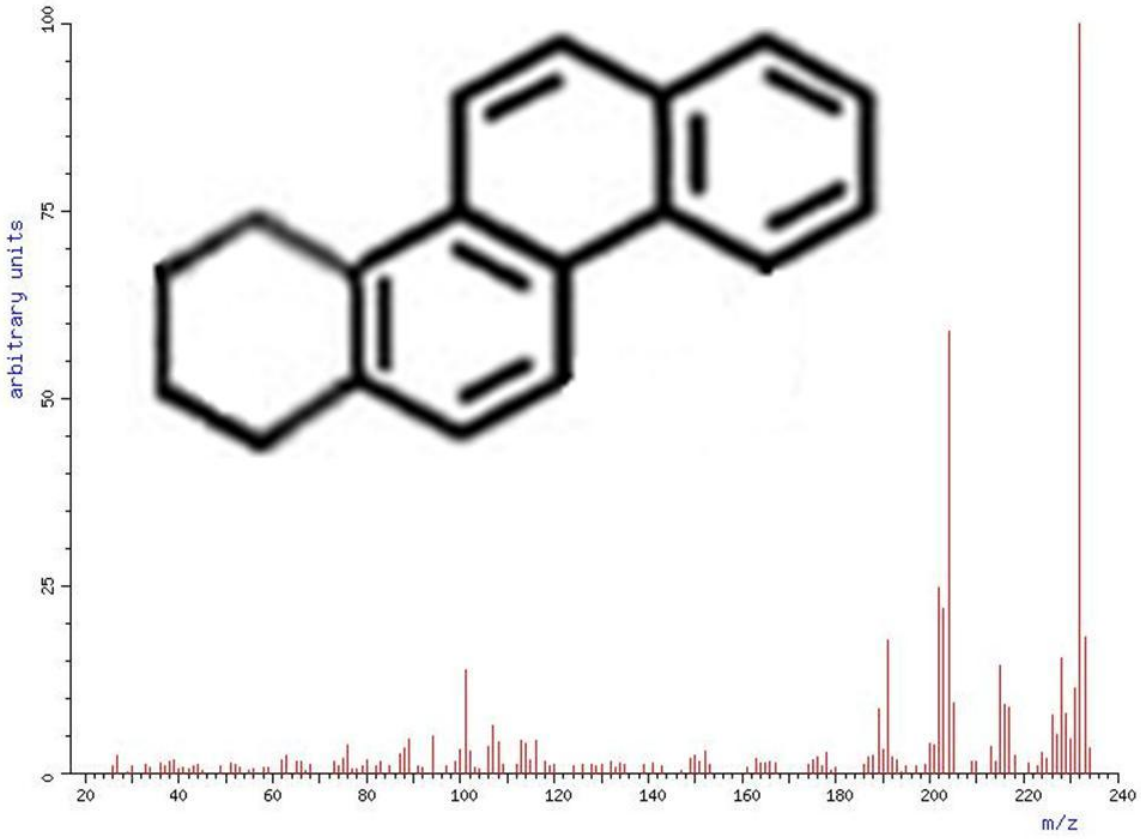

Figure G.9. EI mass spectrum for 1,2,3,4-tetrahydrochrysene.[11] Reprinted with the permission of the American Chemical Society. Copyright 2010 American Chemical Society (ACS). All rights reserved.

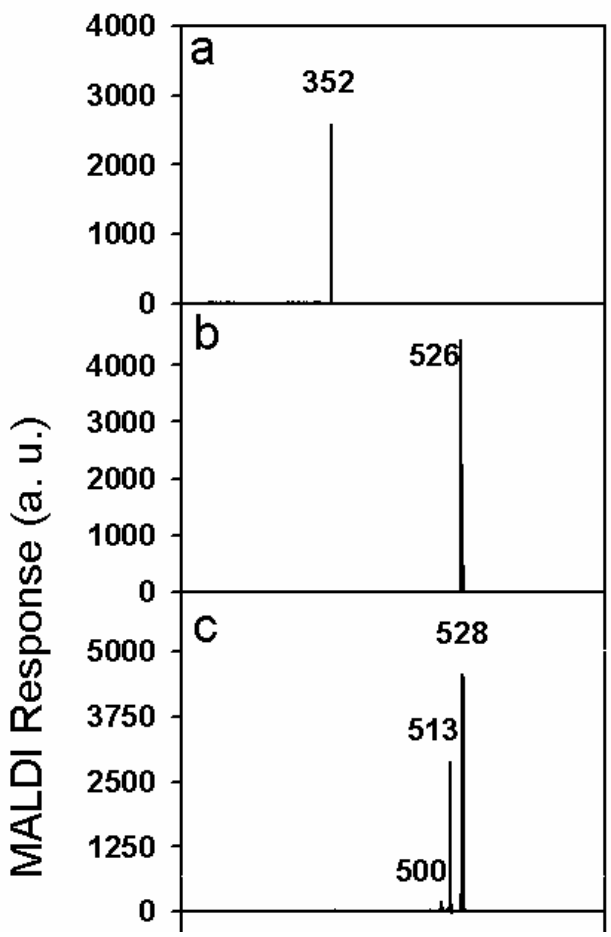

Figure G.10. PSD spectra for selected constituents of anthracene pitch.

Based on a comparison of the above PSD spectra in Figs. G.10a-c to those from the literature presented in Figs. G.1-G.9, it is apparent that the species of m/z = 528 (panel c) possesses naphthenic content (as evidenced by the fragment peaks at m/z values of 15 and 28 less than that of the parent species), while the species of m/z = 352 and m/z = 526 (panels a and b, respectively) do not possess naphthenic content.

References

[1]SciFinder; Chemical Abstracts service: Columbus, OH; Mass spectrum for anthracene; spectrum ID ID_WID-DLO-073970-8; CAS registry number 120-12-7; <https://scifinder.cas.org> (accessed March 2009).

[2]SciFinder; Chemical Abstracts service: Columbus, OH; Mass spectrum for 1,2-dihydroanthracene; spectrum ID 8_LMCM-39905-106L; CAS registry number 58746-82-0; <https://scifinder.cas.org> (accessed March 2009).

[3]SciFinder; Chemical Abstracts service: Columbus, OH; Mass spectrum for 9,10-dihydroanthracene; spectrum ID ID_WID-DLO-018345-9; CAS registry number 613-31-0; <https://scifinder.cas.org> (accessed March 2009).

[4]SciFinder; Chemical Abstracts service: Columbus, OH; Mass spectrum for 1,2,3,4-tetrahydroanthracene; spectrum ID 8_LMCM-92127-474Z; CAS registry number 2141-42-6; <https://scifinder.cas.org> (accessed March 2009).

[5]SciFinder; Chemical Abstracts service: Columbus, OH; Mass spectrum for phenanthrene; spectrum ID ID_WID-DLO-073965-1; CAS registry number 85-01-8; <https://scifinder.cas.org> (accessed March 2009).

[6]SciFinder; Chemical Abstracts service: Columbus, OH; Mass spectrum for 9,10-dihydrophenanthrene; spectrum ID ID_WID-DLO-074105-9; CAS registry number 776-35-2; <https://scifinder.cas.org> (accessed March 2009).

[7]SciFinder; Chemical Abstracts service: Columbus, OH; Mass spectrum for pyrene; spectrum ID ID_WID-DLO-074967-7; CAS registry number 129-00-0; <https://scifinder.cas.org> (accessed March 2009).

[8]SciFinder; Chemical Abstracts service: Columbus, OH; Mass spectrum for 4,5-dihydropyrene; spectrum ID ID_WID-DLO-093070-1; CAS registry number 6628-98-4; <https://scifinder.cas.org> (accessed March 2009).

[9]SciFinder; Chemical Abstracts service: Columbus, OH; Mass spectrum for 1,2,3,6,7,8-hexahydropyrene; spectrum ID 8_LMCM-77344-758R; CAS registry number 1732-13-4; <https://scifinder.cas.org> (accessed March 2009).

[10]SciFinder; Chemical Abstracts service: Columbus, OH; Mass spectrum for chrysene; spectrum ID ID_WID-DLO-075807-6; CAS registry number 218-01-9; <https://scifinder.cas.org> (accessed March 2009).

[11]SciFinder; Chemical Abstracts service: Columbus, OH; Mass spectrum for 1,2,3,4-tetrahydrochrysene; spectrum ID 8_LMCM-66607-141F; CAS registry number 2091-90-9; <https://scifinder.cas.org> (accessed March 2009).

APPENDIX H

EQUIPMENT LIST

Gel permeation chromatography (GPC)

Gel permeation chromatograph. Manufactured by Waters Corp., model Alliance GPCV2000. It comes with an automatic sample injection ststem. This technique is used to fractionate petroleum pitches into fractions of narrow molecular weight distribution that can be subsequently subjected to further analyses.

Preparatory-scale GPC columns. PLgel, manufactured by Polymer Laboratories, a division of Varian, Inc. Particle size is 10 microns, 300 mm x 25 mm. (a) 500 Å pore size, catalog number PL1210-6125. (b) 100 Å pore size, catalog number PL1210-6120.

Analytical-scale GPC Columns. StyragelHT4, manufactured by Waters Corp., part number WAT044209. Particle size is 10 microns, 300 mm x 7.8 mm. Note: the Styragel HT4 column also comes packed in tetrahydrofuran (WAT044210); for future work in which tetrahydrofuran is used as the mobile phase, this column is preferable because no solvent change will be necessary (each solvent change lowers the column separation efficiency; thus, the solvent in which a GPC column is packed should not be changed unless necessary).

Sample Injection Loop. 1.080 mL, obtained from Waters Corp., part number 700001018. The volume of the sample injection loop determines the amount of sample injected into the GPC column.

Solvent Inline Filter. Obtained from Waters Corp., part number WAT088084. This part is used to filter particulate matter from the mobile phase before it is pumped throught he GPC column. Because it becomes clogged over time, it must be changed periodically.

GPC Pump Piston Seal. This part is obtained from Waters Corp.; part number WAT270938. When working with elevated flow rates (> 2.5 mL of mobile phase per minute, it is possible that the piston seal will fail, causing the GPC pump to leak. Therefore, this part must be changed periodically. The procedure for changing the piston seal is given in the Alliance GPCV2000 system software operating manual. When removing, make sure to use something sharp and firm, but that will not scratch and damage the metal fitting (such as a toothpick).

GPC Filter Vial Assembly. Obtained from Waters Corp.; part number 600000186. These vials are used for samples, such as petroleum pitch, that are not fully soluble in the GPC mobile phase.

GPC Filter Vial Caps. Obtained from Waters Corp.; part number 600000138.

Crimping Tool for Securing Caps to Filter Vials. Obtained from Waters Corp.; part number 700000847.

Waters Fraction Collector. Manufactured by Waters Corporation. Used for automated collection of GPC eluent fractions over a constant time interval.

Matrix-Assisted Laser Desorption and Ionization, Time-of-Flight Mass Spectrometry (MALDI)

MALDI Mass Spectrometer. Manufactured by Bruker Daltonics, model Autoflex. Used to obtain mass spectra for pitches and post-source decay spectra for various species within said pitches.

MALDI Target. The sample to be subjected to MALDI analysis is deposited onto the target which is introduced into the MALDI apparatus. The MTP 384 massive target (Part number 26755) was used in carrying out the work in this dissertation.

MALDI Roughing Vacuum Pump Oil. Oil P3, manufactured by Pfeiffer. This oil is used in the MALDI rough vacuum pump and should be changed yearly in order to maintain optimum pump performance.

MALDI Microchannel Plate Detector. Manufactured by Bruker Daltonics, part number S-267682. Over time (the last detector, used when operating in reflectron mode, had a lifetime of 47 months before its performance became unacceptable), the microchannels within the detector become clogged with matrix and analyte, reducing the secondary electron current generated when ions strike the detector walls.

MALDI Laser. Manufactured by Bruker Daltonics; part number S-555636. The 337 nm N_2 laser must be changed, on average, every couple of years.

Miscellaneous

Microcapillary Tubes. Manufactured by Drummond Scientific Company; catalog number 1-000-0200. These tubes, which hold a maximum volume of 20 μL, are used in MALDI sample preparation by both the solvent-based and solvent-free methods.

Sonicator. Manufactured by Mettler Electronics Corp.; model ME 5.5S. The sonicator is used to mix samples prior to their introduction into the GPC apparatus.

Cuvette for UV-Vis Analyses. Fisherbrand part number 14-385-902A, 1 mm optical path length, with Suprasil quartz windows.

Balance. Denver Instrument, model M-310; mass limit 310 g. This instrument was used to measure out pitch in the preparation of pitch solutions for preparatory-scale GPC fractionation.

APPENDIX I

PERMISSIONS

AMERICAN CHEMICAL SOCIETY LICENSE TERMS AND CONDITIONS

Jun 11, 2010

This is a License Agreement between Ward A Burgess ("You") and American Chemical Society ("American Chemical Society") provided by Copyright Clearance Center ("CCC"). The license consists of your order details, the terms and conditions provided by American Chemical Society, and the payment terms and conditions.

All payments must be made in full to CCC. For payment instructions, please see information listed at the bottom of this form.

License Number	2446020071221
License Date	Jun 11, 2010
Licensed content publisher	American Chemical Society
Licensed content publication	Industrial & Engineering Chemistry Research
Licensed content title	SAFT−LC: An Equation of State for Predicting Liquid-Crystalline Phase Behavior in Carbonaceous Pitches
Licensed content author	Ward A. Burgess et al.
Licensed content date	Oct 1, 2007
Volume number	46
Issue number	21
Type of Use	Thesis/Dissertation
Requestor type11	Not specified
Format	Print and Electronic
Portion	Table/Figure/Micrograph
Number of Table/Figure/Micrographs	1
Author of this ACS article	Yes
Order reference number	
Title of the thesis / dissertation	Prediction of Liquid Crystalline Content and Molecular Structures Present in Carbonaceous Pitches
Expected completion date	Jun 2010
Estimated size(pages)	280
Billing Type	Invoice
Billing Address	Clemson University Department of Chemical Engineering Clemson, SC 29630 United States
Customer reference info	
Total	0.00 USD
Terms and Conditions	

AMERICAN CHEMICAL SOCIETY LICENSE TERMS AND CONDITIONS

Jun 11, 2010

This is a License Agreement between Ward A Burgess ("You") and American Chemical Society ("American Chemical Society") provided by Copyright Clearance Center ("CCC"). The license consists of your order details, the terms and conditions provided by American Chemical Society, and the payment terms and conditions.

All payments must be made in full to CCC. For payment instructions, please see information listed at the bottom of this form.

License Number	2446000547830
License Date	Jun 11, 2010
Licensed content publisher	American Chemical Society
Licensed content publication	Energy & Fuels
Licensed content title	Extraction of Petroleum Pitch with Supercritical Toluene: Experiment and Prediction
Licensed content author	Mark S. Zhuang et al.
Licensed content date	Jan 1, 2000
Volume number	14
Issue number	1
Type of Use	Thesis/Dissertation
Requestor type11	Not specified
Format	Print and Electronic
Portion	Table/Figure/Micrograph
Number of Table/Figure/Micrographs	2
Author of this ACS article	No
Order reference number	
Title of the thesis / dissertation	Prediction of Liquid Crystalline Content and Molecular Structures Present in Carbonaceous Pitches
Expected completion date	Jun 2010
Estimated size(pages)	280
Billing Type	Invoice
Billing Address	Clemson University Department of Chemical Engineering Clemson, SC 29630 United States
Customer reference info	
Total	0.00 USD
Terms and Conditions	

JOHN WILEY AND SONS LICENSE TERMS AND CONDITIONS

Jun 11, 2010

This is a License Agreement between Ward A Burgess ("You") and John Wiley and Sons ("John Wiley and Sons") provided by Copyright Clearance Center ("CCC"). The license consists of your order details, the terms and conditions provided by John Wiley and Sons, and the payment terms and conditions.

All payments must be made in full to CCC. For payment instructions, please see information listed at the bottom of this form.

License Number	2446030660564
License date	Jun 11, 2010
Licensed content publisher	John Wiley and Sons
Licensed content publication	Rapid Communications in Mass Spectrometry
Licensed content title	Post-source decay of alkylated and functionalized polycyclic aromatic compounds
Licensed content author	Frache Gilles, Krier Gabriel, Vernex-Loset Lionel, et al
Licensed content date	Jul 17, 2007
Start page	2601
End page	2607
Type of use	Dissertation/Thesis
Requestor type	University/Academic
Format	Print and electronic
Portion	Figure/table
Number of figures/tables	1
Original Wiley figure/table number(s)	Figure 3
Will you be translating?	No
Order reference number	
Total	0.00 USD
Terms and Conditions	

Subject: FW: Concerning my use of pictures of Bruker software screens in my dissertation
From: "Victor Fursey" <vgf@bdal.com>
Date: Mon, June 21, 2010 12:21 pm
To: wburges@clemson.edu
Cc: ms@bdal.de (less)
"Lisa Peters" <lmp@bdal.com>
Priority: Normal
Options: View Full Header | View Printable Version | Download this as a file | View Message details | Add to Addressbook | Bounce

Dear Ward,

Thank you for your recent email to Lisa Peters. You may use the screen shots of our data acquisition and processing software pages specifically in your Ph.D. dissertation. They are for this purpose only and should not be propagated elsewhere. Please could you forward a copy of the final figures you intend to use, just for our records. Thanks in advance.

Yours sincerely,

Victor Fursey

Bruker Daltonics

Victor Fursey,
Vice President, Sales - North America
Bruker Daltonics Inc.
40 Manning Road
Billerica, MA 01821
Ph: 978.663.3660 x1250
vgf@bdal.com <mailto:vgf@bdal.com>

-----Original Message-----
From: wburges@clemson.edu [mailto:wburges@clemson.edu]
Sent: Friday, June 18, 2010 5:01 PM
To: Lisa Peters
Subject: Concerning my use of pictures of Bruker software screens in my dissertation

Lisa,

I am writing several MALDI tutorials for my dissertation which require me to cut and paste pictures of the screen in the FlexControl and Flex Analysis software. May I have a written confirmation of

permission to do so?

I appreciate your time and help in this matter.

Sincerely,

Ward Burgess

Clemson University

Dept. of Chemical Engineering

(864)-656-5904

wburges@clemson.edu

Subject: FW: Request permission to use ACS mass spectra accessed via SciFinder
From: "Berlin, Gary" <gberlin@cas.org>
Date: Wed, June 30, 2010 5:24 pm
To: wburges@clemson.edu
Priority: Normal
Options: View Full Header | View Printable Version | Download this as a file | View Message details | Add to Addressbook | Bounce

Hi Ward,

You may certainly reproduce those 8 spectra within your dissertation. Please follow these guidelines for 1) proper citation and 2) acknowledgment:

1) Identify the individual spectra using the following format, which is a blend of the formats that the ACS Style Guide 3rd ed. recommends for web site (p. 321) and computer programs (p. 324). Currently, no single format in ACS Style 3rd addresses your exact case.

Example:
SciFinder; Chemical Abstracts Service: Columbus, OH; carbon-13 NMR spectrum; spectrum ID CC-03-C_SPC-3734; RN 50-52-2; https://scifinder.cas.org (accessed June 9, 2010).

2) Append the following permission statement so it's clear that it refers to the spectra. (If you want, you can do this for all 8 spectra as a group.)

Reprinted with the permission of the American Chemical Society. Copyright (c) 2010. American Chemical Society (ACS). All Rights Reserved.

Thanks,

Gary Berlin
Customer Service
CAS, a division of the American Chemical Society
2540 Olentangy River Road
Columbus, OH 43202
Phone: 614-447-3764
Fax: 614-447-3751
www.cas.org

-----Original Message-----
From: wburges@clemson.edu [mailto:wburges@clemson.edu]
Sent: Wednesday, June 30, 2010 1:35 PM
To: CAS Customer Care
Subject: Request permission to use ACS mass spectra accessed via SciFinder

I am writing this email to request permission to reproduce several mass spectra copyrighted by ACS in my dissertation. I accessed these mass spectra via the SciFinder program. Their identification codes are as follows:

ID_WID-DLO-073970-8
8_LMCM-39905-106L
ID_WID-DLO-018345-9
8_LMCM-92127-474Z
ID_WID_DLO_073965-1

ID_WID-DLO-074105-9
ID_WID-DLO-074967-7
ID_WID-DLO-093070-1
8_LMCM-77344-758R
ID_WID-DLO-075807-6
8_LMCM-66607-141F
ID_WID-DLO-052568-8

I also need to know the entity to whom I should give credit. Would you please get back to me on this part ASAP?

Thank you very much for your time and attention in this matter.

Regards,

Ward Burgess
Ph. D. Candidate
Clemson University
Dept. of Chemical Engineering
(864)-656-5904
wburges@clemson.edu